

**Anomalous photovoltaic effect
in π -conjugated ferroelectric liquid crystals**

Atsushi Seki

September, 2017

**Anomalous photovoltaic effect
in π -conjugated ferroelectric liquid crystals**

Atsushi Seki

September, 2017
Department of Advanced Material Sciences
School of Engineering
Kagawa University

The study described in this thesis was carried out under the supervision of Professor Masahiro Funahashi at Kagawa University from October, 2014 to September, 2017.

Table of contents

| | |
|--|------------|
| Chapter 1. General introduction | 6 |
| 1.1. Philosophy of this thesis | 6 |
| 1.2. Ferroelectric materials | 8 |
| 1.3. Liquid crystals | 28 |
| 1.4. Liquid-crystalline semiconductors | 47 |
| 1.5. Ferroelectric liquid crystals | 65 |
| 1.6. Multi-functional materials | 72 |
| 1.7. Photovoltaic effect | 72 |
| 1.8. Objective of this thesis | 74 |
| 1.9. Outline of this thesis | 76 |
| 1.10. References | 77 |
| | |
| Chapter 2. Bulk photovoltaic effects in ferroelectric liquid crystals based on phenylterthiophene derivatives | 95 |
| 2.1. Introduction | 95 |
| 2.2. Experimental section | 96 |
| 2.3. Results and discussion | 104 |
| 2.4. Conclusion | 110 |
| 2.5. References | 111 |
| | |
| Chapter 3. Bulk photovoltaic effects based on molecular chirality: the influence of the enantiomer purity on the photocurrent response in π-conjugated ferroelectric liquid crystals | 112 |
| 3.1. Introduction | 112 |
| 3.2. Experimental section | 115 |
| 3.3. Results and discussion | 121 |
| 3.4. Conclusion | 134 |
| 3.5. References | 135 |

| | |
|--|------------|
| Chapter 4. Anomalous Photovoltaic Effect in Chiral Ordered Smectic Phases of Phenylterthiophene Derivatives without Junctions: Immobilization of the Polarized Structure by Surface Stabilization | 138 |
| 4.1. Introduction | 138 |
| 4.2. Experimental section | 140 |
| 4.3. Results and discussion | 142 |
| 4.4. Conclusion | 152 |
| 4.5. References | 152 |
| | |
| Chapter 5. Conclusion of this thesis | 153 |
| 5.1. Overall conclusion | 153 |
| 5.2. Perspective | 153 |
| | |
| Accomplishments | 156 |
| | |
| Acknowledgement | 160 |

Chapter 1

General introduction

1.1. Philosophy of this thesis

The term of “material” indicates “an element constituting a tissue expressing various functions”. Since ancient times, human beings have produced various “tools” and “equipment” to make their lives rich and comfortable. The primitive tools and dwelling were made of “stones”, “woods”, “plant fibers” and “soils”, which is derived from natural products. Along with the development of civilization and the progress of technology, human beings have come to process and manufacture “bronze”, “copper” and “iron”. These ancient metals and alloys are regarded as the first artificial materials. These inorganic materials can be obtained by simple smelting technique that metal ores are ignited with fagots and charcoals. Chemical reactions in these processes can be explained by “reduction reaction” of metal ores. Following the melting of metal ores under the ignition condition, nonmetallic elements such as oxygen, sulfur and hydrogen in the ores can be burned with natural fuel and removed out as oxidized gasses from the molten system. While the manufacturing technology by using the minerals, and processing technology of natural inorganic/organic matters had been developed from ancient, the establishment of organic synthetic materials technology was delayed to modern ages. In fact, the "medieval castle" in Japan consists of various facilities such as "moat", "stone wall", "tower", "hall" and the materials forming them are "earth", "timber", "metal fittings" and so on. Facilities constructed with various materials are appropriately arranged and organized so that the castle can demonstrate its role to the utmost. Here, looking at the material, "earth" is a chemical mixture composed of coarse-grained minerals, colloidal mixtures, and organism-derived organic substances in various compositions. "Stones" are mixtures of inorganic minerals containing silicate as a main component and various minerals. On the other hand, "timbers" are based on organic polymer composed of polysaccharide such as cellulose and hemicellulose and lignin. All of these organic components are synthesized not by artificial but biochemical reactions. In this way, no organic synthetic materials had been used before “urea” was developed in 19th century.¹

Even in present time, many natural materials are used for various “tools” and “equipment” because they are easy to obtain and also apply the conventional methods. However, natural materials such as “stones”, “timbers” and “plant fibers” have serious concerns in that they are not composed of a single and the same chemical species. In addition, they also have big difference in compositions, chemical and physical structures, and physical properties depending on the species, biological environments and production processes. The precise control of chemical compositions and organized structures in natural materials are impracticable in present because the precise conditions such as the formation processes and mechanisms of a lot of natural products are never completely

clarified and understood. Thus, production location, environments and collected portions of natural materials are critical issues in practical use. In contrast, the chemical species and whole compositions of artificial synthetic materials are obvious. Furthermore, the control of well-organized structure and chemical modification are also possible. Thus, various material systems can be designed and developed.

Depending on the function of interest, you can classify the materials in different ways. Based on the chemical elements constituting them, it can be classified into organic materials, inorganic materials and organic-inorganic composite materials.

Since each of these materials is diverse, its physical properties such as density, light and heat absorption characteristics, softening temperature, and other chemical properties (weather resistance including thermal stability and light stability) are different. Therefore, an appropriate material is selected based on the characteristic which is indispensable in the application.

My main scientific interests cover organic materials. This is because organic compounds can be designed in a wide variety of chemical structures and can be arranged in various ways by applying the reaction technique of organic synthetic chemistry.² From this point of view, the combination of several components with possibilities of inducing different features can lead to the construction of functional molecules.³ Especially, low molecular weight organic compounds with stereo-regularity can be synthesized and isolated by common organic synthetic technique in contrast to conventional polymers obtained by radical reactions. Therefore, the structural control of self-assemblies based on single component system as well as the mixtures system with precise compositions can be achieved.

Through my study described in this thesis, it will be considered about the development of multi-functional materials centering on thermotropic LC materials as one of the significant self-assembled systems.⁴ As a model case, the material systems with "carrier transport" and "ferroelectric" properties will be discussed.

What I would like to described in this Ph.D. thesis is "the importance of understanding the various inter- and intra-molecular interactions", "the possibility of controlling a self-assembled structures by an application of those weak interactions in the appropriate balance for the required functions", "the realization of hierarchal and utilized functions along the nano-structurization strategy" and "the development of novel organic-based multifunctional material system by using the conventional technique of organic synthetic chemistry".

I believe that our π -conjugated ferroelectric liquid-crystalline systems are important trajectory on materials science as well as liquid-crystalline science, due to the novel concept which is experimentally demonstrated the efficient carrier generation and transport assisted by ferroelectric internal field in the bulk (Figure 1-1).

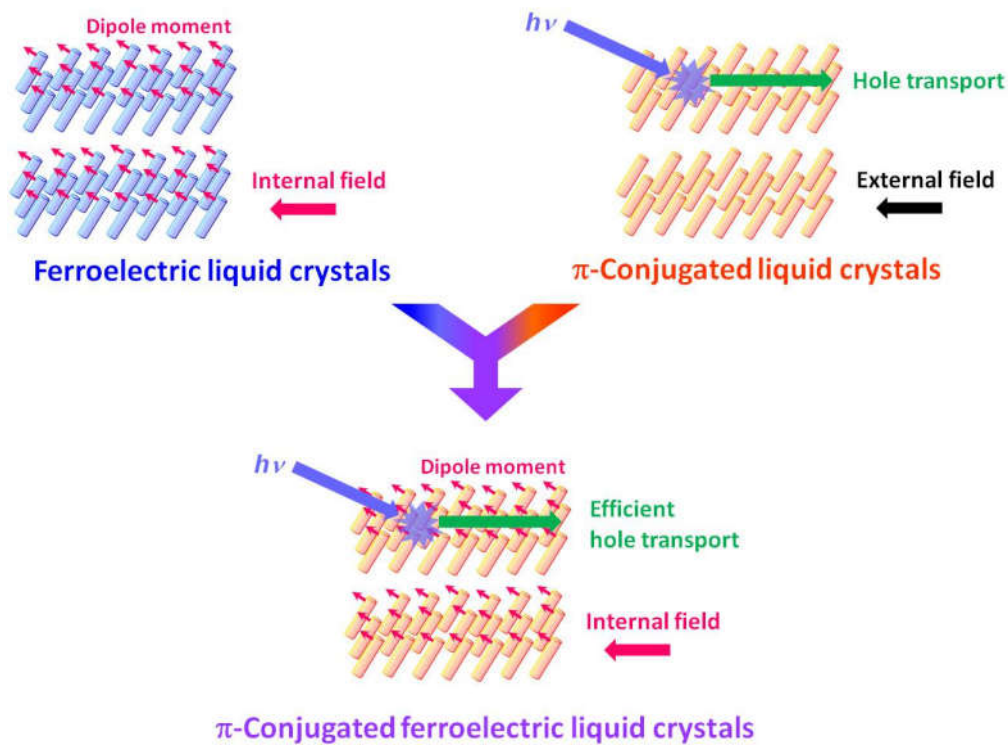


Figure 1-1. Schematic illustrations of π -conjugated ferroelectric liquid-crystalline system as an example of multi-functional materials.

1.2. Ferroelectric materials⁵

1.2.1. Basic concept of ferroelectrics

The existence of spontaneous electric dipoles and their thermal dependence has been known since ancient times. In the 18th and 19th centuries, the quantitative characterization studies on this phenomenon were carried out. These studies have greatly led to the establishment of the perception that the physical effect based on thermal change of electric dipole moment is a "pyroelectric" effect.⁶ Furthermore, the phenomenon that electrical polarity is generated under the application of external stress, which is known as "piezoelectric" behaviors, was discovered by J. Curie and P. Curie in 1880 as a result of systematic study on "pyroelectricity".⁷ The Curie brothers also revealed that charge development upon uniform thermal treatment are different from that upon non-uniform heating due to the thermal stress originated from the "pyroelectricity". From the above description, the "pyroelectric" and "piezoelectric" materials are defined as matter in which the magnitude of the electric dipole moment can be changed by thermal and pressure stimuli, respectively. It is noted that "pyroelectric" materials are subset in "piezoelectric" materials.⁸

The term of "ferroelectricity" indicates a property possessing a spontaneous polarization which can be reversed by the external electric field.^{5, 9} This term got to use in the analogy to "ferromagnetism" which exhibiting a permanent magnetic moment because the "ferromagnetic" phenomenon had been recognized in scientific society before the discovery of "ferroelectricity". The

essential condition for the expression of "ferroelectricity" is a structure that allows uniaxial orientation of permanent dipole moments in the molecular aggregation state as well as dynamic behavior which can reverse a direction of the dipole moment. All "ferroelectric" materials also work as "pyroelectric" and "piezoelectric" materials (Figure 1-2).

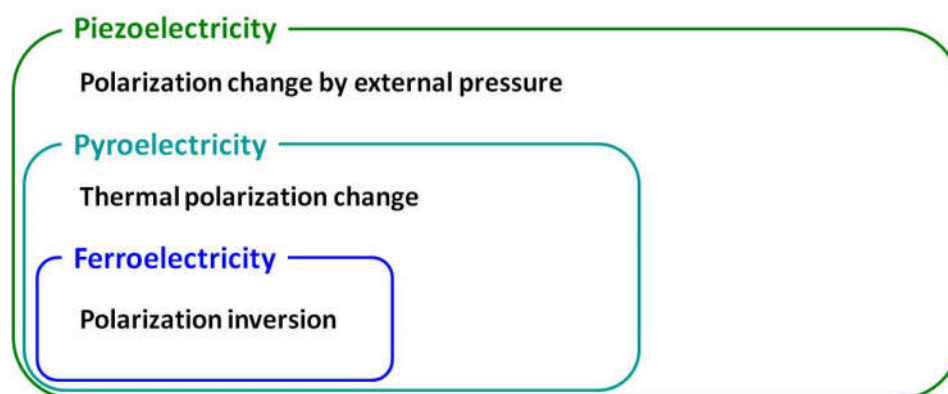


Figure 1-2. Schematic illustrations of ferroelectric system.

In the ferroelectric systems, the polarization state is induced by an electrical poling treatment and the generated polarization state is retained even after removing the external bias. In practical, the ferroelectric polarization and charge accumulation behaviors are important properties as a function which can be applied to sensors, memory and integrated devices.

The hysteresis behaviors are observed in plots of polarization (polarization charge density) as a function of the external voltage (electric field) (Figure 1-3). The ferroelectric hysteresis loop can be experimentally obtained by Sawyer-Tower method. On each region of the loop displayed in Figure 1-3, the dipole distribution inside the aggregation structures is schematically explained as follows. Position (a) is the initial state, in which polarization is still not generated. At position (b) under the positive bias external field ($+E_1$), the electric dipoles can be aligned to compensate for the external stimulus. As a result, the polarization state (internal electric field) is generated in the bulk. The situation after the bias is returned to zero from state (b) corresponds to position (c), where the polarization state with the value of $+P_r$ is maintained even under zero bias. At position (d) under the negative field ($+E_1$), the electric dipoles should be aligned in reversed direction to the case of position (b). At position (e), which corresponds to the state after removed the negative bias, the opposite polarization state with the value of $-P_r$ is induced. On the basis of such behaviors, various devices based on ferroelectrics such as ferroelectric random access memory (FeRAM) can demonstrate their functions. For instance, the FeRAM system is incorporated in a circuit using a large number of electrodes, records binary information as local polarization, and reads and writes by using an electrical signal (voltage, current). Physical values such as coercive electric field, residual polarization, and spontaneous polarization can be estimated from the hysteresis loop. The coercive electric field

($+E_c$, $-E_c$), which is the electric field when the polarization becomes zero, corresponds to the intersection point of E axis and polarization plot. The intersection and extrapolation points of polarization plot and P axis indicate the remanent polarization ($+P_r$, $-P_r$) and the spontaneous polarization ($+P_s$, $-P_s$), respectively.

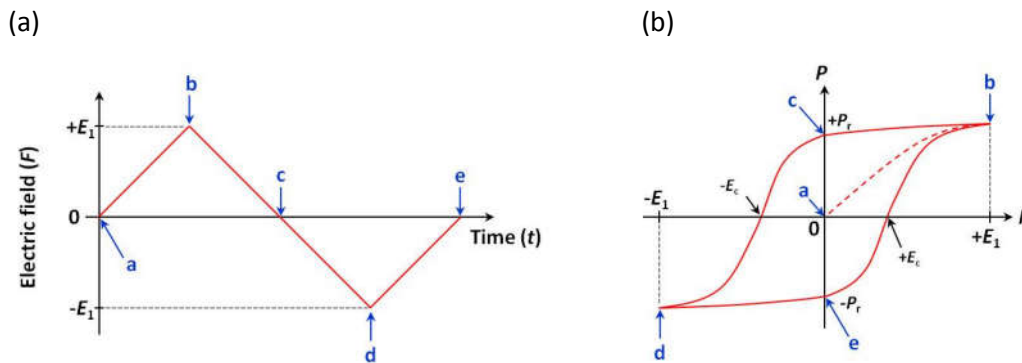


Figure 1-3. Schematic illustrations of (a) application profiles on external electric field, and (b) typical ferroelectric hysteresis loop.

Some analogous substances of ferroelectric materials exhibit double dielectric hysteresis behaviors (Figure 1-4). This phenomenon is defined as “anti-ferroelectricity”. In the anti-ferroelectric system, no spontaneous polarization is generated on zero bias. Under the application of electric field above a certain threshold value, the ferroelectric-like dielectric behaviors are observed and two hysteresis loops according to the positive and negative electric field are induced.

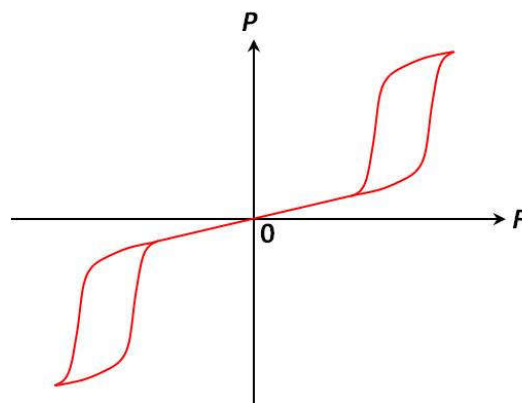


Figure 1-4. The typical anti-ferroelectric double hysteresis loop.

As an extremely rare phenomenon, "ferrielectricity" which displays triple dielectric hysteresis behaviors is also found. In the ferrielectric system, three ferroelectric-like loops are observed in low

electric field range as well as high electric field ranges in positive and negative regions (Figure 1-5).

Under the application of electric field above a certain threshold value, the ferroelectric-like behaviors are observed and two hysteresis loops are induced in the positive and negative field regions.

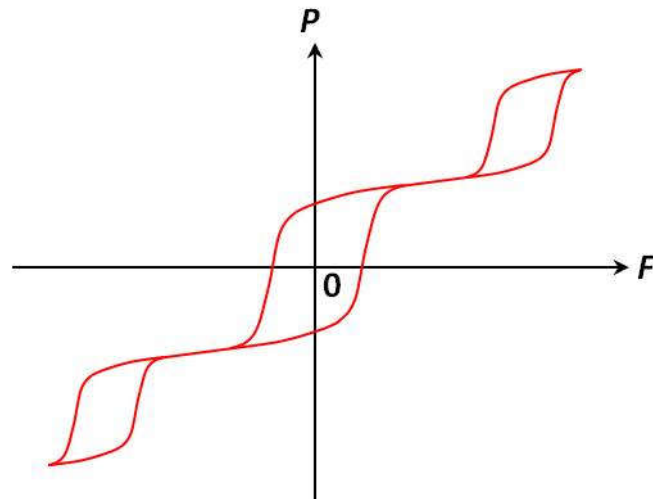


Figure 1-5. The typical ferroelectric triple hysteresis loop.

Temperature-dependence of dielectric constant in ferroelectrics is explained by the Ferroelectric Curie-Weiss law. The Curie-Weiss law expresses the relation between the absolute temperature (T) and the relative dielectric constant of ferroelectrics (ϵ_r) with using specific coefficient (C) and temperature (T_c) (Equation 1-1).

$$\epsilon_r = \frac{C}{T-T_c} \quad [\text{Equation 1-1}]$$

The threshold temperature T_c is called as “Curie temperature”, at which the denominator of equation 1-1 is zero and relative dielectric constant diverges. The Curie temperature indicates the phase transition point from ferroelectric phase to another non-ferroelectric (paraelectric) phase. In the simplest ferroelectric system exhibiting only a ferroelectric-paraelectric transition, the ferroelectric phase lies in low-temperature side to the paraelectric phase in which no spontaneous polarization is generated. In this ferroelectric system, ferroelectric behaviors can be observed below the Curie temperature. However, the ferroelectricity drastically dissappeared above the Curie temperature (after the phase transition).

The typical plot of relative dielectric constant as a function of absolute temperature (T) is as shown in Figure1-6. For the ferroelectric-paraelectric phase transition, the temperature-dependences of the relative permittivity, electrosensitivity, and polarization are different between the first and second order phase transitions. In the case of the first order ferroelectric-paraelectric transition, relative dielectric constant discontinuously jumps up at the Curie temperature (Figure 1-6a). The

relative dielectric constant is maximized on the Curie point and decayed in higher temperature above it. In case of the second order ferroelectric-paraelectric transition, relative dielectric constant is diverged at the Curie temperature (Figure 1-6b).

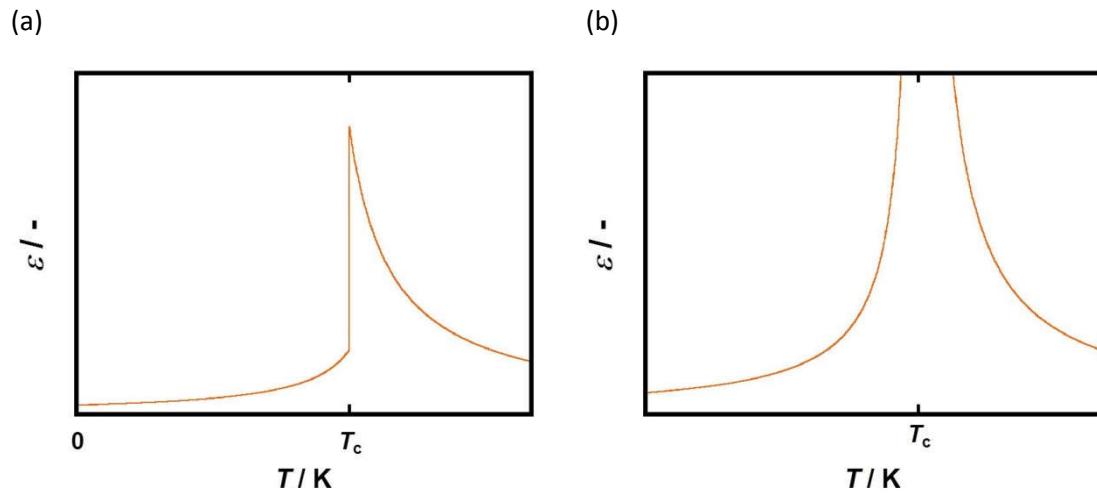


Figure 1-6. The typical plots of relative dielectric constant as a function of the temperature in cases of (a) the first order ferroelectric-paraelectric transition, and (b) second order ferroelectric-paraelectric transition.

Here, the reciprocal of relative dielectric constant are focused on. In general, the inverse for relative dielectric constant (ϵ_r^{-1}) is converted into the form with reciprocal of electrosensitivity (χ^{-1}). The correlation between dielectric polarization vector (\mathbf{P}) and external electric field vector (\mathbf{E}) is expressed as Equation 1-2 with coefficient of electrosensitivity (χ) and permittivity of vacuum (ϵ_0).

$$\mathbf{P} = \epsilon_0 \chi \mathbf{E} \quad (\chi > 0) \quad [\text{Equation 1-2}]$$

In the basic physics of dielectrics system, the correlation between vector of electric flux density (\mathbf{D}) and external electric field vector is defined as Equation 1-3.

$$\mathbf{D} = \epsilon_0 \mathbf{E} + \mathbf{P} = \epsilon_r \epsilon_0 \mathbf{E} \quad [\text{Equation 1-3}]$$

From Equations 1-2 and 1-3, relative dielectric constant can be described as Equation 1-4 with using the coefficient of electrosensitivity.

$$\epsilon_r = 1 + \chi \quad (\chi > 0) \quad [\text{Equation 1-4}]$$

Therefore, the inverse for relative dielectric constant can be expressed with the reciprocal of electrosensitivity as Equation 1-5.

$$\varepsilon_r^{-1} = (1 + \chi)^{-1} \quad (1 + \chi > 1) \quad [\text{Equation 1-5}]$$

The typical plot of reciprocal of electrosensitivity as a function of temperature is as shown in Figure 1-7. In the ferroelectric system based on the first order phase transition at the Curie temperature, the drastic and discontinuous change is observed at the Curie temperature (Figure 1-7a). In this case, the reciprocal of electrosensitivity is linearly changed in ferroelectric and paraelectric phases. The intersection point of plots does not coincide with the Curie point. Extrapolation point on the temperature axis (T_0) of the plot contributing to the paraelectric phase indicates the temperature where the free energy of the system becomes apparently zero. In contrast, the reciprocal of electrosensitivity continuously changes in the ferroelectrics exhibiting the second order phase transition at the Curie temperature (Figure 1-7b).

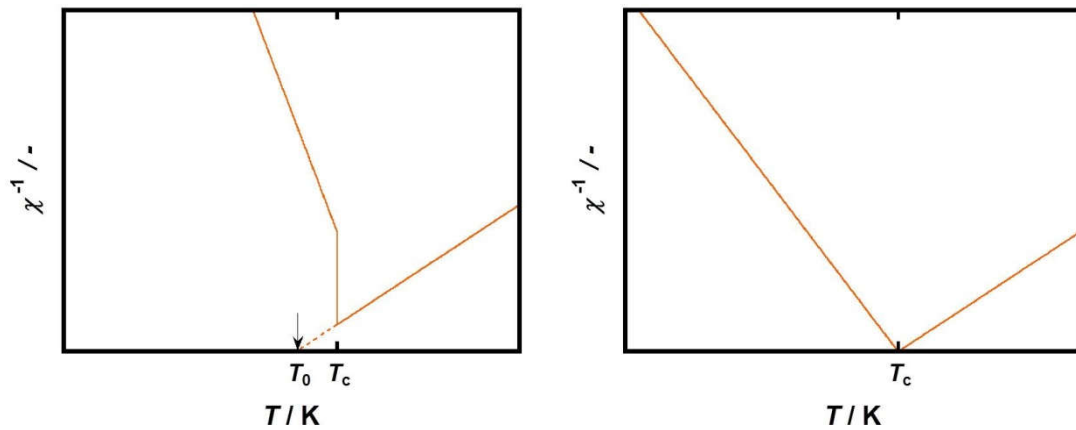


Figure 1-7. Temperature dependence of reciprocal of electrosensitivity (a) in the first-order transition system, and (b) in the second-order transition system.

There is the same difference in the temperature-dependence of spontaneous polarization between the first-order transition system and the second-order transition system (Figure 1-8).

In the first-order transition system, the spontaneous polarization discontinuously and abruptly drops on the Curie temperature (Figure 1-8a). In contrast, continuous and gentle attenuation behavior on spontaneous polarization is observed in the second-order transition system (Figure 1-8b).

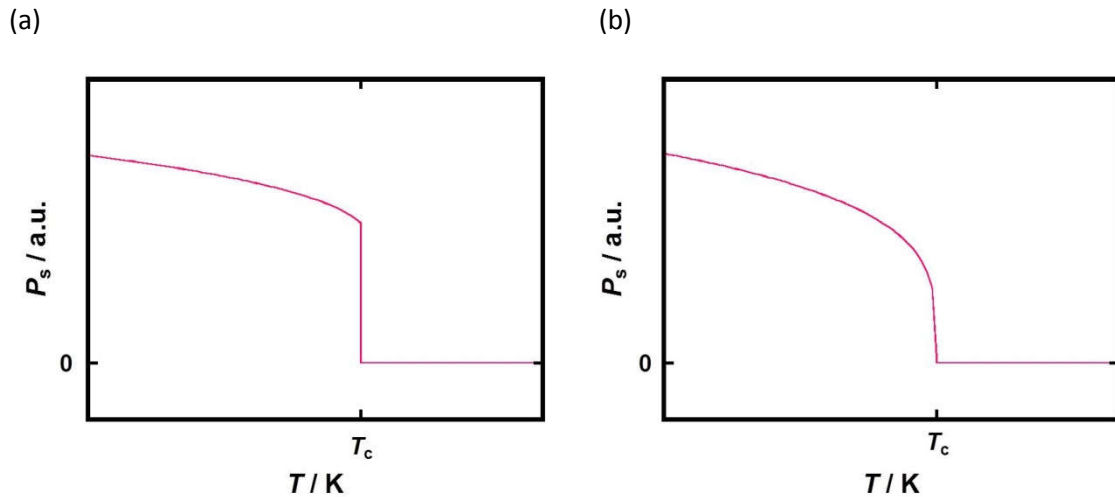


Figure 1-8. Temperature dependence of spontaneous polarization (a) in the first-order transition system, and (b) in the second-order transition system.

The above discussion on dielectric constant is in static condition. It is noted that their dielectric properties depends on frequency of the external AC bias due to the origin of the polarization. Dielectric dispersion phenomenon is observed in common with all these polarizations. The electric dipole moment is generated by “orientation polarization”, “ion polarization” and “electronic polarization”.

“Orientation polarization” can be produced in polar molecular system with permanent dipole moment. To be brief, this phenomenon is caused by the uniaxial orientation of permanent dipole moment under the application of external bias. In polar molecular system, local polarization (in molecular scale) is formed in the initial stage without external electric field, because the electronic density in a molecule is biased by contribution of electronegativity. Although “ion polarization” and “electronic polarization” are considered as the result of “induced dipole” by the external stimulus, therefore, “orientation polarization” is different from those polarizations. The contribution of external electric field is only the induction of the dipole reorientation behavior to compensate for the external stimulus. In the initial state (without external bias), the direction of local dipole moments is random and thus the sum total of local polarization results in zero. Under the application of the appropriate electric field, the sum total of local polarization has some values by the uniaxial orientation of dipoles.

“Ion polarization” can be induced by displacements of cations and anions in the ionic complex when the external electric field is applied. The displacement behavior of ions depends on the electric field intensity.

“Electronic polarization” can be induced by deformation of the molecular (atomic) orbitals as well as displacement of nuclei.

It should be noted that the actual polarization phenomenon is caused by cooperation of these three polarizations. Therefore, the polarization of the whole system is physically treated as the sum of the contributions of all these polarizations.

Here, the situation that the external electric field is applied to any dielectric material will be considered. The correlation between dipole moment (m) of the material and external bias electric field (E) is expressed by the following equation (Equation 1-6) with polarizability factor (α).

$$m = \alpha E \quad [\text{Equation 1-6}]$$

Polarizability factor of ion polarization (α_i) and that of electronic polarization (α_e) are defined in Equation 1-7, 1-8 as analogy of Equation 1-6, respectively. The factors indicated by m_i and m_e are where the moments corresponding to the ionic dipole and electronic dipole, respectively.

$$m_i = \alpha_i E \quad [\text{Equation 1-7}]$$

$$m_e = \alpha_e E \quad [\text{Equation 1-8}]$$

By using a factor of permanent dipole moment (m_p), polarizability factor of orientation polarization (α_p) are described as Equation 1-9 based on classical statistical mechanics.

$$\alpha_p = \frac{m_p^2}{3kT} \quad [\text{Equation 1-9}]$$

In particular to the polar molecular system, therefore, the overall polarizability factor (α) can be expressed as Equation 1-10.

$$\alpha = \alpha_i + \alpha_e + \frac{m_p^2}{3kT} \quad [\text{Equation 1-10}]$$

The dynamics of molecules, atoms and electrons is contributed to frequency dependence of polarizability factor and dielectric constant. In the case of considering the frequency dependence of “induced polarization”, it can be roughly explained by a harmonic oscillator model.

The phenomenon that dielectric constant depends on the frequency of external bias is considered as “dielectric dispersion”. The AC external electric field as a function of time (t) can be defined as Equation 1-11 with using imaginary unit (i) and angular frequency (ω).

$$E = E_0 \exp(i\omega t) \quad (i = \sqrt{-1}) \quad [\text{Equation 1-11}]$$

The frequency dependence of electric flux density is defined as Equation 1-12 by considering the phase shift (Δ).

$$D = D_0 \exp(i\omega t - \Delta) \quad [\text{Equation 1-12}]$$

Following Equation 1-3 which describes the static condition, the linear combination between Equation 1-11 and Equation 1-12 is formally defined as Equation 1-13 with using complex dielectric constant (ϵ_r^*).

$$D = \epsilon_r^* \epsilon_0 E \quad [\text{Equation 1-13}]$$

The definition equation of complex dielectric constant is Equation 1-14.

$$\epsilon_r^* = \epsilon' - i\epsilon'' = \frac{D_0}{\epsilon_0 E_0} \cos\Delta - i \left(\frac{D_0}{\epsilon_0 E_0} \sin\Delta \right) \quad [\text{Equation 1-14}]$$

In physical, ϵ'' and $\tan\Delta$ indicate energy loss when AC electric field is applied to the dielectric. The dielectric is generally considered as an equivalent circuit composed of electrostatic capacity (C_p) and the resistance (R_p). The relation between these factors can be expressed by Equation 1-15.

$$\frac{\epsilon''}{\epsilon'} = \tan\Delta = \frac{1}{R_p C_p \omega} \quad [\text{Equation 1-15}]$$

Dielectric dispersion is explained by two types of mechanism. In the case of orientation polarization, relaxation-type dispersion is observed. In this relaxation-type dispersion, dielectric loss causes due to the delay of the dipole rotation dynamics to the external electric field. On the other hand, resonance-type dispersion is observed for induced (ionic and electronic) polarization. The resonance-type dispersion is considered as elastic vibration system with decay.

To explain the relaxation-type dispersion, the simple one dimensional system which possesses thermodynamic energy potential curve in solid state as shown in Figure 1-9 will be considered. As an assumption, the following conditions shall be applicable to this thermodynamic model. The orientation vector of permanent dipole moment will be parallel or anti-parallel to the horizontal axis in this simplified system. The thermodynamic energy potential barrier (U_a) will be located between two energy potential minimums and the permanent dipole will be vibrating with thermal frequency ($\omega_0/2\pi$).

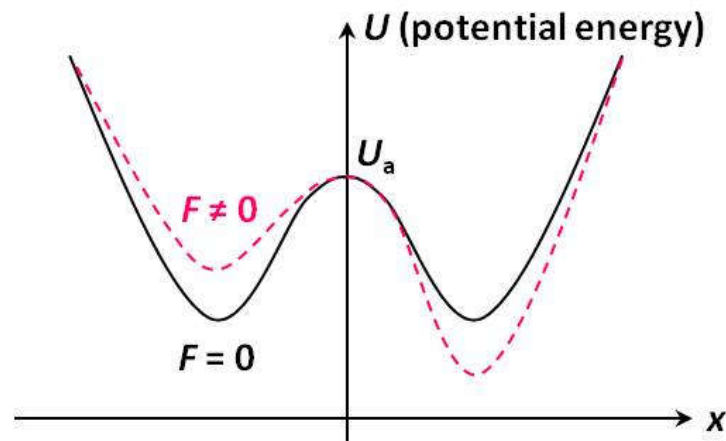


Figure 1-9. Potential curves in solid state with permanent dipole (F : external electric field).

In this model, the Debye dispersion formula described as following equations (Equation 1-15, 1-16) is derived by the Debye theory on dielectric dispersion with using the relaxation time (τ).

$$\varepsilon'(\omega) - \varepsilon(\infty) = \frac{\varepsilon(0) - \varepsilon(\infty)}{1 + \omega^2 \tau^2} \quad [\text{Equation 1-15}]$$

$$\varepsilon''(\omega) = \frac{\{\varepsilon(0) - \varepsilon(\infty)\} \omega \tau}{1 + \omega^2 \tau^2} \quad [\text{Equation 1-16}]$$

These two equations describe the correlation between the complex dielectric constant and the relaxation time. The plot for these equations as functions of $\omega\tau$ is as shown in Figure 1-10. The real part ε' is stepwise decreased along with the increase of external electric field frequency. This change behavior briefly shows that the dipole inversion cannot follow the speed of electric field change gradually. In the small $(\omega\tau)^{-1}$ region, the dipole inversion can follow the electric field change. In contrast, however, the dipole cannot reverse the direction in the region of large enough $(\omega\tau)^{-1}$. The imaginary part ε'' is maximized in the point where is $\omega = \tau^{-1}$. This model describes the system which has only single relaxation time. It is noted that there is a distribution in relaxation time in the actual system.

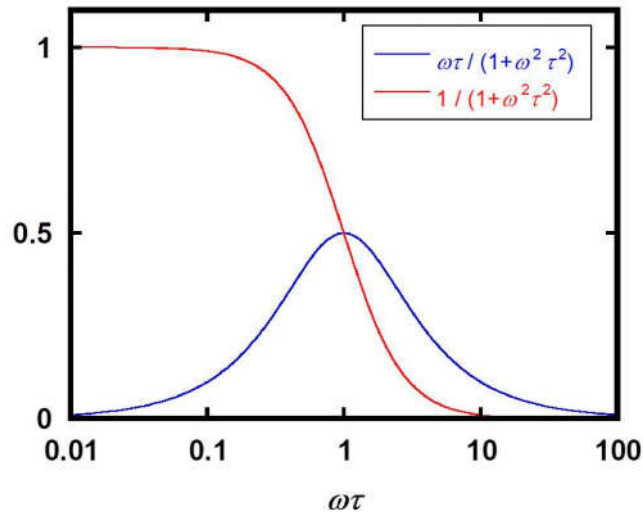


Figure 1-10. Theoretical plots for Debye dispersion formula.

The resonance-type dispersion is considered as the system composed of multicomponent oscillators. In this case, real part ε' and imaginary part ε'' can be expressed as following with using damping coefficient (Γ) (Equation 1-17, 1-18).

$$\varepsilon'(\omega) = \varepsilon(\infty) + \frac{\{\varepsilon(0) - \varepsilon(\infty)\} \omega_0^2 (\omega_0^2 - \omega^2)}{(\omega_0^2 - \omega^2)^2 + \Gamma^2 \omega^2} \quad [\text{Equation 1-17}]$$

$$\varepsilon''(\omega) = \frac{\{\varepsilon(0) - \varepsilon(\infty)\} \omega_0^2 \Gamma \omega}{(\omega_0^2 - \omega^2)^2 + \Gamma^2 \omega^2} \quad [\text{Equation 1-18}]$$

The plot for real and imaginary parts of complex dielectric constant as functions of the frequency ω is as shown in Figure 1-11. The real part ϵ' gets zero on the point where is $\omega = \omega_0$. On the other hand, the imaginary part ϵ'' is maximized on the point where is $\omega = \omega_0$.

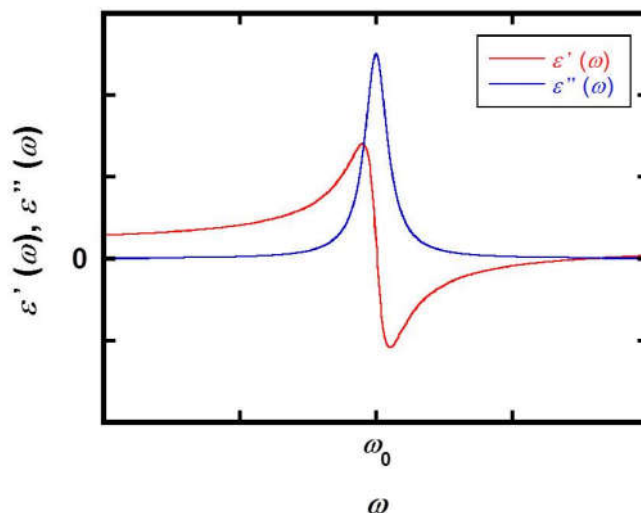


Figure 1-11 Theoretical plots of complex dielectric constant as functions of the frequency for resonance-type dispersion.

The plot for frequency dependence of complex dielectric constant under the contribution of orientation polarization and induced polarization is shown in Figure 1-12. It should be noted that the characteristic frequencies of corresponding dielectric dispersion behaviors are different magnitude and depends on the type of polarization.

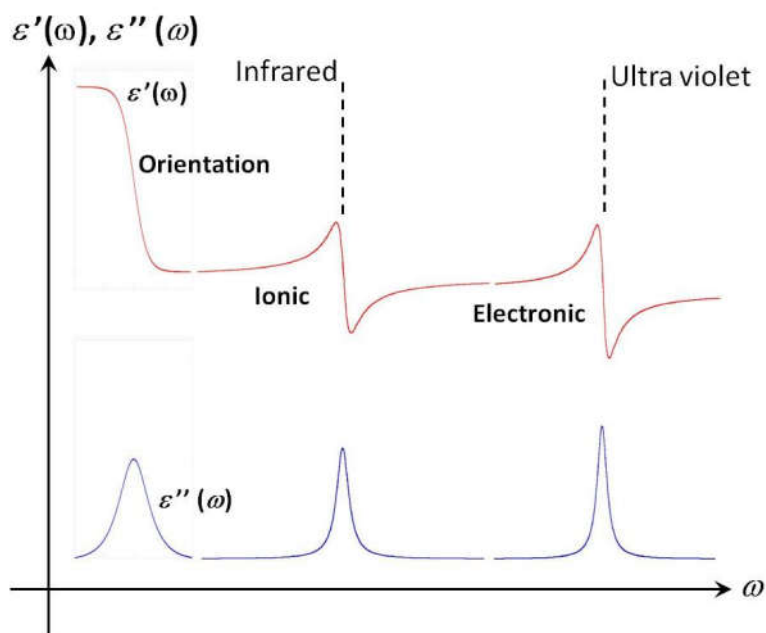


Figure 1-12 Frequency dependence of complex dielectric constant.

1.2.2. Brief history of ferroelectrics¹⁰

Ferroelectricity was first discovered by study on “Rochelle salt” reported by J. Valasek in 1920.¹¹ He investigated the dielectric properties of “Rochelle salt” from 1919 under the supervision of Professor W. F. G. Swann. Then, he observed the uncommon dielectric hysteresis behaviors, that is ferroelectric hysteresis, in “Rochelle salt”. Furthermore, his deep and systematic study revealed the temperature dependence of piezoelectric activity and phase transition behaviors in “Rochelle salt”. Valasek's study was undoubtedly inscribed as a vital milestone in the history of ferroelectricity and ferroelectric materials. Following the first experimental study of the ferroelectric salts, P. Scherrer and G. Bush clarified the ferroelectricity of KH_2PO_4 which exhibits high average dielectric constant. Through their study, KH_2PO_4 shows low critical temperature about 123 K.¹² Up to the present, KH_2PO_4 has been a model and substance in the ferroelectric science.

A little late from the study of ferroelectric salts, ferroelectric ceramics system was found in 1940's by some independent groups in United States and Russia.^{13, 14} After that, the spread and development of ferroelectric ceramics led to the construction of doped ferroelectric ceramics systems such as $\text{Pb}(\text{Zr},\text{Ti})\text{O}_3$ (PZT)¹⁵ and $(\text{Ba},\text{Sr})\text{TiO}_3$ (BST).¹⁶ As the industrial applications, some inorganic ferroelectric materials have been used for ceramics capacitors and ferroelectric random access memory (FeRAM) etc. in the present.¹⁰

The interests of ferroelectric study after 1950's can be roughly classified as two trends. One trend is perovskite-based ferroelectrics and another one is organic ferroelectric materials. In the organic system, the ferroelectric behaviors of thiourea were discovered in 1959.¹⁷ Ferroelectric liquid crystals, which is described in detail on the latter section 1.5., have been developed in 1975.¹⁸ After a while, R. G. Kepler and coworker reported the ferroelectric behavior in poly(vinylidene fluoride) (PVDF) as the first example of ferroelectric polymers.^{19a} Almost at the same time, T. Furukawa and coworkers deeply investigated the ferroelectricity in PVDF^{19b} and copolymer of vinylidene fluoride and trifluoroethylene (P(VDF-TrFE)).^{19c} Compared with ferroelectric ceramics, the reports on ferroelectric polymers are not so much, but nylon (polyamide)-based polymers as well as PVDF-based polymer systems also exhibit ferroelectric properties.²⁰ Focusing on the influence of hydrogen bonds to ferroelectric nature, Y. Tokura and coworkers developed the ferroelectrics based on supramolecular complex and have investigated the issues systematically.²¹

1.2.3. Classification of ferroelectrics

Ferroelectric materials are roughly classified into “displacement-type” and “order–disorder-type” depending on the difference in generation mechanism of spontaneous polarization. The well-known inorganic ferroelectric ceramics such as BaTiO_3 and PZT is typical “displacement-type” materials. In contrast, “Rochelle salt”, the oldest ferroelectrics, belongs to “order-disorder type” materials.^{5, 22}

1.2.3.1. Conventional displacement-type ferroelectrics

Most of the inorganic ferroelectric ceramics are belonging to this type. In this system, the symmetry breaking originated from distorted structures by the displacement of heavy metal and non-metallic elements results in the ferroelectric nature. In general, this displacement-type ferroelectrics exhibit the first-order ferroelectric-paraelectric phase transition behavior. Therefore, relative permittivity, electrosensitivity and spontaneous polarization are discontinuously changed on the Curie temperature. Most of ferroelectric ceramics have perovskite or similar structures in their crystalline states. The displacement behavior in the ferroelectric crystalline phase has anisotropy. The direction of spontaneous polarization is parallel to the displacement axis corresponding to crystal structures of the ferroelectric phase. Considering the crystal structure of the ferroelectric phase, the required crystal systems for exhibiting the ferroelectricity is allowed to generate the spontaneous polarization and to be stable states.

Typical ferroelectric perovskites are BaTiO₃, PbTiO₃, KNbO₃ and BiFeO₃. The representative ferroelectric parameters for these ferroelectrics are summarized in Table 1-1.

Table 1-1 Ferroelectric parameters for typical ferroelectric ternary transition metal oxides.^{5, 23}

| Compounds | $T_c / ^\circ\text{C}$ | $P_s / \mu\text{C cm}^{-2} (T / ^\circ\text{C})$ |
|---------------------|------------------------|--|
| BaTiO ₃ | 135 | 26 (23) |
| PbTiO ₃ | 490 | >50 (23) |
| NaNbO ₃ | -200 | 12 (-200) |
| KNbO ₃ | 435 | 30 (250) |
| BiFeO ₃ | 850 | 6 (—) |
| KIO ₃ | 212 | 3 (-100) |
| CsGeCl ₃ | 155 | 15 (25) |

Perovskite-type compounds are ternary transition metal oxides represented by the general chemical formula AMO₃ composed of the central transition metal species M, the dissimilar metal species A and oxygen atoms. The typical crystal structure is as shown in figure 1-13.

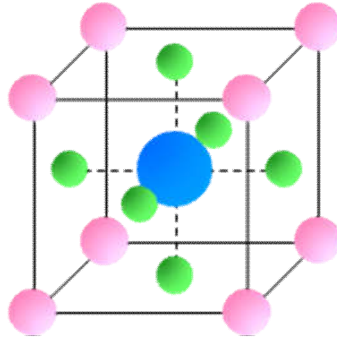


Figure 1-13 A schematic illustration of typical crystal structure for perovskite-type metal oxides.

After the discovery of ferroelectricity in BaTiO_3 , analogous multi-element transition metal oxides extensively were developed and investigated their polarization behaviors. The deep studies revealed that not all of the perovskite-type metal oxides exhibit ferroelectricity. Furthermore, paraelectric perovskites such as KTaO_3 and SrTiO_3 or antiferroelectric perovskites such as PbZrO_3 are found through those investigations. Since the design of ferroelectric perovskites is not limited only to the ternary system, multicomponent ferroelectrics can be also designed and synthesized in which A or M sites are partially substituted by different metal species. Up to now, a lot of partially-substituted ferroelectrics comprised of various metal elements with different compositions have been developed. PZT is the most typical this type of materials. Their ferroelectric parameters depend on the Zr substitution ratio of Ti sites. Typical ferroelectric parameters for partially-substituted ferroelectrics are summarized in Table 1-2.

Table 1-2 Ferroelectric parameters for partially-substituted perovskite-type ferroelectrics.^{5, 23, 24}

| Compounds | $T_c / ^\circ\text{C}$ | $P_s / \mu\text{C cm}^{-2} (T / ^\circ\text{C})$ |
|---|------------------------|--|
| $(\text{K}_{0.5}\text{Bi}_{0.5})\text{TiO}_3$ | 270 | — |
| $(\text{Na}_{0.5}\text{Bi}_{0.5})\text{TiO}_3$ | 200 | 8 (116) |
| $\text{Pb}(\text{Sc}_{0.5}\text{Nb}_{0.5})\text{O}_3$ | 90 | 4 (18) |
| $\text{Pb}(\text{Zn}_{0.33}\text{Nb}_{0.67})\text{O}_3$ | 140 | 24 (25) |
| $\text{Pb}(\text{Cd}_{0.33}\text{Nb}_{0.67})\text{O}_3$ | 270 | 0.65 (25) |
| $\text{Pb}(\text{Zr}_{0.52}\text{Ti}_{0.48})\text{O}_3$ | 386 | ~30 (r.t.) |
| $\text{Pb}(\text{Zr}_{0.25}\text{Ti}_{0.75})\text{O}_3$ | ~450 | >3 (—) |

Some ternary transition metal oxides with similar structures to perovskite such as LiNbO_3 and LiTaO_3 also exhibit ferroelectricity. Their physical properties are listed up in Table 1-3.

Table 1-3 Ferroelectric parameters for metal oxides with similar structures to perovskite.^{5, 23}

| Compounds | $T_c / ^\circ\text{C}$ | $P_s / \mu\text{C cm}^{-2} (T / ^\circ\text{C})$ |
|--------------------|------------------------|--|
| LiNbO ₃ | 1210 | 71 (23) |
| LiTaO ₃ | 665 | 50 (—) |
| YbMnO ₃ | ~720 | ~6 (—) |
| YMnO ₃ | ~640 | ~6 (—) |

The exhibition of ferroelectricity depends on a stability of the polarized structure. The polar vector (the vector of spontaneous polarization) is discussed from the symmetry of the crystal structure. Ferroelectric phenomenon is one of the results from symmetry breaking. In the case of cubic crystal structures where every lattice constants are equivalent, ferroelectricity can not developed. In the other six crystal structure systems except for cubic structures out of the seven crystal systems, some structures permit the existence of polarization vector. Considering the crystal point group, the polar vector can be allowed in ten point groups among all thirty-two point groups. These ten structures are regarded as polar point groups. The characteristics of polar crystal structures are summarized in Table 1-4.

Table 1-4 Classification of polar crystal systems.^{5b}

| Crystal systems | Crystal classes | Point group | Polar vector component |
|-----------------|---|----------------|------------------------|
| Tetragonal | Ditetragonal pyramidal | C_{4v} (4mm) | (0, 0, z) |
| Tetragonal | Tetragonal pyramidal | C_4 (4) | (0, 0, z) |
| Hexagonal | Dihexagonal pyramidal | C_{6v} (6mm) | (0, 0, z) |
| Hexagonal | Hexagonal pyramidal | C_6 (6) | (0, 0, z) |
| Trigonal | Ditrigonal pyramidal rhombohedral hemimorphic | C_{3v} (3m) | (0, 0, z) |
| Trigonal | Pyramidal rhombohedral tetragonal | C_3 (3) | (0, 0, z) |
| Orthorhombic | Pyramidal | C_{2v} (mm2) | (0, 0, z) |
| Monoclinic | Domatic | C_s (m) | (x, 0, z) |
| Monoclinic | Sphenoidal | C_2 (2) | (0, y, 0) |
| Triclinic | Pinacoidal | C_1 (1) | (x, y, z) |

In some ferroelectrics, sequential ferroelectric-ferroelectric phase transitions are observed. The most typical ferroelectric perovskite BaTiO₃ exhibits three phase transitions which come from

paraelectric cubic – ferroelectric tetragonal, ferroelectric tetragonal – ferroelectric orthorhombic and ferroelectric orthorhombic – ferroelectric trigonal transitions. All these transitions are first-order type. All these ferroelectric crystal structure and direction of spontaneous polarization are shown in Figure 1-14.

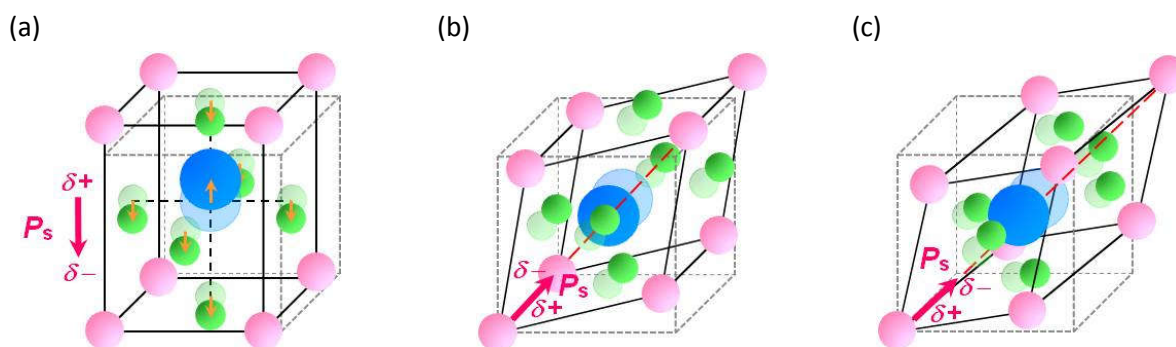


Figure 1-14 Schematic illustrations of crystal structures and polarization direction for BaTiO₃ in (a) ferroelectric tetragonal, (b) ferroelectric orthorhombic, and (c) ferroelectric trigonal phases.

1.2.3.2. Conventional order-disorder-type ferroelectrics

Most of organic ferroelectrics and ferroelectric salts are included to the “order-disorder-type” ferroelectrics. In this type of ferroelectrics, uniaxial arrangement of dipole moments instead of displacement generates spontaneous polarization. The order-disorder-type ferroelectrics generally exhibit the second-order ferroelectric-paraelectric phase transition behavior.** Thus, relative permittivity, electrosensitivity and spontaneous polarization are continuously changed on the Curie temperature.

The typical order-disorder-type ferroelectrics are alkali metal nitrites. The Curie temperature and spontaneous polarization for ferroelectric metal nitrites are summarized in Table 1-5.

Table 1-5 Ferroelectric parameters for alkali metal nitrites.^{5, 23}

| Compounds | $T_c / ^\circ\text{C}$ | $P_s / \mu\text{C cm}^{-2} (T / ^\circ\text{C})$ |
|-------------------------------------|------------------------|--|
| NaNO ₂ | 163 | 8 (100) |
| KNO ₂ | 47 | 2.8 (25) |
| AgNa(NO ₂) ₂ | 38 | 1.5 (37) |

Typical crystal structures of order-disorder-type ferroelectric salts in ordered (ferroelectric) phase and disordered phase are shown in Figure 1-15.

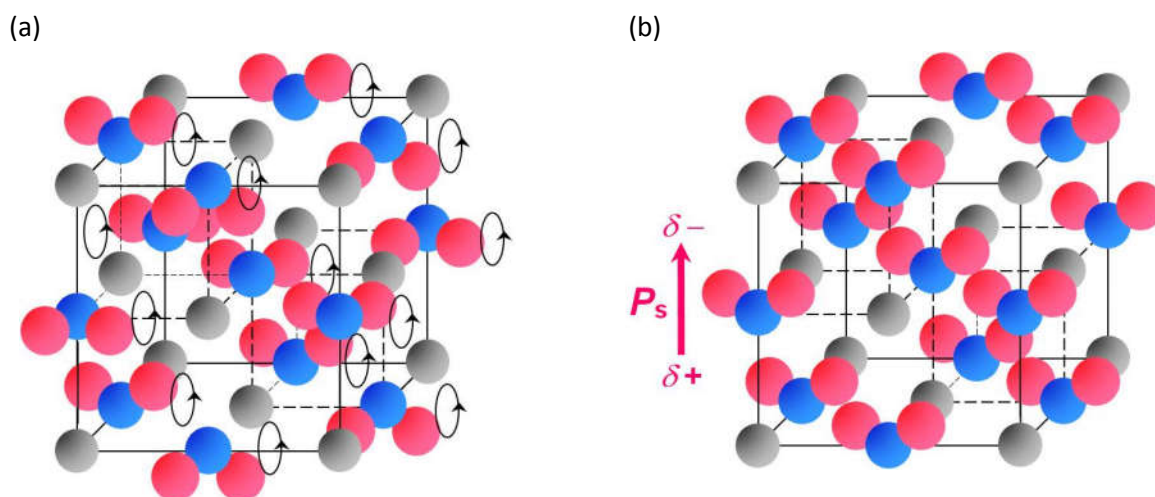


Figure 1-15 Schematic illustrations of crystal structures and polarization direction for order-disorder-type ferroelectric salts in (a) disordered phase, and (b) ferroelectric ordered phase.

“Rochelle salt” and related tartrate salts are also representative “order-disorder-type” ferroelectrics. The physical properties are summarized in Table 1-6.

Table 1-6 Ferroelectric parameters for tartrate salts.^{5, 23}

| Compounds | $T_c / ^\circ\text{C}$ | $P_s / \mu\text{C cm}^{-2} (T / ^\circ\text{C})$ |
|--|------------------------|--|
| Rochelle salt ($\text{NaOCOCH(OH)CH(OH)COOK} \cdot 4\text{H}_2\text{O}$) | -18, 24 | 0.25 (5) |
| $\text{NaOCOCH(OH)CH(OH)COONH}_4 \cdot 4\text{H}_2\text{O}$ | -164 | 0.21 (-181) |
| $\text{LiOCOCH(OH)CH(OH)COONH}_4 \cdot \text{H}_2\text{O}$ | -167 | 0.22 (-178) |
| $\text{LiOCOCH(OH)CH(OH)COOTI} \cdot \text{H}_2\text{O}$ | -263 | 0.14 (-272) |

“Rochelle salt” has specifically two phase transition points (T_c). In the temperature range from -18 °C to 24 °C, “Rochelle salt” forms ferroelectric monoclinic sphenoidal C_2 (2) crystal structures. The high-temperature disordered crystalline phase is piezoelectric orthorhombic D_2 (222) phase. The orthorhombic crystal melts at 70-80 °C. The crystalline phase below -18 °C is considered as re-entrant orthorhombic phase. The orientation of hydroxyl groups could be essential to the ferroelectric nature. From the comparison of the ferroelectricities with deuterated substituted salts, it is conceivable that hydrogen bonding contributes to the ferroelectric nature.

Some glycine derivatives belong to order-disorder-type ferroelectrics. The physical properties are summarized in Table 1-7.

Table 1-7 Ferroelectric parameters for glycine derivatives.^{5, 23}

| Compounds | Chemical Formula | $T_c / ^\circ\text{C}$ | $P_s / \mu\text{C cm}^{-2} (T / ^\circ\text{C})$ |
|--------------------------|--|------------------------|--|
| Triglycine sulphate | $(\text{NH}_2\text{CH}_2\text{COOH})_3 \cdot \text{H}_2\text{SO}_4$ | 49 | 2.8 (20) |
| Triglycine selenate | $(\text{NH}_2\text{CH}_2\text{COOH})_3 \cdot \text{H}_2\text{SeO}_4$ | 22 | 3.2 (10) |
| Triglycine fluoberyllate | $(\text{NH}_2\text{CH}_2\text{COOH})_3 \cdot \text{H}_2\text{BeF}_4$ | 75 | 3.2 (20) |
| Diglycine nitrate | $(\text{NH}_2\text{CH}_2\text{COOH})_2 \cdot \text{HNO}_3$ | -67 | 1.5 (-190) |
| Glycine silver nitrate | $\text{NH}_2\text{CH}_2\text{COOH} \cdot \text{AgNO}_3$ | -55 | 0.6 (-170) |

Glycine is the simplest amino acid which composing the polypeptide in the living body. Glycine and its derivative can form the hydrogen bonding network in the self-assembled structure. The orientation of polar groups is effective to appearance of ferroelectricity. Hydrogen bonding network can also affect to the ferroelectric properties.

Dihydrogenphosphate and dihydrogenarsenate salts also have the formability of hydrogen bond. The representative ferroelectric dihydrogenphosphate and dihydrogenarsenate salts are listed up in Table 1-8. The transition temperature and spontaneous polarization are also described in the same table.

Table 1-8 Ferroelectric parameters for dihydrogenphosphate and dihydrogenarsenate salts.^{5, 23}

| Compounds | $T_c / ^\circ\text{C}$ | $P_s / \mu\text{C cm}^{-2} (T / ^\circ\text{C})$ |
|---------------------------|------------------------|--|
| KH_2PO_4 | -150 | 4.75 (-177) |
| RbH_2PO_4 | -126 | 5.6 (-183) |
| KH_2AsO_4 | -176 | 5.0 (-195) |

The deuterated substitution of salts affects to their ferroelectricity by the change of hydrogen bonding environment. The transition temperature and spontaneous polarization of ferroelectric deuterated salts are displayed in the Table 1-9. These experimental facts indicate that the hydrogen bonding network affects to the ferroelectric nature. In particular, the phase transition temperature rise about 100 K by deuterium substitution in KH_2PO_4 system of which three-dimensional hydrogen bonding network is formed in the crystalline state. Regarding the mechanism of ferroelectricity development in this system, some models (Slater model,²⁵ proton tunneling model,²⁶ over-damped phonon model,²⁷ coupled proton-optic-mode model,²⁸ two coupled oscillators model,²⁹ PO_4 order-disorder model,³⁰ coupled proton-internal vibration model,³¹ asymmetric potential model,³² proton-polaron model³³ etc.) have been proposed. However, all models have some drawbacks in

inconsistency to experimental facts, such as explanation by proton tunneling model in which KH_2PO_4 system is treated as displacement-type ferroelectrics. Therefore, the clarification of the mechanism remains still big issues.

It is noteworthy that more pronounced isotope effect called "deuterium displacement induced phase transition" has been found in O-H-O hydrogen bonds (zero-dimensional hydrogen bonding) system, which is isolated from creating hydrogen bonding network.³⁴

Table 1-9 Ferroelectric parameters for deuterated salts.^{5, 23}

| Compounds | $T_c / ^\circ\text{C}$ | $P_s / \mu\text{C cm}^{-2} (T / ^\circ\text{C})$ |
|--|------------------------|--|
| $\text{NaOCOCD(OD)CD(OD)COOK} \cdot 4\text{D}_2\text{O}$ | -22, 35 | 0.35 (6) |
| $(\text{ND}_2\text{CD}_2\text{COOD})_3 \cdot \text{D}_2\text{SO}_4$ | 60 | 3.2 (-60) |
| $(\text{ND}_2\text{CD}_2\text{COOD})_3 \cdot \text{D}_2\text{BeF}_4$ | 77 | — |
| KD_2PO_4 | -60 | 4.83 (-93) |

1.2.4. Ferroelectric self-assemblies

Ferroelectric property in polymer system was found in 1980 for the first time.¹⁹ The ferroelectricity in PVDF and P(VDF-TrFE) is generated from electric-field-responsive molecular dipoles originated from fluoro groups.³⁵ The ferroelectric behaviour are also found in Nylon system. In the Nylon system, the orientation of amide groups is a key to the ferroelectricity.³⁶ All these ferroelectric polymers are classified into order-disorder-type ferroelectrics.³⁷

FLC materials also are one kind of ferroelectric self-assemblies. The detailed explanation is described in later section.

The background study on supramolecular ferroelectrics were carried out by scientific interests on ferroelectric salts forming the hydrogen bonding network.³⁸ The ferroelectricity originated from positional shift (displacement) of hydrogen atoms was found in the crystal of 1,4-diazabicyclo[2,2,2]octane perchlorate (dabco- HClO_4) and 1,4-diazabicyclo[2,2,2]octane perrhenate (dabco- HReO_4) salts (Figure 1-16). In these dabco salts, one-dimensional intermolecular hydrogen bonds between the same species (dabco units) are essential to the exhibitance of ferroelectricity.^{38b, c} In these ferroelectric dabco salts, one-dimensional intermolecular hydrogen bonds between the same species (dabco units) are essential to the ferroelectric nature.

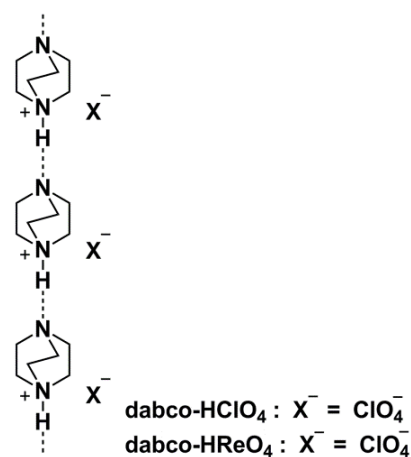


Figure 1-16 One-dimensional hydrogen bonding network in ferroelectric dabco salts.

From the viewpoint of components for forming intermolecular networks, two types of hydrogen bonds can be considered. One is homo-type intermolecular network, in which hydrogen bonds are formed between the same chemical species. The other is hetero-type intermolecular network, in which hydrogen bonds are formed between different species. The ferroelectric hydrogen-bonded complex salts are based on the later hetero-type intermolecular hydrogen bond networks. S. Horiuchi and coworkers have developed ferroelectric supramolecular two-component crystals based on chloranilic acid and phenazine in 2005.³⁹ Also, the analogous ferroelectric co-crystal systems are developed by using bromanilic acid, iodanilic acid, and fluoranilic acid as acidic components with phenazine or 5, 5'-dimethyl-2, 2'-bipyridine as basic components.⁴⁰ The ferroelectric nature originating from dynamic shuttling of protons is found in the co-crystal of 2,3,5,6-tetra(2-pyridinyl)pyrazine with chloranilic acid and related acids.⁴¹

The single component supramolecular ferroelectric system based on proton transfer was first developed in 2010. The supramolecular assemblies of cloconic acid exhibited large spontaneous polarization due to the proton transfer by the enol-ketone tautomerism.⁴² The ferroelectric behaviors originating from tautomerism inspire the recent ferroelectric investigations.

External-stimulus-induced ferroelectric nature in charge-transfer (CT) complexes has been investigated since the 1980's.⁴³ Many studies on ferroelectric neutral-ionic phase transition in CT complexes were carried out.^{38a, 44} However, the leakage current and the difficulty of preparing high quality large-scaled single crystals prevented the obtaining of a ferroelectric hysteresis loop as clear evidence.⁴⁵ The ferroelectric hysteresis loops of CT complexes were obtained for the first time by the study on tetrathiafulvalene (TTF)-(*p*-bromanil) complex in 2010 (Figure 1-17).⁴⁶ For the related complexes TTF-(*p*-chloranil) and TTF-(2-bromo-3,5,6-trichloro-*p*-benzoquinone), clear ferroelectric hysteresis loops were also obtained.⁴⁷ Some ferroelectric CT complexes such as TTF-pyromellitic diimine derivative (PMI) and 1,6-diaminopyrene (DAP)-PMI were recently developed as inspired by these successful achievements (Figure 1-18).⁴⁸

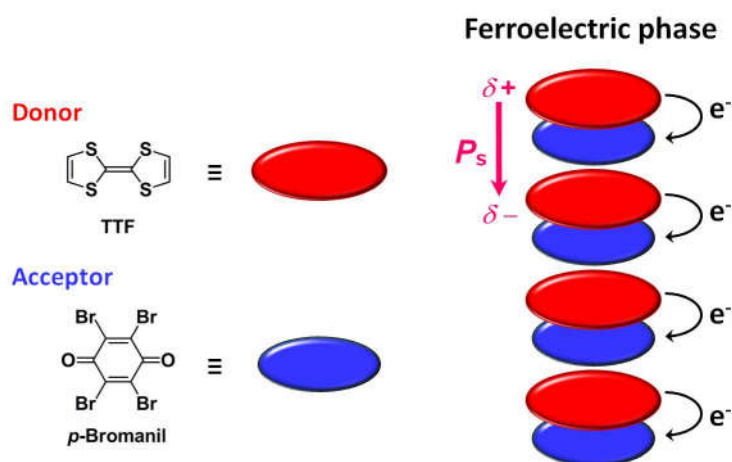


Figure 1-17 Schematic illustrations of self-assembled structure and polarization direction for CT complex TTF-(*p*-bromanil) in the ferroelectric phase.

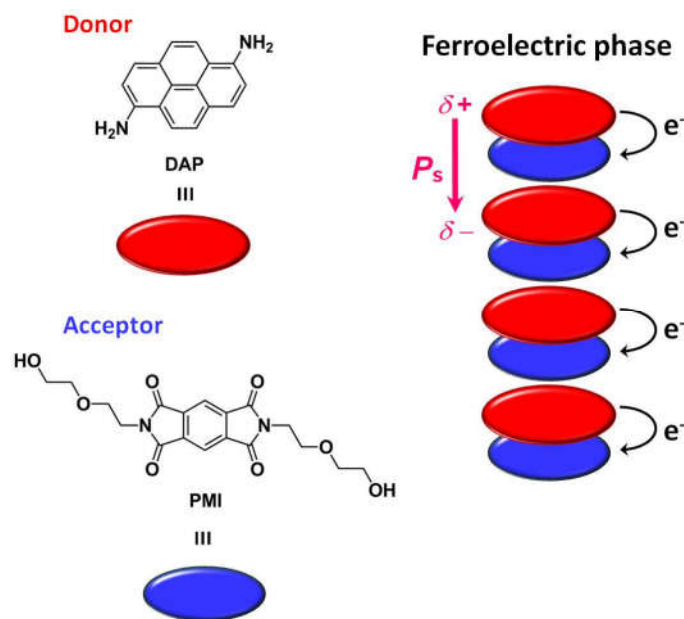


Figure 1-18 Schematic illustrations of self-assembled structure and polarization direction for CT complex DAP-PMI in the ferroelectric phase.

Furthermore, ferroelectric supramolecular systems (metal-organic framework and physical xero-gel etc.), which concerted plural intermolecular interactions such as hydrogen bond, CT interaction and coordination interaction are developed.^{49, 50}

1.3. Liquid crystals⁵¹

1.3.1. Basic concept of liquid crystals⁵²

The term of “Liquid crystal” indicates “a material which forms dynamic ordered structures”. This English term has been widely used as a translation of German word “Flüssige Krystalle” which had named in the early stage of liquid crystal study.⁵³ Liquid-crystalline (LC) phase is a mesophase which lies between crystalline and liquid phases. LC systems generally have molecular orientation order in the mesophase. It should be noted that the molecular aggregation system which has only positional order and not orientation order is “plastic crystal” system. In the most of LC phases, the anisotropic environment is generated due to the LC structures comprised of molecules with a large aspect ratio. The anisotropic LC molecular structures are reflected to the optical, magnetic and electric anisotropies.

The LC properties are generally characterized with using polarizing optical microscopy (POM), powder X-ray diffraction measurement (XRD) and differential scanning calorimetry (DSC).

POM observation is usually carried out under the crossed nicols. The plane of polarization rotates by birefringence, when the polarized light passes through the liquid crystal medium. Since the polarized component of transmitted light which is parallel to the analyzer can pass it, the optical

patterns reflecting the LC molecular ordered structure with some defects can be observed. The optical patterns provide some significant information for the assignment of LC phase.

In XRD, diffraction patterns corresponding to the periodicity of the electron density distribution is obtained. Layer, cubic or cylindrical LC structures give some diffraction peaks corresponding the lattice constants in the LC phases. Since dynamic LC ordered structures is more disordered than crystalline structures, the diffraction peaks in the LC phase are usually weakened and broadened.

DSC thermograms provide the thermodynamic parameters such as transition temperature, transition enthalpies and enthalpies. For the LC compounds, plural phase transition peaks are usually observed on the plots.

1.3.1. History of liquid crystals⁵²

Thermotropic LC phase was first discovered by F. Reinitzer who was an Austrian botanist through the study on phase transition behaviors of benzoate derivatives in 1888.⁵⁴ He observed strange melting behaviors in cholesteryl benzoate on heating process. The stepwise melting behaviors of the cholesterol derivative suggested the appearance of a mesophase between crystalline (solid) and isotropic liquid phases. The crystalline solid of cholesteryl benzoate changed around 145 °C to the cloudy fluids, which is liquid-crystalline state, and then transitioned to the clear molten state around 180 °C.⁵³⁻⁵⁵ F. Reinitzer got interested in the unique cloudy fluids state, and he asked O. Lehman who was a German physicist to scrutinize the properties of the mysterious fluids. O. Lehman clarified by polarizing optical microscopy that the strange fluids show birefringence (optical anisotropy) and named the fluids (fluidy state) as "Flüssige Krystalle" in German.⁵³ As described above, the recorded history of the "thermotropic liquid crystals" began with fundamental research by two scientists in 19th century.

The brief history of liquid crystals is summarized below.

1854: Discovery of myelin sheath based on lyotropic LC system⁵⁶

1888: Discovery of anomalous phase transition behavior in cholesteryl benzoate⁵⁴

1904: Publication of "Flüssige Krystalle"⁵³

1911: Publication on optical characteristics of twisted nematic arrangement for LC compounds⁵⁷

1927: The study on the influence of electric and magnetic fields on LC structures⁵⁸

1949: Suggestion of Onsager's hard-rod model⁵⁹

1959: Establishment of Maier-Saupe theory of liquid crystals⁶⁰

1963: Development of regular domain patterns in nematic liquid crystals under the application of electric field⁶¹

1965: Development of LC polyamide Kevlar® by DuPont Co., Ltd.⁶²

1968: Development of the first LC display by RCA Laboratory⁶³

- 1968: Discovery of guest-host effect with dichroic dye⁶⁴
- 1971: Establishment of drive principles based on "twisted nematic mode" for liquid crystal displays (LCDs)⁶⁵
- 1973: Synthesis of 4-pentyl-4'-cyanobiphenyl (5CB) for the application of displays⁶⁶
- 1973: Placing on the market of portable calculator equipped with LCD based on dynamic scattering mode
- 1975: Discovery of ferroelectric liquid crystals¹⁸
- 1977: Discovery of discotic liquid crystals⁶⁷
- 1986: Commercialization of color liquid crystal televisions based on TFT-LCD by Matsushita Electric Industrial Co., Ltd.
- 1994: Commercialization of FLC display by Canon Co., Ltd.

1.3.2. Classification of LC phases^{51, 68}

Liquid crystals are roughly classified into two types by the factor which induces dynamic properties. One is a temperature transition type as "thermotropic liquid crystal system", and the other is a concentration transition type as "lyotropic liquid crystal system". In the thermotropic LC system, the thermal fluctuation of molecules, which disturbs the crystalline packing and weakens the intermolecular interaction, induces the LC phase. Molecular arrangement and molecular orientation (degrees of structural order) depend on the degree of contribution of thermal fluctuation. As the result, various liquid crystal structures are formed. In the lyotropic LC system, the solvation behavior as alternative of thermal fluctuation inhibits the crystalline packing and weakens the intermolecular interaction for appearance of mesomorphism.

1.3.2.1. Lyotropic LC system^{68a, 69}

Lyotropic LC system is usually composed of amphiphilic molecules such as "soap" with solvents. In the lyotropic LC system, LC molecules exhibit mesophase in a certain concentration range. In general, a solution of lyotropic LC molecules shows isotropic phase in low concentration range below the critical concentration. In high concentration region exceeding the critical concentration, the biphasic state (the coexistence of optically anisotropic and isotropic phases) is appeared. In further higher concentration region, the entire system shows a single liquid crystal phase. In this type of liquid crystal, the solvation environment strongly depends on the concentration. Here, typical lyotropic binary mixture system with amphiphilic molecule and water will be described as an example. Under the condition that the amphiphile concentration exceeds the critical micelle concentration, micelles are formed through the self-organization of each hydrophobic moiety by the hydrophobic interaction. The micelle concentration increases along the increase of the solute concentration. As the micelle concentration increases, each micelle rearranges the aggregation structure and forms lyotropic LC

structure with solvent molecules. The lyotropic self-assembled LC structures are strongly affected by the free volume ratio between hydrophilic part, hydrophobic part and solvating solvent molecules. In the case where there is no big difference in the three-dimensional spreads of free space between non-polar and polar parts, lyotropic LC molecules exhibits lamella (L_α) phase with a layer structure (Figure 1-19a). When the difference between each three-dimensional spreads of free space is gradually increased, lyotropic LC structures change to normal bicontinuous cubic (V_1), reversed bicontinuous cubic (V_2), normal hexagonal (H_1), reversed hexagonal (H_2), normal cubic (I_1) and reversed cubic (I_2) structures. In V_1 and V_2 phases, the slight difference of free volumes between hydrophilic and hydrophobic parts induces the curvature into the layer ordering and forms the bicontinuous cubic structures with double gyroid interface (Figure 1-19b, c). In the case of increasing difference of free volumes of two parts, closely packed hexagonal cylinder structures are formed and assembled into the the H_1 and H_2 phases (Figure 1-19d, e). When there is an extreme bias in their free volumes, I_1 or I_2 phases are induced. In I_1 and I_2 phases, small aggregates of LC molecules have cubic lattice arrangement (Figure 1-19f, g). The lyotropic LC structures are similar to those of thermotropic LC system.

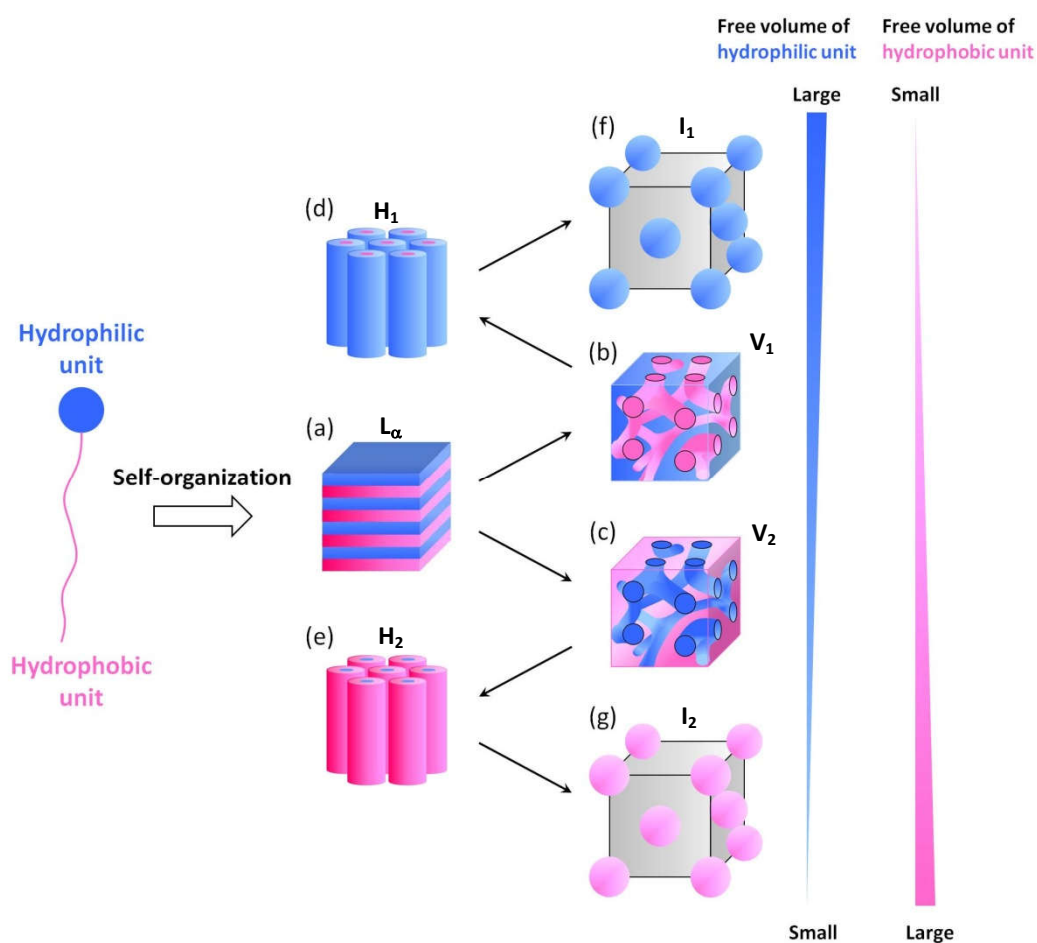


Figure 1-19. Schematic illustrations of self-assembled structures in lyotropic LC system.

In some cases, molecules bearing a rigid central aromatic core working as dye unit (chromophore) or biofunctional unit with flexible side chains can form LC ordered structure with assistance of solvent molecules. Such LC system is called "chromonic liquid crystal".^{51a, 70} In chromonic systems, the aggregation of core unit induces the formation of mesophases.⁷¹ The typical chromonic LC materials are as shown in Figure 1-20.⁷²

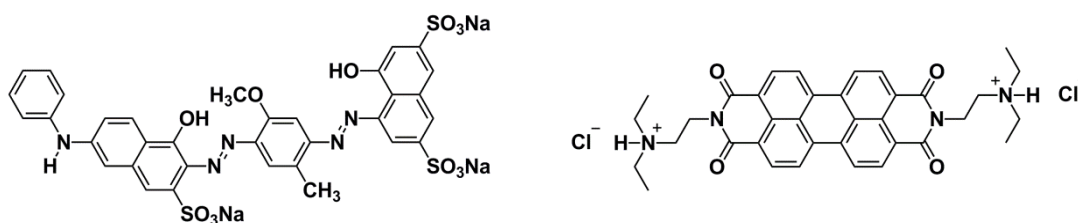


Figure 1-20. Chemical structures of representative chromonic LC compounds.⁷²

As can be easily assumed from the fact that the first discovery of lyotropic LC structures was in myelin sheath,⁵⁶ the lyotropic LC system can be found in living body system. Lipid bilayer membranes (cell membranes), polypeptides, nerve tissues and bacteriophages are biomaterials based on the lyotropic LC system. These hierarchical LC self-assembled structures play important roles in the biological functions.⁷³

1.3.2.2. Thermotropic LC system⁵¹

Unlike lyotropic systems, thermotropic LC systems are possible to exhibit mesophases without the support of solvents. In general, thermotropic LC molecules have flexible chains and a rigid core. Rigid cores are usually comprised of aromatic moieties and determine the optical and electronic property of the LC self-assemblies. In contrast, flexible units are associated with the softness and flexibility of the assemblies. The self-assembled structure in the LC phase reflects molecular shapes and structures of thermotropic LC compounds. The free volumes of flexible side chains have strong dependence on temperature. The balance of free volumes between rigid core and flexible unit is very important for exhibiting the thermotropic LC properties.

A) Calamitic liquid crystal system

From the viewpoint of conventional liquid crystal science, molecules with a large aspect ratio of molecular structure tend to exhibit mesomorphic properties. In particular, rod-like molecular structures are typical mesogen skeleton which has been widely studied. "Calamitic" liquid crystal is the self-assembled system comprised of rod-like molecules.

Nematic phase

Nematic (N) phase is the simplest and most fluidic state in calamitic LC system. LC molecules in N phase do not have a three-dimensional positional order, but only orientational order (Figure 1-21).

In the N phase composed of rod-like molecules with large aspect ratio, characteristic phenomena are generated. The N LC materials exhibit optical, electrical and magnetic anisotropy due to the anisotropic electron density distribution formed on rod-like molecules. The N phase can be regarded as a low viscous LC phase, because the attraction terms of intermolecular interactions in N phase are generally smaller than those in other LC phases. As the offset behavior of the external field due to the polarization produced by permanent or induced dipoles, therefore, LC molecules in N phase respond to the electric field and the molecular reorientation behavior are induced. This field-induced reorientation behavior in the N LC system is utilized for the conventional drive principle of liquid crystal display, which is the most typical and successful application of liquid-crystalline system. In addition, the N LC material is the most suitable LC system for control of molecular orientation. This is because structural defects other than dislocations (point defect) cannot generate in N phase and monodomain N LC structure can be formed by the uniaxial alignment of LC molecules. In fact, the methods to control molecular orientation in N phase by rubbing technique have been established.⁷⁴ The horizontal and vertical alignment films composed of polymers such as polyvinyl alcohols and polyimides are widely utilized. Furthermore, uniaxially aligned monodomain structure of N LC materials can be formed by a rubbing technique for producing uniaxial grooves on substrates. Up to now, deep investigations on orientation control of LC molecules have been made it possible to control the precise orientation angle of LC molecules. Photo-alignment technique applying the photoisomerization behavior of azobenzene has also been established.⁷⁵

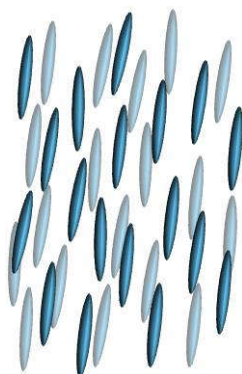


Figure 1-21. A schematic illustration of self-assembled structure in N phase.

Typical N LC molecules are shown in Figure 1-22.^{66, 76}

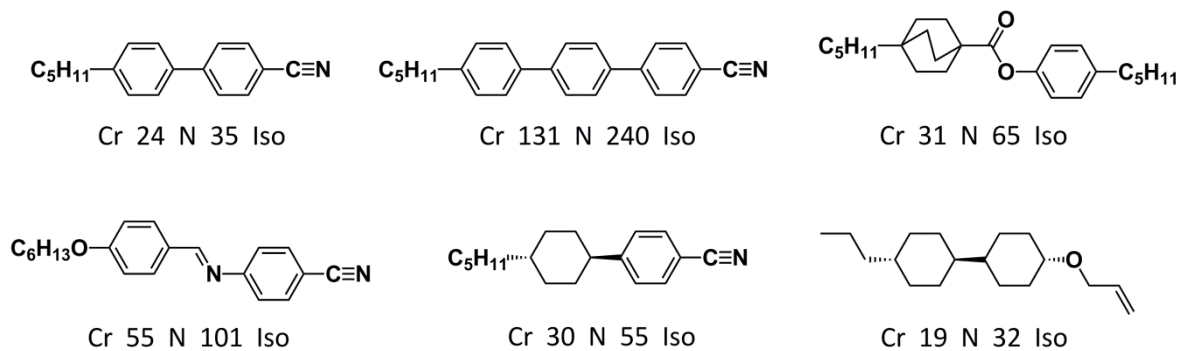


Figure 1-22. Chemical structures of representative N LC compounds.^{66, 76}

As is described former, the structural defects that can exist in the N phase are only dislocations. The feature of the defect formation is reflected to the optical textures under crossed nichol. The typical optical patterns in nematic phase are “Schrielen” textures (Figure 1-23). Although the schrielen textures are also observed in the homeotropic region of a smectic phase, only 4-brush-type can be found for the smectic phase. The coexistence of 2-brush-type and 4-brush-type schrielen patters is strong evidence on the identification of nematic phase.



Figure 1-23. Typical “Schrielen” texture in N LC phase.⁷⁷

Smectic phases

Smectic phases are another type of the calamitic LC phases and have higher structural orders than N phase. Although LC molecules in N phase have only orientation order, LC molecules in smectic phases have positional orders and form the layer structures. Smectic phases are classified more finely according to existence of intralayer positional order and relationship between layer normal and molecular orientation direction. The structural features of each smectic phase are shown in Figure 1-24 below.

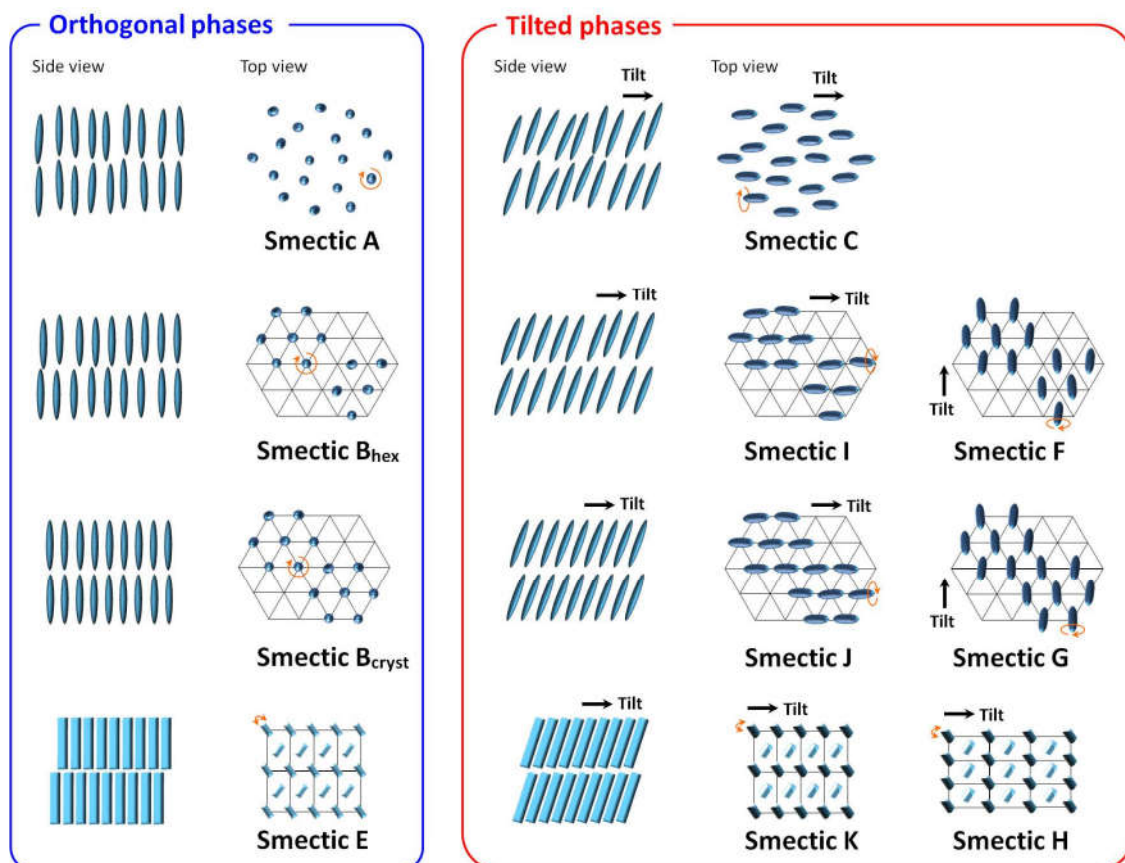


Figure 1-24. Classification of smectic LC phases.

The smectic LC materials also exhibit optical, electrical and magnetic anisotropy originated from the anisotropic electron density distribution of rod-like molecules. Smectic phases are generally regarded as more viscous phase than N phase, because smectic LC molecules are bounded by strong intermolecular interactions than N LC molecules.

Typical smectic LC molecules are shown in Figure 1-25.^{76a, 78}

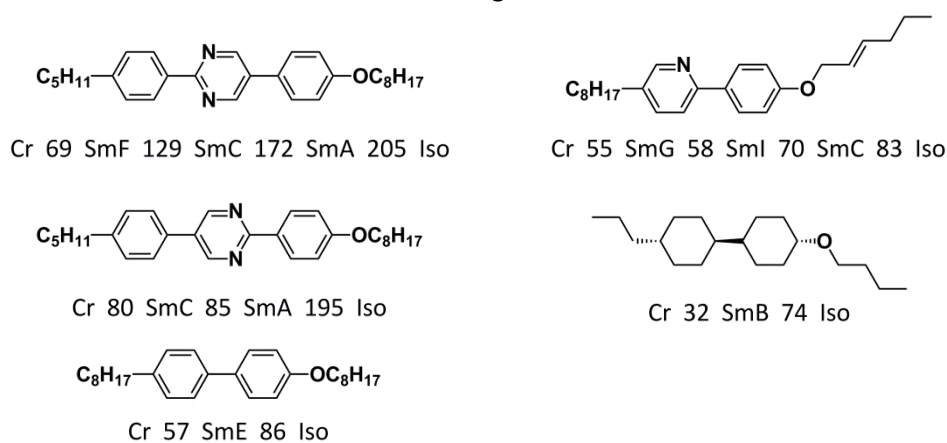


Figure 1-25. Chemical structures of representative smectic LC compounds (SmA: smectic A, SmB: smectic B, SmC: smectic C, SmE: smectic E, SmF: Smectic F).^{76a, 78}

Chiral nematic and chiral smectic phases^{79, 80, 81}

Typical N and smectic phases are achiral calamitic LC system. As the introduction of molecular chirality to calamitic LC molecules brings to the drastically structural change described below, LC system with the chirality is distinguished with the achiral system and considered as independent chiral LC system. Molecular chirality usually induces the formation of helical structures, due to minimization of elastic free energy in the system. The helical structure and helical axis reflect the absolute configuration of the molecules labeled (*R*) or (*S*). The helical nature based on molecular chirality is important for functions such as chiral molecular recognition.⁸² Even when helical structures are not formed, furthermore, molecular chirality breaks the symmetry of a system, which generates the characteristic phenomena such as ferroelectricity.^{18, 81h, 83}

Chiral LC phases can be induced by the introduction of molecular chirality to the LC system. The induction of chiral LC phases is generally achieved by a doping of chiral additives into LC materials. Chiral LC phases also can be found in single component LC molecules with molecular chirality.

When a chiral side chain is introduced to the LC molecule which has a tendency to exhibit N phase, it twists around the axis perpendicular to the molecular long axis (director), resulting in the formation of a helical structure spontaneously (Figure 1-26a). This twisted nematic phase is called as a chiral nematic (N^*) or a cholesteric phase. (The name of cholesteric phase is derived from the fact that this phase was first discovered for cholesteryl esters.) In the N^* phase, specific selective reflection is observed. The characteristic phenomenon is originated from the helical structure of the N^* phase and the helical pitch depends on the temperature of the LC system. Therefore, it has been demonstrated for the application to the thermal sensor.⁸⁴ Moreover, the design of the luminescent LC materials offers circularly polarized light (CPL) emitting devices⁸⁵ and organic lasing media.⁸⁶

In smectic phases, chiral side chains often generate a helical axis along the layer normal. In SmC-type LC phase where the director tilts to the layer normal, the director changes periodically along the layer normal (Figure 1-26b). This tilted Sm phase with chirality is defined as a chiral smectic C (SmC^*) phase. This phase often exhibits ferroelectricity and the application to high speed displays was attempted.⁸⁷

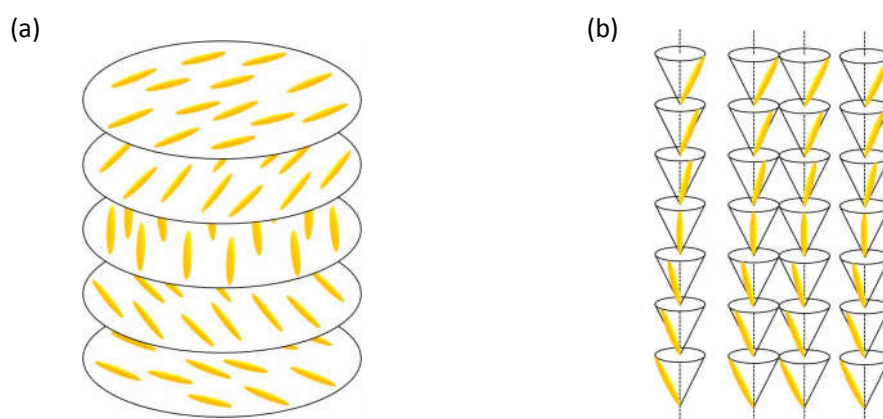


Figure 1-26. Schematic illustrations of the helical structures in (a) N^* and (b) SmC^* phases

Typical chiral LC molecules are shown in Figures 1-27^{53, 54, 88} and 1-28.^{18, 89}

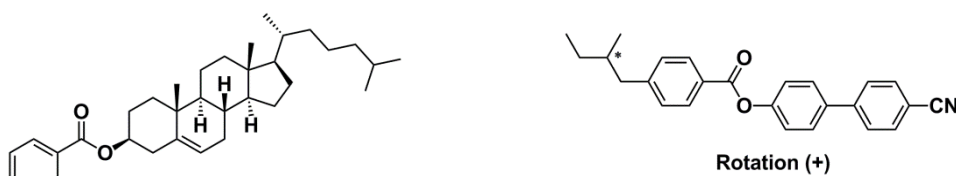


Figure 1-27. Chemical structures of representative N* LC compounds.^{53, 54, 88}

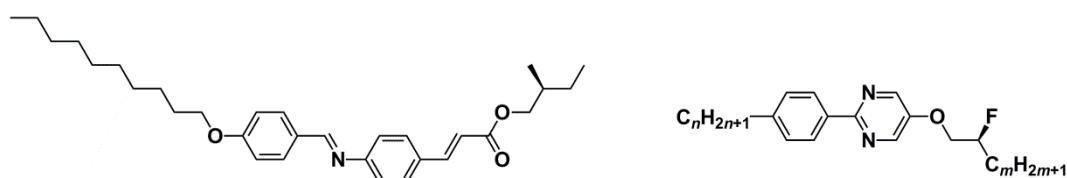


Figure 1-28. Chemical structures of representative chiral smectic LC compounds.^{18, 89}

B) Discotic liquid crystal system

In addition to typical calamitic LC system composed of rod-like molecules, disc-like molecules also are well-known as a mesogenic core. “Discotic” liquid crystal is the self-assembled system comprised of such disk-shaped molecules.⁹⁰

Discotic nematic and columnar nematic phases⁹⁰

Discotic nematic (N_D) phase is the most disordered LC state in discotic LC system. N_D phase corresponds to N phase in the calamitic LC system. LC molecules in N_D phase have only orientation order but no positional order (Figure 1-29a).⁹¹

On the hand, columnar nematic (N_C) phase is slightly more structured LC phase than N_D phase. LC molecules in N_C phase form only small columnar aggregates of which orientational order but not higher positional-order (Figure 1-29b).⁹²

These N_D and N_C LC materials composed of disk-shaped molecules also show optical, electrical and magnetic anisotropic nature. Representative molecules exhibiting these LC phases are shown in Figure 1-30⁹³ and 1-31.⁹⁴

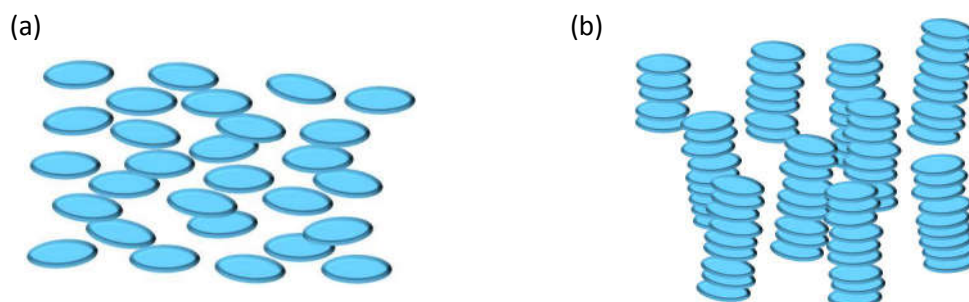
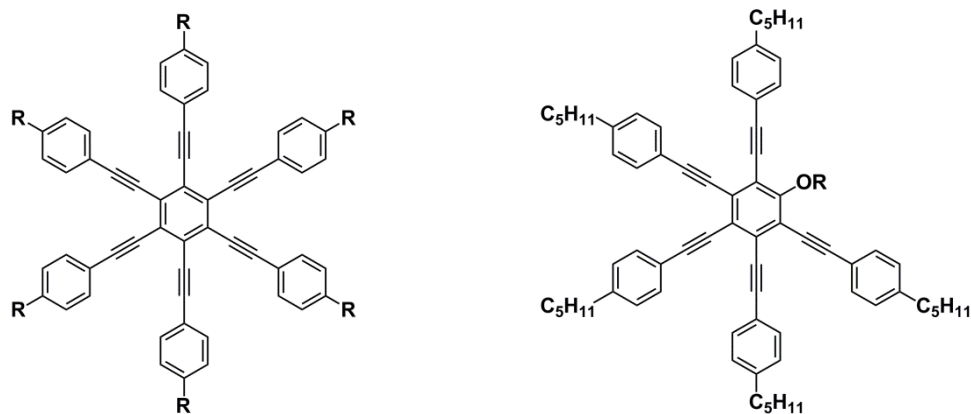


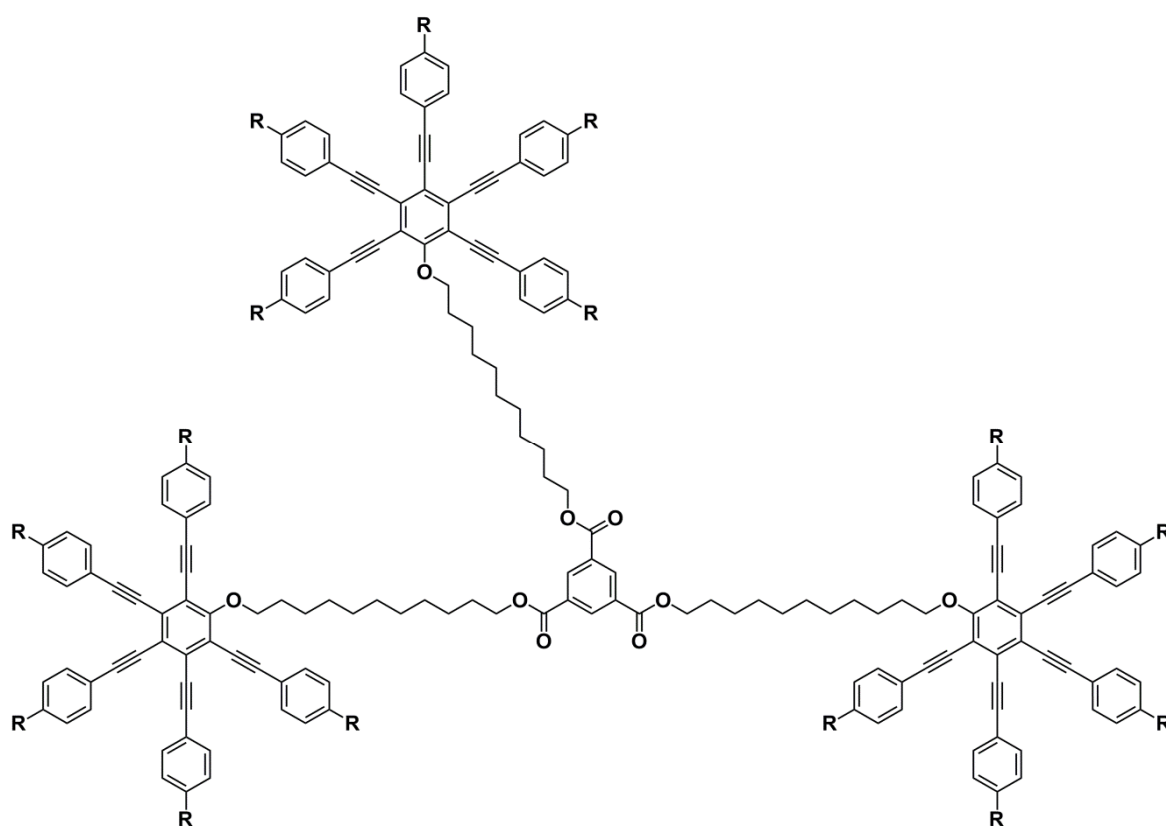
Figure 1-29. Schematic illustrations of the self-assembled structures in (a) N_D and (b) N_C phases.



R = -C₅H₁₁, -C₆H₁₃, -C₇H₁₅, -C₈H₁₇, -C₉H₁₉, -OC₇H₁₅

R = -C₉H₁₉, -(CH₂)₉CH=CH₂

Figure 1-30. Chemical structures of representative N_D LC compounds.⁹³



R = -C₂H₅, -C₃H₇, -C₅H₁₁

Figure 1-31. Chemical structures of representative N_C LC compounds.⁹⁴

Columnar phases⁹⁵

Most of disc-like LC molecules exhibit the columnar (Col) phase. Representative Col LC compounds are shown in Figure 1-32.^{67, 96} Discotic columnar LC molecules have position orders of cylindrical assemblies. The fine classification of columnar phases is essentially based on the position orders (packing styles). The structural features of each columnar phase are shown in Figure 1-33 below.

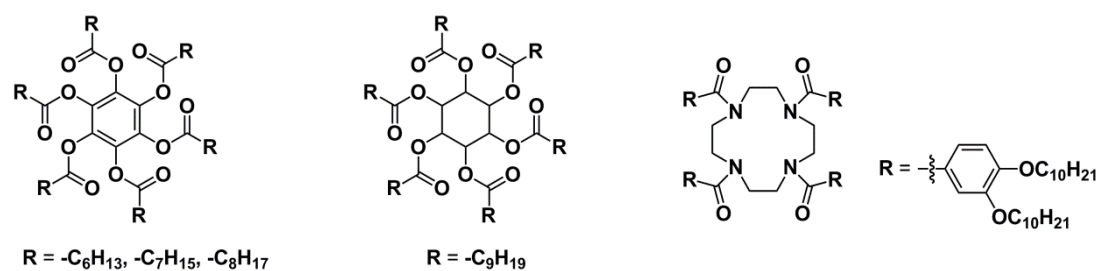


Figure 1-32. Chemical structures of representative Col LC compounds.^{67, 96}

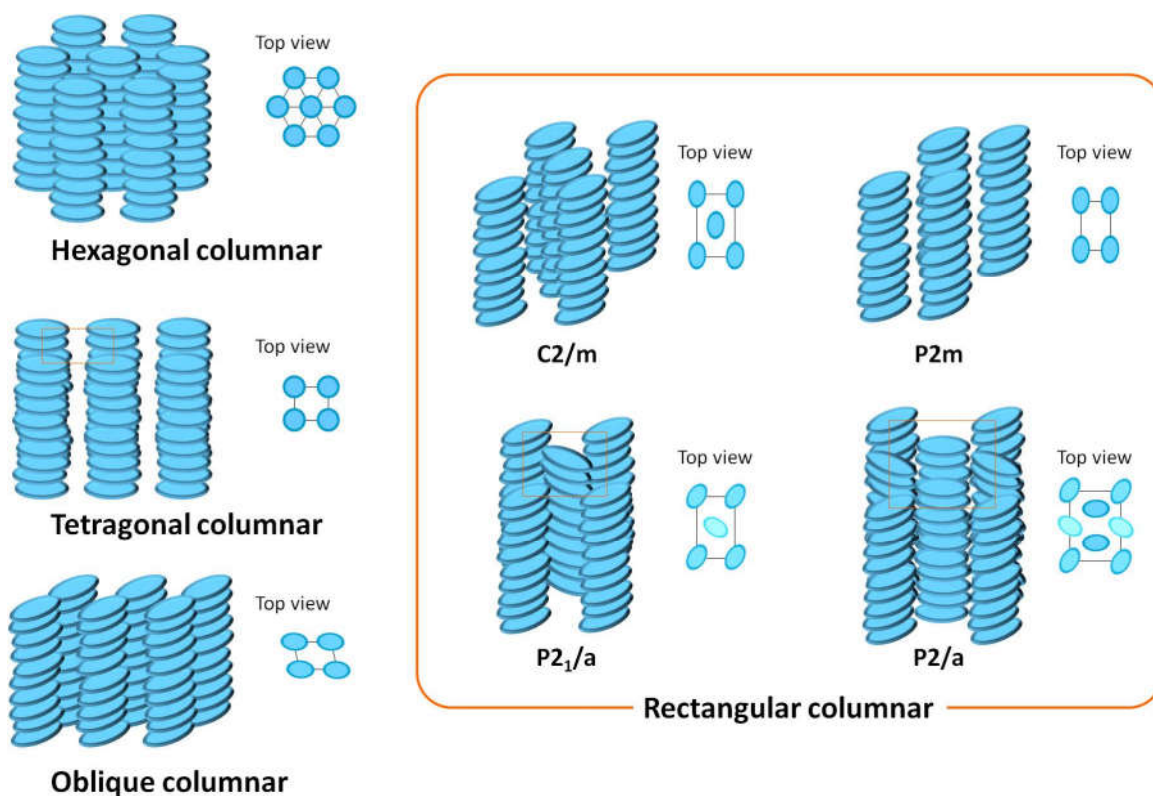


Figure 1-33. Schematic illustrations of self-assembled structures in columnar phases.

C) Other liquid crystal system

*Micellar cubic phase*⁹⁷

Micellar cubic (Cub) phase has an isotropic LC structure in which nanometer scale aggregates are arranged in a cubic lattice (Figure 1-34). When LC molecules have large difference of the free volumes between mesogenic core and dynamic side chains, a large curvature should be generated. Therefore, LC molecules do not behave as rods nor disks in the LC phase. In case of forming the Cub LC structure, small spherical aggregates arranged in a cubic lattice are constructed by several LC molecules with extreme free volume bias between rigid and flexible units. A variety of Cub LC structures can be distinguished by the application of space groups in crystallography to the periodic array of small

aggregates in the self-assembled structure. Representative Cub LC molecules are displayed in Figure 1-35.⁹⁸ It is noted that Cub LC phases are optically isotropic. Therefore, it is only dark and no optical patterns are obtained under the crossed nicols in POM observation. In LC system exhibiting several mesophases, the Cub LC phase always appears as a high-temperature phase above Col LC phases. Because LC materials in the Cub phase show high viscosity and low fluidity, the distinction between Cub and isotropic molten phase would be possible by the application of mechanical shearing. In most cases, the clear evidence of the assignment to the Cub phase is provided by XRD measurement as well as the phase transition peak in the optically isotropic region on the DSC thermograms.

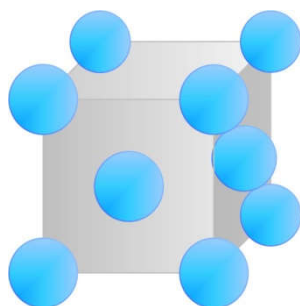


Figure 1-34. Schematic illustrations of self-assembled structures in Cub (Fm3m) phase.

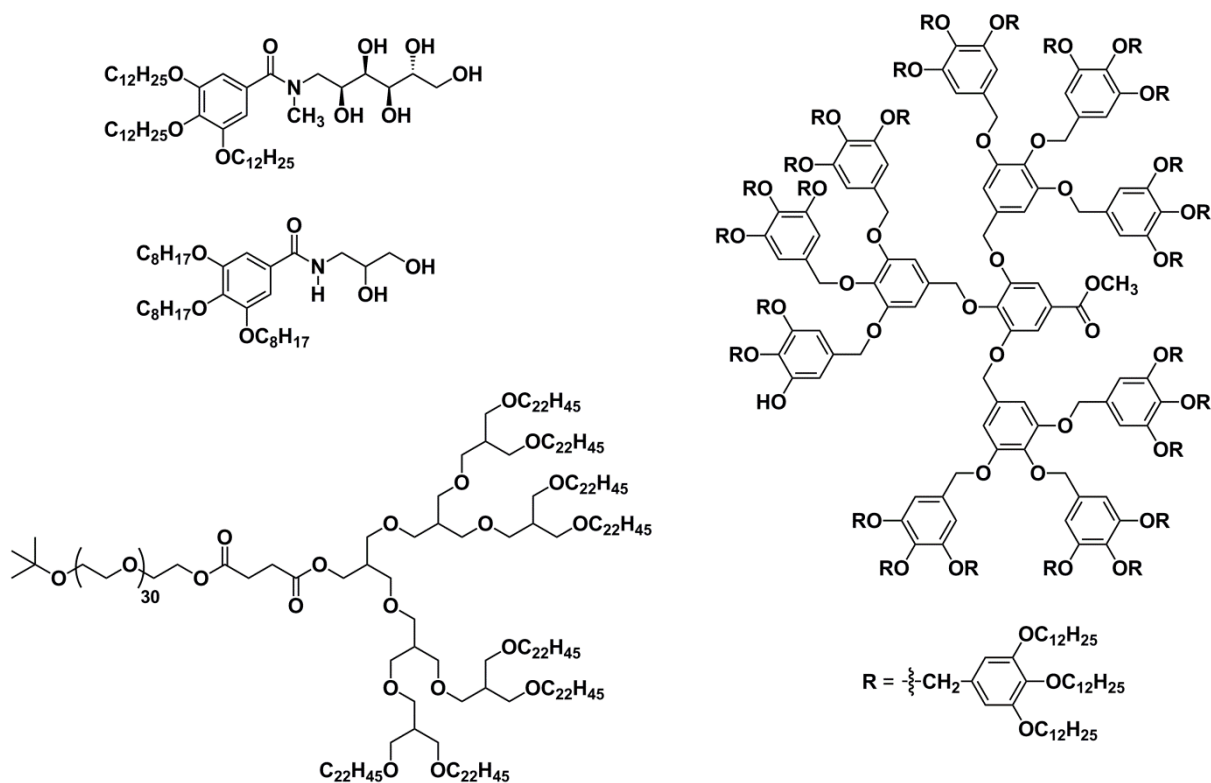


Figure 1-35. Chemical structures of representative Col LC compounds.⁹⁸

Bicontinuous cubic phase^{97d, 99, 100}

Bicontinuous cubic (Cub_{bi}) phase is another type of isotropic LC phase. When the free volume ratio is in the middle of volume ratio for fan-shaped and rod-like molecules, double gyroid interface is induced and Cub_{bi} phase is formed (Figure 1-36). Various Cub_{bi} LC structures can be also described by space groups. Im3m-, Ia3d-, Pn3m- and R3c-type Cub_{bi} structures have been recognized. The similar self-assembled structures are also found in self-assemblies composed of ionic crystals,¹⁰¹ block copolymers¹⁰² or lyotropic LC system.¹⁰³ LC Cub_{bi} phases also work as optically isotropic phase like Cub phase. It is noteworthy that Cub_{bi} LC phase always appears as low-temperature phase below Col LC phases in the LC system showing the several LC-LC phase transitions. The typical Cub_{bi} LC compounds are shown in Figure 1-37.¹⁰⁴

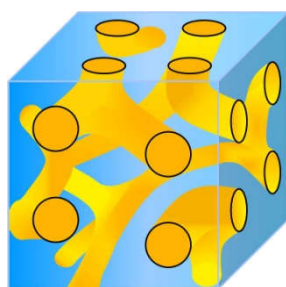


Figure 1-36. Schematic illustrations of the self-assembled structures in Cub_{bi} (Ia3d) phase.

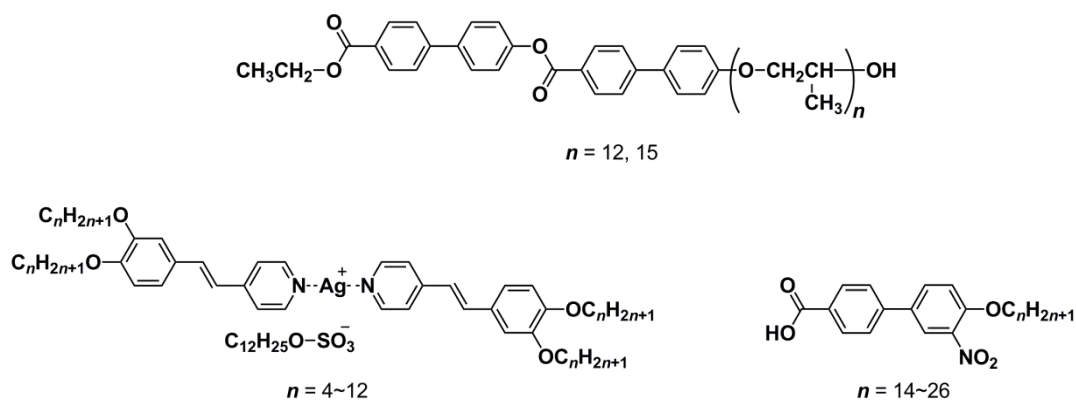


Figure 1-37. Chemical structures of representative Cub_{bi} LC compounds.¹⁰⁴

Blue phase¹⁰⁵

Blue phase (BP) is one of the chiral LC phase and appears between isotropic liquid and N* phases. The existence of BPs seems to have already been found by F. Reinitzer and O. Lehmann in dawn of study on liquid crystals. However, it took more than 80 years to be clarified the detail on BPs, of which pioneering study was carried out by G. W. Gray and A. Saupe in the middle of 20th century.¹⁰⁶

The LC BPs have been extensively studied since 1980, following the advanced study by G. W. Gray, A. Saupe and coworkers.^{105c, 107} The important work by H. Kikuchi and coworkers in 2002 brought the turning point for the study of BPs.¹⁰⁸ They found the stabilization effect of the BPs by complexation with small amount of polymers. The discovery of polymer-stabilized BP contributed to the expansion and deepening of the BPs' study.^{105e} Up to now, LC structures of BPs (BP1, BP2) have been clarified by the contribution of polymer-stabilized system and development of structural analysis technology by synchrotron radiation. There are three types of LC structures in BP phase depending on packing arrangements (Figure 1-38).^{105g} Further aggregation of cylindrical assemblies with N^* helical orientation leads to form the hierarchical order structure with cubic lattice arrangement. Thus, BP exhibits the optically isotropic. The self-assembled structure in blue phase has structural frustration. Therefore, the LC temperature range of blue phase is generally narrow (typically about 1 K). It is noted that LC structure of BP3 is still not clarified.

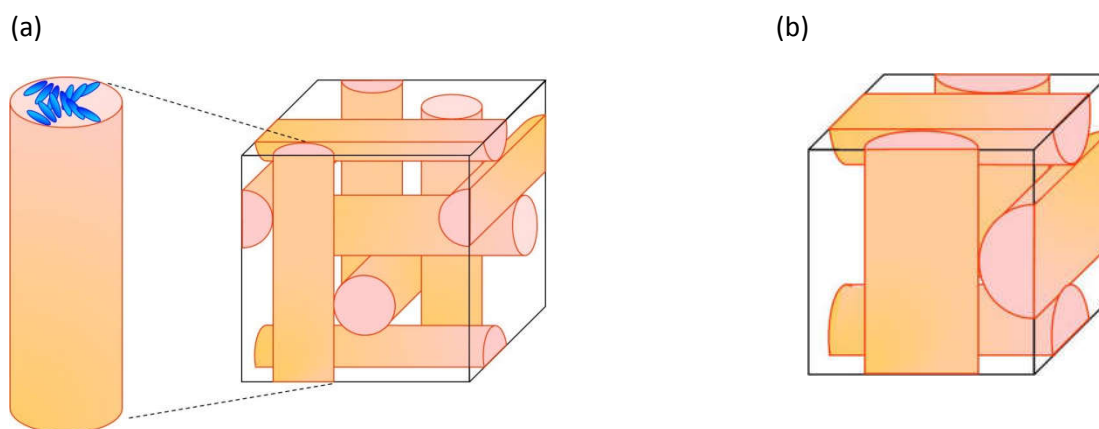


Figure 1-38. Schematic illustrations of LC structures in (a) BP1 and (b) BP2.^{105f, g}

Twist grain boundary phase^{79d, 105h, 109}

Twist grain boundary (TGB) phase is also frustrated liquid-crystalline system under chiral environment. S. R. Renn and T. C. Lubensky reported the existence of TGB phase for the first time in 1988.¹¹⁰ TGB phase appears in the middle of N^* and smectic (SmA^* or SmC^*) phases. In the LC structures of TGB phase, smectic clusters seem to be twisted around an axis perpendicular to the layer normal and periodically arranged in helix (Figure 1-39). The competition between intermolecular interactions to form the smectic layer and N^* -type helical twisting field originated from molecular chirality induces the twisting grain boundaries. As a result, frustrated LC structures of TGB phase are formed. Typical TGB LC compounds are displayed in Figure 1-40.¹¹¹

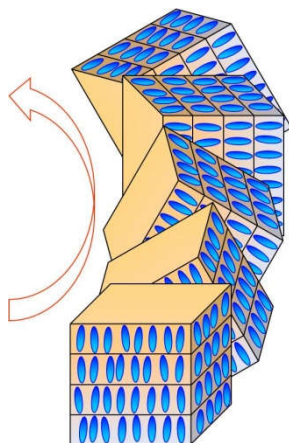


Figure 1-39. Schematic illustrations of LC structures in TGB phase.¹⁰⁹

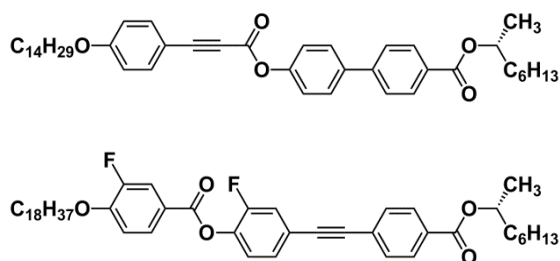


Figure 1-40. Chemical structures of representative TGB LC compounds.¹¹¹

1.3.3. Conventional LC model¹¹²

Conventional LC molecules consist of rigid cores and flexible side chains. The side chains weaken the strong interaction between the aromatic cores by their thermal motion to form LC phases. In conventional molecular designs of the LC compounds, non-polar alkyl chains are usually used as flexible units. The thermodynamic stability of the LC phases has generally explained by a few models based on the classical Onsager hard-rod,^{59, 112} Maier-Saupe,^{60, 112} and Gay-Bern models.^{112, 113} All these models assume simple rigid molecules with a cylindrical symmetry and single intermolecular interaction. They are not proper for the LC molecules consisting of a few incompatible parts causing a competition of plural intermolecular interactions.

1.3.4. nano-segregated LC system¹¹⁴

Soft matter represented by block copolymers, physical gels consisting of fibrous aggregates and liquid crystals are characterized by self-assembled supramolecular structures. Molecules functionalized with aromatic cycles, aliphatic alkyl chains, polar amide groups etc. form the various supramolecular self-assemblies depending on the volume fractions of the incompatible units and intermolecular interactions.^{102, 103, 115} The LC system utilizing segregation of incompatible unit in molecular scale is defined “nano-segregated LC system”.¹¹⁴ Figure 1-41 demonstrates a schematic illustration of supramolecular structures constructed by the molecules bearing incompatible functional moieties. In general, rod-like molecules form layer structures while fan-shaped molecules assemble into cylindrical structures. In the case of the LC molecules bearing incompatible side chains with a large difference of the free volumes, a large curvature should be generated, so that the layer or cylindrical structures are disturbed and gyroid or spherical structures are formed. The self-assembled systems provide an effective methodology for the construction of the novel functional materials based on bottom-up approach.¹¹⁶⁻¹¹⁸

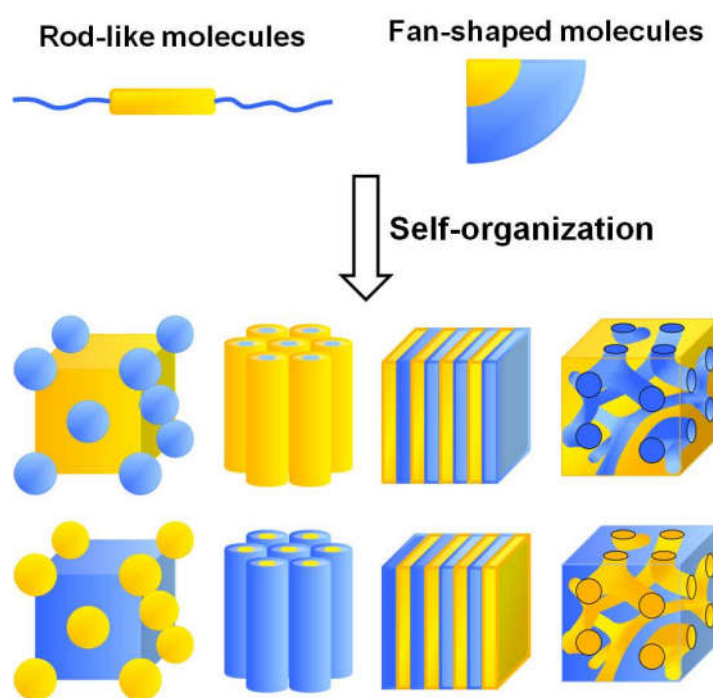


Figure 1-41. A schematic illustration of various self-assembled structures composed of incompatible parts

These LC molecules to produce self-assembled supramolecular structures are composed of several incompatible segments. Dynamic ordered structures of LC phases are originated from the thermal motion of the flexible units. The freedom of the molecular motion is strongly associated with

one of the most significant property of LC materials, the formation of large-area homogeneous thin films.

The side chains of LC molecules not only disturb the molecular aggregation by their thermal motion, but also promote the formation of supramolecular assemblies through nanosegregation. Thus, the optimization of the chemical structures of the flexible side chain units as well as the rigid cores contributes to the developments of the novel multifunctional materials. Especially, the organic materials based on the concept of nanosegregation will contribute to the establishments of the novel functional material development strategies.^{118c}

1.3.5. LC materials as organic functional materials^{115, 118a, 119}

As is mentioned former, LC molecules have dynamic ordered structures in the mesophase. The anisotropic nature in most of LC structures is reflected to the orientation-dependence in some features such as birefringence. In addition, low viscous LC materials can response to the external stimuli. Most typical applications of LC materials are electro-optical devices such as liquid crystal displays (LCDs),^{52, 76a} optical shutters¹²⁰ and dimming windows.¹²¹ These utilizations are based on the optical anisotropy and electric-field responsiveness of LC materials.

The most conventional and typical LCD cell is “twisted nematic (TN) cell”. In this case, LC molecules are in a planer arrangement in the initial condition without an AC bias. In contrast, the molecular orientation can be changed to homeotropic arrangement when the AC external field is applied. In the case of random orientation, both molecular short axis and long axis factors of the dielectric constant contribute to light transmission in crossed nickol. In the homeotropic orientation, however, the contribution of long axis factor is suppressed and that of short axis factor is two-dimenssionally averaged by the spin motion. Therefore, liquid crystal layer in homeotropic orientation bahave as isotropic media and polarized light can be transimited in crossed nickol. In the situation of such planar arrangement, the polarized light can be shut off by the contribution of birefringence in contrast to the situation of homeotropic arrangement. The typical LC materials for LCDs are shown in Figure 1-42.^{76a, 122} LC mixtures are generally used for the application to LCDs, because some properties such as phase transition temperature, viscosity, refractive index and response speed can be easily tuned by optimization of components and their composition ratio.^{76a}

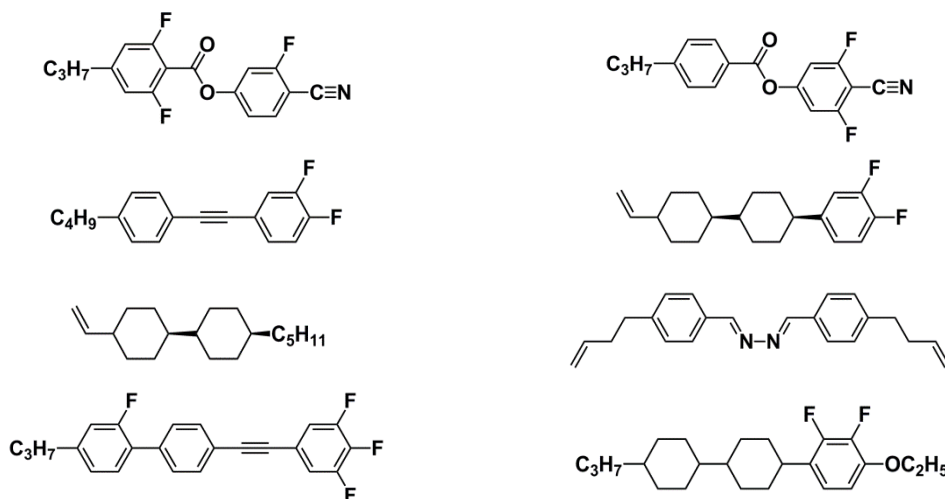


Figure 1-42. Representative LC components for the application to LCDs.^{76a, 122}

As is mentioned in former section, FLC materials are also investigated for electro-optical devices. The detail of FLC materials will be described later.

Representative practical applications of liquid crystal materials system other than electrooptical devices are engineering plastics based on LC polyesters and LC polyamide such as Kevlar[®],¹²³ optical compensation films,¹²⁴ and chiral nematic temperature sensors.⁸⁴ For these functions, LC ordered structures and orientation of LC molecules are important rather than the chemical structures. Molecular designs for these applications are based on conventional LC models.

Needless to say, not only aggregation structures but also chemical structures have a great influence on the function. In contrast to conventional molecular design based on aliphatic side chains, alicyclic ring and aromatic ring, molecular design strategy relied upon the characteristic of functional groups and skeletons can be considered. In a molecular design including the polar units, coordination sites and extended π -conjugated skeleton at the same time, the balance of several intermolecular interactions should be deeply considered. The first consideration focusing on the intermolecular interactions in the LC system is the study and development of supramolecular LC system.^{125, 126} The first example of supramolecular LC materials are based on hydrogen-bond network.^{126a-d} Following the development of hydrogen-bond supramolecular LC materials, variety of supramolecular LC systems have been investigated by utilizing metal coordination bonds,¹²⁷ halogen bonds,¹²⁸ charge-transfer,¹²⁹ dipole-dipole¹³⁰ and ionic interactions.¹³¹ The idea base on cooperation of these intermolecular leads to the construction of nano-segregated LC system. Furthermore, unconventional material designs coupled with exotic functions and LC dynamic ordered structures can be considered.

As focused on the LC self-assembled structures, LC molecules form the well-defined multi-dimensional nano-channels, depending on the balance between the free volumes of central mesogen core and dynamic side chains. The formed nanometer-scaled channels provide conduction pathways for ionic¹³² or electronic charge carriers,¹³³ or mass transport pathways for nanoporous

membranes.¹³⁴

For another application of LC system, light-responsive LC materials,¹³⁵ mechano-responsive LC materials¹³⁶ and biomedical LC materials¹³⁷ have been investigated.

In this thesis, photoconductive LC materials and ferroelectric liquid crystals are focused on. The details of those materials are described in follow.

1.4. LC semiconductors^{133, 138}

LC molecules to produce self-assembled supramolecular structures are composed of several incompatible segments. In general, LC molecules have flexible chains and a rigid core. Rigid cores are usually comprised of aromatic moieties and determine the optical and electronic property of the supramolecular assemblies. In contrast, flexible units are associated with the softness and flexibility of the assemblies. Dynamic ordered structures of LC phases are originated from the thermal motion of the flexible units. The freedom of the molecular motion is strongly associated with one of the most significant property of LC materials, the formation of large-area homogeneous thin films.

Extended π -conjugated molecules can work as organic semiconductors based on the carrier conduction through the π orbitals. Liquid crystals having extended π -conjugated units also exhibit the carrier transport properties. LC semiconductors exhibit good carrier transport properties comparable to organic polycrystalline semiconductors and conjugated polymers. From the viewpoint of the carrier transport property, a single-crystal structure in which π -conjugated molecules are stacked closely in a crystal lattice is most favorable because intermolecular π -orbital overlaps are maximized and structural disorder to inhibit charge carrier movement is minimized. However, the single-crystalline materials generally have a difficulty in the preparation of the thin film with the low defect density. Polycrystalline thin films can be produced by a vacuum process. However, their carrier transport properties are inferior to single-crystalline materials, due to the domain boundaries, which are inconsistency of the molecular orientation and are regarded as a major problem on the carrier transport property. In contrast, LC semiconductors are less affected by the domain boundaries due to their dynamic ordered structures.

In addition, LC materials have good solubility in conventional organic solvents, due to the thermal motion of the flexible side chains. In the processability, crystalline materials are unfavorable because of their poor solubility and the difficulty in the preparation of homogeneous thin films. In contrast, LC semiconductors provide the good solubility and homogeneous thin film formation property, and are suitable for device production with solution processes including a printing technology.

Up to now, the design of aromatic cores has been studied mainly for LC semiconductors. However, the roles of side chains are not negligible. The side chains of LC molecules not only disturb the molecular aggregation by their thermal motion, but also promote the formation of supramolecular assemblies through nanosegregation. Thus, the optimization of the chemical structures of the flexible

side chain units as well as the rigid cores contributes to the developments of the novel multifunctional materials.

The molecular design is very important to develop the novel multifunctional LC materials. The character of molecular structures will be described as follows.

1.4.1. Classical LC semiconductors bearing alkyl side chains

1.4.1.1. LC semiconductors based on aromatic hydrocarbons

Chemical structures of representative LC semiconductors are shown in Figure 1-43. In the aromatic hydrocarbons, triphenylene, phenyl naphthalene and perylene tetracarboxylic acid bisimide (PTCBI) are typical mesogens for LC semiconductors. Haarer's and Boden's groups reported LC semiconductors based on the triphenylene core with high carrier mobilities in their LC phases.^{139a, b} Disk-like shaped LC triphenylene derivatives generally form columnar structures. 2,3,6,7,10,11-Hexahydroxytriphenylene (**1**), and 2,3,6,7,10,11-hexahexylthiotriphenylene (**2**) are well-known examples. The triphenylene cores stack and form one-dimensional conduction paths of electronic charge carriers in their columnar LC phases. The triphenylene cores are an electron-rich aromatic unit and favorable for hole transport. The hole mobilities of these triphenylene-based LC were on the order of 10^{-4} - 10^{-2} $\text{cm}^2 \text{V}^{-1} \text{s}^{-1}$ determined by time-of-flight (TOF) method.^{139a, b, g-i}

In addition to columnar phases consisting of disk-like LC molecules with extended π -conjugated systems, efficient carrier transport was observed in smectic phases consisting of the LC hydrocarbons having relatively small π -conjugated systems. The phenyl naphthalene derivatives (**3**) bearing simple alkyl chains exhibit several smectic LC phases and the hole and electron mobilities in their ordered smectic phases reach the order of 10^{-2} $\text{cm}^2 \text{V}^{-1} \text{s}^{-1}$.¹⁴⁰ The PTCBI is well-known as a representative mesogenic core which shows the electron transporting property.^{141, 142} The PTCBI core has an electron-deficient nature because of four electron-withdrawing carbonyl groups. Most of LC PTCBI derivatives exhibit the columnar phase.^{142d-f, 143} Besides, LC PTCBI derivatives with the asymmetrical side chains or long alkyl chains form the lamellar LC structures.^{142a, g} Sudhölter and coworkers reported a LC PTCBI derivative bearing two octadecyl chains, which form a smectic phase. The electron mobility in the LC phase was evaluated by the pulse-radiolysis time resolved microwave conductivity (PR-TRMC) method and the electron mobility reaches the order of 10^{-1} $\text{cm}^2 \text{V}^{-1} \text{s}^{-1}$.^{142a}

It is noted that the carrier mobility estimated by PR-TRMC method is higher than the value estimated by a TOF method. A carrier mobility obtained by the PR-TRMC method is a band mobility, which corresponds to the rate of intermolecular charge transfer without a carrier trapping process. The value determined by the TOF technique is a drift mobility, which involves detrapping processes of charge carriers from localized states formed by impurities and defects.

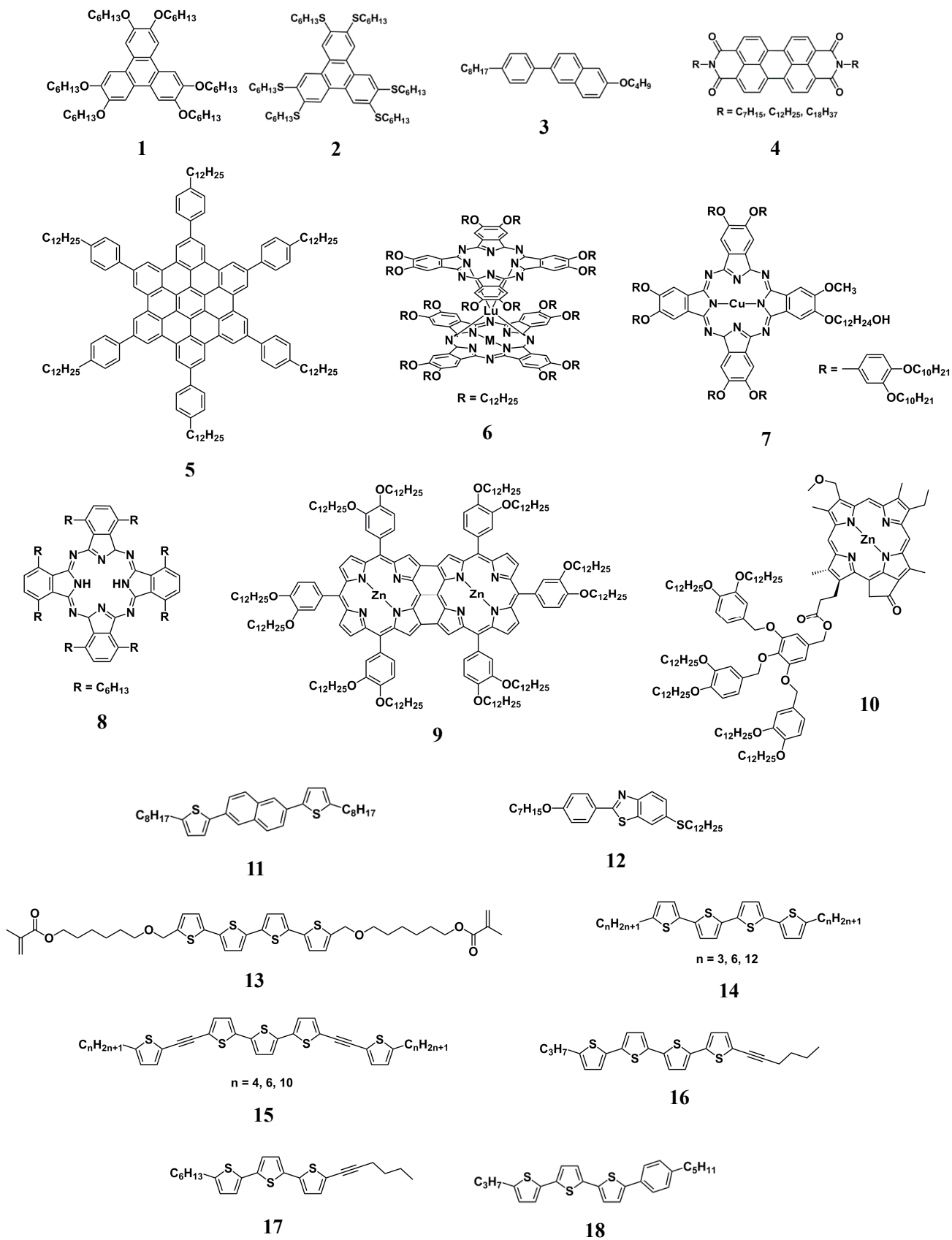


Figure 1-43. Chemical structures of representative LC semiconductors^{139-144, 147-150}

1.4.1.2. LC semiconductors based on heteroaromatic moieties

Not only the aromatic hydrocarbons, but heteroaromatic LC semiconductors also have been reported.¹⁴⁴ Ohta and coworkers synthesized symmetrical and asymmetrical phthalocyanine derivatives (**6**, **7**) which formed the columnar LC structures. They evaluated their carrier transport properties by TOF or PR-TRMC methods.^{139e, 144c, d}

Swarts and Cook's group also synthesized LC metal-free phthalocyanines.^{144e} Cook, Ozaki and coworkers developed a LC phthalocyanine derivative (**8**) octa-substituted at non-peripheral positions. They evaluated the drift carrier mobility in the crystalline and hexagonal disordered columnar phases of the phthalocyanine **8**, which increases to the order of $10^{-1} \text{ cm}^2 \text{ V}^{-1} \text{ s}^{-1}$.^{144f} In addition, they fabricated the bulk heterojunction organic photovoltaic cells using the LC phthalocyanine derivative **8** as a hole-transport material.^{144g} The LC zinc porphyrin oligomer (**9**) was synthesized by Aida's group. The metalloporphyrin **9** exhibited rectangular columnar phases in which band mobilities were on the order of $10^{-2} \text{ cm}^2 \text{ V}^{-1} \text{ s}^{-1}$.^{144h} Würthner *et al.* synthesized an asymmetrical zinc chlorophyll derivative (**10**), of which carrier mobility evaluated by the PR-TRMC method were on the order of $10^{-2} \text{ cm}^2 \text{ V}^{-1} \text{ s}^{-1}$ in the columnar LC phase.¹⁴⁴ⁱ Shimizu and coworkers developed a LC dithienonaphthalene (DTN) derivative (**11**) and fabricated the high performance thin film transistors whose active layer composed of the LC DTN.^{144j} Funahashi, Hanna and coworkers synthesized phenylbenzothiazole derivatives (**12**) which exhibited smectic LC phases. Ambipolar carrier transports were observed in their smectic LC phases. The hole and electron mobilities were of the order of $10^{-3} \text{ cm}^2 \text{ V}^{-1} \text{ s}^{-1}$.^{140, 144k-l}

In this way, the chemical structure of the central aromatic core has an impact on the self-assembled structure, influencing on carrier transport property. The closed packing of the π -conjugated moieties is required for the efficient carrier transport and high carrier mobilities have been observed in ordered LC phases. LC compounds bearing heteroaromatic cores exhibit redox activity,¹⁴⁵ mechanical stimuli-responsiveness¹⁴⁶ as well as carrier transport property.^{139, 140} Especially, oligothiophene frameworks are considered as a substructure of polythiophenes, which are typical π -conjugated polymers. Based on the idea that organization of the oligothiophene cores in LC phases should enhance the electronic properties, LC oligothiophene have been studied for the alternative materials.^{118a, 147} The thiophene rings prefer all-*trans* (transoid) conformation to all-*cis* (cisoid) or twisted conformations generally. As the expanding the π -conjugated planes with increasing the number of thiophene rings, the planarity of the aromatics are maintained. The extended π -conjugated system is preferable for the efficient charge carrier transport, leading to the bathochromic shift of the absorption maxima. However, the melting points of the compounds are remarkably raised and their solubilities are reduced due to the enhanced self-association of the extended π -conjugated plane.

Low solubility of the extended π -conjugated materials causes difficulties in the synthetic and purification processes. For the fabrication of practical electronic devices using wet processes represented by a printing technique, π -conjugated materials with high solubilities are indispensable. One method to increase their solubilities is the introduction of the linear alkyl chains to the

heteroaromatic cores. Conventional LC molecules consist of aromatic cores and alkyl chains, and exhibit good solubility in organic solvents.

A lot of LC oligothiophene derivatives have been reported up to the present time.¹⁴⁸ McCulloch *et al.* reported that the quaterthiophene derivatives (**13**) bearing the polymerizable acrylate groups in the terminal of the side-chains exhibit the LC properties. In the report, they prepared the field-effect transistors (FETs) with using the LC quaterthiophenes as the active layers and demonstrated the performances of the devices.^{148a} Garnier and Horowitz *et al.* reported that 5,5'''-dihexyl-2,2':5', 2'':5'',2'''-quaterthiophene (DH4T) shows a smectic phase, indicating the formation of the layer structure at an elevated temperature. They also demonstrated the performance of the FETs based on the DH4T and showed that the field-effect mobility reached on the order of $10^{-2} \text{ cm}^2 \text{ V}^{-1} \text{ s}^{-1}$.^{148c} Although various symmetrically alkylated terthiophene and quaterthiophene derivatives have been synthesized,^{148d, 149} the melting points of these compounds are generally above 100 °C and room-temperature LC oligothiophenes are quite limited.

Funahashi *et al.* have synthesized room-temperature oligothiophene liquid crystals bearing the normal linear alkyl chains.¹⁵⁰ Especially, 3-TTPPh-5 (**18**) shows the ordered smectic phase in a wide temperature range including room temperature. We have observed that high hole mobility in the ordered smectic phase of 3-TTPPh-5 exceeding $10^{-1} \text{ cm}^2 \text{ V}^{-1} \text{ s}^{-1}$. We have explained that the hole transport in the LC system of 3-TTPPh-5 is based on the band-like conduction mechanism by the observation of temperature- and field-independent mobility over wide temperature range.^{150c} Using this compound, field-effect transistors were produced by a spin-coating method. When the transistors were fabricated on polymer films, their performance was retained under the application of the strain around 10%.

Heteroaromatic LC semiconductors with heavy chalcogens have an advantage over aromatic hydrocarbon-based LC semiconductors because they have relatively large van der Waals' radii. Increase in the overlaps between the π -molecular orbitals enhances the carrier transport. In fact, high carrier mobilities comparable to those of amorphous silicon have been achieved in the crystal phase of heteroaromatic compounds.

Recently, organic crystalline semiconductors based on thienothiophene units have been reported. The representative crystalline semiconductors based on sulfur containing aromatics are shown in Figure 1-44.¹⁵¹⁻¹⁵⁴ Takimiya's group reported that the preparation of the high performance organic field-effect-transistors using the [1]benzothieno[3,2-*b*][1]benzothiophene (BTBT) derivatives for crystalline active layer.¹⁵¹ The high carrier mobility in this system derived from the large transfer integral which is affected by the large van der Waals' radius of sulfur atoms on the BTBT core and the Sulfur-Sulfur interaction.

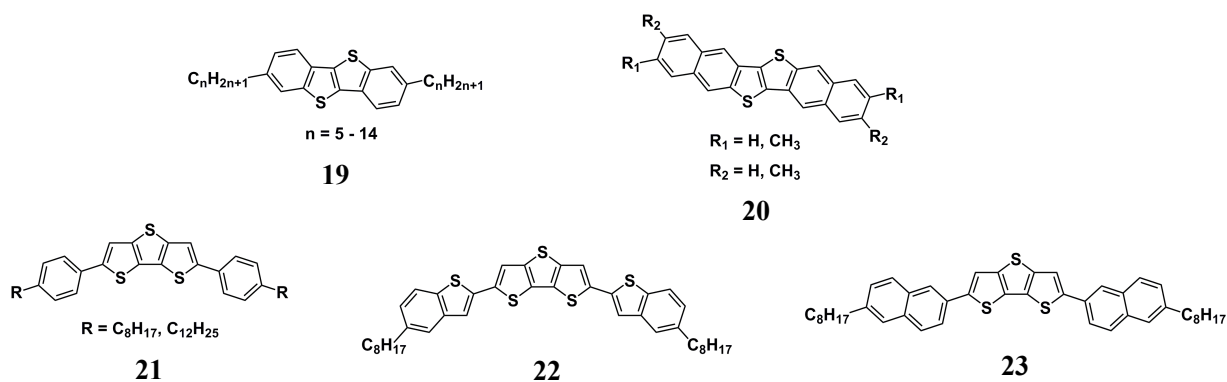


Figure 1-44. Crystalline semiconductors based on sulfur-containing aromatics¹⁵¹⁻¹⁵⁴

Bao's and Tsukagoshi's groups reported that the achievements of high field-effect mobilities on the order of $10^1 \text{ cm}^2 \text{ V}^{-1} \text{ s}^{-1}$ by controlling the molecular orientations with 2,7-dioctyl[1]benzothieno[3,2-*b*]-[1]benzothiophene (C8-BTBT) and the analogues (**19**) for active layers.¹⁵² Dinaphtho[2, 3-*b*:2', 3'-*f*]thieno[3, 2-*b*]thiophene derivatives (**20**) also have good field-effect mobilities up to the order of $10^1 \text{ cm}^2 \text{ V}^{-1} \text{ s}^{-1}$.¹⁵³ In addition, Yasuda and Adachi's group recently reported fast carrier transport in the crystal phases of sulfur-containing aromatics (**21-23**) expanded the π -electron system of the dithienothiophene (DTT) skeleton utilizing the S-S contact.¹⁵⁴ Thus, it is significant to optimize the intermolecular interactions which directly contribute to the self-assembled structures of low molecular-weight heteroaromatic compounds for the carrier transport property.

Single-crystalline materials are the most suitable for high performance devices at the sacrifice of their processability. In polycrystalline materials, the grain boundaries are an obstacle to efficient carrier transport. In contrast, LC semiconductors have a big advantage over crystalline materials in the film-forming property and processability.

In the conventional molecular design of LC semiconductors, flexible long alkyl chains are introduced to the central extended π -conjugated aromatic core. It is reported that C8-BTBT and the analogous compounds C_n -BTBT ($n = 6, 10, 12$) form smectic mesophases.¹⁵⁵ In the C8-BTBT system, liquid-crystallinity of the C8-BTBT improves the solubility in the organic solvents and the molecular orientation. The DTT derivatives (**21**) also form smectic phases^{154a} and the same effect should contribute to their processability. The LC systems can be considered for the construction strategy on the low-cost and high-performance electronic devices. Iino, Hanna and coworkers ascertained the effect of the LC property to the device performance. They fabricated thin film transistors using C10-BTBT, whose active layers prepared by a spin-coating technique in different temperatures at crystalline and LC phases. The device based on polycrystalline thin films spin-coated in the LC phase exhibited superior performance to the devices using the active layers spin-coated at room temperature.¹⁵⁶ Gomez and coworkers demonstrated the optimization of the quenching temperature from melting state to crystalline phase on the C8-BTBT system. They obtained the thin film with suitable morphology for field-effect transistors by controlling of crystallization.¹⁵⁷

As shown in Figure 1-45, BTBT-based LC compounds were synthesized aiming for the improvement of the device performance by structural reorganization effect in the LC system.¹⁵⁸ Iino, Hanna and coworkers synthesized a thienyl substituted BTBT derivative (**24**), which exhibits smectic A and smectic E phases. They fabricated thin film transistors whose active layer was composed of the thienyl-BTBT derivative. The active layers were prepared by the spin-coating technique in the LC temperature range. They also studied on the thermal treatment effect upon the film morphology and the device performance.^{152a} A phenyl substituted BTBT derivative (**25**), which exhibits smectic A and smectic E phases, was also synthesized by the same group. The device performance of the thin film transistors based on the phenyl-BTBT derivative were evaluated in wide temperature range including the LC phase temperature.^{158b} Hasegawa *et al.* synthesized analogous phenyl-BTBT derivatives. They studied on the influence of the alkyl chain length upon the solubility and thermal property.^{158c} Méry, Shimizu and coworkers synthesized a dialkenyl substituted BTBT derivative (**26**), which forms the lamella-columnar LC structure. They evaluated the carrier transport property by time-of-flight technique. The drift mobility in the LC phase of the compound was on the order of $10^{-2} \text{ cm}^2 \text{ V}^{-1} \text{ s}^{-1}$.^{158d} Choi's group synthesized thienylethenyl-BTBT derivatives (**27**), which exhibit smectic phases. They fabricated thin film transistors based on the thienylethenyl-BTBT derivatives.^{158e}

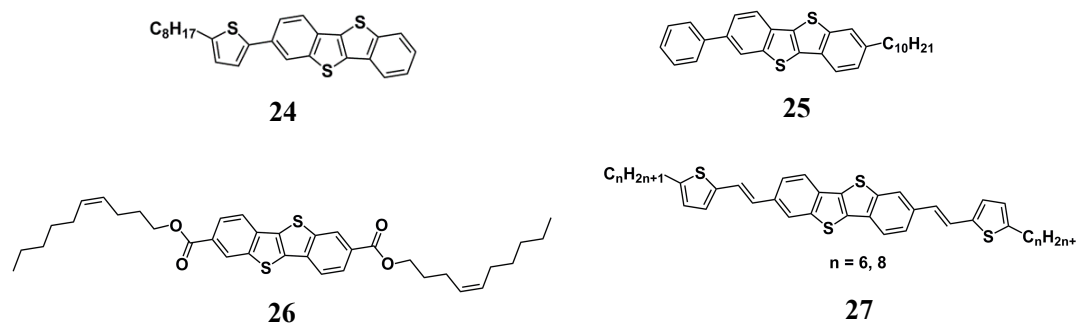


Figure 1-45. BTBT-based LC semiconductors¹⁵⁸

On the other hand, the various aromatic systems behave as the rigid core. The aromatic rings are also electronically and spectroscopically active units due to the π -electrons. From these characteristic properties of aromatic rings, the aromatic cores have been mainly focused upon for the conventional molecular design of the functional soft materials. So far, the expansion and modification of π -conjugated moiety have been studied for the tuning of HOMO and LUMO energy levels and/or the intramolecular charge-transfer. As a result of these studies, the tuning of the redox activities and absorption properties as well as the enhancement of the carrier mobilities have been achieved.^{144a-b,}
¹⁵⁹ In these molecular designs, not only the aromatic hydrocarbons but also heterocycles and fused aromatic rings are used for a central core.¹⁶⁰

1.4.2. Nanosegregated LC semiconductors

1.4.2.1. LC semiconductors bearing polar side chains

Some characteristic unconventional LC systems, which are not possible to be explained by the classical theoretical models, have recently reported.¹⁶¹ For the explanation of these unconventional LC systems, the concept of nanosegregation has been proposed.^{81h, 114g, 162} This model describes that the various LC structures are formed by the nanosegregation between the incompatible segments (e.g. polar and non-polar units) of the LC molecules. In the molecules having both the polar ionic unit and non-polar alkyl chains, the incompatible units are independently assembled to form the nanosegregated structures. We focus on the structures of side chains of the LC molecules and describe the LC material design based on nanosegregation.

The LC systems based on the polar side chains such as oligo(ethylene oxide) units,¹⁶³ propylene oxide units,¹⁶⁴ fluoroalkyl chains¹⁶⁵ and perfluoroalkyl chains have been reported.¹⁶⁶ These polar side-chains having larger dipole moments compared to the non-polar aliphatic and/or aromatic rings. Therefore, the side chains are immiscible with aromatic cores and aliphatic side chains, resulting in microscopic segregation on the order of nm scale. It has recently been pointed out that the nanosegregation strongly contributes to the stabilization of the LC phases.¹⁶⁷

Figure 1-46 exhibits molecular structures of π -conjugated LC's bearing polar side chains. Tschierske *et al.* reported that oligothiophene derivatives (**28**) bearing glycerol groups and lateral alkyl chains formed the hexagonal and tetragonal columnar superstructures.¹⁶⁸ Schenning and Meijer *et al.* synthesized sexithiophene derivatives (**29**) functionalized by oligo(ethylene oxide) chains. These compounds formed the smectic layer structures associated with coiled aggregates. In the self-assembled coils, π -conjugated rigid cores and flexible polar side chains were separately assembled.¹⁶⁹ Gregg *et al.* synthesized LC PTCBI derivatives (**30**, **31**) bearing the linear or branched oligo(ethylene oxide) chains. These compounds formed interdigitated or tilted lamellar structures. Moreover, they also evaluated the electronic properties of the PTCBI derivatives.¹⁷⁰ Shimizu and coworkers developed the perfluoroalkyl-substituted LC triphenylene (**32**)¹⁷¹ and phthalocyanine (**33**).¹⁷² Aida's group synthesized an LC metalloporphyrin dyad (**34**) asymmetrically substituted by polar and non-polar side chains.¹⁷³

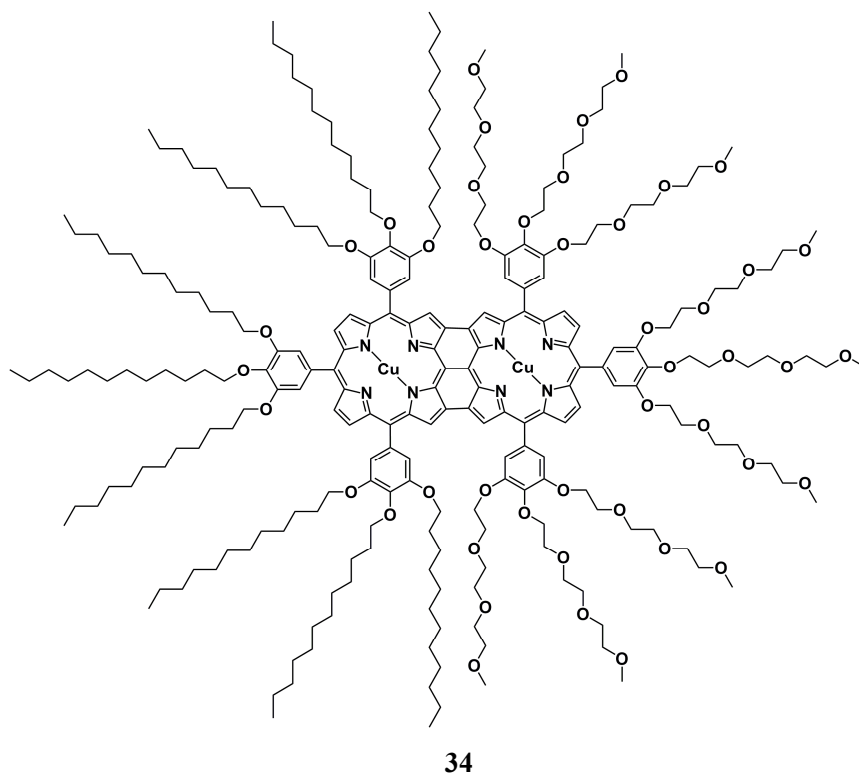
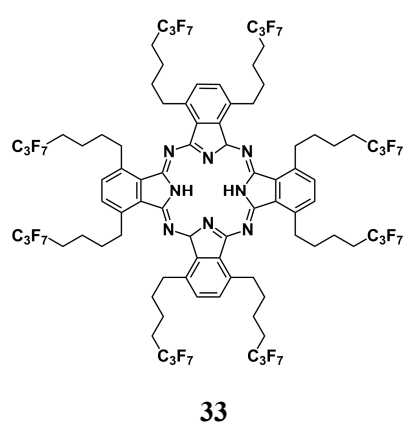
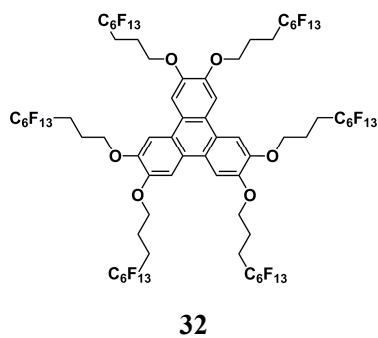
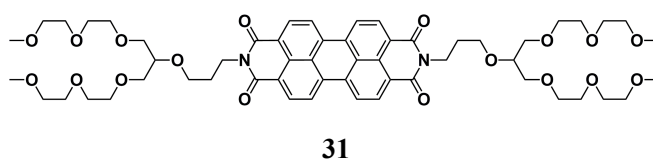
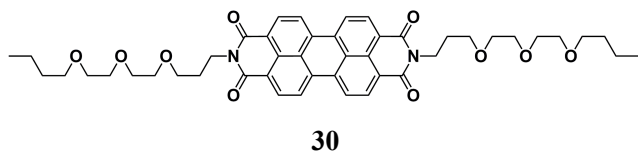
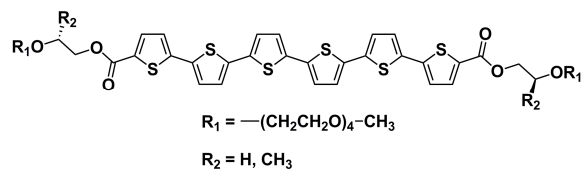
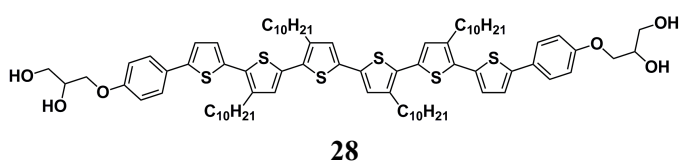


Figure 1-46. Nanosegregated π -conjugated LC compounds¹⁶⁸⁻¹⁷³

1.4.2.2. LC semiconductors bearing side chains with ionic moiety

Other than the polar side chains described in the preceding section, LC molecules having an ionic unit at the terminal of the alkyl side chain have been reported so far. The LC molecules having ammonium,¹⁷⁴ phosphonium,^{174d} sulfonium,¹⁷⁵ imidazolium,¹⁷⁶ and pyridinium moieties¹⁷⁷ have been synthesized. The main driving force of the formation of their LC phases is nanosegregation.^{131b} This phenomenon is similar to the micelles and vesicles in water in the surfactant systems.

Figure 1-47 shows molecular structure of LC semiconductors bearing ionic moieties at the terminals of the alkyl chains. Funahashi and Kato *et al.* synthesized a phenylterthiophene derivative (35) having ionic imidazolium units at the terminal of side chains. These compounds formed nanosegregated smectic layer structures, in which ionic units and rigid π -conjugated aromatic cores were separately assembled. In these LC systems, the electrochromism was observed under the application of a DC bias without any electrolytes. In the nanosegregated smectic phases, ions can be transported within the two-dimensional mantles while the electronic charge carriers can also move within the layers made from aromatic cores.¹⁷⁸ Fukushima *et al.* synthesized triphenylene derivatives (36), in which six imidazolium groups and central aromatic core were connected via aliphatic linkers. These compounds exhibited columnar LC phases. Moreover, the triphenylene derivative having the tetrafluoroborate anions as counterparts can be hybridized with ionic liquids and carbon nanotubes.^{176h, 179}

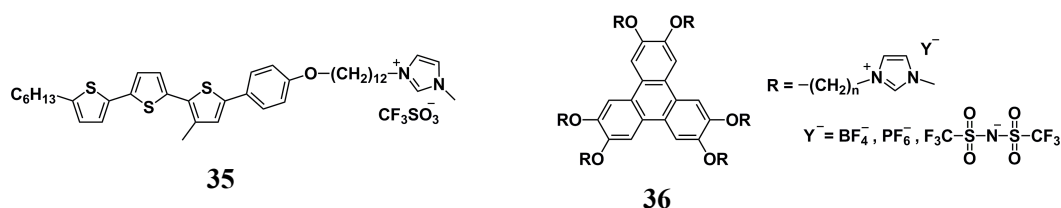


Figure 1-47. Chemical structures of π -conjugated LC compounds bearing the side chains with ionic moieties^{176h, 178, 179}

1.3.2.3. Nanosegregated LC semiconductors bearing non-polar side chains

As mentioned in former section, nanosegregation effect is remarkable in the formation of the LC phases of the molecules bearing polar functional groups. Even in the LC phases of the molecules bearing non-polar side chains, this nanosegregation effect is also significant. Non-polar side chains do not only weaken the strong interaction between π -conjugated cores to induce LC phase, but also promote structural formation by their attractive interaction.

Most general flexible units are linear alkyl chains while rigid cores are often heteroaromatic units. Thermal motion of the alkyl chains weaken the strong interaction between the heteroaromatic cores, resulting in the appearance of LC phases and increase in the solubility. On the other hand, heteroaromatic cores are self-organized in soft aggregates by the attractive interaction and

nanosegregation of the alkyl chains. Yasuda and Kato *et al.* synthesized LC oligothiophenes (**37-39**) with polycatenar structures, as shown in Figure 1-48. It should be noted that various LC structures such as micellar cubic (0D), columnar (1D) and smectic (2D) phases were formed due to the nanosegregation between π -conjugated oligothiophene units and alkyl side chains. In addition, they verified the ambipolar carrier transporting properties in the columnar and smectic phases.^{145c, 148g} In the polycatenar LC molecules, nanosegregation effect of alkyl chains should be more remarkable, compared to the classical LC molecules bearing one or two alkyl chains.

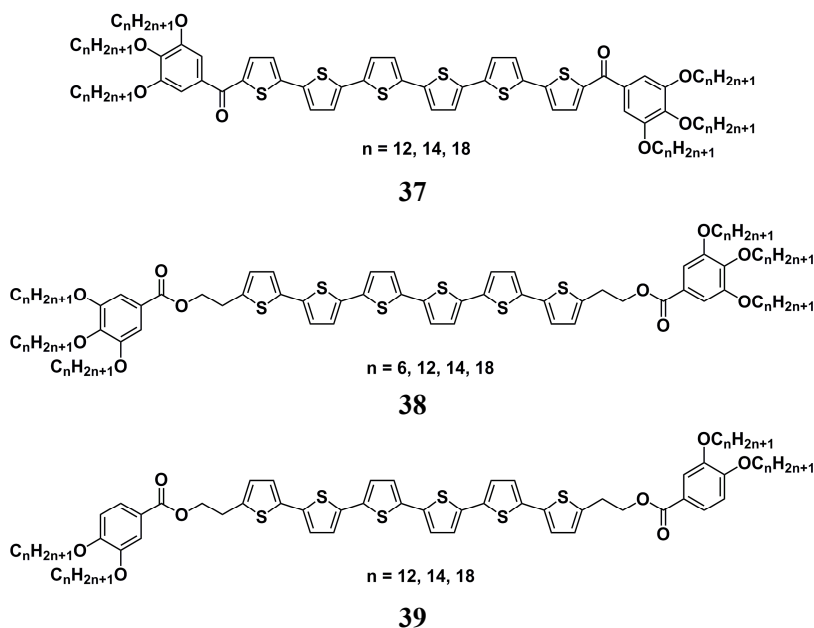


Figure 1-48. The chemical structure of LC oligothiophene derivatives^{145c, 148g}

Ohta *et al.* reported an evidence of an attractive interaction between alkyl chains in LC systems. They synthesized octaalkoxy bis(diphenyldioximato) metal complexes (**40**) and octaalkoxy bis(diphenyldithiolene) metal complexes (**41**) (Figure 1-49).¹⁸⁰ The alkylated complexes exhibited bathochromic shift in UV-VIS absorption spectra compared to non-alkylated analogues. This result is attributed to the compression of the columnar aggregates by the attractive interaction between the alkyl chains.^{180c}

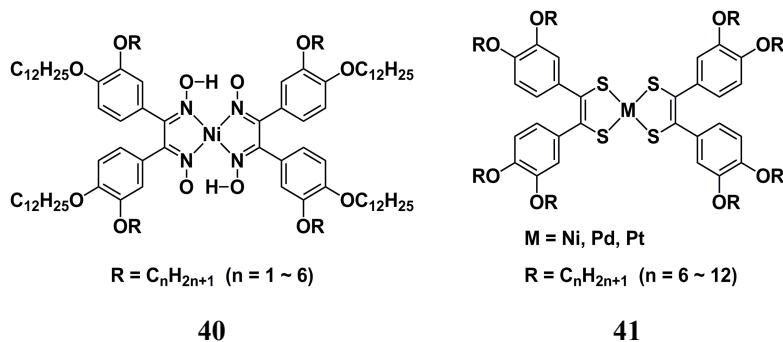


Figure 1-49. The chemical structure of LC metal complexes¹⁸⁰

Branched alkyl chains are more bulky than the linear alkyl chains. The branched chains have low interfacial free volumes and high surface coverage. Therefore, the aggregation of the molecules bearing the branched alkyl chains should be relatively weakened compared to those bearing linear alkyl chains.¹⁸¹

Figure 1-50 demonstrates the molecular structures of LC semiconductors bearing branched alkyl chains. Funahashi and Kato reported that phenylterthiophene derivative (**42**) with 3,7,11-trimethyldecyloxy groups exhibits a nematic phase around room temperature.¹⁸² This report provides one example of the effectiveness of the branched alkyl groups for the formation of LC phases with the low order. The introduction of the branched aliphatic unit results the appearance of the nematic phase around room temperature. The hole mobility in the nematic phase of the compound was $4 \times 10^{-4} \text{ cm}^2 \text{ V}^{-1} \text{ s}^{-1}$. Recently, Isoda and Tadokoro *et al.* reported that tetraazanaphthacene (TANC) derivatives (**43**) bearing the 3,7,11-trimethyldecyloxy or 3,7-dimethyloctyloxy group as branched chains show the smectic phases.¹⁸³ In spite of the high crystallinity of the TANC core, the compounds surprisingly shows the mesomorphism. The electron mobilities of these LC TANC derivatives are of the order of $10^{-4} \text{ cm}^2 \text{ V}^{-1} \text{ s}^{-1}$.

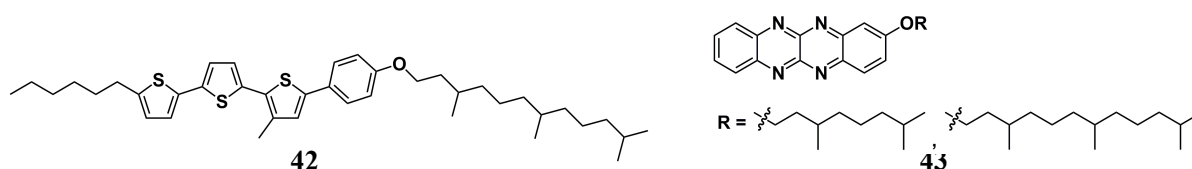


Figure 1-50. Photoconductive LC compounds bearing the branched alkyl chain^{182, 183}

Among branched alkyl chains, chiral alkyl chains play significant roles in the living body systems. Formation of supramolecular aggregates of chiral molecules for chiral molecular recognition has been main research topics in biology, physics, pharmacy and chemistry. In chiral LC systems, helical structures are formed so that in order to minimize the elastic free energy in the system. The helical structure and helical axis reflect the absolute configuration of the molecules labeled (*R*) or (*S*).

When a chiral alkyl chain is introduced to the LC molecule which has a tendency to exhibit a nematic phase, it twists around the axis perpendicular to the director, resulting in the formation of a helical structure spontaneously. This twisted nematic phase is N* phase.

In the N* phase, specific selective reflection is observed. The characteristic phenomenon is originated from the helical structure of the N* phase and the helical pitch depends on the temperature of the LC system. Therefore, it has been demonstrated for the application to the thermal sensor. Moreover, the design of the luminescent LC molecules offers materials emitting circularly polarized light (CPL) and organic lasing media.

In the smectic phases, chiral alkyl side chains often generate a helical axis along the layer normal. In the smectic phases in which the director tilts to the layer normal, the director changes periodically along the layer normal (Figure 10b). Such a phase is called as a chiral smectic C (SmC*) phase. This phase exhibits ferroelectricity and the application to high speed displays was attempted.

Figure 1-51 shows molecular structures of chiral LC semiconductors. Kelly, O'Neil and coworkers developed a photoluminescent chiral nematic LC material **44**, as shown in Figure 1-51. Compound **44** exhibits glassy N* phase at room temperature and its thin film exhibits a reflection band with a wide wavelength range covering visible light region. The thin film emits high quality CPL fluorescence over a wide wavelength range. They have also studied on the carrier transport properties in the N* phase of the compound.¹⁸⁴

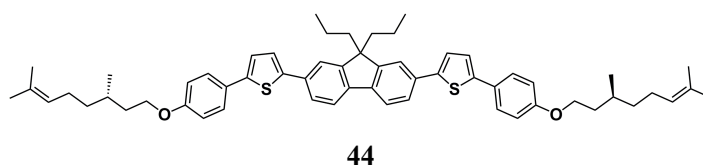


Figure 1-51. Photoconductive LC compounds bearing the chiral alkyl chain¹⁸⁴

As we describes in this section, the introduction of chirality to LC systems leads to the formation of the helical structures in which optical and electronic properties couple to create new opto-electronic functions.

1.4.2.4. Nanosegregated LC semiconductors based on oligosiloxane units

Goodby *et al.* first reported the LC compounds (**45-47**) bearing the disiloxane and cage-shaped silsesquioxane units in 1999 (Figure 1-52).¹⁸⁵ In this report, the cyanobiphenyl as the representative mesogen with the side chain modified by the siloxane moieties were synthesized and they studied the influence of the siloxane moieties on their LC properties. The stabilization of LC phases and drops of their melting points were observed. Their mesomorphisms are based on the formation of core-shell structures resulting from the nanosegregation between the siloxane moieties and the rigid biphenyl cores.

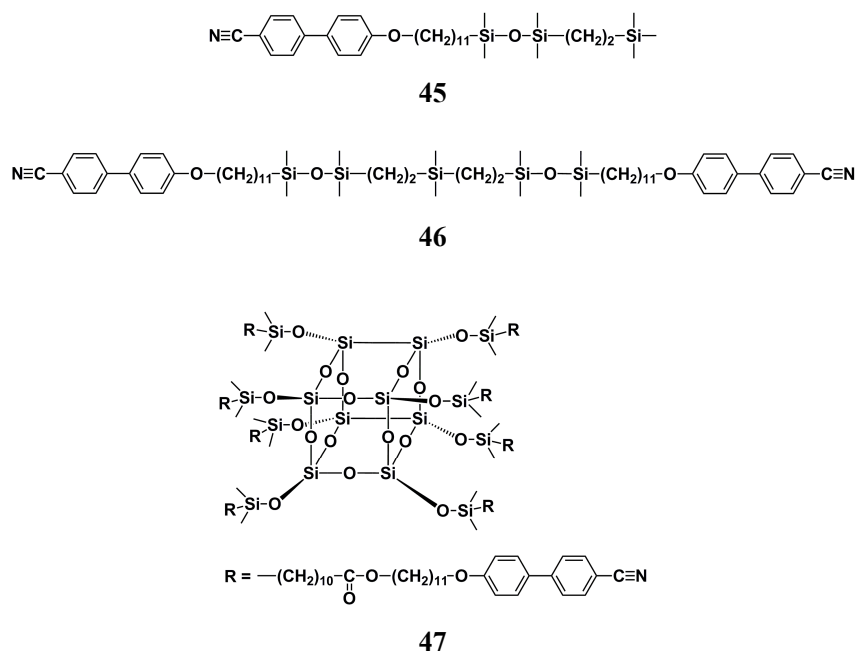


Figure 1-52. Chemical structures of LC cyanobiphenyl derivatives having oligosiloxane moieties¹⁸⁵

In past years, it has been revealed that the linear siloxane chains instead of the alkyl chains are effective to the stabilization of the LC phases. The rotational barrier of the siloxane bond is lower than that of the carbon-carbon bonds of the alkyl groups, and the dimethylsiloxane unit is bulkier than the methylene unit in alkyl chains. Apparently oligosiloxane units should have a tendency to destabilize the formation of LC phases. However, some experimental results described later have indicated that linear siloxane units contribute to the stabilization of the LC phases. This remarkable stabilization of LC phases should be owing to the nanosegregation between dynamic siloxane units and closely aggregated cores. The nanosegregation was driven by difference in the van der Waals interactions between the siloxane units and the π - π interactions between the cores. Based on this idea, some LC π -conjugated materials bearing the siloxane units have been designed and synthesized. Figure 1-53 shows molecular structures of LC PTCBI derivatives bearing oligosiloxane chains. LC PTCBI

derivatives (**48**, **49**) bearing four linear siloxane units were synthesized in our group. The LC PTCBI derivative (**49**) connected four trisiloxane moieties via swallow tail type linkers has lower melting point than the PTCBIs functionalized with normal alkyl chains. The columnar phases of LC PTCBIs are thermodynamically stable in a wide temperature range including a room temperature. They exhibit high electron mobilities up to $10^{-1} \text{ cm}^2 \text{ V}^{-1} \text{ s}^{-1}$ in the columnar phase at room temperature. In spite of this high electron mobility comparable to those of molecular crystals, the LC phases are soft at room temperature and soluble even in nonpolar solvents. Uniaxially aligned thin films can be produced on friction-transferred substrates by a spin-coating method. This efficient electron mobility should be attributed to a nanosegregated columnar structure. In the LC phase, one-dimensional stacking aggregates of π -conjugated cores is formed and they are surrounded by liquid-like mantle consisting of disordered oligosiloxane chains.¹⁸⁶

Moreover, a hybridized LC system with a polar substituent and oligosiloxane units has been reported. The PTCBI derivative (**50**) bearing two disiloxane units and a triethylene oxide chain was synthesized. This PTCBI derivative exhibits a smectic phase at room temperature, which has a bilayer structure and can form the complex with Li ion maintaining the LC structures.¹⁸⁷ In this LC phase of this compound, ion-conductive and electron-conductive layers are assembled separately on nanometer scale through nanosegregation.

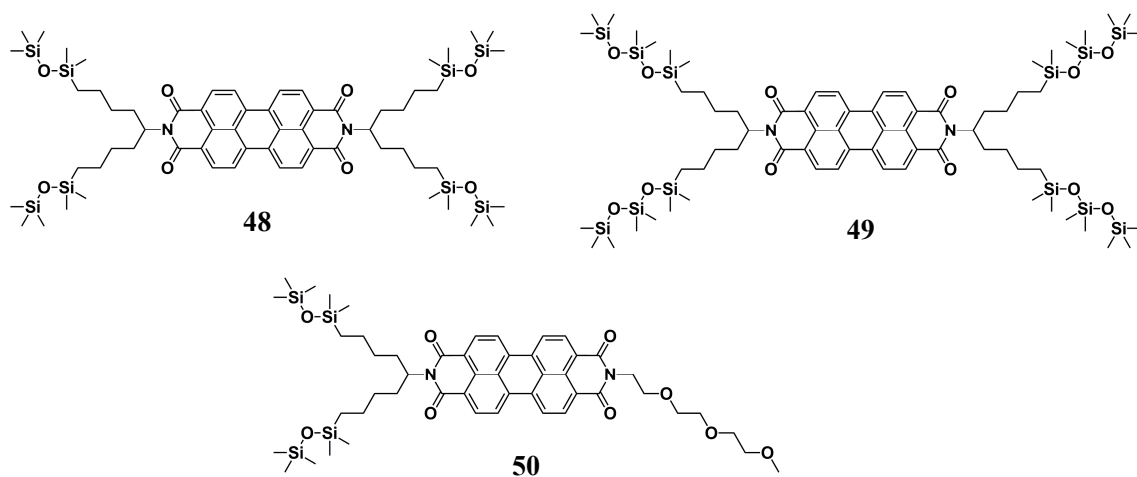


Figure 1-53. LC PTCBIs bearing linear oligosiloxane chains^{186, 187}

Not only linear oligosiloxane chains, but cyclic oligosiloxane moieties can also function as side chains of LC molecules. We have demonstrated the introduction of polymerizable siloxane rings to PTCBI and oligothiophene skeletons in order to stabilize the LC structures (Figure 1-54). The PTCBI derivative (**51**) bearing the four cyclotetrasiloxane units through the branched linkers exhibit the rectangular columnar disordered (Col_{rd}) phase in a wide temperature range including room temperature. Interestingly, the LC PTCBI derivative transitions around $-35 \text{ }^\circ\text{C}$ to the LC glass state

without crystallization. While maintaining the softness originated from core-shell type supramolecular organization, the electron mobility at room temperature exceeds the order of $10^{-2} \text{ cm}^2 \text{ V}^{-1} \text{ s}^{-1}$.¹⁸⁸ Apparently the cyclotetrasiloxane rings are bulky and should inhibit LC molecular order. However, LC phases are stabilized over wide temperature ranges for oligothiophene and PTCBI derivatives. We can design electronic functional materials which exhibit the LC phases over wide temperature ranges, considering the volume balance between the core, chains and rings.

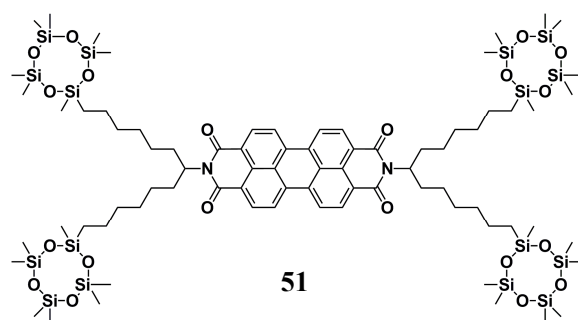


Figure 1-54. LC π -conjugated compounds bearing cyclic siloxane units¹⁸⁸

1.4.3. Physics of LC semiconductors¹⁸⁹

Carrier transport of LC semiconductors is generally explained by diverting the mechanism models for molecular crystals and amorphous solids. It is noted that both models are not perfectly applicable for LC semiconductors. Electronic structures in the molecular aggregation state depend on the molecular packing and ordered structures. In organic molecular crystals with highly oriented and arranged, band structures are generated due to overlaps between many molecular orbitals. The bandwidth is generally narrow and on the orders of 10^{-1} - 10^2 meV. Unlike inorganic crystalline semiconductors, charge carriers in organic molecular crystals are tightly bound in the molecular potential. Electron conduction in solid state is physically explained by two different conduction mechanisms, that is band conduction and hopping conduction. Charge carrier mobilities are drastically changed according to their contributions. In general, band conduction can be realized in the highly pure single-crystalline semiconductors and leads to high carrier mobilities exceeding $10^{-1} \text{ cm}^2 \text{ V}^{-1} \text{ s}^{-1}$. In contrast, charge carriers in amorphous solids or crystalline materials with low purity should be transported by hopping conduction exhibiting low carrier mobilities. The disturbance of energy levels hinders fast band conduction and results in charge transport by the hopping mechanism. The difference of carrier transport mechanism is reflected to temperature- and electric field-dependence of carrier mobilities.

In general, carrier mobility (μ) is defined as equation 1-19 and 1-20, where v_{th} , m^* , e , τ and F are thermal speed, effective mass, elementary charge, carrier relaxation time and electric field intensity, respectively.

$$v_{th} = \frac{e}{m^*} \tau F \quad \text{[Equation 1-19]}$$

$$\mu = \frac{e}{m^*} \tau \quad \text{[Equation 1-20]}$$

Carrier mobility is strongly affected by the transfer integral between proximity molecular orbitals. In band conduction model, band width (B) is linear proportion to the transfer integral. Therefore, equation 1-20 can be rewritten as follows.

$$\mu = \frac{e}{m^*} \tau \propto B \quad \text{[Equation 1-21]}$$

Theoretically, the correlation between carrier mobility (μ) and absolute temperature (T) in the band conduction model is given by the following equation, where λ and v_{th} are mean free path and thermal speed respectively.¹⁹⁰

$$\mu \propto \frac{\lambda}{v_{th}} \propto T^{-\frac{3}{2}} \quad \text{[Equation 1-22]}$$

The above equation does not usually fit temperature dependence of carrier mobilities for real organic molecular crystals. The experimental result for crystalline materials with high purity revealed that carrier transport by hopping occurs in high temperature region and band conduction was generated in a low temperature region. Thus, the correlation between absolute temperature and carrier mobilities can be described as follow equation.¹⁹⁰

$$\mu \propto T^{-\left(\frac{3}{2}+n\right)} \quad \text{[Equation 1-23]}$$

For band conduction in which there are shallow trap sites and the detrapping process is rate-limiting, Hoesterey-Letson (HL) model has been proposed as equation 1-24, where μ_0 , N_T , N_0 and E_T indicate Intrinsic carrier mobility, number of carrier trap sites, number of transport sites (number of molecules) and potential energy of trap level, respectively.¹⁹¹

$$\ln \left[\frac{\mu_0(T)}{\mu(T)} - 1 \right] = \ln \left(\frac{N_T}{N_0} \right) + \frac{E_T}{k_B T} \quad \text{[Equation 1-24]}$$

According to HL model, temperature dependence of carrier mobilities is defined by the balance between the phonon scattering and the detrapping behaviors.

For band conduction, carrier mobilities are basically independent to electric field except for the high-field condition.¹⁹²

On the other hand, hopping conduction shows different temperature- and field-dependence of carrier mobilities. Carrier transport in organic crystalline system by hopping conduction is explained by polaron hopping model^{192a} and Marcus theory.¹⁹³

In energetically and structurally disordered system dominated by hopping conduction, charge carriers are localized for most times in transport process. The localization of charge carriers can be considered as the expression of local radical cation or radical anion. The radical species are stabilized by formation of polaron states. Carrier transport by the hopping mechanism can be regarded as

propagation of the polaron state. The hopping probability of polarons (P_H) is described by the following equation 1-25 as a function of absolute temperature (T) and electric field strength (F) with using polaron binding energy (P_H).^{192a}

$$P_H \propto \exp\left(-\frac{E_p}{k_B T} + \frac{e F E_p}{2 k_B T}\right) \quad \text{[Equation 1-25]}$$

Temperature- and field-dependence of carrier mobilities in this condition follow the equation 1-26 by using averaged intermolecular distance (a).

$$\mu = \mu_0 \cdot \exp\left(-\frac{e^2 a^2 F^2}{8 E_p k_B T}\right) \frac{\sinh\left(\frac{e a F}{2 k_B T}\right)}{\left(\frac{e a F}{2 k_B T}\right)} \quad \text{[Equation 1-26]}$$

Marcus theory describes charge transfer rate between donor and acceptor species from electromagnetic consideration. Although Marcus theory originally describes the behaviors of charged species in a polar solvent, charge transfer reactions shows typical Arrhenius-type temperature dependence. Because the carrier hopping probability in organic solids is linearly correlated to the theoretical model, Marcus theory is sometimes utilized on discussion of carrier mobilities. It should be noticed that temperature-dependence of carrier mobilities in organic solids does not always shows Arrhenius-type behavior and is not always applicable of the theory. Charge transfer rate (k) based on Marcus theory can be expressed as following equation, where h , J , λ and ΔG_0 indicate Planck coefficient, the degree of molecular orbital coupling between initial and final conditions, rearrangement energy of electronic state associated with charge transfer and free energy change of the reaction, respectively.¹⁹³

$$k = \frac{4\pi^2 |J|^2}{h \sqrt{4\pi\lambda k_B T}} \cdot \exp\left[-\frac{\lambda}{4k_B T} \left(1 + \frac{\Delta G_0}{\lambda}\right)^2\right] \quad \text{[Equation 1-27]}$$

For hopping conduction in amorphous solids, Miller-Abrahams model,¹⁹⁴ Mott theory¹⁹⁵ and Gaussian disorder model¹⁹⁶ have been suggested. In the Gaussian disorder model assumes a density of state (DOS) for explanation of hopping rate of charge carriers. In this model, carrier transport between adjacent hopping sites with Gaussian energy state distribution is considered. Here, standard deviation of energy dispersion is defined as σ . Temperature dependence of hopping mobility in the Gaussian disorder model is shown by following equation.

$$\mu(T) \propto \exp\left[-\left(\frac{2\sigma}{3k_B T}\right)^2\right] \quad \text{[Equation 1-28]}$$

Given that the hopping probability is expected to increase under the presence of an electric field, hopping mobility is expressed by Equation 1-29 as a function of the electric field and absolute temperature.

$$\begin{aligned} \mu &= \mu_0 \cdot \exp\left[-\left(\frac{2\sigma}{3k_B T}\right)^2\right] \cdot \exp\left[C(\sigma^2 - \Sigma^2)F^{\frac{1}{2}}\right] \quad (\Sigma > 1.5) \\ \mu &= \mu_0 \cdot \exp\left[-\left(\frac{2\sigma}{3k_B T}\right)^2\right] \cdot \exp\left[C(\sigma^2 - 2.25)F^{\frac{1}{2}}\right] \quad (\Sigma < 1.5) \end{aligned} \quad \text{[Equation 1-29]}$$

In this equation, μ_0 is prefactor and C is constant. Σ indicates positional disorder and reflects fluctuations of geometry on molecular arrangement. $F^{1/2}$ is included as a result of Pool-Frenkel type carrier propagation.¹⁹⁷

Some LC semiconductors exhibit high carrier mobilities exceeded $10^{-1} \text{ cm}^2\text{V}^{-1}\text{s}^{-1}$ around room temperature.^{139i, 144f, 150c, 186b, 198} The order of carrier mobility reaching $10^{-1} \text{ cm}^2\text{V}^{-1}\text{s}^{-1}$ is located on the borderline of band-like conduction and hopping conduction.¹⁹⁹ These high carrier mobilities are realized in the high-ordered columnar or smectic LC phases.

In most case of LC semiconductors, carrier transport is realized by hopping mechanism, due to structural and energetic disorders by thermal fluctuation.²⁰⁰ Temperature- and electric field-dependence of carrier mobilities are case by case.

In N and N* phase, the thermal-activated tendency is usually observed.²⁰¹ The average intermolecular distance in N (N*) phases is relatively longer than those in the other LC phases. In addition, π - π interactions between the central π -conjugated cores are weak in N (N*) phases. Therefore, the transfer integral (overlap between π -molecular orbitals) is small. Since hopping of carriers occurs with high probability in the condition that central π -conjugated cores are close, carrier transport is activated in high temperature region in which molecular motion is vigorous. Thus, carrier mobilities show positive temperature dependency.

In some cases, negative temperature dependency of carrier mobilities is observed in LC phases.²⁰² In this case, hindering effect for carrier propagations seems to be dominant rather than the promoting effect by thermal activation. The essence of hindering effect is phonon scattering accompanying grating vibrations. The negative effect is originated from the decrease of the transfer integral due to the vigorous molecular motion. The negative tendency of carrier mobilities to temperature can be observed in the mesophase with the dense aggregation structures with few deep trapping sites.

In another case, temperature-independence of mobilities can be observed.²⁰³ It is considered that thermal activation and disturbance effects are balanced in this situation.

1.5. Ferroelectric liquid crystals^{81h, 83c, 204, 205}

McMillan described the speculation on the possibility of ferroelectric liquid crystalline phases in 1973.²⁰⁶ After showing this theoretical consideration, Meyer *et al.* reported the first experimental result of FLC system by using a chiral 4-((4-decyloxybenzylidene)amino)cinnamate derivative frequently called as abbreviation "DOBAMBC" in 1975 (as described in 1.3.2.2, Figure 1-28, left).¹⁸ Most ferroelectric liquid crystals can be classified as order-disorder-type ferroelectrics,⁸⁷ with the exception of FLC surfactant complexes based on phosphonium salts.²⁰⁷ Anyway, the structural symmetry breaking is indispensable to exhibit ferroelectricity.

Most of ferroelectric liquid crystals, including DOBAMBC, are based on chiral smectic LC system. The essential requirements for chiral smectic FLC compounds are as follows.²⁰⁸

- 1) LC molecules must have chiral atoms and are not racemic.
- 2) The molecules must have a component of permanent dipole perpendicular to the long axis (parallel to the short axis).
- 3) They must form tilted smectic structures.

The above two requirements can be easily reflected to molecular design and synthetic routes. However, the satisfaction of last requirement is the most difficult because it is difficult to predict the phase transition behaviors and their self-assembled structures strictly. Since the molecular design reflects the empirical rules, usually several kinds of analogous compounds is synthesized and evaluated.

The expression mechanism of ferroelectric property is based on the precession of LC molecules. As described in former section, the helical structures are formed on the electrically neutral state in SmC* phase (Figure 1-55, center). The formed helical structures reflect the molecular chirality on the LC molecules. In this neutral state, the random arrangement of the individual dipoles cancels each other for an overall dipole moment of zero. When a DC bias is applied, the dipoles can be aligned to compensate for the external electric field. As a result, polarized smectic structures are formed. The polarization produces an internal electric field in the whole (Figure 1-55, left and right). After removing the external bias, polarization are retained. The polarization can be inverted by the application of reverse bias. Thus, the chiral smectic LC compounds can exhibit ferroelectric nature.

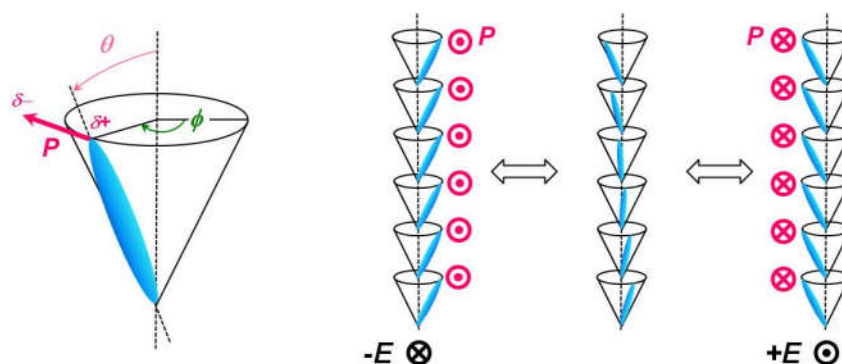


Figure 1-55. Schematic illustrations of molecular orientation in SmC* phase under the external field.

Characteristics in chemical structures of typical ferroelectric liquid crystal compounds are shown below. The basic strategy of molecular design is followed the conventional calamitic LC models. The remarkable features are that molecules have chiral side chain(s) and polar group(s) such as fluorine group on the lateral position.

The first FLC compound DOBAMBC is Schiff's base derivatives modified with chiral alkyl ester.¹⁸ Inspired from DOBAMBC, some FLC Schiff's bases were developed as shown in Figure 1-56.²⁰⁹

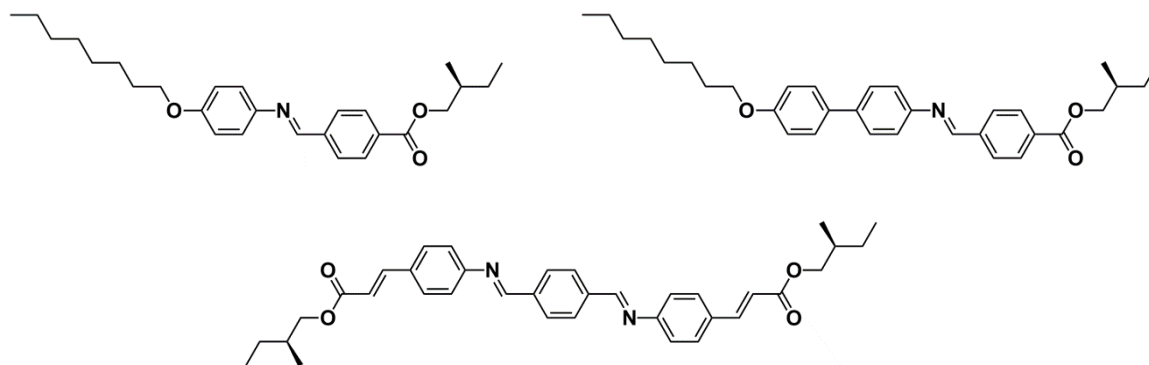


Figure 1-56. Chemical structures of FLC Schiff's bases compounds.²⁰⁹

Schiff's bases are generally poor in chemical stability because they are hydrolyzable. For improving the chemical stability, some azoxy- and azo-based FLC compounds were developed (Figure 1-57).²¹⁰

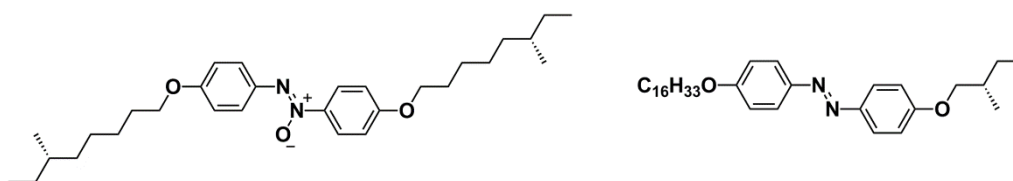


Figure 1-57. Chemical structures of typical azoxy- and azo-based FLC compounds.²¹⁰

FLC compounds based on conventional biphenyl and cyclohexane skeletons were also studied (Figure 1-58).²¹¹

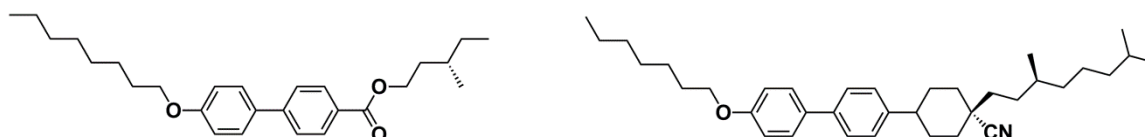


Figure 1-58. Chemical structures of FLC biphenyl derivatives.²¹¹

For increase of the pontaneous polarization, a lot of FLC compounds in which ester units are arranged in the center of core unit are reported (Figure 1-59).²¹²

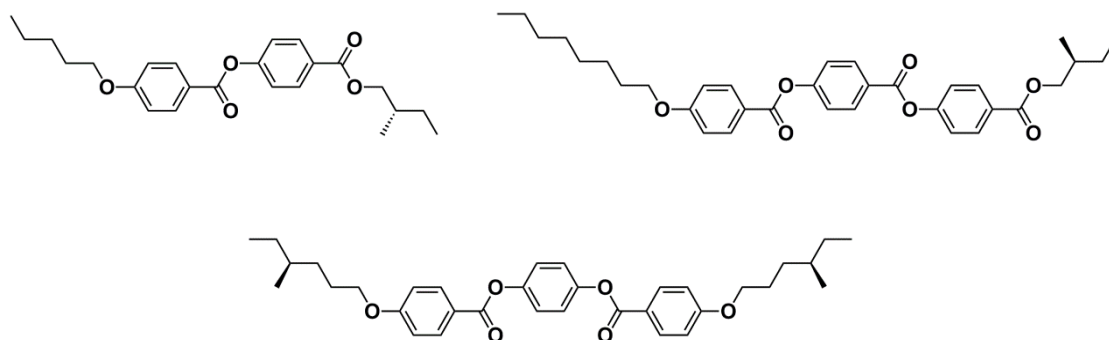


Figure 1-59. Chemical structures of FLC biphenyl derivatives.²¹²

FLC compounds containing the heterocycle unit are also reported (Figure 1-60).²¹³

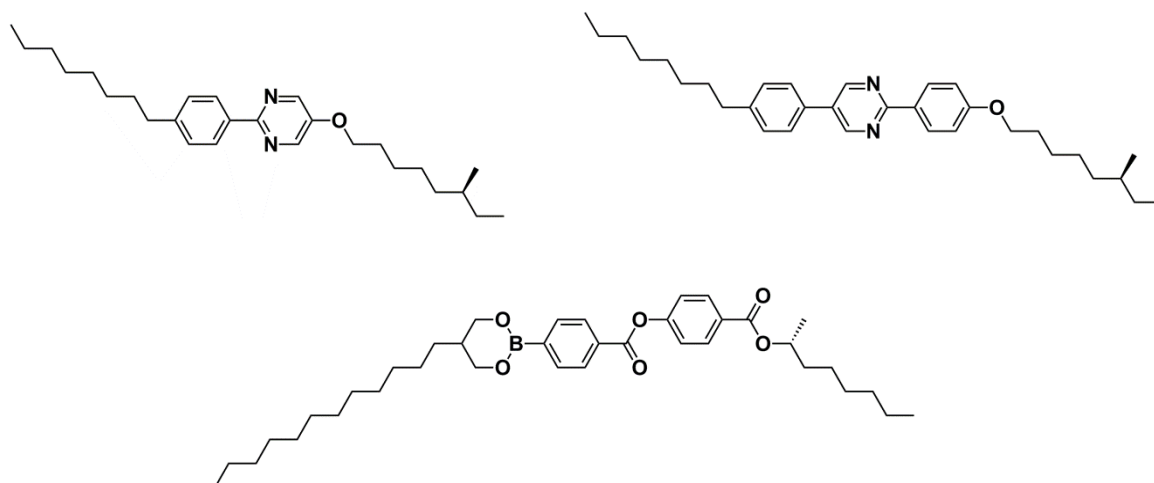


Figure 1-60. Chemical structures of FLC compounds containing the heterocycle unit.²¹³

As displayed above, many FLC compounds are bearing ester groups as polar unit. Some FLC system introducing the different polar units such as fluorine, chlorine, bromine and cyano groups were also developed (Figure 1-61).²¹⁴

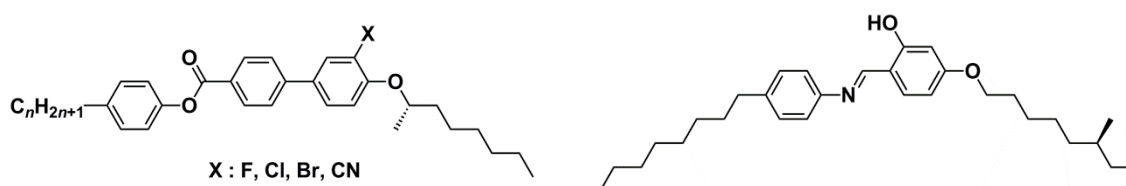


Figure 1-61. Chemical structures of FLC compounds bearing the additional polar units.²¹⁴

Focussing on the origin of chiral unit, alcohol, lactate, amino acid, chiral epoxide and fluorinated side chains are selected as chiral origins. The representative chiral moieties for FLC compounds are shown in Figure 1-62.

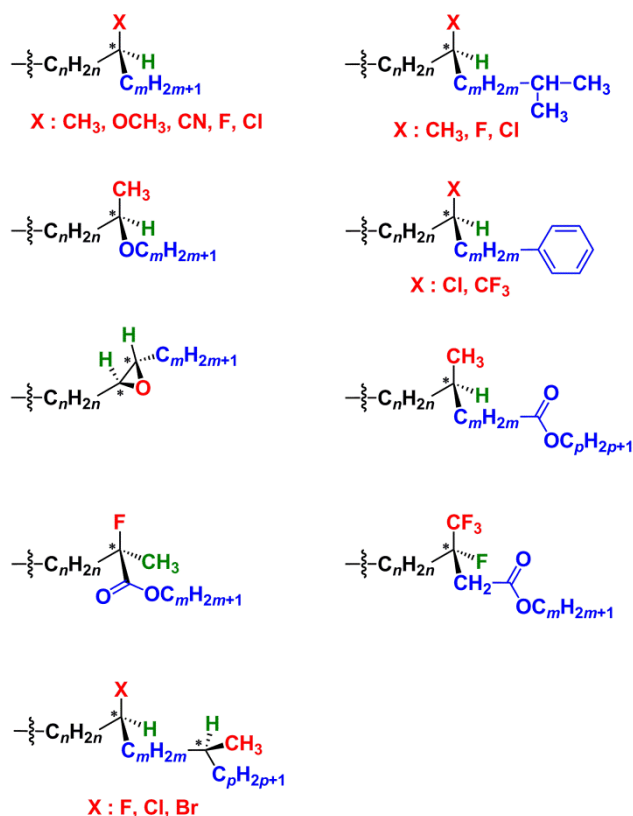


Figure 1-62. Chemical structures of typical chiral units for chiral smectic-based FLC compounds.

Dispite of normal alkyl chains, another types of side chains can be applied to FLC system. As shown in Figure 1-63, FLC molecules bearing a disiloxane or trisiloxane unit have been reported. These ferroelectric LC materials exhibit temperature-independent interlayer distances.²¹⁵

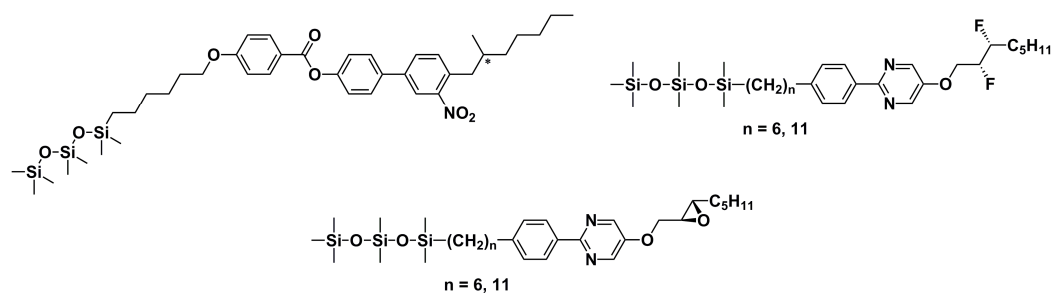
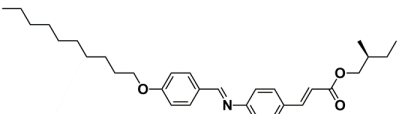
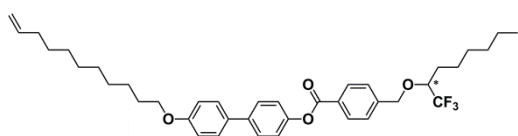
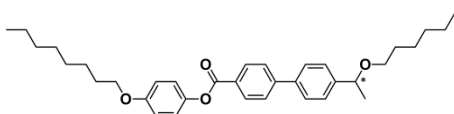
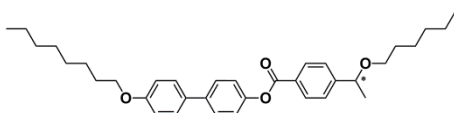
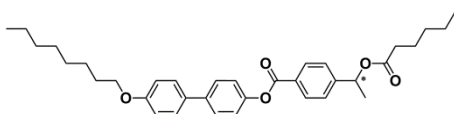
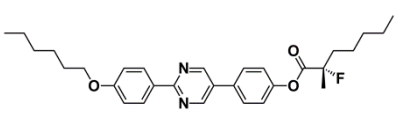
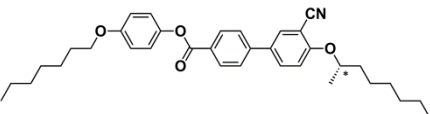
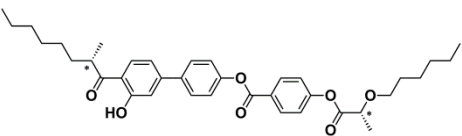


Figure 1-63. FLC compounds bearing a linear oligosiloxane chain.²¹⁵

In general, the values of spontaneous polarization for FLC compounds are on the orders of 10^0 – 10^2 nC cm⁻². For improving the value of spontaneous polarization, many researchers synthesized and investigated variety of FLC materials. As a result, the empirical molecular design strategy for realizing the large spontaneous polarization in FLC system was developed.

The typical FLC materials showing the large spontaneous polarization are listed up in table 1-10.²¹⁶

Table 1-10 The values of spontaneous polarization for typical FLC materials.²¹⁶

| Entry | Compounds | P_s / nC cm ⁻² |
|------------------------|--|-----------------------------|
| 1 (Reference: DOBAMBC) |  | 2–5 |
| 2 |  | 76 |
| 3 |  | 48 |
| 4 |  | 114 |
| 5 |  | 250 |
| 6 |  | 400 |
| 7 |  | 190 |
| 8 |  | 1130 |

For realizing the large spontaneous polarization, some key points of molecular design are suggested as follows.

- (1) The distance between mesogenic core and chiral carbon atom.
- (2) The number of chiral units.
- (3) Rotation barrier by introduction of lateral substituents and bulky rings.
- (4) Polar unit with large dipole moment on the chiral atoms.

To my best knowledge, the maximum record on the spontaneous polarization in the FLC system is $1.1 \times 10^3 \text{ nC cm}^{-2}$ of the FLC compound shown in Table 1-10, entry 8. It is noted that the spontaneous polarization can change by the molecular arrangement, domain size, LC film thickness and purity as well as measurement conditions and methods. In addition, the ferroelectric property is strongly influenced by structural disorder, viscosity and molecular packing in the chiral smectic phase. Therefore,

Although details are omitted, a bent-core-type FLC system based on a unique aggregate structure of an achiral bent-shaped molecule (Figure 1-64) and ferroelectric columnar liquid crystals (Figure 1-65) have been also developed.^{217, 218}

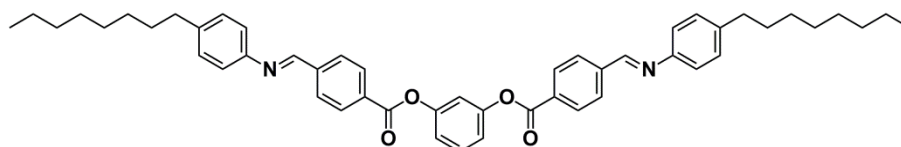


Figure 1-64. A chemical structure of bent-shaped FLC compounds.²¹⁷

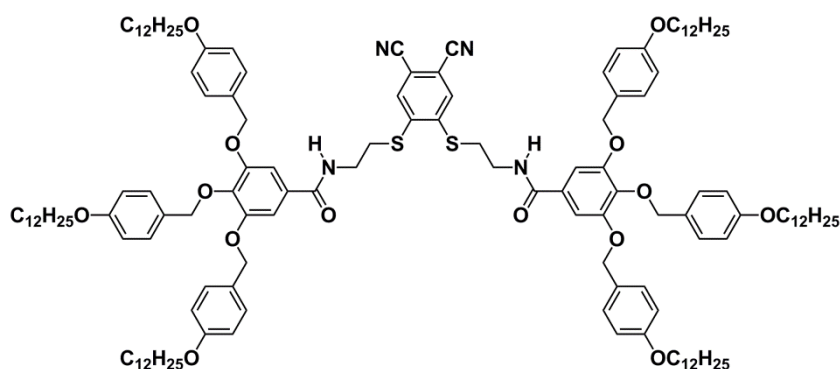


Figure 1-65. A chemical structure of ferroelectric columnar liquid crystals.²¹⁸

1-6. Multi-functional materials

In general, most of present tools and equipments are composed of various units, for which every different functions are required. Thus, they are not composed of only single material. As constructing equipment systems exhibiting advanced and complex functions, the simplest approach is to select and arrange every parts corresponding to each functions according to their applications. If high functional equipment is constructed by the method, however, the whole system becomes bulky and heavy depending on the quantity of parts. Therefore, the integration of some different functions is one of the attractive approaches for the development of advanced system complexes. The application of the integration strategy to materials as basic units of each parts results in multi-functional materials. The multi-functional materials expand the diversity of material systems.

There are some strategies for constructing the multi-functional system. The simplest strategy is based on the mixtures system. In a simple composite system, the dispersibility of each functional component is a critical challenge to be overcome in order to balance each of functions.

The other strategy is that the introduction of several different functional units into a single molecule. Single molecular system composed of several functional units can be an effective approach to the challenge of function compatibility. The segregation of incompatible functional moieties in block molecules leads to the formation of various self-assembled supramolecular structures depending on the volume fractions of the incompatible units and intermolecular interactions. The microphase separation behavior in block copolymer system forms the sub-micron scaled channel structures through the self-organization process. Liquid-crystalline (LC) system provides the dynamic nanosegregated suprastructure which act in the nanometer-scale order.

1.7. Photovoltaic effect

1.7.1. Conventional photovoltaic effect²¹⁹

Conventional photovoltaic effect is based on Schottky's junction or p-n heterojunction. The energy levels of metal are different from those of semiconductors. When metal and semiconductor are contacted, their Fermi levels become equal immediately by inducing the electron transfer at the interface. Thus, the internal built-in potentials are generated near the interface. Here, the case of contact between metal and p-type semiconductor is regarded. In the case of using the p-type semiconductor which has shallow HOMO level than Fermi level of metal, Ohmic junction is generated after the contact of the semiconductor and metal. On the other hand, Schottky's junction is produced by contact of metal with semiconductor having deep HOMO level than Fermi level of metal. For Schottky's junction based on the metal—p-type semiconductor contact, the direction of charge carrier transport is limited to one direction. The rectification behaviours are applicable to diodes. In addition, the built-in potential promotes the charge-separation and leads to the photovoltaic effect. It is noted that Ohmic junction and Schottky's junction are also formed in the couple with

metal and n-type semiconductor.

Next, the contact p-type semiconductor with n-type semiconductor is considered. The energy levels of p- and n-type semiconductors are also different. Therefore, the contact of these semiconductors induces the electron transfer at the interface. The built-in potential is also produced by p-n heterojunction. The rectification and photovoltaic effects can be also observed.

The conventional photovoltaic effect is based on these Schottky's junction or p-n heterojunction. The mechanism of conventional photovoltaic effect is explained as follows. In the first step, excitons are generated by the light absorption. Then, charge separations from excitons are promoted by the internal field originated from heterojunctions. The generated charge carriers transport to two electrodes. Finally, the carriers are collected as electrical power in electrodes.

This mechanism of conventional photovoltaic effect is applicable to both inorganic semiconductors and organic systems. However, the diffusion distance of excitons is quite different between inorganic and organic systems. The photoexcitons in organic semiconductors cannot diffuse exceeding around 10 nm in most cases. Charge separation occurs at the heterojunction interface. Because most of excitons generated by photoexcitation annihilate, the charge generation efficiency becomes low. For the improvement of charge separation efficiency, bulk-hetero junction and similar junctions with micro interface structures have been developed.²²⁰ In addition, the other drawback of conventional photovoltaic effect is the limitation of output (open circuit) voltage. The open circuit voltage is limited to the band-gap of active materials. Therefore, photovoltaic devices showing high output voltage is unrealistic for the simple single unit cell.

1.7.2. Anomalous photovoltaic effect²²¹

Anomalous photovoltaic (APV) effect is defined as band-gap-independent photovoltaic effect. The first report on this specific phenomenon was described by Starkiewicz and co-workers in 1946 for PbS films.²²² Following this first report, similar observations were reported for polycrystalline film of CdTe, ZnTe and InP.²²³⁻²²⁵ It is scientifically valuable and interesting that the photovoltaic effect observed with these inorganic thin films has resulted in a large photovoltage which is more than two to three orders of magnitude larger than the band gap. However, the reproducibility of these phenomena was very low. This drawback came from the fact that such a strange phenomenon is observed under the singular sample conditions. The common point in these reports is that the anomalous phenomena were observed in thin films deposited on angularly inclined substrates under the heating condition.

The mechanism of APV effect can be roughly explained by the model of inhomogeneity in the charge distribution. The inhomogeneity can be generated by some situations. The situations are generally explained by some categorized models.

The Dember effect is a phenomenon in which an electric field is generated due to the difference in diffusion speed between holes and electrons in photoconductive materials. In the surface of the photoconductive materials, a pair of positive and negative charge carriers (holes and electrons) is

generated by light illumination. In many cases, electron diffusion is faster than hole diffusion. Thus, the difference between electron and hole diffusion rates induces the internal electric field and results in an photovoltage derived from the inhomogeneous density distribution of holes and electrons in the active materials.²²⁶ This unique phenomenon is also called “photo Dember effect”²²⁷ or “light diffusion effect”²²⁸.

Ionic impurities and asymmetric aliovalent defects or dopant also cause inhomogeneous environment and form the internal electric field for charge separation. As the generated charge is transported to the electrode, APV effect can be developed.²²⁹

Ferroelectric domains have a large internal electric field originated from spontaneous polarization. Some ferroelectric materials also exhibit the APV effect. The typical ferroelectric exhibiting the APV effect is BiFeO₃. In the single-crystalline BFO films which precisely controlled the crystal orientation, the realization of high open circuit voltage exceeding 10 V was achieved.²³⁰ It is noted that high vacuum process and precise condition are required for preparation of the suitable thin films.²³¹

Most of study is based on the inorganic ferroelectric system. The study on APV phenomena in organic ferroelectrics is limited as two reports.²³²

1.8. Objective of this thesis

Our group focus on the development of multifunctional LC semiconductors based on nanosegregated LC supramolecular systems. The most important concept of nanosegregated functional LC materials is how to compete and arrange the several intermolecular interactions by the suitable molecular design. Not only the molecular shape, aspect ratio and substitution positions but also the kinds of π -conjugated unit, additional functional units and suitable flexible side chains is important issues for the molecular design.

In this doctor thesis, the molecular design philosophy is refelcted to the development of π -conjugated ferroelectric liquid crystals. Moreover, APV effect in the π -conjugated FLC system, which is coupled with charge transporting property based on the extended π -conjugated site and spontaneous polarization derived from ferroelectricity, is investigated. For construction of multifunctional materials, the study described in this thesis is considered to provide an example of demonstrations with the single component soft material system with several different functional units.

The essential point in this study is how to break the symmetry of the aggregation structure and how to hold it below. As described in former section, chiral LC systems provide the one approach for the structural symmetry breaking.

Recently, our group developed (*R*)- and (*S*)-dimers based on phenylterthiophene skelton exhibit the N* phases (Figure 1-66). In the mixtures of the (*R*)- and (*S*)-enantiomers, the helical pitches were tuned by changing the composition ratio of the both enantiomers. As optimizing the composition so that the reflection band covers the luminescent band of the phenylterthiophene core, the prominent

CPL emission was observed.²³³ It should be considered that this chiral LC oligothiophenes shows one application of chiral LC semiconductors.

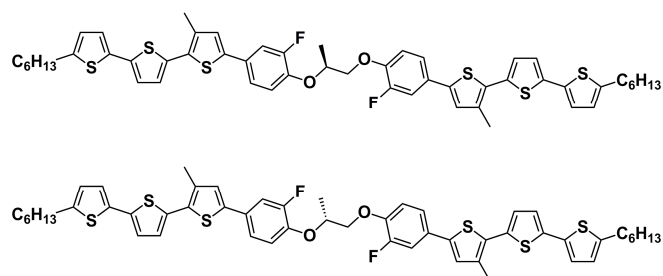


Figure 1-66. Chemical structure of chiral LC semiconductors exhibiting CPL emission.²³³

Another function of the chirality is breaking the symmetry of the systems, which is a key in this study. In the ferroelectric phase, a macroscopic polarization is induced by the application of the DC bias and the spontaneous polarization is maintained after switching off the bias. Recently, fluorophenylterthiophene derivatives exhibiting the hole transport property in the ferroelectric SmC* phases were developed (Figure 1-67).²³⁴ In this system, APV-like response was observed. This photovoltaic response should be caused by the internal electric field derived from the spontaneous polarization of the ferroelectric materials while the conventional photovoltaic effect is originated from the built-in potential formed at p-n junction.²²¹ However, the mechanism of the photovoltaic response has not been clarified.

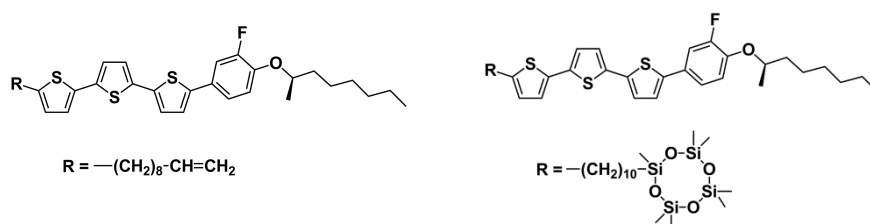


Figure 1-67. Chemical structures of FLC fluorophenylterthiophene derivatives.²³⁴

Based on the above, some smectic LC systems based on chiral phenylterthiophene derivatives were investigated for exploring the possibilities of APV effect in LC system.

1.9. Outline of this thesis

Following the general introduction as described in this chapter (Chapter 1), the APV phenomena in some LC phases based on phenylterthiophene derivatives will be discussed.

In chapter 2, the study on the APV response of analogous compounds will be described. The spontaneous polarization and carrier mobilities are strongly affected by the disorder of the molecular aggregation structure. Chiral phenylterthiophene derivatives with a different side chain moiety were designed and synthesized. As the introduced side chain unit, a hexenyl group with a small steric hindrance and a bulky cyclic siloxane moiety were selected. These two compounds exhibit ferroelectric chiral smectic C phases, in which carrier mobilities are different magnitude. From the comparison of the APV response between these compounds, the relationship between their APV photocurrents, spontaneous polarizations, and carrier mobilities was investigated.

In chapter 3, the influence of the molecular chirality to the APV phenomena will be discussed by the study on LC enantiomer mixtures with some different composition. While spontaneous polarization linearly depends on the enantiomer purity, carrier mobility is independent to the enantiomer composition. The direct evidence of the correlation between the spontaneous polarization and APV effect was indicated.

In chapter 4, the fixation of polarization state was investigated by the applying of surface stabilization technique and the structural immobilization method through the phase transition under DC bias.

Finally, overall conclusion and some perspectives will be given in chapter 5.

1.10. References

1. F. Wöhler, *Annalen der Physik und Chemie*, 1828, **88**, 253.
2. Reactions and Syntheses: In the Organic Chemistry Laboratory, 2nd, Completely Revised and Updated Edition, Edited by L. F. Tietze, T. Eicher, U. Diederichsen, A. Speicher and N. Schutzenmeister, Wiley-VCH, Weinheim, 2014.
3. (a) S. C. Abeylath, S. Ganta, A. K. Iyer and M. Amiji, *Acc. Chem. Res.*, 2011, **44**, 1009. (b) S. Kango, S. Kalia, P. Thakur, B. Kumari and D. Pathania, *Adv. Polym. Sci.*, 2015, **267**, 283. (c) M. Šupová, G. S. Martynková and K. Barabaszová, *Sci. Adv. Mater.*, 2011, **3**, 1. (d) S. Savagatrup, A. D. Printz, T. F. O'Connor, A. V. Zaretski and D. J. Lipomi, *Chem. Mater.*, 2014, **26**, 3028.
4. T. Kato, N. Mizoshita and K. Kishimoto, *Angew. Chem. Int. Ed.*, 2006, **45**, 38.
5. (a) M. E. Lines and A. M. Glass, *Principles and Applications of Ferroelectrics and Related Materials*, Oxford, New York, 2001. (b) M. Takashige, *Introduction to Materials Structure and Dielectric Physics (Ver. 5)*, Shokabo, Tokyo, 2013.
6. (a) M. Année, *Histoire de l'Académie des Sciences: Phisique Generale*, 1717, 7. (b) C. von Linné, *Flora Zeylanica: Sistens Plantas Indicas Zeylonae Insulae*, 1747, 8. (c) F. U. T. Aepinus, *Histoire de l'Académie royale des sciences et des belles lettres* (Berlin), 1756, **12**, 105. (d) D. Brewster, *Edinburgh J. Sci.*, 1824, **1**, 208.
7. (a) J. Curie and P. Curie, *Compt. Rend.*, 1880, **91**, 294. (b) J. Curie and P. Curie, *Compt. Rend.*, 1880, **91**, 383.
8. P. T. Moseley and A. J. Crocker, *Sensor Materials*, Institute of Physics Publishing, Bristol, 1996.
9. W. Känzig, *Solid State Phys.*, 1957, **4**, 1.
10. A. Lüker, *Sol-Gel derived Ferroelectric Thin Films for Voltage Tunable Applications*, VDM Publishing, Saarbrücken, 2010.
11. J. Valasek, *J. Phys. Rev.*, 1920, **15**, 537.
12. G. Busch and P. Scherrer, *Naturwiss*, 1935, **23**, 737.
13. A. von Hippel, R. G. Breckenbridge, F. G. Chesley and L. Tisza, *Ind. Eng. Chem.*, 1946, **38**, 1097.
14. B. Wul and J. M. Goldman, *C. R. Acad. Sci. URSS*, 1946, **51**, 21.
15. E. Sawaguchi, *J. Phys. Soc. Jpn.*, 1953, **8**, 615.
16. D. F. Rushman and M. A. Strivens, *Trans. Faraday Soc.*, 1946, **42**, A231.
17. G. J. Goldsmith and J. G. White, *J. Chem. Phys.*, 1959, **31**, 1175.
18. R. B. Meyer, L. Libert, L. Strzelecki and P. Keller, *J. Phys.*, 1975, **36**, L69.
19. (a) R. G. Kepler and R. A. Anderson, *J. Appl. Phys.*, 1978, **49**, 1232. (b) T. Furukawa, M. Date and E. Fukada, *J. Appl. Phys.*, 1980, **51**, 1135. (c) T. Furukawa, M. Date, E. Fukada, Y. Tajitsu and A. Chiba, *Jpn. J. Appl. Phys.*, 1980, **19**, L109.
20. (a) D. Katz and V. Gelfandbein, *J. Phys. D: Appl. Phys.*, 1982, **15**, L115. (b) A. J. Lovinger, *Science*, 1983, **220**, 1115. (c) T. Furukawa, *Phase Transitions*, 1989, **18**, 143.
21. (a) S. Horiuchi, R. Kumai and Y. Tokura, *Kotai Butsuri*, 2007, **42**, 283. (In Japanese)
22. (a) C. A. Beevers and P. W. Hughes, *Proc. Roy. Soc. (London)*, 1941, **177**, 251. (b) B. C. Frazer, M. McKeown and R. Pepinsky, *Phys. Rev.*, 1954, **94**, 1435. (c) F. sandy and R. V. Jones, *Phys. Rev.*, 1968, **168**, 481.

23. (a) E. C. Subbarao, *Ferroelectrics*, 1973, **5**, 267. (b) *Ferro- and Antiferroelectric Substances*, edited by K.-H. Hellwege and A. M. Hellwege, Springer-Verlag, Berlin, 1975.
24. (a) A. G. Boni, C. Chirila, L. Hrib, I. Pintilie and L. Pintilie, *Dig. J. Nanomater. Bios.*, 2015, **10**, 1257. (b) C. A. Randall, N. Kim, J. -P. Kucera, W. Cao and T. R. Shrout, *J. Am. Ceram. Soc.*, 1998, **81**, 677. (c) C. E. Zybill, *Mater. Sci. Eng. C*, 2001, **18**, 191.
25. J. C. Slater, *J. Chem. Phys.*, 1941, **9**, 16.
26. R. Blinc, *J. Phys. Chem. Solids*, 1960, **13**, 204.
27. I. P. Kaminow and T. C. Damen, *Phys. Rev. Lett.*, 1968, **20**, 1105.
28. K. K. Kobayashi, *J. Phys. Soc. Jpn.*, 1968, **24**, 497.
29. (a) R. S. Katiyar, *Phys. Rev. J. F. Ryan and J. F. Scott.*, 1971, **B4**, 2685. (b) N. Lagakos and H. Z. Cummins, *Phys. Rev. B*, 1974, **10**, 1063. (c) P. S. Peercy, *Phys. Rev. B*, 1975, **12**, 2725.
30. Y. Tominaga, H. Urabe and M. Tokunaga, *Sol. Stat. Commun.*, 1983, **48**, 265.
31. P. Simon, F. Gervais and E. Courtens, *Phys. Rev. B*, 1988, **37**, 1969.
32. H. Sugimoto and S. Ikeda, *Phys. Rev. Lett.*, 1991, **67**, 1306.
33. Y. Yamada, *J. Phys. Soc. Jpn.*, 1994, **63**, 3691.
34. (a) T. Matsuo, *J. Korean Phys. Soc.*, 1996, **29**, S409. (b) M. Fukai, A. Inaba, T. Matsuo, H. Suga and M. Ichikawa, *Sol. Stat. Commun.*, 1993, **87**, 939. (c) T. Matsuo, K. Kohno and M. Ichikawa, *J. Korean Phys. Soc.*, 1996, **29**, S432. (d) C. Totsuji and T. Matsubara, *Sol. Stat. Commun.*, 1998, **107**, 741. (e) S. P. Dolin, A. A. Levin, T. Y. Mikhailova, M. V. Solin, N. S. Strokach and N. I. Kirillova, *Int. J. Quant. Chem.*, 2004, **96**, 247. (f) S. P. Dolin, A. A. Khrulev, E. V. Polyakov, T. Y. Mikhailova and A. A. Levin, *Int. J. Quant. Chem.*, 2006, **106**, 2297. (g) S. P. Dolin, I. S. Flyagina, M. V. Tremasova, T. Y. Mikhailova, A. B. Gavriljuk and A. A. Levin, *Int. J. Quant. Chem.*, 2007, **107**, 2409. (h) A. A. Levin, S. P. Dolin and T. Y. Mikhailova, *J. Mol. Struct.*, 2008, **880**, 44.
35. A. J. Lovinger, *Science*, 1983, **220**, 1115.
36. (a) D. Katz and V. Gelfandbein, *J. Phys. D: Appl. Phys.*, 1982, **15**, L115. (b) S. C. Mathur, J. I. Scheinbeim and B. A. Newman, *J. Appl. Phys.*, 1984, **56**, 2419. (c) H. S. Nalwa, *J. Macromol. Sci., Rev. Macromol. Chem. Phys.*, 1991, **C31**, 341. (d) J. W. Lee, Y. Takase, B. A. Newman and J. I. Scheinbeim, *J. Polym. Sci. Polym. Phys.*, 1991, **29**, 273. (e) J. I. Scheinbeim, J. W. Lee and B. A. Newman, *Macromolecules*, 1992, **25**, 3729. (f) B. A. Newman, J. I. Scheinbeim, J. W. Lee and Y. Takase, *Ferroelectrics*, 1992, **127**, 1565. (g) B. Z. Mei, J. I. Scheinbeim and B. A. Newman, *Ferroelectrics*, 1993, **144**, 51. (h) T. Itoh, T. Tanaka, M. Hashimoto and T. Konishi, *Jpn. J. Appl. Phys.*, 1995, **34**, 6164.
37. (a) M. Mai, S. Ke, P. Lin and X. Zeng, *J. Nanomater.*, 2015, **16**, 181. (b) R. G. Kepler and R. A. Anderson, *Adv. Phys.*, 1992, **41**, 1. (c) H. S. Nalwa, *J. Macromol. Sci., Rev. Macromol. Chem. Phys.*, 1991, **C31**, 341. (d) *Ferroelectric Polymers: Chemistry: Physics, and Applications*, Edited by H. S. Nalwa, Marcel Dekker, Inc., New York, 1995.
38. (a) A. S. Tayi, A. Kaeser, M. Matsumoto, T. Aida and S. I. Stupp, *Nat. Chem.*, 2015, **7**, 281. (b) A. Katrusiak and M. Szafranski, *Phys. Rev. Lett.*, 1999, **82**, 576. (c) M. Szafranski, A. Katrusiak and G. J. McIntyre, *Phys. Rev. Lett.*, 2002, **89**, 215507.

39. S. Horiuchi, F. Ishii, R. Kumai, Y. Okimoto, H. Tachibana, N. Nagaosa and Y. Tokura, *Nat. Mater.*, 2005, **4**, 163.
40. (a) R. Kumai, S. Horiuchi, H. Sagayama, T. Arima, M. Watanabe, Y. Noda and Y. Tokura, *J. Am. Chem. Soc.*, 2007, **129**, 12920. (b) S. Horiuchi, R. Kumai and Y. Tokura, *Angew. Chem. Int. Ed.*, 2007, **46**, 3497.
41. S. Horiuchi, R. Kumai, Y. Tokunaga and Y. Tokura, *J. Am. Chem. Soc.*, 2008, **130**, 13382.
42. S. Horiuchi, Y. Tokunaga, G. Giovannetti, S. Picozzi, H. Itoh, R. Shimano, R. Kumai and Y. Tokura, *Nature*, 2010, **463**, 789.
43. (a) J. B. Torrance, J. E. Vazquez, J. J. Mayerle and V. Y. Lee, *Phys. Rev. Lett.*, 1981, **46**, 253. (b) A. Girlando and C. Pecile, *Sol. St. Commun.*, 1986, **57**, 891. (c) H. Okamoto, T. Mitani, Y. Tokura, S. Koshihara, T. Komatsu, Y. Iwasa, T. Koda and G. Saito, *Phys. Rev. B*, 1991, **43**, 8224. (d) H. Matsuzaki, H. Takamatsu, H. Kishida and H. Okamoto, *J. Phys. Soc. Jpn.*, 2005, **74**, 2925.
44. (a) Y. Iwasa, T. Koda, S. Koshihara, Y. Tokura and G. Saito, *Mol. Cryst. Liq. Cryst.*, 1992, **216**, 195. (b) M. Le Cointe, M.-H. Lemeé-Cailleau, H. Cailleau and B. Toudic, *J. Mol. Struct.*, 1996, **374**, 147. (c) M.-H. Lemeé-Cailleau, H. Cailleau and M. Le Cointe, *Ferroelectrics*, 1996, **183**, 123. (d) S. Horiuchi, R. Kumai and Y. Tokura, *J. Am. Chem. Soc.*, 1998, **120**, 7379. (e) S. Horiuchi, Y. Okimoto, R. Kumai and Y. Tokura, *J. Phys. Soc. Jpn.*, 2000, **69**, 1302. (f) S. Horiuchi, Y. Okimoto, R. Kumai and Y. Tokura, *J. Am. Chem. Soc.*, 2001, **123**, 665. (g) H. Kishida, K. Fujinuma and H. Okamoto, *Syn. Met.*, 2001, **120**, 909.
45. S. Horiuchi and Y. Tokura, *Nat. Mater.*, 2008, **7**, 357.
46. F. Kagawa, S. Horiuchi, M. Tokunaga, J. Fujioka and Y. Tokura, *Nat. Phys.*, 2010, **6**, 169.
47. K. Kobayashi, S. Horiuchi, R. Kumai, F. Kagawa, Y. Murakami and Y. Tokura, *Phys. Rev. Lett.*, 2012, **108**, 237601.
48. A. S. Tayi, A. K. Shveyd, A. C.-H. Sue, J. M. Szarko, B. S. Rolczynski, D. Cao, T. J. Kennedy, A. A. Sarjeant, C. L. Stern, W. F. Paxton, W. Wu, S. K. Dey, A. C. Fahrenbach, J. R. Guest, H. Mohseni, L. X. Chen, K. L. Wang, J. F. Stoddart and S. I. Stupp, *Nature*, 2012, **488**, 485.
49. (a) H. B. Cui, K. Takahashi, Y. Okano, Z. M. Wang, H. Kobayashi and A. Kobayashi, *Angew. Chem. Int. Ed.*, 2005, **44**, 6508. (b) H. B. Cui, Z. M. Wang, K. Takahashi, Y. Okano, H. Kobayashi and A. Kobayashi, *J. Am. Chem. Soc.*, 2006, **128**, 15074. (c) Q. Ye, Y.-M. Song, G.-X. Wang, K. Chen, D.-W. Fu, P. W. H. Chan, J.-S. Zhu, S. D. Huang and R.-G. Xiong, *J. Am. Chem. Soc.*, 2006, **128**, 6554. (d) H. B. Cui, B. Zhou, L. S. Long, Y. Okano, H. Kobayashi and A. Kobayashi, *Angew. Chem. Int. Ed.*, 2008, **47**, 3376. (e) C.-F. Wang, Z.-G. Gu, X.-M. Lu, J.-L. Zuo and X.-Z. You, *Inorg. Chem.*, 2008, **47**, 7957. (f) C.-F. Wang, D.-P. Li, X. Chen, X.-M. Li, Y.-Z. Li, J.-L. Zuo and X.-Z. You, *Chem. Commun.*, 2009, 6940. (g) G. Rogez, N. Viart and M. Drillon, *Angew. Chem. Int. Ed.*, 2010, **49**, 1921. (h) M. Guo, H. L. Cai and R. G. Xiong, *Inorg. Chem. Commun.*, 2010, **13**, 1590. (i) W. Zhang and R. G. Xiong, *Chem. Rev.*, 2012, **112**, 1163. (j) J. Li, Y. Liu, Y. Zhang, H. L. Cai and R. G. Xiong, *Phys. Chem. Chem. Phys.*, 2013, **15**, 20786. (k) K. Asadi and M. A. van der Veen, *Eur. J. Inorg. Chem.*, 2016, **2016**, 4332.
50. M. Pandeewar, S. P. Senanayak, K. S. Narayan and T. Govindaraju, *J. Am. Chem. Soc.*, 2016, **138**, 8259.

51. (a) *Handbook of liquid crystals, 2nd edition*, edited by J. W. Goodby, P. J. Collings, T. Kato, C. Tschierske, H. F. Gleeson and P. Raynes, Wiley-VCH, Weinheim, 2014. (b) *Handbook of Liquid Crystals*, edited by D. Demus, J. W. Goodby, G. W. Gray, H.-W. Spiess, V. Vill, Wiley-VCH, Weinheim, 1998. (c) *Thermotropic Liquid Crystals*, edited by G. W. Gray, Wiley, Chichester, 1987.
52. D. Dunmur and T. Sluckin, *Soap, Science and Flat-Screen TVs: A History of Liquid Crystals*, Oxford, New York, 2010.
53. O. Lehmann, *Flüssige Kristalle: sowie Plastizität von Kristallen im allgemeinen, molekulare Umlagerungen und Aggregatzustandsänderungen*. Wilhelm Engelmann, Leipzig, 1904.
54. F. Reinitzer, *Monatsh. Chem.*, 1888, **9**, 421.
55. (a) F. Reintzer, *Liq. Cryst.*, 1989, **5**, 7. (b) H. Kelker and P. M. Knoll, *Liq. Cryst.*, 1989, **5**, 19.
56. R. Virchow, *Archiv f. pathol. Anat.*, 1854, **6**, 562.
57. (a) C. Mauguin, *Bull. Soc. Fr. Min.*, 1911, **34**, 71. (b) C. Mauguin, *Physik Zeitschrift*, 1911, **12**, 1011.
58. V. Fredericksz and A. Repiewa, *Z. Phys.*, 1927, **42**, 532.
59. L. Onsager, *Ann. N. Y. Acad. Sci.*, 1949, **51**, 627.
60. W. Maier and A. Saupe, *Z. Naturforsch.*, 1959, **13a**, 564.
61. (a) R. Williams, *J. Chem. Phys.*, 1963, **39**, 384. (b) R. Williams, *Nature*, 1963, **199**, 273.
62. S. Kwolek, H. Mera and T. Takata, "High-Performance Fibers" in *Ullmann's Encyclopedia of Industrial Chemistry*, Wiley-VCH, Weinheim, 2002.
63. (a) G. H. Heilmair, L. A. Zanoni and L. A. Barton, *Appl. Phys. Lett.*, 1968, **13**, 46. (b) W. Helfrich, *J. Chem. Phys.*, 1969, **51**, 4092.
64. G. H. Heilmair and L. A. Zanoni, *Appl. Phys. Lett.*, 1969, **13**, 91.
65. M. Schadt and W. Helfrich, *Appl. Phys. Lett.*, 1971, **18**, 127.
66. G. W. Gray, K. S. Harrison and J. A. Wash, *Electron. Lett.*, 1973, **9**, 130.
67. S. Chandrasekhar, B. K. Sadashiva and K. A. Suresh, *Pramana*, 1977, **9**, 471.
68. (a) A. Derzhanski and A. Petrov, *Mol. Cryst. Liq. Cryst.*, 1982, **89**, 339. (b) A. Adamczyk, *Mol. Cryst. Liq. Cryst. Sci. Technol., Sect. A*, 1994, **249**, 75.
69. C. Tschierske, *Prog. Polym. Sci.*, 1996, **21**, 775.
70. (a) J. Lydon, *Curr. Opin. Colloid Interface Sci.*, 1998, **3**, 458. (b) J. Lydon, *Curr. Opin. Colloid Interface Sci.*, 2004, **8**, 480. (c) S.-W. Tam-Chang and L. Huang, *Chem. Commun.*, 2008, 1957. (d) J. Lydon, *J. Mater. Chem.*, 2010, **20**, 10071. (e) J. Lydon, *Liq. Cryst.*, 2011, **38**, 1663.
71. (a) P. J. Collings, A. J. Dickinson and E. C. Smith, *Liq. Cryst.*, 2010, **37**, 701. (b) A. J. Dickinson, N. D. LaRacunte, C. B. McKitterick, and P. J. Collings, *Mol. Cryst. Liq. Cryst.*, 2009, **509**, 751.
72. (a) C. Ruslim, D. Matsunaga, M. Hashimoto, T. Tamaki and K. Ichimura, *Langmuir*, 2003, **19**, 3686. (b) S.-W. Tam-Chang, I. K. Iverson and J. Helbley, *Langmuir*, 2004, **20**, 342.
73. (a) J. W. Gopdby, *Liq. Cryst.*, 1998, **24**, 25. (b) Y. Gohon and J.-L. Popot, *Curr. Opin. Colloid Interface Sci.*, 2003, **8**, 15. (c) K. Urata, *PharmaChem*, 2012, **11**, 38. (d) H. Chaudhary, B. Gautam and V. Kum, *Asian J. Pharm.*, 2014, **8**, 70.
74. (a) S. Kobayashi and Y. Iimura, *Proc. SPIE 2175, Liquid Crystal Materials, Devices, and Applications III*, 1994,

122. (b) S.-H. Paek, C. J. Durning, K.-W. Lee and A. Lien, *J. Appl. Phys.*, 1998, **83**, 1270. (c) L. Parry-Jones, "Alignment Properties of Liquid Crystals" in *Handbook of Visual Display Technology*, Edited by J. Chen, W. Cranton and M. Fihn, Springer-Verlag, New York, 2014.
75. (a) K. Ichimura, *Chem. Rev.*, 2000, **100**, 1847. (b) M. O'Neill and S. M. Kelly, *J. Phys. D: Appl. Phys.*, 2000, **33**, R67. (c) N. Kawatsuki, *Chem. Lett.*, 2011, **40**, 548. (d) T. Seki, S. Nagano and M. Hara, *Polymer*, 2013, **54**, 6053.
76. (a) S. M. Kelly and M. O'Neill, "Liquid Crystals for Electro-Optic Applications" in *Handbook of Advanced Electronic and Photonic Materials and Devices, Volume 7: Liquid Crystals, Display and Laser Materials*, Edited by H. S. Nalwa, Academic Press, San Diego, 2001. (b) G. W. Gray, K. J. Harrison and J. A. Nash, *J. Chem. Soc., Chem. Commun.*, 1974, 431. (c) G. W. Gray and S. M. Kelly, *Mol. Cryst. Liq. Cryst.*, 1981, **75**, 109. (d) J. A. Castellano, *German Patent Application DE-OS*, 1971, 2,024,269. (e) R. Eidenschink, D. Erdmann, J. Krause and L. Pohl, *Angew. Chem.*, 1977, **89**, 103. (f) R. Buchecker and M. Schadt, *Mol. Cryst. Liq. Cryst.*, 1987, **149**, 359.
77. Reproduced from A. Seki, *Master's Thesis*, Department of Chemistry and Biotechnology, School of Engineering, The University of Tokyo, 2009, 43.
78. (a) S. M. Kelly and J. Fünfschilling, *Liq. Cryst.*, 1995, **19**, 519. (b) S. M. Kelly and J. Fünfschilling, *Ferroelectrics*, 1996, **180**, 269. (c) R. Eidenschink, G. W. Gray, K. J. Toyne and A. E. F. Waechtler, *Mol. Cryst. Liq. Cryst. Lett.*, 1988, **5**, 177.
79. (a) E. J. Davis and J. W. Goodby, "Symmetry and chirality in liquid crystals" in *Handbook of liquid crystals, 2nd edition*, edited by J. W. Goodby, P. J. Collings, T. Kato, C. Tschierske, H. F. Gleeson and P. Raynes, Wiley-VCH, Weinheim, 2014. (b) J. W. Goodby, S. J. Cowling, E. J. Davis and X. Jia, "Chiral structures in liquid crystals of calamitic systems" in *Handbook of liquid crystals, 2nd edition*, edited by J. W. Goodby, P. J. Collings, T. Kato, C. Tschierske, H. F. Gleeson and P. Raynes, Wiley-VCH, Weinheim, 2014. (c) K. A. Suresh, *Mol. Cryst. Liq. Cryst. Sci. Technol., Sect. A*, 1997, **302**, 1223. (d) G. Chilaya, *Mol. Cryst. Liq. Cryst.*, 2012, **561**, 8. (e) H. Takezoe, *Top. Curr. Chem.*, 2012, **318**, 303.
80. (a) D. G. Gray, *Carbohydr. Polym.*, 1994, **25**, 277. (b) N. Katsonis E. Lacaze and A. Ferrarini, *J. Mater. Chem.*, 2012, **22**, 7088. (c) H. Coles, "Chiral nematics: physical properties and applications" in *Handbook of Liquid Crystals*, edited by D. Demus, J. W. Goodby, G. W. Gray, H.-W. Spiess, V. Vill, Wiley-VCH, Weinheim, 1998. (d) G. Chilaya, "Cholesteric liquid crystals: Optics, electro-optics, and photo-optics" in *Chirality in Liquid Crystals*, edited by H.-S. Kitzerow and C. Bahr, Springer-Verlag, New York, 2001. (e) C. J. Booth, "The synthesis of chiral nematic liquid crystals" in *Handbook of Liquid Crystals*, edited by D. Demus, J. W. Goodby, G. W. Gray, H.-W. Spiess, V. Vill, Wiley-VCH, Weinheim, 1998. (f) D. G. Gray and B. R. Harkness, "Chiral Nematic Mesophases of Lyotropic and Thermotropic Cellulose Derivatives" in *Liq. Cryst. Mesomorphic Polym.*, edited by V. P. Shibaev and L. Lam, Springer-Verlag, New York, 1994. (g) A. Taugerbeck and J. Christopher, "Design and synthesis of chiral nematic liquid crystals", *Handbook of liquid crystals, 2nd edition*, edited by J. W. Goodby, P. J. Collings, T. Kato, C. Tschierske, H. F. Gleeson and P. Raynes, Wiley-VCH, Weinheim, 2014.
81. (a) S. M. Kelly, "Synthesis of chiral smectic liquid crystals" in *Handbook of Liquid Crystals*, edited by D.

- Demus, J. W. Goodby, G. W. Gray, H.-W. Spiess, V. Vill, Wiley-VCH, Weinheim, 1998. (b) P. J. Collings, "High chirality smectic mesophases" in *Handbook of liquid crystals, 2nd edition*, edited by J. W. Goodby, P. J. Collings, T. Kato, C. Tschierske, H. F. Gleeson and P. Raynes, Wiley-VCH, Weinheim, 2014. (c) C. Bahr, "Smectic liquid crystals: ferroelectric properties and electroclinic effect" in *Chirality in Liquid Crystals*, edited by H.-S. Kitzerow and C. Bahr, Springer-Verlag, New York, 2001. (d) G. S. Chilaya and V. G. Chigrinov, *Usp. Fiz. Nauk*, 1993, **163**, 1. (e) B. Pansu, *Pramana*, 2003, **61**, 285. (f) S. T. Lagerwall, *Adv. Colloid Interface Sci.*, 2014, **208**, 1. (g) M. Brunet and N. Isaert, *Ferroelectrics*, 1988, **84**, 25. (h) J. P. F. Lagerwall and F. Giesselmann, *ChemPhysChem*, 2006, **7**, 20.
82. A. M. Castilla, W. J. Ramsay and J. R. Nitschke, *Acc. Chem. Res.*, 2014, **47**, 2063.
83. (a) C. Y. Young, R. Pindak, N. A. Clark and R. B. Meyer, *Phys. Rev. Lett.*, 1978, **40**, 773. (b) N. A. Clark and S. T. Lagerwall, *Appl. Phys. Lett.*, 1980, **36**, 899. (c) S. T. Lagerwall and I. Dahl, *Mol. Cryst. Liq. Cryst.*, 1984, **114**, 151. (d) Y. Takanishi, H. Takezoe, Y. Suzuki, I. Kobayashi, T. Yajima, M. Terada and K. Mikami, *Angew. Chem., Int. Ed.*, 1999, **38**, 2353.
84. (a) V. R. Brown, *U.S. Patent*, 1972, 3651695A. (b) J. Li, S. Gauza and S. T. Wu, *J. Appl. Phys.*, 2004, **96**, 19.
85. (a) S. H. Joo, J. K. Kim and J. K. Song, *J. Appl. Phys.*, 2013, **114**, 083508. (b) K. Driesen, D. Moors, J. Beeckman, K. Neyts, C. Görrler-Walrand and K. Binnemans, *J. Lumin.*, 2007, **127**, 611. (c) M. Rumi, V. P. Tondiglia, L. V. Natarajan, T. J. White and T. J. Bunning, *ChemPhysChem*, 2014, **15**, 1311.
86. (a) I. P. Il'chishin, E. A. Tikhonov, V. G. Tishchenko and M. T. Shpak, *JETP Lett.*, 1980, **32**, 24. (b) H. Finkelmann, S. T. Kim, A. Muñoz, P. Palffy-Muhoray and B. Taheri, *Adv. Mater.*, 2001, **14**, 1069. (c) M. Ozaki, M. Kasano, T. Kitasho, D. Ganzke, W. Haase and K. Yoshino, *Adv. Mater.*, 2003, **12**, 974. (d) S. Furumi and N. Tamaoki, *Adv. Mater.*, 2010, **22**, 886. (e) A. Chanishvili, G. Chilaya, G. Petriashvili, R. Barberi, R. Bartolino, G. Cipparrone, A. Mazzulla and L. Oriol, *Adv. Mater.*, 2004, **16**, 791. (f) L.-W. Li and L.-G. Deng, *Eur. Phys. J. B*, 2013, **86**, 112. (g) S. Furumi, S. Yokoyama, A. Otomo and S. Mashiko, *Appl. Phys. Lett.*, 2004, **84**, 2491. (h) V. I. Kopp, Z.-Q. Zhang and A. Z. Genack, *Prog. Quant. Electron.*, 2003, **27**, 369.
87. W. J. A. M. Hartmann, *Ferroelectrics*, 1991, **122**, 1.
88. G. W. Gray and D. G. McDonnell, *Mol. Cryst. Liq. Cryst.*, 1976, **37**, 189.
89. S. Saito, K. Murashiro, M. Kikuchi, D. Demus, T. Inukai, M. Neundorf and S. Diele, *Ferroelectrics*, 1993, **147**, 367.
90. (a) H. K. Bisoyi and S. Kumar, *Chem. Soc. Rev.*, 2010, **39**, 264. (b) D. W. Bruce, *Acc. Chem. Res.*, 2000, **33**, 831.
91. N. H. Tinh, C. Destrade and H. Gasparoux, *Phys. Lett. A*, 1979, **72**, 251.
92. H. Ringsdorf, R. Wustefeld, E. Zerta, M. Ebert and J. H. Wendorff, *Angew. Chem., Int. Ed. Engl.*, 1989, **28**, 914.
93. (a) B. Kohne and K. Praefcke, *Chimia*, 1987, **41**, 196. (b) M. Ebert, D. A. Jungbauer, R. Kleppinger, J. H. Wendorff, B. Kohne and K. Praefcke, *Liq. Cryst.*, 1989, **4**, 53.
94. A. Grafe, D. Janietz, T. Frees and J. H. Wendorff, *Chem. Mater.*, 2005, **17**, 4979.
95. (a) S. Chandrasekhar, *Curr. Sci.*, 1981, **50**, 47. (b) C. Destrade, P. Foucher, H. Gasparoux, H. T. Nguyen, A. M. Levelut and J. Malthete, *Mol. Cryst. Liq. Cryst.*, 1984, **106**, 121. (c) C. Tschierske, *J. Mater. Chem.*,

- 1998, **8**, 1485. (d) C. Tschierske, *J. Mater. Chem.*, 2001, **11**, 2647. (e) D. Guillon, *Struct. Bond.*, in *Liquid Crystals II*, edited by D. M. P. Mingos, Springer-Verlag, Berlin, 1999, 41.
96. (a) J. Billard and B. K. Sadashiva, *Pramana*, 1979, **13**, 309. (b) S. Chandrasekhar, B. K. Sadashiva, K. A. Suresh, N. V. Madhusudana, S. Kumar, R. Shashidhar and G. Venkatesh, *J. de Phys., Colloque*, 1979, 120. (c) B. Kohne, K. Praefcke and J. Billard, *Zeitschrift fuer Naturforschung, Teil B: Anorganische Chemie, Organische Chemie*, 1986, **41B**, 1036. (d) H. W. Neuling, H. Stegemeyer, K. Praefcke and B. Kohne, *Zeitschrift fuer Naturforschung, A: Physical Sciences*, 1987, **42**, 631. (e) H. Fischer, S. S. Ghosh, P. A. Heiny, N. C. Maliszewskyj, T. Plesniviy, H. Ringsdorf and M. Seitz, *Angew. Chem.*, 1995, **107**, 879; *Angew. Chem., Int. Ed. Engl.*, 1995, **34**, 795.
97. (a) S. Diele and P. Goring, *Handbook of Liquid Crystals*, Edited by D. Demus, Wiley-VCH, Weinheim, 1998, **2B**, 887. (b) G. Ungar, F. Liu, and X. Zeng, Xiangbing, *Handbook of Liquid Crystals (2nd Edition)*, Edited by J. W. Goodby, Wiley-VCH, Weinheim, 2014, **5**, 363. (c) C. Tschierske, *Angew. Chem. Int. Ed.*, 2013, **52**, 8828. (d) S. Diele, *Curr. Opin. Colloid Interface Sci.*, 2002, **7**, 333.
98. (a) K. Borisch, S. Diele, P. Göring and C. Tschierske, *Chem. Commun.*, 1996, 237. (b) K. Borisch, S. Diele, P. Göring, H. Muller and C. Tschierske, *Liq. Cryst.*, 1997, **22**, 427. (c) K. Borisch, C. Tschierske, P. Goering and S. Diele, *Langmuir*, 2000, **16**, 6701. (d) K. Borisch, S. Diele, P. Göring, H. Kresse and C. Tschierske, *J. Mater. Chem.*, 1998, **8**, 529. (e) G. Dlubek, D. Bamford, I. Wilkinson, K. Borisch, M. A. Alam and C. Tschierske, *Liq. Cryst.*, 1999, **26**, 863. (f) B.-K. Cho, A. Jain, S. M. Gruner and U. Wiesner, *Science*, 2004, **305**, 1598. (g) B.-K. Cho, A. Jain, S. M. Gruner and U. Wiesner, *Chem. Commun.*, 2005, 2143. (h) B.-K. Cho, *Polym. J.*, 2012, **44**, 475. (i) V. S. K. Balagurusamy, G. Ungar, V. Percec and G. Johansson, *J. Am. Chem. Soc.*, 1997, **119**, 1539. (j) D. J. P. Yeardley, G. Ungar, V. Percec, M. N. Holerca and G. Johansson, *J. Am. Chem. Soc.*, 2000, **122**, 1684. (k) K. Borisch, S. Diele, P. Goring, H. Kresse and C. Tschierske, *Angew. Chem., Int. Ed. Engl.*, 1997, **36**, 2087. (l) A. Kohlmeier, D. Janietz and S. Diele, *Chem. Mater.*, 2006, **18**, 1483. (m) S. H. Seo, J. H. Park, G. N. Tew and J. Y. Chang, *Tetrahedron Lett.*, 2007, **48**, 6839.
99. (a) C. Tschierske, *Curr. Opin. Colloid Interface Sci.*, 2002, **7**, 69. (b) M. Imperor-Clerc, *Curr. Opin. Colloid Interface Sci.*, 2005, **9**, 370. (c) S. Kutsumizu, *Isr. J. Chem.*, 2012, **52**, 844.
100. A. Tardieu and J. Billard, *J. Phys. Colloques*, 1976, **37**, C3-79.
101. R. Nesper R and H. G. Von Schnering, *Angew. Chem.*, 1986, **98**, 111.
102. (a) M. Wohlgemuth, N. Yufa, J. Hoffman and E. L. Thomas, *Macromolecules*, 2001, **34**, 6083. (b) C. A. Lambert, L. H. Radzilowski and E. L. Thomas, *Philos. Trans. R. Soc. Lond. Ser. A*, 1996, **354**, 2009. (c) H.-A. Klok and S. Lecommandoux, *Adv. Mater.*, 2001, **13**, 1217.
103. (a) A. Fogden and S. Lidin, *J. Chem. Soc. Faraday Trans.*, 1994, **90**, 3423. (b) K. Fontell, *Colloid Polym. Sci.*, 1990, **268**, 264. (c) B. R. Wiesenauer, D. L. Gin, *Polym. J.*, 2012, **44**, 461.
104. (a) M. Lee, B.-K. Cho, H. Kim and W.-C. Zin, *Angew. Chem. Int. Ed.*, 1998, **37**, 638. (b) B. Donnio, B. Heinrich, T. Gulik-Krzywicki, H. Delacroix, D. Guillon and D. W. Bruce, *Chem. Mater.*, 1997, **9**, 2951. (c) S. Kutsumizu, K. Morita, T. Ichikawa, S. Yano, S. Nojima and T. Yamaguchi, *Liq. Cryst.*, 2002, **29**, 1447. (d) S. Kutsumizu, M. Yamada, S. Yano, K. Tadano, S. Nojima and T. Yamaguchi, *Mol. Cryst. Liq. Cryst.*, 2004, **412**, 1659. (e) K. Saito, T. Shinhara, T. Nakamoto, S. Kutsumizu, S. Yano and M. Sorai, *Phys. Rev. E*, 2002, 65,

031719.

105. (a) D. C. Wright and N. D. Mermin, N. David, *Rev. Mod. Phys.*, 1989, **61**, 385. (b) H. Stegemeyer, T. Bluemel, K. Hiltrop, H. Onusseit and F. Porsch, *Liq. Cryst.*, 1986, **1**, 3. (c) P. P. Crooker, "Blue phases" in *Chirality in Liquid Crystals*, edited by H.-S. Kitzerow and C. Bahr, Springer-Verlag, New York, 2001. (d) H. K. Bisoyi and Q. Li, *Acc. Chem. Res.*, 2014, **47**, 3184. (e) H. Kikuchi, *Struct. Bond.*, in *Liquid Crystalline Functional Assemblies and Their Supramolecular Structures*, Springer-Verlag, Berlin, 2008, **128**, 99. (f) H.-S. Kitzerow, *ChemPhysChem*, 2006, **7**, 63. (g) E. Dubois-Violette and B. Pansu, *Mol. Cryst. Liq. Cryst.*, 1988, **165**, 151. (h) J. W. Goodby, *Curr. Opin. Colloid Interface Sci.*, 2002, **7**, 326. (i) A. Yoshizawa, *RSC Adv.*, 2013, **3**, 25475. (j) T. Seideman, *Rep. Prog. Phys.*, 1990, **53**, 659.
106. (a) G. W. Gray, *J. Chem. Soc.*, 1956, 3733. (b) A. Saupe, *Mol. Cryst. Liq. Cryst.*, 1969, **7**, 59.
107. (a) R. M. Hornreich and S. Shtrikman, *J. Phys.*, 1980, **41**, 335. (b) D. L. Johnson, J. H. Flack and P. P. Crooker, *Phys. Rev. Lett.*, 1980, **45**, 641. (c) R. M. Hornreich and S. Shtrikman, *Phys. Lett. A*, 1981, **82**, 345. (d) S. Meiboom, M. Sammon and W. F. Brinkman, *Phys. Rev. A*, 1983, **27**, 438.
108. H. Kikuchi, M. Yokota, Y. Hisakado, H. Yang and T. Kajiyama, *Nature Mater.*, 2002, **1**, 64.
109. (a) J. W. Goodby, *Struct. Bond.*, in *Liquid Crystals II*, edited by D. M. P. Mingos, Springer-Verlag, Berlin, 1999, 83. (b) H.-S. Kitzerow, "Twist grain boundary phases" in *Chirality in Liquid Crystals*, edited by H.-S. Kitzerow and C. Bahr, Springer-Verlag, New York, 2001, 296. (c) M. Brunet, L. Navailles and N. A. Clark, *Eur. Phys. J. E: Soft Matter*, 2002, **7**, 5. (d) R. Dhar, *Phase Trans.*, 2006, **79**, 175. (e) Y. Galerne, *J. Phys. II*, 1994, **4**, 1699. (f) Y. Hidaka, N. Oikawa and S. Kai, *Ekisho*, 2006, **10**, 82. (f) I. Nishiyama, *Chem. Rec.*, 2009, **9**, 340.
110. S. R. Renn and T. C. Lubensky, *Phys. Rev. A*, 1988, **38**, 2132
111. (a) J. W. Goodby, M. A. Waugh, S. M. Stein, E. Chin, R. Pindak and J. S. Patel, *Nature*, 1989, **337**, 449. (b) J. W. Goodby, M. A. Waugh, S. M. Stein, E. Chin, R. Pindak and J. S. Patel, *J. Am. Chem. Soc.*, 1989, **111**, 8119. (c) C. C. Huang, D. S. Lin, J. W. Goodby, M. A. Waugh, S. M. Stein and E. Chin, *Phys. Rev. A*, 1989, **40**, 4153. (d) G. Srajer, R. Pindak, M. A. Waugh, J. W. Goodby and J. S. Patel, *Phys. Rev. Lett.*, 1990, **64**, 1545. (e) J. W. Goodby, I. Nishiyama, A. J. Slaney, C. J. Booth and K. J. Toyne, *Liq. Cryst.*, 1993, **14**, 37. (f) C. J. Booth, J. W. Goodby, K. J. Toyne, D. A. Dunmur and J. S. Kang, *Mol. Cryst. Liq. Cryst.*, 1995, **260**, 39. (g) J. W. Goodby, *Mol. Cryst. Liq. Cryst.*, 1997, **292**, 245. (h) M.-H. Li, V. Laux, H.-T. Nguyen, G. Sigaud, P. Barois and N. Isaert, *Liq. Cryst.*, 1997, **23**, 389. (i) M. Young, G. Pitsi, M.-H. Li, H.-T. Nguyen, P. Jamée, G. Sigaud and J. Thoen, *Liq. Cryst.*, 1998, **25**, 387.
112. (a) S. Singh, *Phys. Rep.*, 2000, **324**, 107; (b) C. Zannoni, *J. Mater. Chem.*, 2001, **11**, 2637.
113. J. G. Gay and B. J. Berne, *J. Chem. Phys.*, 1981, **74**, 3316.
114. (a) M. Yoneya, E. Nishikawa and H. Yokoyama, *J. Chem. Phys.*, 2002, **116**, 5753. (b) P. Zhang, E. Buncel and R. P. Lemieux, *Adv. Mater.*, 2005, **17**, 567. (c) C. Keith, R. A. Reddy, A. Hauser, U. Baumeister and C. Tschierske, *J. Am. Chem. Soc.*, 2006, **128**, 3051. (d) R. P. Lemieux, *Chem. Soc. Rev.*, 2007, **36**, 2033. (e) B. Rodriguez-Spong, A. Acciaccia, D. Fleisher and N. Rodriguez-Hornedo, *Mol. Pharm.*, 2008, **5**, 956. (f) M. Lehmann, M. Jahr, F. C. Grozema, R. D. Abellon, L. D. A. Siebbeles and M. Mueller, *Adv. Mater.*, 2008, **20**, 4414. (g) J. W. Goodby, E. J. Davis, R. J. Mandle and S. J. Cowling, *Isr. J. Chem.*, 2012, **52**, 863.

- (h) M. Lehmann, *Top. Curr. Chem.*, 2012, **318**, 193. (i) H. Shimura, M. Yoshio and T. Kato, *Org. Biomol. Chem.*, 2009, **7**, 3205.
115. T. Kato, N. Mizoshita, and K. Kishimoto, *Angew. Chem. Int. Ed.*, 2006, **45**, 38.
116. (a) E. S. Gil and S. M. Hudson, *Prog. Polym. Sci.*, 2004, **29**, 1173. (b) H. Otsuka, Y. Nagasaki and K. Kataoka, *Adv. Drug Deliv. Rev.*, 2003, **55**, 403. (c) R. A. Segalman, *Mater. Sci. Eng. R Rep.*, 2005, **48**, 191. (d) M. R. Bockstaller, R. A. Mickiewicz and E. L. Thomas, *Adv. Mater.*, 2005, **17**, 1331. (e) H.-A. Klok and S. Lecommandoux, *Adv. Mater.*, 2001, **13**, 1217.
117. (a) O. Gronwald, E. Snip and S. Shinkai, *Curr. Opin. Colloid Interface Sci.*, 2002, **7**, 148. (b) Y. Noda, Y. Hayashi and K. Ito, *J. Appl. Polym. Sci.*, 2014, **131**, 40509.
118. (a) M. Funahashi, H. Shimura, M. Yoshio and T. Kato, *Struct. Bond.*, 2008, **128**, 151. (b) T. Kato, T. Yasuda, Y. Kamikawa and M. Yoshio, *Chem. Commun.*, 2009, 729. (d) M. Funahashi, *J. Mater. Chem. C*, 2014, **2**, 7451.
119. (a) M. Schadt, *Annu. Rev. Mater. Sci.*, 1997, **27**, 305. (b) C. F. van Nostrum and R. J. M. Nolte, *Chem. Commun.*, 1996, 2385. (c) T. Kato, T. Yasuda, Y. Kamikawa and M. Yoshio, *Chem. Commun.*, 2009, 729. (d) D. L. Gin, W. Gu, B. A. Pindzola and W.-J. Zhou, *Acc. Chem. Res.*, 2001, **34**, 973. (e) B. Donnio, S. Buathong, I. Bury and D. Guillon, *Chem. Soc. Rev.*, 2007, **36**, 1495. (f) T. Kato, Y. Hirai, S. Nakaso and M. Moriyama, *Chem. Soc. Rev.*, 2007, **36**, 1857. (g) A. Angelova, B. Angelov, R. Mutafchieva, S. Lesieur and P. Couvreur, *Acc. Chem. Res.*, 2011, **44**, 147. (h) S.-W. Tam-Chang and L. Huang, *Chem. Commun.*, 2008, 1957. (i) D. J. Broer, C. M. W. Bastiaansen, M. G. Debije and A. P. H. J. Schenning, *Angew. Chem. Int. Ed.*, 2012, **51**, 7102. (j) T. Seki, S. Nagano and M. Hara, *Polymer*, 2013, **54**, 6053. (k) T. Chuard and R. Deschenaux, *Chimia*, 2003, **57**, 597. (l) D. S. Miller, X. Wang and N. L. Abbott, *Chem. Mater.*, 2014, **26**, 496. (m) H. K. Bisoyi and Q. Li, *Chem. Rev.*, 2016, **116**, 15089.
120. (a) Y. Arai, S. Kinoshita and K. Kimura, *Jpn. Kokai Tokkyo Koho*, 1972, JP47027187. (b) H. J. Coles, *Mol. Cryst. Liq. Cryst.*, 1978, **41**, 231. (c) H. J. Coles, *Mol. Cryst. Liq. Cryst.*, 1978, **41**, 281. (d) H. J. Coles, *Mol. Cryst. Liq. Cryst.*, 1978, **49**, 13. (e) S. Kurihara, S. Nomiyama and T. Nonaka, *Chem. Mater.*, 2000, **12**, 9.
121. (a) T. Kajiyama, J. Ono, T. Kashiwagi and K. Hara, *PCT Int. Appl.*, 1992, WO9214185. (b) H. Khandelwal, R. C. G. M. Loonen, J. L. M. Hensen, M. G. Debije and A. P. H. J. Schenning, *Sci. Rep.*, 2015, **5**, 11773. (c) R. Baetens, B. P. Jelle and A. Gustavsen, *Sol. Energy Mater. Sol. Cells*, 2010, **94**, 87. (d) C.M. Lampert, *Sol. Energy Mater. Sol. Cells*, 2003, **76**, 489. (e) Y. Kim, D. Jung, S. Jeong, K. Kim, W. Choi and Y. Seo, *Curr. Appl. Phys.*, 2015, **15**, 292. (f) S. Park and J. W. Hong, *Thin Solid Films*, 2009, **517**, 3183. (g) D. J. Gardiner, S. M. Morris and H. J. Coles, *Sol. Energy Mater. Sol. Cells*, 2009, **93**, 301. (h) H.-K. Kwon, K.-T. Lee, K. Hur, S. H. Moon, M. M. Quasim, T. D. Wilkinson, J.-Y. Han, H. Ko, I.-K. Han, B. Park, B. K. Min, B.-K. Ju, S. M. Morris, R. H. Friend and D.-H. Ko, *Adv. Energy Mater.*, 2015, **5**, 1401347.
122. (a) H. Takatsu, *DIC Technical Review*, 2005, **11**, 29. (b) H. Takatsu, *J. Syn. Org. Chem. Jpn.*, 2000, **58**, 444.
123. (a) C. Robinson and J. C. Ward, *Nature*, 1957, **180**, 1183. (b) S. L. Kwolek, P. W. Morgan, J. R. Schaeffgen, and L. W. Gulrich, *Macromolecules*, 1977, **10**, 1390. (c) T. I. Bair, P. W. Morgan and F. L. Killian, *Macromolecules*, 1977, **10**, 1396. (d) B. A. Kowalski, T. C. Guin, A. D. Auguste, N. P. Godman and T. J. White, *ACS Macro Lett.*, 2017, **6**, 436.

124. (a) M. Okazaki, K. Kawata, H. Nishikawa and M. Negoro, *Polym. Adv. Technol.*, 2000, **11**, 398. (b) K. Kawata, *Chem. Rec.*, 2002, **2**, 59. (c) K. Kawata, M. Negoro, H. Nishikawa and M. Okazaki, *Ekisho*, 1997, **1**, 45.
125. (a) C. M. Paleos and D. Tsiourvas, *Angew. Chem. Int. Ed. Engl.*, 1995, **34**, 1696. (b) T. Kato, *Supramol. Sci.*, 1996, **3**, 53. (c) T. Kato, *Struct. Bond.*, 2000, **96**, 95. (d) T. Kato, N. Mizoshita and K. Kanie, *Macromol. Rapid Commun.*, 2001, **22**, 797. (e) T. Kato and N. Mizoshita, *Curr. Opin. Solid State Mater. Sci.*, 2002, **6**, 579. (f) S. C. Zimmerman and P. S. Corbin, *Struct. Bond.*, 2000, **96**, 64. (g) G. Brinke, J. Ruokolainen and O. Ikkala, *Adv. Polym. Sci.*, 2007, **207**, 113. (h) U. Beginn, *Prog. Polym. Sci.*, 2003, **28**, 1049. (i) J. W. Goodby, I. M. Saez, S. J. Cowling, V. Gortz, M. Draper, A. W. Hall, S. Sia, G. Cozquer, S.-E. Lee and E. P. Raynes, *Angew. Chem. Int. Ed.*, 2008, **47**, 2754.
126. (a) T. Kato and J. M. J. Frechet, *Macromolecules*, 1989, **22**, 3818. (b) T. Kato and J. M. J. Frechet, *Macromolecules*, 1990, **23**, 360. (c) M.-J. Brienne, J. Gabard, J.-M. Lehn and I. Stibor, *J. Chem. Soc., Chem. Commun.*, 1989, 1868. (d) T. Kato and J. M. J. Frechet, *J. Am. Chem. Soc.*, 1989, **111**, 8533. (e) C. Fouquey, J.-M. Lehn and A.-M. Levelut, *Adv. Mater.*, 1990, **2**, 254. (f) C. Alexander, C. P. Jariwara, C. M. Lee and A. C. Griffin, *Macromol. Symp.*, 1994, **77**, 283. (g) R. Kleppinger, C. P. Lillya and C. Yang, *Angew. Chem. Int. Ed.*, 1995, **34**, 1637. (h) M. SuTrez, J.-M. Lehn, S. C. Zimmerman, A. Skoulios and B. Heinrich, *J. Am. Chem. Soc.*, 1998, **120**, 9526.
127. (a) D. W. Bruce, D. A. Dunmur, E. Lalinde, P. M. Maitlis and P. Styring, *Nature*, 1986, **323**, 791. (b) D. W. Bruce, E. Lalinde, P. Styring, D. A. Dunmur and P. M. Maitlis, *J. Chem. Soc., Chem. Commun.*, 1986, 581. (c) D. W. Bruce, *J. Chem. Soc., Dalton Trans.*, 1993, **20**, 2983.
128. (a) H. L. Nguyen, P. N. Horton, M. B. Hursthouse, A. C. Legon and D. W. Bruce, *J. Am. Chem. Soc.*, 2004, **126**, 16. (b) C. Präsang, H. L. Nguyen, P. N. Horton, A. C. Whitwood and D. W. Bruce, *Chem. Commun.*, 2008, 6164.
129. (a) H. Ringsdorf, R. Wüstefeld, E. Zerta, M. Ebert and J. H. Wendorff, *Angew. Chem. Int. Ed.*, 1989, **28**, 914. (b) M. M. Green, H. Ringsdorf, J. Wagner and R. Wüstefeld, *Angew. Chem. Int. Ed.*, 1990, **29**, 1478. (c) Y. Kamikawa and T. Kato, *Org. Lett.*, 2006, **8**, 2463.
130. (c) I. A. Levitsky, K. Kishikawa, S. H. Eichhorn and T. M. Swager, *J. Am. Chem. Soc.*, 2000, **122**, 2474. (b) K. Kishikawa, S. Furusawa, T. Yamaki, S. Kohmoto, M. Yamamoto and K. Yamaguchi, *J. Am. Chem. Soc.*, 2002, **124**, 1597. (c) S. H. Eichhorn, A. J. Paraskos, K. Kishikawa and T. M. Swager, *J. Am. Chem. Soc.*, 2002, **124**, 12742.
131. (a) S. Ujiie and K. Iimura, *Macromolecules*, 1992, **25**, 3174. (b) K. Binnemans, *Chem. Rev.*, 2005, **105**, 4148.
132. (a) S. Chen and S. H. Eichhorn, *Isr. J. Chem.*, 2012, **52**, 830. (b) M. Yoshio, T. Mukai, H. Ohno and T. Kato, *ACS Symp. Ser.*, 2007, **975**, 161. (c) B.-K. Cho, *RSC Adv.*, 2014, **4**, 395. (d) M. Yoshio and T. Kato, "Liquid crystals as ion conductors" in *Handbook of liquid crystals, 2nd edition*, edited by J. W. Goodby, P. J. Collings, T. Kato, C. Tschierske, H. F. Gleeson and P. Raynes, Wiley-VCH, Weinheim, 2014.
133. (a) S. Sergeev, W. Pisula and Y. H. Geerts, *Chem. Soc. Rev.*, 2007, **36**, 1902. (b) W. Pisula, M. Zorn, J. Y. Chang, K. Müllen and R. Zentel, *Macromol. Rapid Commun.*, 2009, **30**, 1179. (c) Y. Shimizu, K. Oikawa, K.

- Nakayama and D. Guillon, *J. Mater. Chem.*, 2007, **17**, 4223. (d) R. J. Bushby and O. R. Lozman, *Curr. Opin. Sol. Stat. Mater. Sci.*, 2003, **6**, 569. (e) M. Funahashi, *Polym. J.*, 2009, **41**, 459. (f) B. Roy, N. De and K. C. Majumdar, *Chem.-Eur. J.*, 2012, **18**, 14560. (g) K. Ohta, K. Hatsusaka, M. Sugibayashi, M. Ariyoshi, K. Ban, F. Maeda, R. Naito, K. Nishizawa, A. M. van de Craats and J. M. Warman, *Mol. Cryst. Liq. Cryst.*, 2003, **397**, 325.
134. M. Henmi, K. Nakatsuji, T. Ichikawa, H. Tomioka, T. Sakamoto, M. Yoshio and T. Kato, *Adv. Mater.*, 2012, **24**, 2238.
135. (a) V. Shibaev, A. Bobrovsky and N. Boiko, *J. Photochem. Photobiol. A: Chem.*, 2003, **155**, 3. (b) T. Seki, "Light-responsive 2-D motions and manipulations in azobenzene-containing liquid crystalline polymer materials" in *Smart Light-Responsive Materials: Azobenzene-Containing Polymers and Liquid Crystals*, edited by Y. Zhao and T. Ikeda, John Wiley & Sons, Inc., Hoboken, 2009. (c) H. Yu and Q. Li, "Photomechanical liquid crystalline polymers: motion in response to light" in *Intelligent Stimuli-Responsive Materials*, edited by Q. Li, John Wiley & Sons, Inc., Hoboken, 2013. (d) S. De, R. Luciano, U. C. Loredana, S. Serak and N. Tabiryan, "Photophysical properties of light responsive liquid crystals in polymeric templates" in *Series on Liquid Crystals*, edited by H.-S. Kwok, S. Naemura and H. L. Ong, World Scientific Publishing Co. Pte. Ltd., Toh Tuck Link, 2013.
136. S. Yamane, K. Tanabe, Y. Sagara and T. Kato, *Top. Curr. Chem.*, 2012, **318**, 395.
137. (a) Y.-H. Lin, *Top. Appl. Phys.*, 2015, **129**, 337. (b) L. V. Elnikova, *J. Surface Investigation: X-Ray, Synchrotron and Neutron Techniques*, 2015, **9**, 257. (c) S. J. Woltman, G. D. Jay and G. P. Crawford, *Nat. Mater.*, 2007, **6**, 929. (d) Y.-Y. Luk, M. L. Tingey, K. A. Dickson, R. T. Raines and N. L. Abbott, *J. Am. Chem. Soc.*, 2004, **126**, 9024. (e) M. L. Tingey, E. J. Snodgrass and N. L. Abbott, *Adv. Mater.*, 2003, **16**, 1331. (f) J.-S. Park and N. L. Abbott, *Adv. Mater.*, 2008, **20**, 1185.
138. (a) M. O'Neill and S. M. Kelly, *Adv. Mater.*, 2011, **23**, 566. (b) M. Funahashi, *J. Mater. Chem. C*, 2014, **2**, 7451. (c) M. Funahashi and T. Kato, *Liq. Cryst.*, 2015, **42**, 909. (d) A. Seki and M. Funahashi, *Heterocycles*, 2016, **92**, 3. (e) T. Kato, M. Yoshio, T. Ichikawa, B. Soberats, H. Ohno and M. Funahashi, *Nat. Rev. Mater.*, 2017, **2**, 17001.
139. (a) D. Adam, F. Closs, T. Frey, D. Funhoff, D. Haarer, H. Ringsdorf, P. Schuhmacher and K. Siemensmeyer, *Phys. Rev. Lett.*, 1993, **70**, 457. (b) N. Boden, R. J. Bushby, J. Clements, B. Movaghar, K. J. Donovan and T. Kreouzis, *Phys. Rev. B*, 1995, **52**, 13274. (c) A. M. van de Craats, J. M. Warman, A. Fechtenkötter, J. B. Brand, M. A. Harbison and K. Müllen, *Adv. Mater.*, 1999, **11**, 1469. (d) M. Ichihara, A. Suzuki, K. Hatsusaka and K. Ohta, *Liq. Cryst.*, 2007, **34**, 555. (e) K. Ban, K. Nishikawa, K. Ohta, A. M. van de Craats, J. M. Warman, I. Yamamoto and H. Shirai, *J. Mater. Chem.*, 2001, **11**, 321. (f) A. Demenev, S. H. Eichhorn, T. Taerum, D. Perepichka, S. Patwardhan, F. C. Grozema, L. D. A. Siebbeles and R. Klenkler, *Chem. Mater.*, 2010, **22**, 1420. (g) I. Bleyl, C. Erdelen, H.-W. Schmidt and D. Haarer, *Phil. Mag. B*, 1999, **79**, 463. (h) J. Simmerer, B. Glösen, W. Paulus, A. Kettner, P. Schuhmacher, D. Adam, K.-H. Etzbach, K. Siemensmeyer, J. H. Wendorf, H. Ringsdorf and D. Haarer, *Adv. Mater.*, 1996, **8**, 815. (i) D. Adam, P. Schumacher, J. Simmerer, L. Haussling, K. Siemensmeyer, K. H. Etzbach, H. Ringsdorf and D. Haarer, *Nature*, 1994, **371**, 141.

140. (a) M. Funahashi and J. Hanna, *Phys. Rev. Lett.*, 1997, **78**, 2184. (b) M. Funahashi and J. Hanna, *Appl. Phys. Lett.*, 1997, **71**, 602. (c) M. Funahashi and J. Hanna, *Appl. Phys. Lett.*, 1998, **73**, 3733. (d) M. Funahashi and J. Hanna, *Jpn. J. Appl. Phys.*, 1999, **38**, L132. (e) K. Kogo, H. Maeda, H. Kato, M. Funahashi, and J. Hanna, *Appl. Phys. Lett.*, 1999, **75**, 3348. (f) H. Zhang and J. Hanna, *J. Phys. Chem. B*, 1999, **103**, 7429.
141. F. Würthner, C. R. Saha-Möller, B. Fimmel, S. Ogi, P. Leowanawat and D. Schmidt, *Chem. Rev.*, 2016, **116**, 962.
142. (a) C. W. Struijk, A. B. Sieval, J. E. J. Dakhorst, M. van Dijk, P. Kimkes, R. B. M. Koehorst, H. Donker, T. J. Schaafsma, S. J. Picken, A. M. van de Craats, J. M. Warman, H. Zuilhof and E. J. R. Sudhölter, *J. Am. Chem. Soc.*, 2000, **122**, 11057. (b) J. Y. Kim and A. J. Bard, *Chem. Phys. Lett.*, 2004, **383**, 11. (c) J. Y. Kim, I. J. Chung, Y. C. Kim and J.-W. Yu, *Chem. Phys. Lett.*, 2004, **398**, 367. (d) Z. An, J. Yu, S. C. Jones, S. Barlow, S. Yoo, B. Domercq, P. Prins, L. D. A. Siebbeles, B. Kippelen and S. R. Marder, *Adv. Mater.*, 2005, **17**, 2580. (e) Z. Chen, V. Stepanenko, V. Dehm, P. Prins, L. D. A. Siebbeles, J. Seibt, P. Marquetand, V. Engel and F. Würthner, *Chem.-Eur. J.*, 2007, **13**, 436. (f) V. Duzhko, E. Aqad, M. R. Imam, M. Peterca, V. Percec and K. D. Singer, *Appl. Phys. Lett.*, 2008, **92**, 113312. (g) M.-A. Muth, G. Gupta, A. Wicklein, M. Carrasco-Orozco, T. Thurn-Albrecht and M. Thelakkat, *J. Phys. Chem. C*, 2014, **118**, 92. (h) J. A. Quintana, J. M. Villalvilla, A. de la Peña, J. L. Segula and M. A. Díaz-García, *J. Phys. Chem. C*, 2014, **118**, 26577.
143. (a) F. Würthner, C. Thalacker, S. Diele and C. Tschierske, *Chem.-Eur. J.*, 2001, **7**, 2245. (b) J. van Herrikhuyzen, A. Syamakumari, A. P. H. J. Schenning and E. W. Meijer, *J. Am. Chem. Soc.*, 2004, **126**, 10021. (c) Z. Chen, U. Baumeister, C. Tschierske and F. Würthner, *Chem.-Eur. J.*, 2007, **13**, 450. (d) A. Wicklein, A. Lang, M. Muth and M. Thelakkat, *J. Am. Chem. Soc.*, 2009, **131**, 14442.
144. (a) F. S. Kim, G. Ren and S. A. Jenekhe, *Chem. Mater.*, 2011, **23**, 682. (b) M. O'Neill and S. M. Kelly, *Adv. Mater.*, 2011, **23**, 566. (c) A. M. van de Craats, J. M. Warman, H. Hasebe, R. Naito and K. Ohta, *J. Phys. Chem. B*, 1997, **101**, 9224. (d) H. Fujikake, T. Murashige, M. Sugibayashi and K. Ohta, *Appl. Phys. Lett.*, 2004, **85**, 3474. (e) J. C. Swarts, E. H. G. Langner, N. Krokeide-Hove and M. J. Cook, *J. Mater. Chem.*, 2001, **11**, 434. (f) Y. Miyake, Y. Shiraiwa, K. Okada, H. Monobe, T. Hori, N. Yamasaki, H. Yoshida, M. J. Cook, A. Fujii and M. Ozaki, *Appl. Phys. Express*, 2011, **4**, 021604. (g) T. Hori, N. Fukuoka, T. Masuda, Y. Miyake, H. Yoshida, A. Fujii, Y. Shimizu and M. Ozaki, *Sol. Energy Mater. Sol. Cells*, 2011, **95**, 3087. (h) S. Tanaka, T. Sakurai, Y. Honsho, A. Saeki, S. Seki, K. Kato, M. Takata, A. Osuka and T. Aida, *Chem.-Eur. J.*, 2012, **18**, 10554. (i) S. Sengupta, S. Uemura, S. Patwardhan, V. Huber, F. C. Grozema, L. D. A. Siebbeles, U. Baumeister and F. Würthner, *Chem.-Eur. J.*, 2011, **17**, 5300. (j) K. Oikawa, H. Monobe, K. Nakayama, T. Kimoto, K. Tsuchiya, B. Heinrich, D. Guillon, Y. Shimizu and M. Yokoyama, *Adv. Mater.*, 2007, **19**, 1864. (k) K. Tokunaga, H. Iino and J. Hanna, *J. Phys. Chem. B*, 2007, **111**, 12041. (l) K. Tokunaga, H. Iino and J. Hanna, *Mol. Cryst. Liq. Cryst.*, 2009, **510**, 241.
145. (a) H.-C. Chang, K. Komasa, K. Kishida, T. Shiozaki, T. Ohmori, T. Matsumoto, A. Kobayashi, M. Kato and S. Kitagawa, *Inorg. Chem.*, 2011, **50**, 4279. (b) H.-C. Chang, T. Shiozaki, A. Kamata, K. Kishida, T. Ohmori, D. Kiriya, T. Yamauchi, H. Furukawa and S. Kitagawa, *J. Mater. Chem.*, 2007, **17**, 4136. (c) T. Yasuda, H. Ooi, J. Morita, Y. Akama, K. Minoura, M. Funahashi, T. Shimomura and T. Kato, *Adv. Funct. Mater.*, 2009, **19**,

411.

146. M. Mitani, S. Yamane, M. Yoshio, M. Funahashi and T. Kato, *Mol. Cryst. Liq. Cryst.*, 2014, **594**, 1.
147. R. Azumi, *Ekisho*, 2006, **10**, 52.
148. (a) I. McCulloch, W. Zhang, M. Heeney, C. Bailey, M. Giles, D. Graham, M. Shkunov, D. Sparrowe and S. Tierney, *J. Mater. Chem.*, 2003, **13**, 2436. (b) D. Byron, A. Matharu, R. Wilson and G. Wright, *Mol. Cryst. Liq. Cryst.*, 1995, **265**, 61. (c) F. Garnier, R. Hajlaoui, A. El Kassmi, G. Horowitz, L. Laigre, W. Porzio, M. Armanini and F. Provasoli, *Chem. Mater.*, 1998, **10**, 3334. (d) R. Azumi, G. Götz and P. Bäuerle, *Synth. Met.*, 1999, **101**, 544. (e) S. Ponomarenko and S. Kirchmeyer, *J. Mater. Chem.*, 2003, **13**, 197. (f) H. Wada, T. Taguchi, M. Goto, T. Kambayashi, T. Mori, K. Ishikawa and H. Takezoe, *Chem. Lett.*, 2006, **35**, 280. (g) T. Yasuda, K. Kishimoto and T. Kato, *Chem. Commun.*, 2006, 3399.
149. (a) J. Leroy, J. Levin, S. Sergeev and Y. Geerts, *Chem. Lett.*, 2006, **35**, 166. (b) J. Leroy, N. Boucher, S. Sergeev, M. Sferrazza and Y. Geerts, *Eur. J. Org. Chem.*, 2007, 1256. (c) N. Boucher, J. Leroy, S. Sergeev, E. Pouzet, V. Lemaury, R. Lazzaroni, J. Cornil, Y. H. Geerts and M. Sferrazza, *Synth. Met.*, 2009, **159**, 1319. (d) A. J. J. M. van Breemen, P. T. Herwig, C. H. T. Chlon, J. Sweelssen, H. F. M. Schoo, S. Setayesh, W. M. Hardeman, C. A. Martin, D. M. de Leeuw, J. J. P. Valetton, C. W. M. Bastiaansen, D. J. Broer, A. R. Popa-Merticaru and S. C. J. Meskers, *J. Am. Chem. Soc.*, 2006, **128**, 2336.
150. (a) M. Funahashi, F. Zhang and N. Tamaoki, *Adv. Mater.*, 2007, **19**, 353. (b) F. Zhang, M. Funahashi and N. Tamaoki, *Appl. Phys. Lett.*, 2007, **91**, 063515. (c) M. Funahashi, T. Ishii and A. Sonoda, *ChemPhysChem*, 2013, **14**, 2750.
151. T. Izawa, E. Miyazaki and K. Takimiya, *Adv. Mater.*, 2008, **20**, 3388.
152. (a) A. Kumatani, C. Liu, Y. Li, P. Darmawan, K. Takimiya, T. Minari and K. Tsukagoshi, *Sci. Rep.*, 2012, **2**, 393. (b) Y. Li, C. Liu, A. Kumatani, P. Darmawan, T. Minari and K. Tsukagoshi, *Org. Electron.*, 2012, **13**, 264. (c) Y. Li, C. Liu, Y. Xu, T. Minari, P. Darmawan and K. Tsukagoshi, *Org. Electron.*, 2012, **13**, 815. (d) Y. Yuan, G. Giri, A. L. Ayzner, A. P. Zoombelt, S. C. B. Mannsfeld, J. Chen, D. Nordlund, M. F. Toney, J. Huang and Z. Bao, *Nat. Commun.*, 2014, **5**, 3005.
153. M. J. Kang, T. Yamamoto, S. Shinamura, E. Miyazaki and K. Takimiya, *Chem. Sci.*, 2010, **1**, 179.
154. (a) Y. S. Yang, T. Yasuda, H. Kakizoe, H. Mieno, H. Kino, Y. Tateyama and C. Adachi, *Chem. Commun.*, 2013, **49**, 6483. (b) H. Mieno, T. Yasuda, Y. S. Yang and C. Adachi, *Chem. Lett.*, 2014, **43**, 293.
155. B. Košata, V. Kozmik, J. Svoboda, V. Novotná, P. Vaněk and M. Glogarová, *Liq. Cryst.*, 2003, **30**, 603.
156. H. Iino and J. Hanna, *Adv. Mater.*, 2011, **23**, 1748.
157. J. M. Adhikari, K. Vakhshouri, B. D. Calitree, A. Hexemer, M. A. Hickner and E. D. Gomez, *J. Mater. Chem. C*, 2015, **3**, 8799.
158. (a) H. Iino, T. Kobori and J. Hanna, *J. Non-Cryst. Solids*, 2012, **358**, 2516. (b) H. Iino, T. Usui and J. Hanna, *Nat. Commun.*, 2015, **6**, 6828. (c) S. Inoue, H. Minemawari, J. Tsutsumi, M. Chikamatsu, T. Yamada, S. Horiuchi, M. Tanaka, R. Kumai, M. Yoneya and T. Hasegawa, *Chem. Mater.*, 2015, **27**, 3809. (d) S. Méry, D. Haristoy, J.-F. Nicoud, D. Guillon, S. Diele, H. Monobe and Y. Shimizu, *J. Mater. Chem.*, 2002, **12**, 37.
159. (a) A. C. Arias, J. D. MacKenzie and I. McCulloch, *Chem. Rev.*, 2010, **110**, 3. (b) C. R. Newman, C. D. Frisbie, D. A. da Silva Filho, J.-L. Brédas, P. C. Ewbank and K. R. Mann, *Chem. Mater.*, 2004, **16**, 4436.

160. (a) B. Roy, N. De and K. C. Majumdar, *Chem.-Eur. J.*, 2012, **189**, 14560. (b) E. Yashima, K. Maeda, H. Iida, Y. Furusho and K. Nagai, *Chem. Rev.*, 2009, **109**, 6102. (c) D. Janietz, *J. Mater. Chem. C*, 1998, **8**, 265. (d) T. Kato, N. Mizoshita, and K. Kanie, *Macromol. Rapid Commun.*, 2001, **22**, 797. (e) D. J. Broer, C. M. W. Bastiaansen, M. G. De Bije and A. P. H. J. Schenning, *Angew. Chem. Int. Ed.*, 2012, **51**, 7102. (f) H. Li, J. Choi and T. Nakanishi, *Langmuir*, 2013, **29**, 5394.
161. (a) D. Vorländer, *Ber. Dtsch. Chem. Ges.*, **1929**, 62, 2831. (b) G. Pelzl, I. Wirth and W. Weissflog, *Liq. Cryst.*, 2001, **28**, 969. (c) H. Takezoe and Y. Takanishi, *Jpn. J. Appl. Phys.*, 2006, **45**, 597. (d) M. Sawamura, K. Kawai, Y. Matsuo, K. Kanie, T. Kato and E. Nakamura, *Nature*, 2002, **419**, 702.
162. (a) J. Charvolin, *J. Chim. Phys.*, 1983, **80**, 15. (b) C. Tschierske, *Angew. Chem. Int. Ed.*, 2013, **52**, 8828. (c) C. Tschierske, *Isr. J. Chem.*, 2012, **52**, 935.
163. (a) R. Duran, P. Gremain, D. Guillon and A. Skoulios, *Mol. Cryst. Liq. Cryst. Lett.*, 1986, **3**, 23. (b) N. H. Tinh, J. Malthete and C. Destrade, *Mol. Cryst. Liq. Cryst. Lett.*, 1985, **2**, 133. (c) J.-K. Kim, M.-K. Hong, J.-H. Ahn and M. Lee, *Angew. Chem. Int. Ed.*, 2005, **44**, 328. (d) F. Hildebrandt, J. A. Schröter, C. Tschierske, R. Festag, M. Wittenberg and J. H. Wendorff, *Adv. Mater.*, 1997, **9**, 564. (e) N.-K. Oh, W.-C. Zin, J.-H. Im, J.-H. Ryu, M. Lee, *Chem. Commun.*, 2004, 1092.
164. (a) M. Lee, B.-K. Cho, Y.-G. Jang and W.-C. Zin, *J. Am. Chem. Soc.*, 2000, **122**, 7449; (b) M. Lee, B.-K. Cho, K. J. Ihn, W.-K. Lee, N.-K. Oh and W.-C. Zin, *J. Am. Chem. Soc.*, 2001, **123**, 4647.
165. (a) K. Hoshino, K. Kanie, T. Ohtake, T. Mukai, M. Yoshizawa, S. Ujiie, H. Ohno and T. Kato, *Macromol. Chem. Phys.*, 2002, **203**, 1547; (b) B. Bilgin-Eran, C. Tschierske, S. Diele and U. Baumeister, *J. Mater. Chem.*, 2006, **16**, 1145. (c) B. Bilgin-Eran, Ç. Yörür, C. Tschierske, M. Prehm and U. Baumeister, *J. Mater. Chem.*, 2007, **17**, 2319. (d) N. Terasawa, H. Monobe, K. Kiyohara and Y. Shimizu, *Chem. Lett.*, 2003, **32**, 214; (e) Y. Yang, H. Li and J. Wen, *Liq. Cryst.*, 2007, **34**, 1167. (f) N. Terasawa, H. Monobe and K. Kiyohara, *Liq. Cryst.*, 2007, **34**, 311.
166. (a) S. Pensec and F.-G. Tournilhac, *Chem. Commun.*, 1997, 441. (b) M. Murase, Y. Takanishi, I. Nishiyama, A. Yoshizawa and J. Yamamoto, *RSC Adv.*, 2015, **5**, 215.
167. M. Yoneya, *Chem. Rec.*, 2011, **11**, 66.
168. (a) M. Prehm, G. Götz, P. Bäuerle, F. Liu, X. Zeng, G. Ungar and C. Tschierske, *Angew. Chem. Int. Ed.*, 2007, **46**, 7856. (b) W. Bu, H. Gao, X. Tan, X. Dong, X. Cheng, M. Prehm and C. Tschierske, *Chem. Commun.*, 2013, **49**, 1756.
169. A. P. H. J. Schenning, A. F. M. Kilbinger, F. Biscarini, M. Cavallini, H. J. Cooper, P. J. Derrick, W. J. Feast, R. Lazzaroni, P. Leclère, L. A. McDonnell, E. W. Meijer and S. C. J. Meskers, *J. Am. Chem. Soc.*, 2002, **124**, 1269.
170. (a) R. A. Cormier and B. A. Gregg, *Chem. Mater.*, 1998, **10**, 1309. (b) B. A. Gregg and R. A. Cormier, *J. Am. Chem. Soc.*, 2001, **123**, 7959. (c) S.-G. Liu, G. Sui, R. A. Cormier, R. M. Leblanc and B. A. Gregg, *J. Phys. Chem. B*, 2002, **106**, 1307. (d) S.-G. Chen, P. Stradins and B. A. Gregg, *J. Phys. Chem. B*, 2005, **109**, 13451. (e) B. A. Gregg and M. E. Kose, *Chem. Mater.*, 2008, **20**, 5235.
171. Y. Miyake, A. Fujii, M. Ozaki and Y. Shimizu, *Synth. Met.*, 2009, **159**, 875.
172. L. Sosa-Vargas, F. Nekelson, D. Okuda, M. Takahashi, Y. Matsuda, Q.-D. Dao, H. Yoshida, A. Fujii, M. Ozaki

- and Y. Shimizu, *J. Mater. Chem. C*, 2015, **3**, 1757.
173. T. Sakurai, K. Shi, H. Sato, K. Tashiro, A. Osuka, A. Saeki, S. Seki, S. Tagawa, S. Sasaki, H. Masunaga, K. Osaka, M. Takata and T. Aida, *J. Am. Chem. Soc.*, 2008, **130**, 13812.
174. (a) F. Tittarelli, P. Masson and A. Skoulios, *Liq. Cryst.*, 1997, **22**, 721. (b) M. Huskic and M. Zigon, *Liq. Cryst.*, 2002, **29**, 1217. (c) S. Ujiie and Y. Yano, *Chem. Commun.*, 2000, 79. (d) T. Ichikawa, M. Yoshio, A. Hamasaki, S. Taguchi, F. Liu, X.-B. Zeng, G. Ungar, H. Ohno and T. Kato, *J. Am. Chem. Soc.*, 2012, **134**, 2634.
175. (a) T. Matsumoto, T. Ichikawa, J. Sakuda, T. Kato and H. Ohno, *Bull. Chem. Soc. Jpn.*, 2014, **87**, 792. (b) T. Ichikawa, T. Kato and H. Ohno, *J. Am. Chem. Soc.*, 2012, **134**, 11354.
176. (a) M. Yoshio, T. Mukai, H. Ohno and T. Kato, *J. Am. Chem. Soc.*, 2004, **126**, 994. (b) M. Yoshio, T. Kato, T. Mukai, M. Yoshizawa and H. Ohno, *Mol. Cryst. Liq. Cryst.*, 2004, **413**, 2235. (c) M. Yoshio, T. Kagata, K. Hoshino, T. Mukai, H. Ohno and T. Kato, *J. Am. Chem. Soc.*, 2006, **128**, 5570. (d) M. Yoshio, T. Ichikawa, H. Shimura, T. Kagata, A. Hamasaki, T. Mukai, H. Ohno and T. Kato, *Bull. Chem. Soc. Jpn.*, 2007, **80**, 1836. (e) D. Högberg, B. Soberats, S. Uchida, M. Yoshio, L. Kloo, H. Segawa and T. Kato, *Chem. Mater.*, 2014, **26**, 6496. (f) J. Sakuda, E. Hosono, M. Yoshio, T. Ichikawa, T. Matsumoto, H. Ohno, H. Zhou and T. Kato, *Adv. Funct. Mater.*, 2015, **25**, 1206. (g) H. Yoshizawa, T. Mihara and N. Koide, *Mol. Cryst. Liq. Cryst.*, 2004, **423**, 61. (h) J. Motoyanagi, T. Fukushima and T. Aida, *Chem. Commun.*, 2005, 101.
177. (a) D. Navarro-Rodriguez, Y. Frere, P. Gramain, D. Guillon and A. Skoulios, *Liq. Cryst.*, 1991, **9**, 321. (b) E. Bravo-Grimaldi, D. Navarro-Rodriguez, A. Skoulios and D. Guillon, *Liq. Cryst.*, 1996, **20**, 393. (c) L. Cui, V. Sapagovas, and G. Lattermann, *Liq. Cryst.*, 2002, **29**, 1121. (d) V. Hessel, H. Ringsdorf, R. Festag and J. H. Wendorff, *Makromol. Chem. Rapid Commun.*, 1993, **14**, 707. (e) S. Kumar and S. K. Pal, *Tetrahedron Lett.*, 2005, **46**, 4127.
178. (a) S. Yazaki, M. Funahashi and T. Kato, *J. Am. Chem. Soc.*, 2008, **130**, 13206. (b) S. Yazaki, M. Funahashi, J. Kagimoto, H. Ohno and T. Kato, *J. Am. Chem. Soc.*, 2010, **132**, 7702.
179. J. J. Lee, A. Yamaguchi, M. A. Alam, Y. Yamamoto, T. Fukushima, K. Kato, M. Takata, N. Fujita and T. Aida, *Angew. Chem. Int. Ed.*, 2012, **51**, 8490.
180. (a) K. Ohta, R. Higashi, M. Ikejima, I. Yamamoto and N. Kobayashi, *J. Mater. Chem.*, 1998, **8**, 1979. (b) K. Ohta, H. Hasebe, M. Moriya, T. Fujimoto and I. Yamamoto, *Mol. Cryst. Liq. Cryst.*, 1991, **208**, 33. (c) K. Ohta, Y. Inagaki-Oka, H. Hasebe and I. Yamamoto, *Polyhedron*, 2000, **19**, 267.
181. M. J. Hollamby and T. Nakanishi, *J. Mater. Chem. C*, 2013, **1**, 6178.
182. M. Naita, J. Sakuda, Y. Hirai, M. Funahashi and T. Kato, *Chem. Lett.*, 2011, **40**, 412.
183. K. Isoda, T. Abe, M. Funahashi and M. Tadokoro, *Chem.-Eur. J.*, 2014, **20**, 7232.
184. (a) S. R. Farrar, A. E. A. Contoret, M. O'Neill, J. E. Nicholls, G. J. Richards and S. M. Kelly, *Phys. Rev. B*, 2002, **66**, 125107. (b) K. L. Woon, M. O'Neill, G. J. Richards, M. P. Aldred, S. M. Kelly and A. M. Fox, *Adv. Mater.*, 2003, **15**, 1555. (c) K. L. Woon, M. O'Neill, P. Vlachos, M. P. Aldred and S. M. Kelly, *Liq. Cryst.*, 2005, **32**, 1191. (d) K. L. Woon, M. O'Neill, G. J. Richards, M. P. Aldred and S. M. Kelly, *J. Opt. Soc. Am. A*, 2005, **22**, 760. (e) K. L. Woon, M. O'Neill, G. J. Richards, M. P. Aldred and S. M. Kelly, *Phys. Rev. E*, 2005, **71**, 041706.
185. G. H. Mehl, A. J. Thornton and J. W. Goodby, *Mol. Cryst. Liq. Cryst.*, 1999, **332**, 455.

186. (a) M. Funahashi and A. Sonoda, *Org. Electron.*, 2012, **13**, 1633; (b) M. Funahashi and A. Sonoda, *J. Mater. Chem.*, 2012, **22**, 25190.
187. M. Funahashi and A. Sonoda, *Dalton Trans.*, 2013, **42**, 15987.
188. M. Funahashi, M. Yamaoka, K. Takenami and A. Sonoda, *J. Mater. Chem. C*, 2013, **1**, 7872.
189. *Device Physics of Organic Semiconductors*, edited by C. Adachi, Kodansha Co. Ltd., Tokyo, 2012.
190. *Organic Electronic Materials*, edited by R. Farchioni and G. Grosso, Springer, Berlin, 2001.
191. D. C. Hoesterey and G. M. Letson, *J. Phys. Chem. Sol.*, 1963, **24**, 1609.
192. (a) W. Warta, R. Stehle and N. Karl, *Appl. Phys. A*, 1985, **36**, 163. (b) W. Shockley, *Bell Syst. Tech. J.*, 1951, **4**, 990.
193. (a) R. A. Marcus and N. Sutin, *Biochim. Biophys. Acta*, 1985, **811**, 265. (b) R. A. Marcus, *Rev. Modern Physics*, 1993, **65**, 599.
194. (a) A. Miller and E. Abrahams, *Phys. Rev.*, 1958, **109**, 1492. (b) V. Ambegaokar, B. I. Halperin and J. S. Langer, *Phys. Rev. B*, 1971, **4**, 2612.
195. N. F. Mott and W. D. Twose, *Adv. Phys.*, 1961, **10**, 107.
196. H. Bässler, *Phys. Status Solidi (b)*, 1993, **175**, 15.
197. (a) J. Frenkel, *Phys. Rev.*, 1938, **54**, 647. (b) D. M. Pai, *J. Chem. Phys.*, 1970, **52**, 2285. (c) W. D. Gill, *J. Appl. Phys.*, 1972, **43**, 5033.
198. (a) K. Oikawa, H. Monobe, J. Takahashi, K. Tsuchiya, B. Heinrich, D. Guillon and Y. Shimizu, *Chem. Commun.*, 2005, 5337. (b) M. Funahashi and J. Hanna, *Adv. Mater.*, 2005, **17**, 594. (c) H. Iino, J. Hanna, R. Bushby, B. Movaghar, B. J. Whitaker and M. J. Cook, *Appl. Phys. Lett.*, 2005, **87**, 132102. (d) K. Takenami, S. Uemura and M. Funahashi, *RSC Adv.*, 2016, **6**, 5474.
199. L. Friedman, *Phys. Rev.*, 1964, **133**, A1668.
200. Y. Shimizu, K. Oikawa, K. Nakayama and D. Guillon, *J. Mater. Chem.*, 2007, **17**, 4223.
201. (a) S. R. Farrar, A. E. A. Contoret, M. O'Neill, J. E. Nicholls, G. J. Richards and S. M. Kelly, *Phys. Rev. B*, 2002, **66**, 125107. (b) M. Funahashi and N. Tamaoki, *ChemPhysChem*, 2006, **7**, 1193. (c) M. Funahashi and N. Tamaoki, *Chem. Mater.*, 2007, **19**, 608. (d) K. L. Woon, M. P. Aldred, P. Vlachos, G. H. Mehl, T. Stirner, S. M. Kelly and M. O'Neill, *Chem. Mater.*, 2006, **18**, 2311. (e) K. Tokunaga, H. Iino, J. Hanna, *Mol. Cryst. Liq. Cryst.*, 2009, **510**, 241.
202. (a) A. M. van de Craats, J. M. Warman, M. R. de Haas, D. Adam, J. Simmerer, D. Haarer and P. Schuhmacher, *Adv. Mater.*, 1996, **8**, 823. (b) Y. Hirai, H. Monobe, N. Mizoshita, M. Moriyama, K. Hanabusa, Y. Shimizu and Takashi Kato, *Adv. Funct. Mater.*, 2008, **18**, 1668.
203. (a) M. Funahashi and J. Hanna, *Mol. Cryst. Liq. Cryst.*, 1997, **304**, 429. (b) M. Funahashi and J. Hanna, *Mol. Cryst. Liq. Cryst.*, 1999, **331**, 509. (c) M. Funahashi and J. Hanna, *Mol. Cryst. Liq. Cryst.*, 2001, **368**, 303.
204. (a) R. B. Meyer, *Mol. Cryst. Liq. Cryst.*, 1977, **40**, 33. (b) K. Skarp and M. A. Handschy, *Mol. Cryst. Liq. Cryst.*, 1988, **165**, 439. (c) M. Hird, *Liq. Cryst.*, 2011, **38**, 1467.
205. S. T. Lagerwall, "Ferroelectric Liquid Crystals" in *Handbook of Liquid Crystals*, ed. D. Demus, J. Goodby, G. W. Gray, H.-W. Spiess and V. Vill, Wiley-VCH, Weinheim, 1998, **2B**, 515.
206. W. L. McMillan, *Phys. Rev. A*, 1973, **8**, 1921.

207. A. Kanazawa, T. Ikeda and J. Abe, *Angew. Chem., Int. Ed.*, 2000, **39**, 612.
208. Structures and Properties of Ferroelectric Liquid Crystals, edited by A. Fukuda and H. Takezoe, Corona Publishing Co. Ltd., Tokyo, 1990.
209. (a) S. Hattori, M. Isogai, K. Iwasaki, T. Kitamura, A. Kobi, T. Inukai, K. Furukawa, K. Terajima and S. Saito, *Jpn. Kokai Tokkyo Koho*, 1985, JP60199865A. (b) R. Blinc, J. Dolinsek, M. Luzar and J. Seliger, *Liq. Cryst.*, 1988, **3**, 663.
210. (a) P. Keller, *Ann. Phys.*, 1978, **3**, 139. (b) T. Inukai, S. Saito, H. Inoue, K. Miyazawa, K. Terajima and M. Ichihashi, *Jpn. Kokai Tokkyo Koho*, 1986, JP61183256A.
211. (a) J. W. Goodby, E. Chin, T. M. Leslie, J. M. Geary and J. S. Patel, *J. Am. Chem. Soc.*, 1986, **108**, 4729. (b) A. Buka and H. Stegemeyer, *Liq. Cryst.*, 1990, **8**, 229.
212. (a) J. W. Goodby and T. M. Leslie, "Some Novel Ferroelectric Smectic Liquid Crystals" in *Liquid Crystals & Ordered Fluids vol. 1*, edited by A. C. Griffin and J. F. Johnson, Plenum, New York, 1982. (b) E. Chin and J. W. Goodby, *Mol. Cryst. Liq. Cryst.*, 1986, **141**, 311. (c) G. Decobert and J. C. Dubois, *Mol. Cryst. Liq. Cryst.*, 1984, **114**, 237.
213. (a) M. Taguchi, T. Harada and H. Suenaga, *PCT Int. Appl.*, 1986, WO8600087A1. (b) H. Suenaga, M. Taguchi and T. Harada, *Jpn. Kokai Tokkyo Koho*, 1986, JP61215373A. (c) K. Seto, H. Matsubara, S. Takahashi, T. Tahara, M. Murakami, S. Miyake, T. Masumi, T. Ando and A. Fukami, *J. Chem. Soc., Chem. Commun.*, 1988, 56.
214. (a) K. Furukawa, K. Terashima, M. Ichihashi, S. Saitoh, K. Miyazawa, and T. Inukai, *Ferroelectrics*, 1988, **85**, 451. (b) J. Billard, A. Dahlgren, K. Flatischler, S. T. Lagerwall and B. Otterholm, *J. Phys.*, 1985, **46**, 1241. (c) J. Billard, A. Dahlgren, K. Flatischler, S. T. Lagerwall and B. Otterholm, *Mol. Cryst. Liq. Cryst.*, 1986, **135**, 265.
215. (a) J. P. F. Lagarwall and F. Giesselmann, *ChemPhysChem*, 2006, **7**, 20. (b) J. Naciri, J. Ruth, G. Crawford, R. Shashidhar and B. R. Ratna, *Chem. Mater.*, 1995, **7**, 1397. (c) M. Spector, P. Heiney, J. Naciri, B. Weslowski, D. Holt and R. Shashidhar, *Phys. Rev. E*, 2000, **61**, 1579. (d) J. V. Selinger, P. J. Collings and R. Shashidhar, *Phys. Rev. E*, 2001, **64**, 061705. (e) O. Panarina, Y. Panarin, J. Vij, M. Spector and R. Shashidhar, *Phys. Rev. E*, 2003, **67**, 051709. (f) P. J. Collings, B. R. Ratna and R. Shashidhar, *Phys. Rev. E*, 2003, **67**, 021705. (g) D. Nonnenmacher, M. A. Osipov, J. C. Roberts, R. P. Lemieux, and F. Giesselmann, *Phys. Rev. E*, 2010, **82**, 031703. (h) D. Nonnenmacher, R. P. Lemieux, M. A. Osipov, and F. Giesselmann, *ChemPhysChem*, 2014, **15**, 1368.
216. (a) N. Maruyama, *Ferroelectrics*, 1985, **63**, 49. (b) S. Dumrongrattana and C. C. Huang, *Phys. Rev. Lett.*, 1986, **56**, 464. (c) H. Nohira, M. Yamada, D. Terunuma and M. Nohira, *Kobunshi Ronbunshu*, 1999, **56**, 401. (d) K. Fujisawa, C. Sekine, Y. Uemura, T. Higashii, M. Minai and I. Dohgane, *Ferroelectrics*, 1991, **121**, 167. (e) M. Minai, T. Higashii, *Jpn. Kokai Tokkyo Koho*, 1989, JP01305055A. (f) N. Shiratori, I. Nishiyama, A. Yoshizawa and T. Hirai, *Jpn. J. Appl. Phys.*, 1990, **29**, L2086. (g) K. Furukawa, K. Terashima, M. Ichihashi, S. Saitoh, K. Miyazawa and T. Inukai, *Ferroelectrics*, 1988, **85**, 451. (h) S. Kobayashi and S. Ishibashi, *Mol. Cryst. Liq. Cryst. Sci. Technol., Sect. A*, 1992, **220**, 1.
217. (a) T. Niori, T. Sekine, J. Watanabe, T. Furukawa and H. Takezoe, *J. Mater. Chem.*, 1996, **6**, 1231. (b) D. A.

- Coleman, J. Fernsler, N. Chattham, M. Nakata, Y. Takanishi, E. Korblova, D. R. Link, R.-F. Shao, W. G. Jang, J. E. Maclennan, O. Mondainn-Monval, C. Boyer, W. Weissflog, G. Pelzl, L.-C. Chien, J. Zasadzinski, J. Watanabe, D. M. Walba, H. Takezoe and N. A. Clark, *Science*, 2003, **301**, 1204. (c) S. K. Lee, S. Heo, J. G. Lee, K. -T. Kang, K. Kumazawa, K. Nishida, Y. Shimbo, Y. Takanishi, J. Watanabe, T. Doi, T. Takahashi and H. Takezoe, *J. Am. Chem. Soc.*, 2005, **127**, 11085. (d) F. Araoka, N. Y. Ha, Y. Kinoshita, B. Park, J. W. Wu and H. Takezoe, *Phys. Rev. Lett.*, 2005, **94**, 137801. (e) Y. Shimbo, Y. Takanishi, K. Ishikawa, E. Gorecka, D. Pocięcha, J. Mieczkowski, K. Gomola and H. Takezoe, *Jpn. J. Appl. Phys.*, 2006, **45**, L282. (f) K. Nishida, M. Čepič, W.-J. Kim, S.-K. Lee, S. Heo, J.-G. Lee, Y. Takanishi, K. Ishikawa, K.-T. Kang, J. Watanabe and H. Takezoe., *Phys. Rev. E*, 2006, **74**, 021704.
218. (a) F. Araoka and H. Takezoe, *Jpn. J. Appl. Phys.*, 2014, **53**, 01AA01. (b) D. Miyajima, F. Araoka, H. Takezoe, J. Kim. K. Kato, M. Takata and T. Aida, *Science*, 2012, **336**, 209. (c) F. Araoka, S. Masuko, A. Kogure, D. Miyajima, T. Aida and H. Takezoe, *Adv. Mater.*, 2013, **25**, 4014.
219. K. W. Böer, *Survey of Semiconductor Physics Volume II*, Springer Science+Business Media, New York, 1992.
220. (a) A. Mishra, P. Baeuerle, *Angew. Chem. Int. Ed.*, 2012, **51**, 2020. (b) A. Facchetti, *Chem. Mater.*, 2011, **23**, 733. (c) Y. Lin, Y. Li and X. Zhan, *Chem. Soc. Rev.*, 2012, **41**, 4245.
221. K. T. Butler, J. M. Frost and A. Walsh, *Energy Environ. Sci.*, 2015, **8**, 838.
222. J. Starkiewicz, L. Sosnowski and O. Simpson, *Nature*, 1946, **158**, 28.
223. H. R. Johnson, R. H. Williams and C. H. B. Mee, *J. Phys. D: Appl. Phys.*, 1975, **8**, 1530.
224. B. Goldstein and L. Pensak, *J. Appl. Phys.*, 1959, **30**, 155.
225. M. D. Uspenskii, N. G. Ivanova and I. E. Malkis, *Semiconductors*, 1968, **1**, 1059.
226. H. Dember, *Phys. Zeits.*, 1931, **32**, 554.
227. (a) T. Dekorsy, X. Q. Zhou, K. Ploog and H. Kurz, *Mater. Sci. Eng. B Solid State M.*, 1993, **B22**, 68. (b) T. Dekorsy, H. Kurz, X. Q. Zhou and K. Ploog, *Appl. Phys. Lett.*, 1993, **63**, 2899. (c) C.-H. Liu, Y.-C. Chang, S. Lee, Y. Zhang, Y. Zhang, T. B. Norris and Z. Zhong, *Nano Lett.*, 2015, **15**, 4234.
228. V. Strano, E. Smecca, V. Depauw, C. Trompoukis, A. Alberti, R. Reitano, I. Crupi, I. Gordon and S. Mirabella, *Appl. Phys. Lett.*, 2015, **106**, 013901.
229. T. Zhao, W. Shi, J. Xi, D. Wang and Z. Shuai, *Sci. Rep.*, 2016, **7**, 19968.
230. S. Nakashima, K. Takayama, K. Shigematsu, H. Fujisawa and M. Shimizu, *Jpn. J. Appl. Phys.*, 2016, **55**, 10TA07
231. S. Nakashima, T. Uchida, K. Doi, K. Saitoh, H. Fujisawa, O. Sakata, Y. Katsuya, N. Tanaka and M. Shimizu, *Jpn. J. Appl. Phys.*, 2016, **55**, 10I501.
232. (a) A. Sugita, K. Suzuki and S. Tasaka, *Phys. Rev. B*, 2004, **69**, 212201. (b) H. Sasabe, T. Nakayama, K. Kumazawa, S. Miyata and E. Fukuda, *Polym. J.*, 1981, **13**, 967.
233. T. Hamamoto and M. Funahashi, *J. Mater. Chem. C*, 2015, **3**, 6891.
234. Y. Funatsu, A. Sonoda and M. Funahashi, *J. Mater. Chem. C*, 2015, **3**, 1982.

Chapter 2

Bulk photovoltaic effect in ferroelectric liquid crystals based on phenylterthiophene derivatives

Abstract: Photovoltaic effect in ferroelectrics has attracted much attention, due to their potential of generating a large open-circuit voltage. Recently, we focus on APV effect in FLC phase. In this work, we have synthesized FLC phenylterthiophene derivatives, whose carrier mobilities are different magnitude. They exhibit bulk photovoltaic effect in FLC phases. The photocurrent response is correlated with the carrier mobility and spontaneous polarization in the FLC phase instead of ionic impurities.

2.1. Introduction

As described in chapter 1, a few inorganic ferroelectric ceramics such as BaTiO_3 exhibits bulk photovoltaic effect.¹⁻⁵ The photovoltaic effect in ferroelectrics can produce a large open-circuit voltage based on spontaneous polarization without p-n or Schottky junctions.⁶ However, most typical inorganic ferroelectrics exhibiting the APV effect are unsuitable materials for the application of solution-processes and the use for light-weight flexible devices. In addition, the absorption bands of these ceramics lies in UV area, which results in low power conversion efficiency.²⁻⁵ The diversity of molecular designs in organic materials provides some advantages in design and processability for flexible and light-weight devices over the inorganic system. However, the report of bulk photovoltaic effect based on organic ferroelectrics is much less. Only two organic ferroelectric systems based on thin films of dye doped poly (vinylidene fluoride) and triphenylene ester have been investigated on the APV effect.⁷ These compounds are insulative and have no absorption bands in near UV and visible areas. Thus, the power conversion efficiencies were less than 1%.⁷

Most of FLC materials have been developed for the application to high speed liquid crystal displays.⁸ Although ferroelectric columnar phases have been recently discovered, the ferroelectric columnar LC materials are also electrically insulative and do not exhibit the photovoltaic effect.⁹ A SmC^* phase consisting of chiral LC molecules has a helical structure, which is unwound to produce spontaneous polarization under the application of the DC electric field. The ferroelectric properties are strongly influenced by the molecular aggregation structure and molecular ordering.

On the other hand, LC molecules comprised of extended π -conjugated systems work as organic semiconductors which can be applied to some electronic devices such as FETs and solar cells.¹⁰ Carrier transport properties are also affected by the molecular packing in the self-assembled structures.

Recently, a few groups synthesized extended π -conjugated FLC compounds, which exhibits photorefractive and rectification effects.¹¹ Bulk photovoltaic effect in the FLC compounds based on a phenylterthiophene moiety was found for the first time by our group.¹² However, polarization of ionic impurities should also cause photovoltaic effect without an external electric field, as observed in perovskite compounds.¹³

In this study, we verify that this photovoltaic phenomena in the ferroelectric SmC* phase is originated from the spontaneous polarization. We have synthesized analogous compounds bearing an alkenyl chain and a bulky cyclotetrasiloxane ring (Figure 1). We studied the relationship between their photocurrents, spontaneous polarizations, and hole mobilities.

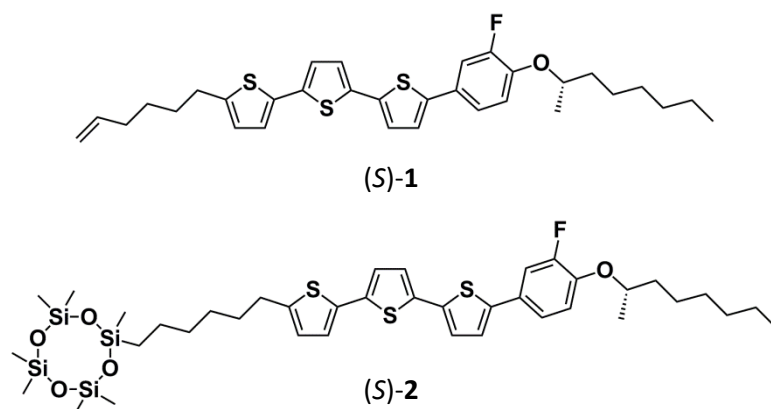


Figure 2-1. Chemical structures of chiral phenylterthiophene derivatives (S)-1 and (S)-2.

2.2. Experimental Section

2.2.1. General Methods

All ^1H - and ^{13}C -NMR spectra were performed by solutions in CDCl_3 on a Varian UNITY INOVA400NB spectrometer. Matrix-assisted laser desorption ionization time-of-flight (MALDI-TOF) mass spectra were performed by Bruker Daltonics ultrafleXtremeTM. A polarizing optical microscope, Olympus DP70, equipped with a handmade hot stage was used for visual observation of optical textures. DSC measurements were conducted with a NETZSCH DSC 204 Phoenix. XRD patterns were acquired with a Rigaku Rapid II diffractometer equipped with a handmade hot stage with the use of Ni-filtered $\text{Cu K}\alpha$ radiation. Hole mobilities were measured by a time-of-flight (TOF) method. A liquid crystal cell was fabricated by combining two glass plates. The cell was put on a hot stage and heated above the clearing temperature. The sample was melted and capillary filled into the cell. The liquid crystal cell was placed on a hot stage, DC voltage was applied to the cell using an electrometer (ADC R8252), and a pulse laser illuminated the cell. The excitation source was the third harmonic generation of a Nd:YAG laser (Continuum MiniLite II, wavelength = 356 nm, pulse duration = 2 ns) and the induced displacement currents were recorded using a digital oscilloscope (Tektronix TDS 3044B) through a serial resistor. Spontaneous polarizations were evaluated by the Sawyer-Tower method

using triangular-wave bias (± 5 V, 100 Hz) with 2 μ m thick cells. The hysteresis loops were recorded using a digital oscilloscope (Tektronix TDS 3044B) through a serial capacitor. The steady state photocurrent response measurements were performed with a using of high-pressure mercury lamp as a light source (light intensity: ~ 17 mW/cm²). In this measurement, a UV cut filter, an IR cut filter, and some lenses were appropriately set on optical system. The induced photocurrents were recorded using the digital oscilloscope through a serial resistor.

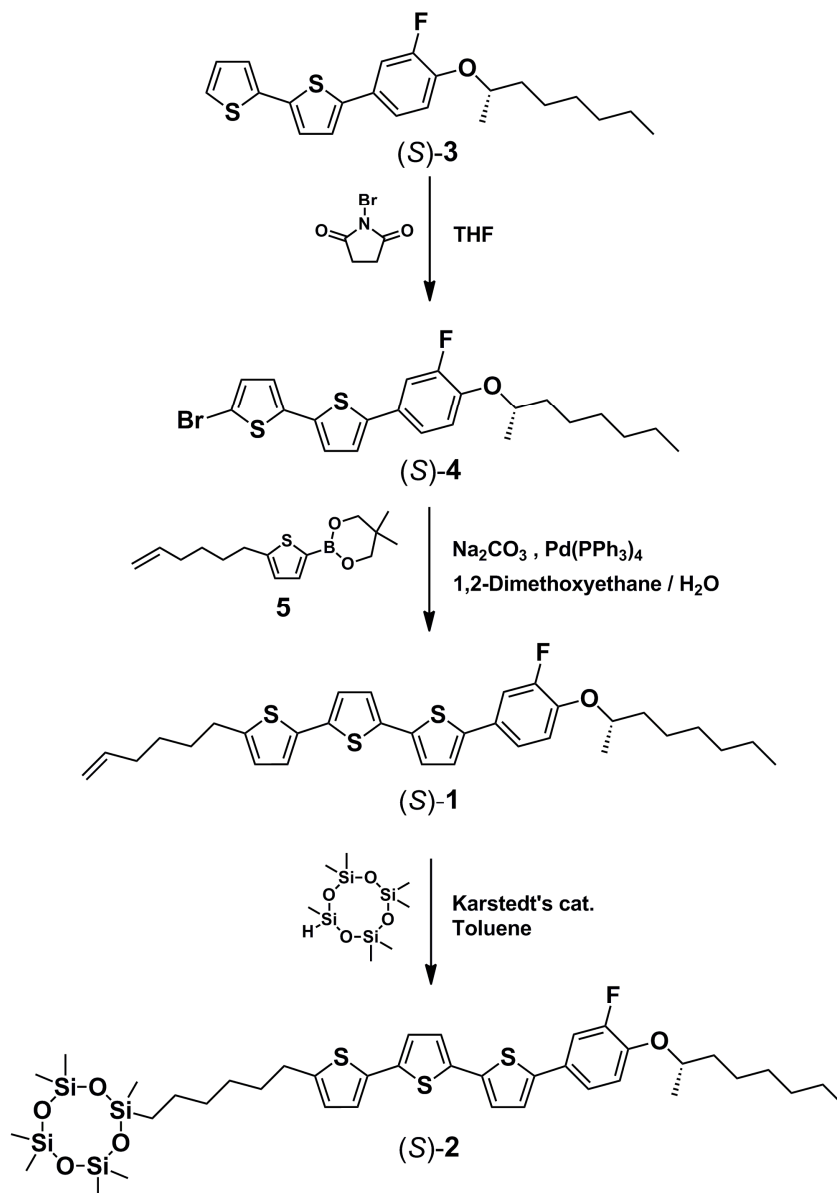
2.2.2. Materials

4-Bromo-2-fluorophenol, (*R*)-2-octanol, diethyl azodicarboxylate (40% in Toluene), thiophene, 2-bromothiophene, *N*-bromosuccineimide, 5-hexen-1-ol, phosphorus tribromide, trimethyl borate, 2, 2-dimethylpropanediol, tetrakis(triphenylphosphine)palladium(0), and [1,3-bis(diphenylphosphino)propane]nickel(II) dichloride were purchased from Tokyo Chemical Industry. 1, 3, 3, 5, 5, 7, 7- Heptamethyl-1, 3, 5, 7-cyclotetrasiloxane and the Karstedt's catalyst were purchased from Gelest Inc. Tetrahydrofuran, toluene, 1, 2-dimethoxyethane, *n*-butyllithium (1.6 M hexane soln.), and the other inorganic reagents were obtained from Wako Pure Chemical Industries. All of them were used without further purification. Silica gel was purchased from Kanto Chemicals.

2.2.3. Synthesis

All reactions were performed under nitrogen atmosphere in a well-dried three-necked flask equipped with a magnetic stirring bar.

Compounds (*S*)-**1** and (*S*)-**2** were synthesized as shown in scheme 2-1. The starting compounds (*S*)-**3** was synthesized via the Suzuki-Miyaura reaction between 2-bromo-5:2'-bithiophene and (*S*)-2-octyloxy-fluorophenyl borate, under the similar conditions to the previous report.¹ The bromination reaction of compound (*S*)-**3** with using *N*-bromosuccinimide was afforded to the compound (*S*)-**4**. Then, phenylterthiophene derivatives (*S*)-**1** bearing an alkenyl side chain was synthesized via Suzuki-Miyaura reaction between brominated phenylbithiophene derivative (*S*)-**4** and alkenylthienyl borate **5**. Compound (*S*)-**2** was obtained via hydrosilylation of compound (*S*)-**1**.



Scheme 2-1. Synthetic route of fluorophenylterthiophene derivatives (S)-1 and (S)-2.

6-Bromo-1-hexene

To stirred *N,N*-dimethylformamide (DMF; 600 mL) was slowly added dropwise phosphorus tribromide (PBr_3 , 28.5 mL, 300 mmol) at 0 °C over 20 min and gradually warmed to room temperature. The mixture was stirred over 30 min. Then, 5-hexen-1-ol (50.0 g, 499 mmol) with dry THF (90 mL) was slowly added to the cream-colored suspension cooling with ice-bath. After the addition of 5-hexen-1-ol, the mixture was gradually warmed to room temperature and stirred for 24 h. The reaction mixture was quenched by H_2O (300 mL). The organic layer was separated and the aqueous layer was extracted with hexane (100 mL \times 2, 50 mL \times 1). The collected organic fractions were combined and dried over Na_2SO_4 . After filtration, the crude solution was passed the short silica gel

column (eluent: *n*-hexane) and distilled to give 6-Bromo-1-hexene as a colorless clear liquid (48.6 g, 60 % yield).

¹H-NMR (400 MHz, CDCl₃): δ = 7.39 (d, 1H, *J* = 3.4 Hz), 6.83 (d, 1H, *J* = 3.4 Hz), 5.79 (ddt, 1H, *J* = 17.0, 10.2, 6.8 Hz), 3.42 (t, 2H, *J* = 6.8 Hz), 2.09 (quartet, 2H, *J* = 7.2 Hz), 1.88 (quintet, 2H, *J* = 7.2 Hz), 1.54 (quintet, 2H, *J* = 7.4 Hz).

2-(5-Hexenyl)thiophene

To a solution of thiophene (16.8 g, 200 mmol) in dry THF (250 mL) was slowly added *n*-buthyllithium (*n*-BuLi, 1.6 M in *n*-hexane soln., 114 mL, 185 mmol) with dry THF (50 mL) at -78 °C. After the addition of *n*-BuLi, the mixture was allowed to warm to 0 °C and stirred for 1 h. Then, 6-Bromo-1-hexene (25.0 g, 153 mmol) with dry THF (50 mL) was slowly added to reactant mixture at 0 °C. The obtained pale-yellow suspension was gradually warmed to room temperature and stirred for overnight at room temperature. The mixture was quenched by H₂O (150 mL) cooling with ice-bath. The product was extracted with hexane (100 mL \times 3, 50 mL \times 1). The organic layer was washed with brine (150 mL) and water (100 mL) in this order. The collected organic fractions were combined and dried over Na₂SO₄. After filtration, the crude solution was passed the silica gel column (eluent: *n*-hexane) and distilled *in vacuo* to give 2-(5-hexenyl)thiophene as a pale-yellow clear liquid (17.1 g, 67 % yield).

¹H-NMR (400 MHz, CDCl₃): δ = 7.10 (m, 1H), 6.91 (m, 1H), 6.77 (m, 1H), 5.80 (ddt, 1H, *J* = 17.0, 10.2, 6.6 Hz), 5.00 (ddd, 1H, *J* = 17.0, 3.2, 1.6 Hz), 4.95 (ddt, 1H, *J* = 10.2, 3.4, 1.2 Hz), 2.83 (t, 2H, *J* = 7.6 Hz), 2.08 (quartet, 2H, *J* = 7.2 Hz), 1.69 (quintet, 2H, *J* = 7.6 Hz), 1.46 (quintet, 2H, *J* = 7.6 Hz).

2-(5-hexenyl)thienylboric acid 2,2-dimethyl-1,3-propanediyl ester

To a solution of 2-(5-Hexenyl)thiophene (10.3 g, 62.1 mmol) in dry THF (200 mL) was slowly added *n*-BuLi (1.6 M in *n*-hexane soln., 44.5 mL, 71.7 mmol) with dry THF (10 mL) at -78 °C. After the addition of *n*-BuLi, the mixture was stirred for 1 h at -78 °C. Then, the mixture was allowed to warm to 0 °C for 10 min and cooled down to -78 °C again. Trimethyl borate (8.4 mL, 75.2 mmol) was slowly dropwised over 20 min. to reactant mixture at -78 °C. The obtained pale-yellow suspension was gradually warmed to room temperature and stirred for 20 h. Then, 2, 2-dimethylpropanediol (7.53 g, 72.3 mmol) with dry THF (30 mL) was added to the orange reactant mixture at 0 °C. The mixture was warmed to room temperature and stirred for 4.5 h. After the addition of H₂O (20 mL), the product was separated and washed with sat. NH₄Cl aq. (100 mL), brine (100 mL) and H₂O (100 mL) in this order. The aqueous layer was extracted with ethyl acetate (100 mL \times 1, 50 mL \times 2). The collected organic fractions were combined and dried over Na₂SO₄. After filtration and evaporation, the crude solution was purified by the silica gel column chromatography (eluent: *n*-hexane \rightarrow *n*-hexane/ethyl acetate = 5/1; v/v, gradient) and dried *in vacuo* to give 2-(5-hexenyl)thienylboric acid 2,2-dimethyl-1,3-propanediyl ester as a brown liquid (10.6 g, 61 % yield).

¹H-NMR (400 MHz, CDCl₃): δ = 7.39 (d, 1H, *J* = 3.4 Hz), 6.83 (d, 1H, *J* = 3.4 Hz), 5.79 (ddt, 1H, *J* = 17.0,

10.2, 6.8 Hz), 5.00 (ddd, 1H, $J = 17.2, 3.6, 1.6$ Hz), 4.94 (m, 1H), 3.74 (s, 4H, $J = 7.6$ Hz), 2.85 (t, 2H, $J = 7.6$ Hz), 2.07 (quartet, 2H, $J = 7.2$ Hz), 1.70 (quintet, 2H, $J = 7.6$ Hz), 1.46 (quintet, 2H, $J = 7.6$ Hz), 1.02 (s, 6H).

3-Fluoro-4-*[(S)-2-octyloxy]*-bromobenzene

To a mixture of triphenylphosphine (24.8 g, 94.5 mmol), (*R*)-2-octanol (10.7 g, 81.9 mmol) and 4-bromo-2-fluorophenol (15.0 g, 78.6 mmol) in dry THF (100 mL) was slowly added dropwise diethyl azodicarboxylate (DEAD, 2.2 M in toluene soln., 43.0 mL, 94.6 mmol) cooling with ice-bath. Then, the mixture was gradually warmed to room temperature and stirred for 4 h. Most of the precipitate of triphenylphosphine oxide generated by the reaction was removed by repeated concentration and filtration. The residue of concentrated filtrate was purified by the silica gel column chromatography (eluent: *n*-hexane) and dried *in vacuo* to give 3-fluoro-4-*[(S)-2-octyloxy]*-bromobenzene as a slight pale pink clear liquid (23.3 g, 98 % yield).

$^1\text{H-NMR}$ (400 MHz, CDCl_3): $\delta = 7.23$ (dd, 1H, $J = 10.6, 2.4$ Hz), 7.17 (ddd, 1H, $J = 8.6, 2.4, 1.6$ Hz), 6.85 (t, 1H, $J = 8.6$ Hz), 4.31 (sextet, 1H, $J = 6.0$ Hz), 1.81-1.72 (m, 1H), 1.63-1.53 (m, 1H), 1.49-1.27 (m, 8H), 1.30 (d, 3H, $J = 6.4$ Hz), 0.89 (t, 3H, $J = 7.0$ Hz).

3-Fluoro-4-*[(S)-2-octyloxy]* phenylboric acid 2,2-dimethyl-1,3-propanediyl ester

To a mixture of magnesium (1.12 g, 46.3 mmol) and iodine (one grain; 0.02 g) in dry THF (50 mL) was slowly added 3-fluoro-4-*[(S)-2-octyloxy]*-bromobenzene (10.0 g, 33.1 mmol) with dry THF (26 mL). The reactant mixture was stirred under gently reflux for 1 h, and then cooled down with dry ice/acetone bath. Trimethyl borate (4.80 mL, 43.0 mmol) was added dropwise at -78 °C around 5 min. The mixture was gradually warmed to room temperature and stirred for 18 h. Then, 2,2-dimethylpropanediol (5.17 g, 49.6 mmol) with dry THF (50 mL) was added to the reactant mixture at room temperature. After the reactant mixture was further stirred for 3 h, H_2O (100 mL) was added. The product was extracted with *n*-hexane (100 mL $\times 3$, 50 mL $\times 1$). The collected organic fractions were combined and dried over MgSO_4 . After filtration and evaporation, the crude product was purified by the silica gel column chromatography (eluent: *n*-hexane/ethyl acetate = 10/1; v/v) and dried *in vacuo* to give 2-(5-hexenyl)thienylboric acid 2,2-dimethyl-1,3-propanediyl ester as a pale yellow liquid (9.04 g, 81 % yield).

$^1\text{H-NMR}$ (400 MHz, CDCl_3): $\delta = 7.47$ (d, 2H, $J = 10.6$ Hz), 6.93 (t, 1H, $J = 8.0$ Hz), 4.40 (sextet, 1H, $J = 6.0$ Hz), 3.74 (s, 4H), 1.82-1.73 (m, 1H), 1.63-1.54 (m, 1H), 1.49-1.27 (m, 8H), 1.31 (d, 3H, $J = 6.4$ Hz), 1.01 (s, 6H), 0.87 (t, 3H, $J = 6.8$ Hz); exact mass: 336.23; molecular weight: 336.25; m/z : 374.83, 375.83, 376.83, 377.84 (All signals were indicated the $[\text{M}+\text{K}]^+$ fragments pattern).

2,2'-Bithiophene

To a mixture of magnesium (2.98 g, 123 mmol) and iodine (one grain; 0.03 g) in dry diethylether (110 mL) was slowly added 2-bromothiophene (21.6 g, 133 mmol) while cooling appropriately with

ice bath. The prepared thienyl Grignard reagent was slowly added over 30 min to the suspension of 2-bromothiophene (10.1 g, 62.2 mmol) and [1,3-bis(diphenylphosphino)propane]nickel(II) dichloride ($\text{NiCl}_2(\text{dppp})$, 2.34 g, 4.31 mmol) in dry diethylether (60 mL). The reactant mixture was stirred under gently reflux for 20 h, and then poured into cold water (100 mL). The product was extracted with *n*-hexane (120 mL \times 3, 60 mL \times 2). The collected organic fractions were combined and dried over MgSO_4 . After filtration and evaporation, the crude product was purified by the silica gel column chromatography (eluent: *n*-hexane) and dried *in vacuo* to give 2,2'-bithiophene as a colorless crystal (11.8 g, 94 % yield).

$^1\text{H-NMR}$ (400 MHz, CDCl_3): δ = 7.20 (dd, 2H, J = 5.2, 1.2 Hz), 7.17 (dd, 2H, J = 3.6, 1.2 Hz), 7.01 (dd, 2H, J = 5.2, 3.6 Hz).

5-Bromo-2,2'-bithiophene

To a solution of 2,2'-bithiophene (2.49 g, 15.0 mmol) in dry THF (70 mL) was slowly added *N*-bromosuccinimide (NBS, 2.00 g, 11.2 mmol) over 1 h at 0 °C. Then, the mixture was allowed to warm to room temperature and stirred for overnight. After the addition of 4 wt% Na_2CO_3 aqueous solution (50 mL), the product was extracted with hexane (30 mL). The organic layer was washed with brine (50 mL) and water (50 mL). The aqueous layer was extracted with hexane (100 mL \times 1, 50 mL \times 3) and all organic layers were combined. The extract was dried over anhydrous MgSO_4 . After filtration and evaporation, the crude product was purified by flash silica gel column chromatography (eluent: *n*-hexane) and dried *in vacuo* to give 5-bromo-2,2'-bithiophene as a colorless crystal (2.29 g, 83 % yield).

$^1\text{H-NMR}$ (400 MHz, CDCl_3): δ = 7.23 (dd, 1H, J = 5.2, 1.2 Hz), 7.11 (dd, 1H, J = 3.6, 1.2 Hz), 7.01 (dd, 1H, J = 5.2, 3.6 Hz), 6.97 (d, 1H, J = 3.8 Hz), 6.91 (d, 1H, J = 3.8 Hz).

5-[4-*{(S)}*-2-octyloxy]-3-fluorophenyl]-2,2'-bithiophene

To a stirred solution of 5-bromo-2,2'-bithiophene (2.51 g, 10.3 mmol), 3-fluoro-4-*{(S)}*-2-octyloxy phenylboric acid 2,2-dimethyl-1,3-propanediyl ester (4.32 g, 12.8 mmol) and tetrakis(triphenylphosphine)palladium(0) ($\text{Pd}(\text{PPh}_3)_4$, 1.19 g, 1.03 mmol) in 1,2-dimethoxyethane (250 mL) was added 2 mol/L Na_2CO_3 aqueous solution (155 mL, 306 mmol). After the reaction mixture was stirred under reflux for 6 h, 1,2-dimethoxyethane was removed from the reaction mixture under the reduced pressure. The produced precipitates were collected by filtration. The filtrate was extracted with *n*-hexane (200 mL \times 1, 100 mL \times 1). The extract was dried over anhydrous MgSO_4 . After filtration and evaporation, obtained solid was combined with former precipitate. The crude product was purified by silica gel column chromatography (eluent: *n*-hexane/toluene = 5/1; v/v). The product was recrystallized from *n*-hexane and dried *in vacuo* to give 5-[4-*{(S)}*-2-octyloxy]-3-fluorophenyl]-2,2'-bithiophene as a white-light pale green crystal (3.58 g, 90 % yield).

$^1\text{H-NMR}$ (400 MHz, CDCl_3): δ = 7.32 (dd, 1H, J = 12.2, 2.2 Hz), 7.27 (dd, 1H, J = 8.2, 2.4 Hz), 7.22 (d, 1H, J = 5.2 Hz), 7.18 (dd, 1H, J = 3.6, 0.8 Hz), 7.12 (d, 1H, J = 3.8 Hz), 7.11 (d, 1H, J = 3.8 Hz), 7.03 (dd, 1H, J

= 5.2, 3.6 Hz), 6.96 (t, 1H, J = 8.6 Hz), 4.37 (sextet, 1H, J = 6.0 Hz), 1.84-1.75 (m, 1H), 1.65-1.56 (m, 1H), 1.51-1.25 (m, 8H), 1.33 (d, 3H, J = 6.0 Hz), 0.88 (t, 3H, J = 6.8 Hz); exact mass: 388.13; molecular weight: 388.56; m/z : 288.80, 389.82, 390.82, 391.82, 392.03.

5-Bromo-5'-[4-*(S)*-2-octyloxy]-3-fluorophenyl]-2,2'-bithiophene

To a solution of 5-[4-*(S)*-2-octyloxy]-3-fluorophenyl]-2,2'-bithiophene (3.11g, 7.99 mmol) in dry THF (50 mL) was slowly added NBS (1.45 g, 8.15 mmol) at 0 °C. Then, the mixture was allowed to warm to room temperature and stirred for overnight. After the addition of 2 wt% Na₂CO₃ aqueous solution (50 mL), the product was extracted with hexane (50 mL). The organic layer was washed with brine (50 mL) and water (100 mL). The aqueous layer was extracted with hexane (100 mL ×1, 50 mL ×3) and all organic layers were combined. The extract was dried over anhydrous MgSO₄. After filtration and evaporation, the crude product was purified by flash silica gel column chromatography (eluent: *n*-hexane/ethyl acetate = 10/1; v/v). The product was recrystallized from *n*-hexane and dried *in vacuo* to afford 5-bromo-5'-[4-*(S)*-2-octyloxy]-3-fluorophenyl]-2,2'-bithiophene as light-yellow solid (3.45 g, 92 % yield).

¹H-NMR : δ = 7.30 (dd, 1H, J = 12.0, 2.4 Hz), 7.25 (ddd, 1H, J = 8.4, 2.4, 1.2 Hz), 7.09 (d, 1H, J = 4.0 Hz), 7.05 (d, 1H, J = 4.0 Hz), 6.98 (d, 1H, J = 4.0 Hz), 6.96 (t, 1H, J = 8.8 Hz), 6.92 (d, 1H, J = 3.6 Hz), 4.38 (sextet, 1H, J = 6.0 Hz), 1.84-1.74 (m, 1H), 1.65-1.35 (m, 1H), 1.53-1.24 (m, 8H), 1.33 (d, 3H, J = 6.0 Hz), 0.88 (t, 3H, J = 7.2 Hz); FT-IR (ATR): ν = 2984, 2976, 2949, 2931, 2919, 2854, 1611, 1577, 1522, 1504, 1466, 1418, 1374, 1296, 1268, 1243, 1182, 1124, 1066, 995, 966, 940, 861, 806, 790, 786, 727, 668, 646, 622, 475, 445 cm⁻¹; elemental analysis calcd (%) for C₂₂H₂₄BrFOS₂: C 56.53, H 5.17, Br 17.09, F 4.06, O 3.42, S 13.72; found: C 56.7, H 5.2; exact mass: 466.04; molecular weight: 467.46; m/z : 465.85, 466.81, 467.82, 468.82, 469.82.

5-(5-Hexenyl)-5''-[4-*(S)*-2-octyloxy]-3-fluorophenyl]-2,2':5',2''-terthiophene : (S)-1

To a stirred solution of 5-bromo-5'-[4-*(S)*-2-octyloxy]-3-fluorophenyl]-2,2'-bithiophene (1.10 g, 2.35 mmol), 2-(5-hexenyl)thienylboric acid 2,2-dimethyl-1,3-propanediyl ester (0.98 g, 3.53 mmol) and Pd(PPh₃)₄ (110 mg, 0.095 mmol) in 1,2-dimethoxyethane (60 mL) was added 2 mol/L Na₂CO₃ aqueous solution (35 mL, 70 mmol). After the reaction mixture was refluxed 6 h, 1,2-dimethoxyethane was removed from the reaction mixture under the reduced pressure. The produced precipitates were collected by filtration. The filtrate was extracted with THF/hexane (100 mL/50 mL ×1) and hexane (50 mL ×1). The extract was dried over anhydrous MgSO₄. After filtration and evaporation, obtained solid was combined with former precipitate. The crude product was purified by silica gel column chromatography (eluent: *n*-hexane/toluene = 5/1; v/v). The product was recrystallized from hexane and dried *in vacuo* to give 5-(5-hexenyl)-5''-[4-*(S)*-2-octyloxy]-3-fluorophenyl]-2,2':5',2''-terthiophene (**1**) as a pale yellow crystal (1.02 g, 78 % yield).

¹H-NMR (400 MHz, CDCl₃): δ = 7.31 (dd, 1H, J = 12.4, 2.4 Hz), 7.26 (ddd, 1H, J = 8.4, 2.4, 1.2 Hz), 7.10 (d, 1H, J = 3.6 Hz), 7.09 (d, 1H, J = 4.0 Hz), 7.06 (d, 1H, J = 3.6 Hz), 7.00 (d, 1H, J = 3.6 Hz), 6.98 (d, 1H, J

= 3.6 Hz), 6.96 (t, 1H, J = 8.8 Hz), 6.69 (d, 1H, J = 3.6 Hz), 5.81 (ddt, 1H, J = 17.2, 10.4, 6.8 Hz), 5.02 (ddd, 1H, J = 17.2, 3.6, 1.6 Hz), 4.96 (ddt, 1H, J = 10.4, 3.2, 1.2 Hz), 4.37 (sextet, 1H, J = 6.0 Hz), 2.81 (t, 2H, J = 7.6 Hz), 2.10 (quartet, 2H, J = 7.6 Hz), 1.84-1.74 (m, 1H), 1.71 (quintet, 2H, J = 7.6 Hz), 1.65-1.55 (m, 1H), 1.53-1.24 (m, 11H), 1.33 (d, 3H, J = 6.0 Hz), 0.89 (t, 3H, J = 6.8 Hz); ^{13}C -NMR (100 MHz, CDCl_3): δ = 145.5, 141.9, 138.7, 136.9, 136.4, 135.6, 134.7, 127.8, 125.1, 124.5, 124.3, 123.8, 123.6, 123.6, 121.6, 121.5, 117.9, 114.8, 113.9, 113.7, 76.7, 36.6, 33.6, 31.9, 31.2, 30.2, 29.4, 28.4, 25.6, 22.8, 20.0, 14.2; FT-IR (ATR): ν = 2956, 2920, 2854, 1574, 1545, 1524, 1502, 1445, 1378, 1298, 1234, 1131, 1061, 944, 833, 786, 726, 625, 475, 447 cm^{-1} ; elemental analysis calcd (%) for $\text{C}_{32}\text{H}_{37}\text{FOS}_3$: C 69.52, H 6.75, F 3.44, O 2.89, S 17.40; found: C 69.5, H 6.8; exact mass: 552.20; molecular weight: 552.83; m/z : 552.12, 553.13, 554.16, 555.17, 556.17, 557.17.

5-{10-(1,3,3,5,5,7,7-heptamethyl-1,3,5,7-cyclotetrasiloxan-1-yl)hexan-1-yl}-5''-[4-{{(S)-2-octyloxy}-3-fluorophenyl}-2,2':5',2''-terthiophene: (S)-2

To a solution of 5-(5-hexenyl)-5''-[4-{{(S)-2-octyloxy}-3-fluorophenyl}-2,2':5',2''-terthiophene (0.77 g, 1.39 mmol), 1,3,3,5,5,7,7-heptamethyl-1,3,5,7-cyclotetrasiloxane (0.59 g, 2.09 mmol) in toluene (60 mL) was added the Karstedt's catalyst (10 μL , 2.1-2.4 % in xylene). The reaction mixture was stirred for 18 h at room temperature. After removing the solvent by vacuum evaporation, the crude product was purified by silica gel column chromatography (eluent: *n*-hexane/toluene = 5/1; v/v). The product was reprecipitated from *n*-hexane and dried *in vacuo* to give 5-{10-(1,3,3,5,5,7,7-heptamethyl-1,3,5,7-cyclotetrasiloxan-1-yl)hexan-1-yl}-5''-[4-{{(S)-2-octyloxy}-3-fluorophenyl}-2,2':5',2''-terthiophene (**2**) as a pale yellow wax (0.74 g, 64 % yield).

^1H -NMR (400 MHz, CDCl_3): δ = 7.31 (dd, 1H, J = 12.0, 2.0 Hz), 7.26 (ddd, 1H, J = 8.4, 2.2, 1.0 Hz), 7.10 (d, 1H, J = 4.0 Hz), 7.09 (d, 1H, J = 3.6 Hz), 7.06 (d, 1H, J = 3.6 Hz), 7.00 (d, 1H, J = 4.0 Hz), 6.98 (d, 1H, J = 3.6 Hz), 6.96 (t, 1H, J = 8.8 Hz), 6.69 (d, 1H, J = 4.0 Hz), 4.38 (sextet, 1H, J = 6.0 Hz), 2.79 (t, 2H, J = 7.4 Hz), 1.84-1.56 (m, 4H), 1.53-1.27 (m, 14H), 1.33 (d, 3H, J = 6.0 Hz), 0.89 (t, 3H, J = 6.8 Hz), 0.54 (br-t, 2H, 7.4 Hz), 0.10 (s, 18H), 0.07 (s, 3H); ^{13}C -NMR (100 MHz, CDCl_3): δ = 146.4, 142.4, 137.6, 136.9, 136.0, 135.1, 128.4, 125.5, 125.0, 124.8, 124.3, 124.1, 122.1, 122.1, 118.5, 114.5, 114.3, 77.2, 37.1, 33.5, 32.5, 32.2, 30.9, 29.9, 29.5, 26.1, 23.5, 23.3, 20.5, 17.8, 14.8, 1.48, 1.45; FT-IR (ATR): ν = 2962, 2927, 2857, 1546, 1524, 1506, 1446, 1378, 1299, 1259, 1234, 1055, 942, 855, 789, 696, 552, 478 cm^{-1} ; elemental analysis calcd (%) for $\text{C}_{39}\text{H}_{59}\text{FO}_5\text{S}_3\text{Si}_4$: C 56.07, H 7.12, F 2.27, O 9.58, S 11.51, Si 13.45; found: C 55.9, H 7.2; exact mass: 834.26; molecular weight: 835.42; m/z : 835.60, 836.61, 837.61, 838.61, 839.61, 840.61.

2.3. Results and Discussion

2.3.1. Mesomorphic Properties of chiral phenylterthiophene derivatives

Compounds (*S*)-1 and (*S*)-2 exhibited SmC* and chiral smectic G (SmG*) phases, which were characterized by polarizing optical microscopy (POM), differential scanning calorimetry (DSC), and a X-ray diffraction measurement. In POM, typical broken fan-like (Figure 2-2a, b) and tile-like (Figure 2c, d) textures were observed in high-temperature and low-temperature phases, respectively.

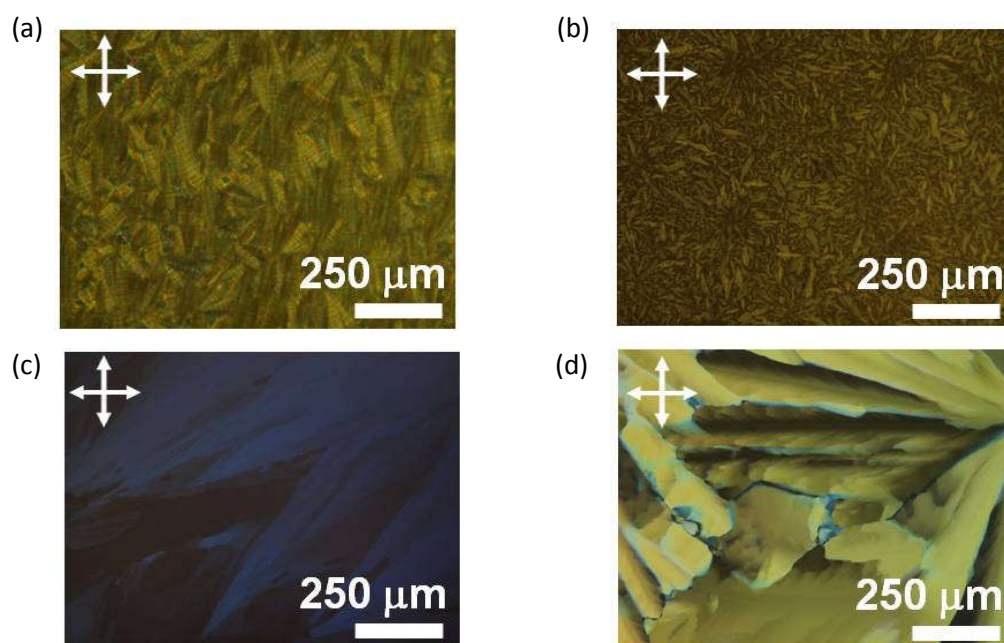


Figure 2-2. Polarizing optical micrographs in the SmC* phases of (a) compound (*S*)-1 (140 °C) and (b) compound (*S*)-2 (85 °C). Those in the SmG* phases of (c) compound (*S*)-1 (120 °C) and (d) compound (*S*)-2 (60 °C).

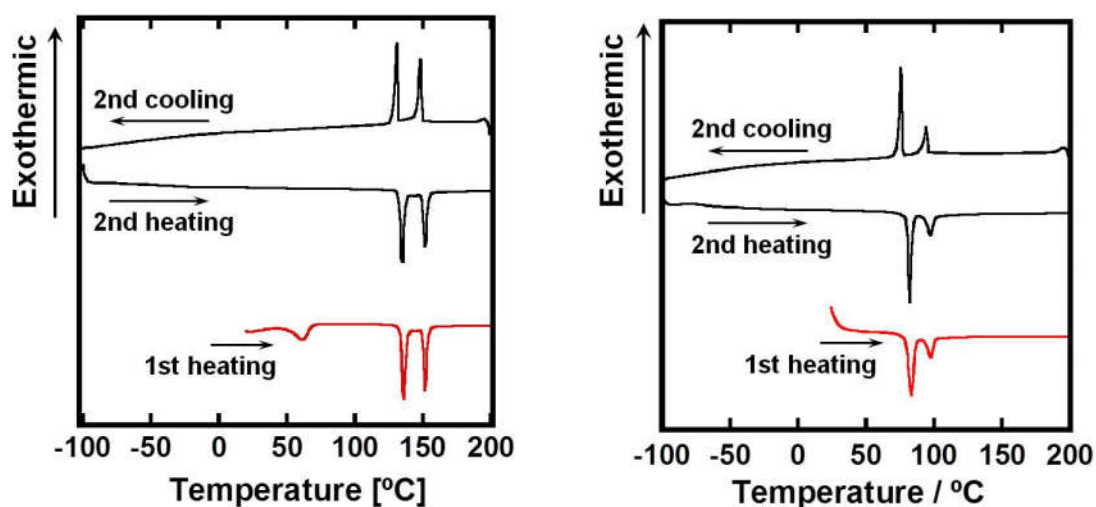


Figure 2-3. DSC thermograms of (a) compound (*S*)-1 and (b) compound (*S*)-2. The scanning rates are 10 K/min. The red curves exhibit thermograms of obtained materials from recrystallization.

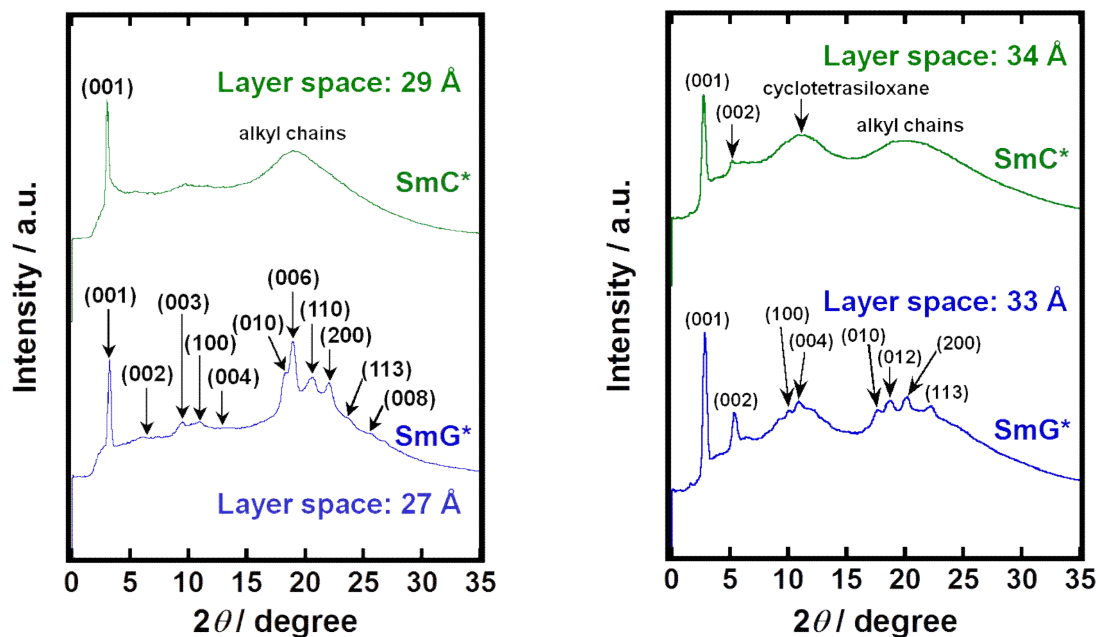


Figure 2-4. XRD patterns in the LC phases of (a) compound (S)-1 at 132 °C (SmC*) and 100 °C (SmG*), (b) compound (S)-2 at 85 °C (SmC*) and 70 °C (SmG*).

Table 2-1 shows phase transition temperatures and enthalpies of two compounds. These compounds maintained LC phases without crystallization when they were cooled below room temperature. The introduction of a bulky cyclotetrasiloxane unit lowered the phase transition temperature, due to a steric effect of the bulky unit.

Table 2-1. Phase transition behaviors of compounds (S)-1 and (S)-2.

| Compounds | Phase transition temperature / °C (enthalpy / kJ mol ⁻¹) ^a |
|-----------|--|
| (S)-1 | SmG* 133 (11) SmC* 149 (8) Iso |
| (S)-2 | SmG* 80 (12) SmC* 94 (4) Iso |

a) Phase transition temperature [°C] (phase transition enthalpy [kJ mol⁻¹]) estimated from DSC measurements on 2nd heating. (The scanning rate: 10 K/min.)

2-3-2. Response to the DC bias

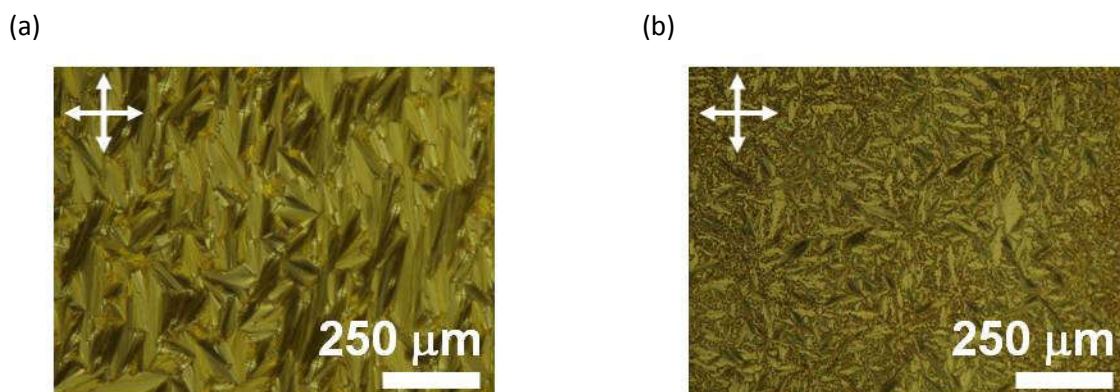


Figure 2-5. Polarizing optical micrographs in the SmC* phases of (a) compound (S)-1 (140 °C) and (b) compound (S)-2 (85 °C) under the application of DC bias (+50 V) to 25 μm-thick ITO glass sandwich cells.

Under the application of DC bias (+50 V), the initial helical structures were unraveled for both compounds (S)-1 and (S)-2. In this condition, the stripe patterns in their LC textures were lost and clear broken-fan textures were observed (Figure 2-5). Applied the higher DC bias above +50 V to the LC cells, the LC textures were not changed from the one shown in Figure 2-5. When the higher DC bias above the coercive electric-fields was applied, the dipole moments should be oriented along the electric field. The TOF measurements described in latter section were carried out under those conditions.

2.3.3. Dielectric Properties of chiral phenylterthiophene derivatives

Spontaneous polarizations were evaluated by the Sawyer-Tower method using triangular-wave bias (± 5 V, 100 Hz). Figure 2-6 shows hysteresis loops in their SmC* phases of compounds (S)-1 and (S)-2. These hysteresis loops indicate the ferroelectricity in the SmC* phases of these compounds. The estimated values of spontaneous polarizations are 50 nC cm^{-2} (compound (S)-1) and 40 nC cm^{-2} (compound (S)-2). These values of spontaneous polarizations should be affected by the disorder of the molecular aggregation structure. The coercive voltages (electric-fields) in SmC* phases of compounds (S)-1 and (S)-2 were around 0.5 V ($2.5 \times 10^3 \text{ V cm}^{-1}$) and 2.5 V ($1.3 \times 10^4 \text{ V cm}^{-1}$), respectively.

The polarization inversion current curves in their SmC* phases were also measured under the application of triangular wave bias (± 5 V, 100 Hz). In each case, current peaks derived from the polarization inversion were observed (see supporting information). The polarization inversion current peaks of compound (S)-2 were broader than those of compound (S)-1.

The larger molecular mass and the lower temperature range of the SmC* phase of compound (S)-2 increase the viscosity of the SmC* phase compared to that of compound (S)-1. This larger

viscosity of compound (S)-2 should cause the slower response in the polarization inversion and the larger coercive voltage in the SmC* phase of compound (S)-2.

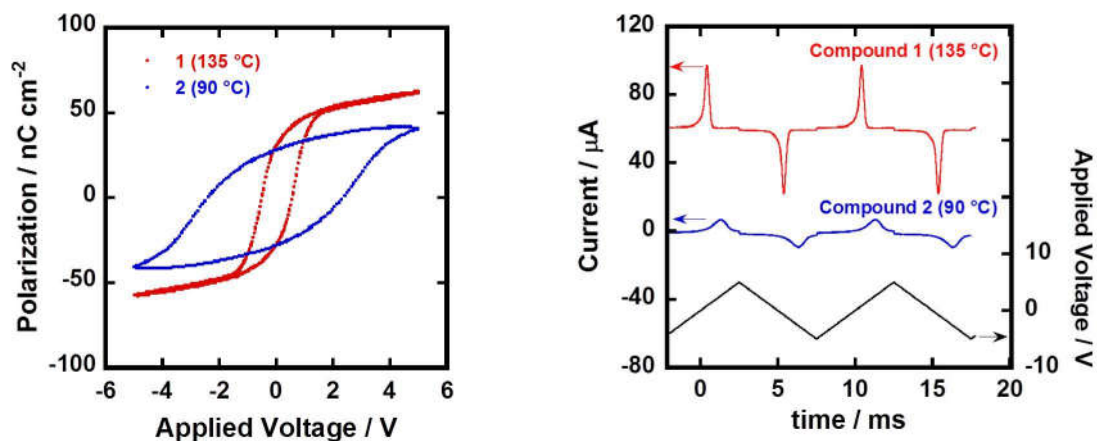


Figure 2-6. (a) Hysteresis loops in SmC* phases of compounds (S)-1 (135 °C) and (S)-2 (90 °C), (b) polarization inversion current in SmC* phases of compounds (S)-1 (135 °C) and (S)-2 (90 °C) measured by the triangular wave method. (± 5 V, 100 Hz, 2 μm thick sample.)

2.3.4. Carrier Transport Properties of chiral phenylterthiophene derivatives

The carrier mobilities in the SmC* phases of compounds (S)-1 and (S)-2 were determined by a TOF technique.

Figure 2-7 shows transient photocurrent curves for holes in the SmC* phases of compound (S)-1 and (S)-2. In their SmC* phases of these compounds, non-dispersive transient photocurrent curves for the holes were observed. The kink point on the linear plot of the curve provided a transit time. In contrast, dispersive and weak transient photocurrent curves generated by negative charge carrier transport were observed, so that the mobilities of the negative carrier could not be estimated.

In the SmC* phase of compound (S)-1 at 135 °C, the hole mobility estimated from the transit time was $4.8 \times 10^{-4} \text{ cm}^2 \text{ V}^{-1} \text{ s}^{-1}$. This value was one or two orders of magnitude larger than the ionic carrier mobility in nematic phases.¹⁴ The hole mobility was independent of the temperature and the electric field in the SmC* phase. The value of the hole mobility was on the same order of those in the SmC* and SmC phases of other LC semiconductors.¹⁵

In the SmC* phase of compound (S)-2, the hole mobility at 85 °C was $3.9 \times 10^{-5} \text{ cm}^2 \text{ V}^{-1} \text{ s}^{-1}$. In the SmC* phase, the temperature- and field-dependent mobility was observed. This should be attributed to structural disorder in the SmC* phase of compound (S)-2. The bulky cyclotetrasiloxane rings should inhibit the close aggregation of the π -conjugated units.

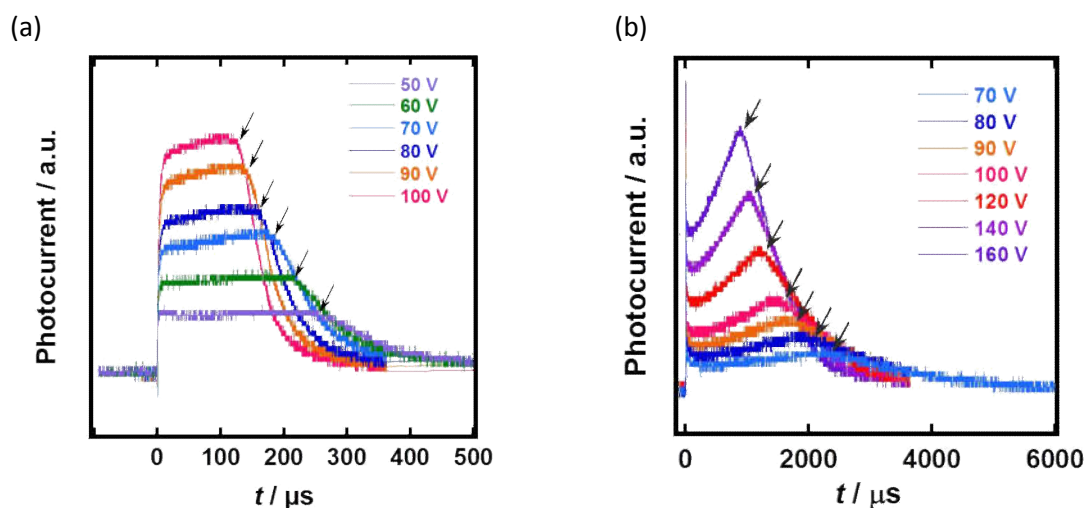


Figure 2-7. Transient photocurrent curves for positive charge in SmC* phases of (a) compound (S)-1 at 140 °C, (b) compound (S)-2 at 85 °C. The measurements were performed using ITO/ ITO sandwich cells whose thickness was 25 μm . The arrows indicate kink points corresponding to the transit times.

2.3.5. APV response of chiral phenylterthiophene derivatives

APV effect in their SmC* phases was confirmed by the measurement of steady state photocurrent under zero bias. Cooling the LC samples from their isotropic phases without the DC bias, helical structures are formed (initial state). In this state, no internal field is formed. When illuminated electrode is biased positively, the internal field is generated in the reversed direction. After removing the DC external bias, the backward internal field should be maintained (second state). UV illumination on the positively biased electrode should produce photocurrent with the reversed polarity. In contrast, the opposite internal field should be induced when the illuminated electrode is biased negatively prior to UV light illumination. After the removal of the external DC bias, the forward internal field should be formed (third state). In this series of experiments, light irradiation was started just after the removing the DC voltages.

Figure 2-7 shows the steady state photocurrent response curves under zero bias in the SmC* phases of compounds (S)-1 and (S)-2. For compound (S)-1, the ambiguous photocurrent response was observed in the initial state of the SmC* phase. After generation of the internal field, clear photocurrent response was observed in the second and third states. It should be noted that the polarity of the photocurrent was opposite to the polarity of the DC bias prior to UV light illumination. Stronger photocurrent response was observed in the third state than in the second state. In the third state, the illuminated electrode should be charged positively.

For compound (S)-2, clear photocurrent response was observed when the positive internal field was generated in the third state. However, the photocurrent was one fourth as large as that of compound (S)-1. In the second state, photocurrent was smaller than that in the third state.

Throughout these steady state photocurrent measurements of compounds (S)-1 and (S)-2, the generated photocurrent at zero bias in the third state was stronger than that in the second state. Compounds (S)-1 and (S)-2 have a strong absorption band in the near UV area, and the penetration depth of the excitation UV light is less than 100 nm. Under the condition of the third state, majority photocarriers are holes, which are generated and transported more efficiently than electrons. In contrast, electrons are the majority carrier in the second state and lower photocurrent was observed.

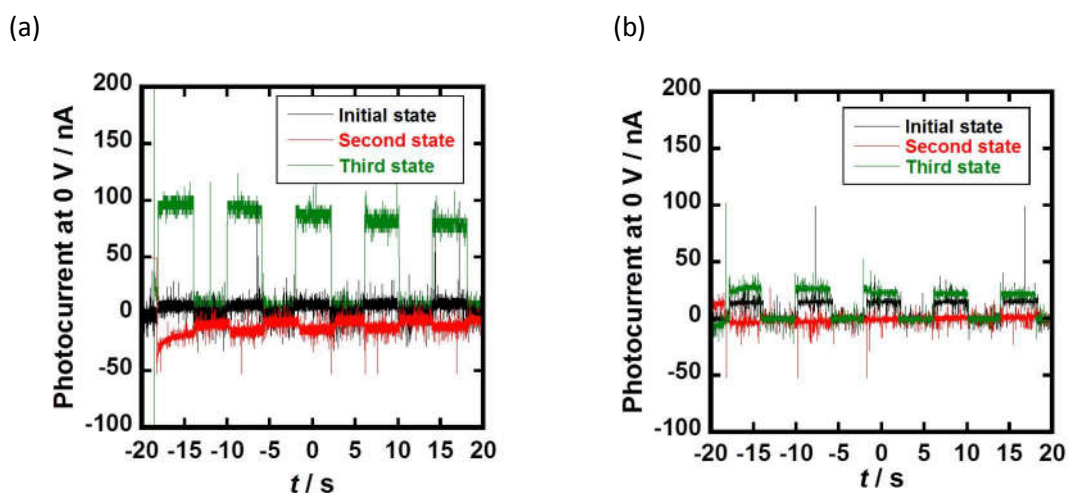


Figure 2-7. Steady state photocurrent response profiles in SmC* phases of (a) compound (S)-1 (135 °C), (b) compound (S)-2 (90 °C). The measurements were performed using ITO/ ITO sandwich cells whose thickness was 2 μm .

As mentioned above, compound (S)-1 has larger spontaneous polarization and higher APV efficiency than compound (S)-2. This result suggested that the spontaneous polarization contributes to the APV efficiency. However, it should be noted that the spontaneous polarization in the bulk should be relaxed on the measurement time scale. This might mean that the retained spontaneous polarization in the interface region contributed to the APV phenomena. Actually, their open-circuit voltages were less than 1 V, which is much lower than the latent power of the ferroelectric system.

Although the spontaneous polarization of compound (S)-1 is 1.2 times larger than that of compound (S)-2, the APV photocurrent of compound (S)-1 in the third state is around 4 times larger than that of compound (S)-2. This implies the contribution of other factors than the spontaneous polarization to APV effect. We consider that the APV effect should be affected by the carrier transport property, because photocurrent is proportional to the product of the density of photocarriers and the carrier mobility. In fact, the value of hole mobility in the FLC phase of compound (S)-1 is one order of magnitude larger than that of compound (S)-2, resulting in the higher APV efficiency of compound (S)-1. For visible light, the APV effect was not observed, because

compounds (S)-1 and (S)-2 have no absorption in long-wavelength visible area. Their strong absorption bands are spread in near-UV area. This result indicates photocarriers are originated from the excitation states of the LC molecules.

2.4. Conclusion

From the above, we suggest the mechanism of APV effect in the FLC system which described following. In the first step, the internal field is generated by the spontaneous polarization in the SmC* phase. In the second step, excitons are generated by UV light excitation. Next, charge separation occurs with the assistance of the internal field. In the final step, the photocarriers are transported to electrodes.

In summary, we have synthesized ferroelectric LC fluorophenylterthiophene derivatives exhibiting SmC* phases. Spontaneous polarizations in SmC* phases of these compounds were on the order of 10^1 nC cm⁻². In the SmC* phase of compound (S)-1, the hole mobility was on the order of 10^{-4} cm²V⁻¹s⁻¹, which was one order of the magnitude higher than that of compound (S)-2. These compounds exhibit APV effect in their SmC* phases. Compound **1** has qualitatively higher conversion efficiency than compound (S)-2. The carrier transport property and spontaneous polarization in SmC* phases should contribute these behaviors.

2.5. References

1. *Ferroelectrics – Physical Effects*, ed. by M. Lallart, Intech, Rijeka, Croatia, 2011.
2. Y. Yuan, Z. Xiao, B. Yang and J. Huang, *J. Mater. Chem. A.*, 2014, **2**, 6027.
3. V. M. Fridkin and B. N. Popov, *Phys. Stat. Sol. (a)*, 1978, **46**, 729.
4. A. M. Glass, D. von der Linde and T. J. Negran, *Appl. Phys. Lett.*, 1974, **25**, 233.
5. (a) T. Choi, S. Lee, Y. J. Choi, V. Kiryukhin and S.-W. Cheong, *Science*, 2009, **324**, 63. (b) A. Bhatnagar, A. R. Chaudhuri, Y. H. Kim, D. Hesse and M. Alexe, *Nat. Commun.*, 2013, **4**, 2835.
6. K. T. Butler, J. M. Frost and A. Walsh, *Energy Environ. Sci.*, 2015, **8**, 838.
7. (a) A. Sugita, K. Suzuki and S. Tasaka, *Phys. Rev. B*, 2004, **69**, 212201. (b) H. Sasabe, T. Nakayama, K. Kumazawa, S. Miyata and E. Fukuda, *Polym. J.*, 1981, **13**, 967.
8. W. J. A. M. Hartmann, *Ferroelectrics*, 1991, **122**, 1.
9. D. Miyajima, F. Araoka, H. Takezoe, J. Kim, K. Kato, M. Takata and T. Aida, *Science*, 2012, **336**, 209.
10. (a) W. Pisula, M. Zorn, J. Y. Chang, K. Müllen and R. Zentel, *Macromol. Rapid Commun.*, 2009, **30**, 1179. (b) M. O'Neill and S. M. Kelly, *Adv. Mater.*, 2011, **23**, 566. (c) M. Funahashi, *Polymer J.*, 2009, **41**, 459. (d) M. Funahashi, *J. Mater. Chem. C*, 2014, **2**, 7451. (e) M. Funahashi and T. Kato, *Liq. Cryst.*, 2015, **42**, 909. (f) A. Seki and M. Funahashi, *Heterocycles*, 2016, **92**, 3.
11. (a) T. Sasaki, *Chem. Rec.*, 2006, **6**, 43. (b) H. Anetai, Y. Wada, T. Takeda, N. Hoshino, S. Yamamoto, M. Mitsuishi, T. Takenobu and T. Akutagawa, *J. Phys. Chem. Lett.*, 2015, **6**, 1813.
12. Y. Funatsu, A. Sonoda and M. Funahashi, *J. Mater. Chem. C*, 2015, **3**, 1982.
13. T. Zhao, W. Shi, J. Xi, D. Wang, Z. Shuai, *Sci. Rep.*, 2016, **7**, 19968.
14. (a) S. Murakami, H. Naito, M. Okuda and A. Sugimura, *J. Appl. Phys.*, 1995, **78**, 4533. (b) A. Sawada and S. Naemura, *Jpn. J. Appl. Phys.*, 2002, **41**, L195.
15. (a) M. Funahashi and J. Hanna, *Appl. Phys. Lett.*, 2000, **76**, 2574. (b) K. Kogo, H. Maeda, H. Kato, M. Funahashi and J. Hanna, *Appl. Phys. Lett.*, 1999, **75**, 3348. (c) M. Funahashi and N. Tamaoki, *Chem. Mater.*, 2007, **19**, 608.

Chapter 3

Bulk photovoltaic effects based on molecular chirality:

the influence of the enantiomer purity on the photocurrent response in π -conjugated ferroelectric liquid crystals

Abstract: (*S*)- and (*R*)-forms of chiral π -conjugated ferroelectric liquid crystals were synthesized. The dielectric properties in the FLC phases were evaluated by the Sawyer–Tower method. Spontaneous polarization of (*S*)-**1** reached 68 nC cm^{-2} at $127 \text{ }^\circ\text{C}$. Hole mobilities in the FLC phases estimated by the TOF method were on the order of $10^{-4} \text{ cm}^2 \text{ V}^{-1} \text{ s}^{-1}$. Each chiral π -conjugated compound exhibited a photovoltaic effect based on spontaneous polarization without p-n or Schottky junctions. This phenomenon could be attributed to APV effect that has been observed in ferroelectric ceramics. In addition, liquid-crystalline enantiomeric mixtures of (*S*)-**1** and (*R*)-**1** were prepared and the APV response under UV illumination was studied. The APV response was enhanced with an increase in enantiomeric purity and was minimized in the racemic mixture. From this result, it was concluded that the APV effect in this FLC compound originated from the molecular chirality.

3.1. Introduction

One of the significant phenomena induced by molecular chirality is the formation of helical structures, which are promising for chiral recognition and optical functions. Chiral functional molecules bearing hydrogen-bonding sites form helical nanofibrous aggregates.¹ Polymers consisting of chiral monomer units form helical structures that can recognize chiral molecules.² Circularly polarized fluorescence has been observed from chiral π -conjugated polymers and oligomers,³ as well as from the cholesteric phase of chiral LC molecules.⁴

Molecular chirality can break the symmetry of a system even when helical structures are not formed. In molecular motors, molecular chirality breaks the balance between right-handed and left-handed photochemical rotations.⁵ For enhanced magnetic Faraday effects in chiral metal complexes, the symmetry of the interaction between the 4f-electron spins of terbium and the magnetic field of the incident light is broken.⁶

Ferroelectric liquid crystals are also based on symmetry breaking by molecular chirality.⁷ A typical ferroelectric SmC* phase consists of chiral LC molecules. In the SmC* phase, a helical structure is unwound to produce spontaneous polarization under the application of a DC electric field. FLC materials have been developed for application in high-speed LC displays.⁸ These conventional FLC materials are electrically insulative and have no absorption bands in the near-UV and visible regions.

LC molecules with an extended π -conjugated unit form anisotropic electronic systems.⁹ Electronic charge carrier transport in columnar and smectic LC materials has been studied by the time-of-flight (TOF) technique,^{10a-g} the microwave absorption method,^{10h-j} and the space-charge-limited current method.^{10k,l} Light-emitting diodes,^{11a-c} field-effect transistors,^{11d-g} and solar cells using LC semiconductors have been studied.^{11h,i}

Our intention is to couple this ferroelectricity with electronic charge carrier transport in LC supramolecular systems. We have already reported preliminary results on a photovoltaic effect in the SmC* phase of phenylterthiophene derivatives.¹² We observed zero-biased photoconductivity with a polarity opposite to that of the DC bias applied prior to UV illumination and inversion of the photocurrent polarity by changing the pre-illumination DC bias polarity. This photovoltaic effect should be attributable to photocarrier generation and transport by the electric field produced by ferroelectric polarization, and not to a p-n junction. However, such a bulk photovoltaic effect could also be caused by polarization of ionic impurities and space charges trapped in defects or electrode surfaces.

In this study, we examined the dependence of the photovoltaic effect on the enantiomeric purity of π -conjugated FLCs and verified that this photovoltaic effect is attributable to ferroelectric spontaneous polarity based on molecular chirality.

Figure 3-1 depicts the mechanism of photovoltaic effects schematically. Conventional photovoltaic devices require p-n junction that generate a built-in internal electric field to promote charge carrier generation and transport, as shown in Figure 3-1a. In conventional devices, the open-circuit voltage is restricted by the band gap of the active materials. Therefore, the open circuit voltage in conventional photovoltaic devices should be around 1 V.¹³

An APV effect is defined as a band-gap-independent photovoltaic effect. The APV effect is mainly observed in inorganic displacement-type ferroelectrics such as BiFeO₃ and BaTiO₃.^{14, 15} As shown in Figure 3-1b, the photovoltage is generated by an internal electric field originating from spontaneous polarization of the ferroelectrics instead of the junction. The APV effect can produce an open circuit voltage that is greater than the band gap. Further, the polarity of the photovoltage can be inverted by application of a DC voltage prior to illumination. Ferroelectric ceramics have wide band gaps and cannot absorb visible light, resulting in low conversion efficiencies. Moreover, vacuum processes are required to produce thin films for these devices.¹⁴

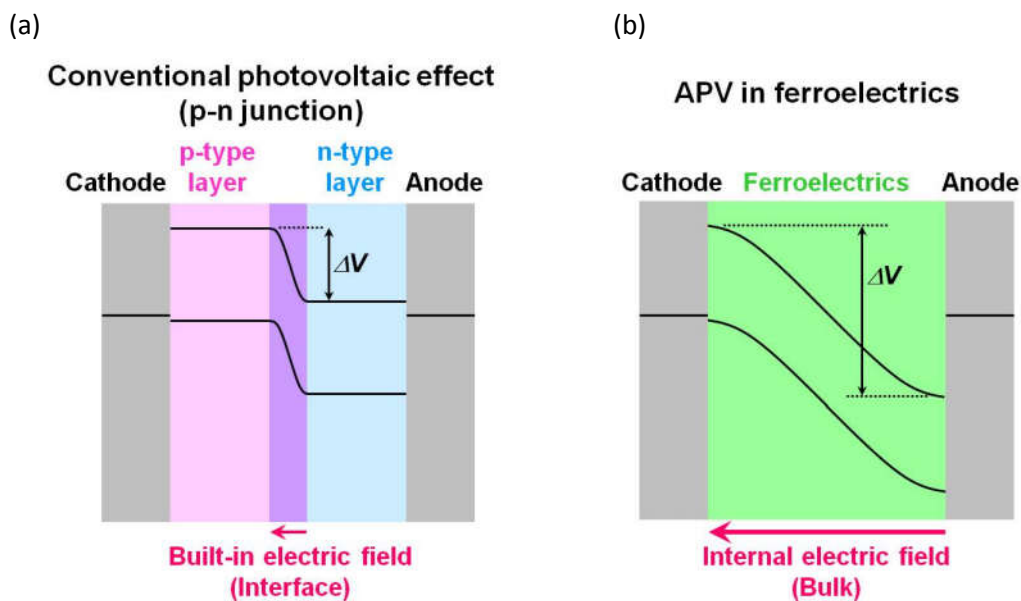


Figure 3-1. Schematic illustrations of the formation of (a) a built-in electric field in a p-n junctions and (b) an internal electric field in a ferroelectrics. ΔV denotes the potential drops.

On the other hand, most organic ferroelectrics are order–disorder-type systems,¹⁶ and studies of APV phenomena in organic ferroelectrics have been quite limited.¹⁷ However, organic materials have a diversity of chemical structures with absorption bands that can be tuned by a chemical modification. In addition, solution-processable ferroelectrics can be designed.

Most FLCs are classified as order–disorder-type ferroelectrics,⁸ with the exception of FLC surfactant complexes based on phosphonium salts.¹⁸ The schematic illustrations in Figure 3-2 display the basic strategy for achieving the APV effect based on order–disorder-type ferroelectric materials bearing an extended π -conjugated unit. In order–disorder-type ferroelectrics, a nonpolarized state is formed without poling treatment (Figure 3-2a). In the initial state, the dipole moment should be cancelled out in the whole. When a DC bias is applied, the dipoles can be aligned to compensate for the external stimulus. As a result, an internal electric field is generated in the bulk (Figure 3-2b). After removing the external bias, ferroelectric polarization can be retained. Then, excitons generated by light absorption can be separated into positive and negative charge carriers by the internal field originating from the spontaneous polarization. The charge carriers can be transported to both electrodes through the electronic conduction pathway derived from orbital overlap between extended π -conjugated units (Figure 3-2c). Thus, the bulk internal field efficiently assists charge-separation and carrier-transport processes.

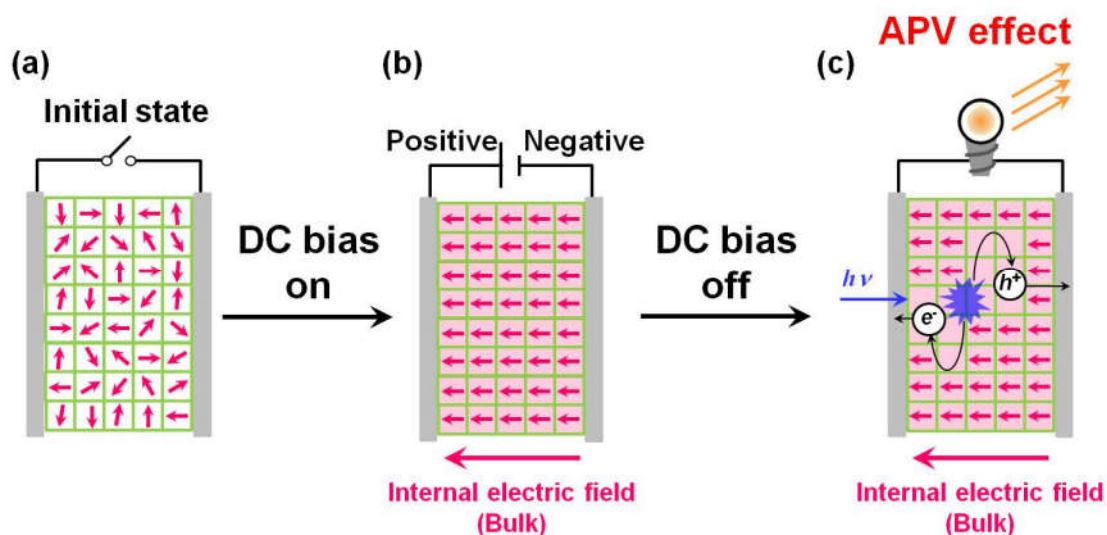


Figure 3-2. Schematic illustrations of the elementary processes for achieving the APV effect based on order–disorder ferroelectrics. (The red arrows indicate the direction of the dipole moments.)

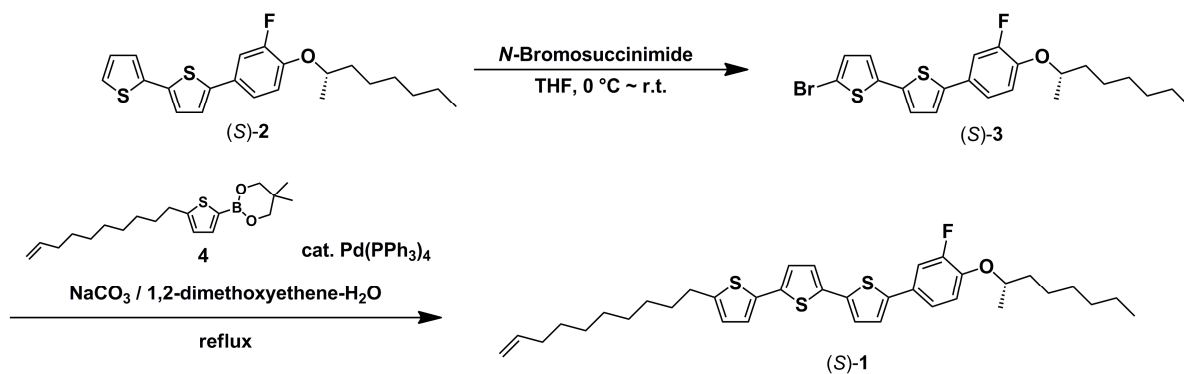
3.2. Experimental Section

3.2.1. Synthesis of materials

All ^1H - and ^{13}C -NMR spectra were performed by solutions in CDCl_3 on a Varian UNITY INOVA400NB spectrometer. Matrix-assisted laser desorption ionization time-of-flight (MALDI-TOF) mass spectra were performed by Bruker Daltonics ultrafleXtreme(TM). FT-IR measurements were carried out on a JASCO FT/IR-660 Plus spectrometer.

[1,3-Bis(diphenylphosphino)propane]nickel(II) dichloride, 4-bromo-2-fluorophenol, 2-bromobithiophene, 9-decen-1-ol, 2, 2-dimethylpropanediol, diethyl azodicarboxylate (40% in toluene), *N*-bromosuccinimide, (*R*)-2-octanol, phosphorus tribromide, thiophene, trimethyl borate, and tetrakis(triphenylphosphine)palladium(0) were purchased from Tokyo Chemical Industry. *n*-Hexane, tetrahydrofuran, toluene, 1, 2-dimethoxyethane, *n*-butyllithium (1.6 M hexane soln.), and the other inorganic reagents were obtained from Wako Pure Chemical Industries. All of them were used without further purification. Silica gel was purchased from Kanto Chemicals. A used mirror enantiomer (*R*)-**1** was synthesized in the previous work. All reactions were performed under nitrogen atmosphere in a well-dried three-necked flask equipped with a magnetic stirring bar.

Compound (*S*)-**1** was synthesized as shown in scheme 1. Compound (*S*)-**2** was synthesized via the Suzuki-Miyaura reaction between 2-bromo-5:2'-bithiophene and 3-fluoro-4- $\{(S)\text{-}2\text{-octyloxy}\}$ phenyl boric acid ester by the same procedure reported previously.¹² The bromination reactions of compound (*S*)-**2** with using *N*-bromosuccineimide were afforded to the compound (*S*)-**3**. Then, phenylterthiophene derivative (*S*)-**1** bearing an alkenyl side chain was synthesized via Suzuki-Miyaura reaction between brominated phenylbithiophene derivative (*S*)-**3** and alkenylthienyl boric acid ester **4**.



Scheme 3-1. Synthetic route to compounds (S)-1.

5-Bromo-5'-[4-((S)-2-octyloxy)-3-fluorophenyl]-2,2'-bithiophene ((S)-3)

The synthetic procedure is described in former chapter (2.2.1. Synthesis of materials).

$^1\text{H-NMR}$: δ = 7.30 (dd, 1H, J = 12.0, 2.4 Hz), 7.25 (ddd, 1H, J = 8.4, 2.4, 1.2 Hz), 7.09 (d, 1H, J = 4.0 Hz), 7.05 (d, 1H, J = 4.0 Hz), 6.98 (d, 1H, J = 4.0 Hz), 6.96 (t, 1H, J = 8.8 Hz), 6.92 (d, 1H, J = 3.6 Hz), 4.38 (sextet, 1H, J = 6.0 Hz), 1.84-1.74 (m, 1H), 1.65-1.35 (m, 1H), 1.53-1.24 (m, 8H), 1.33 (d, 3H, J = 6.0 Hz), 0.88 (t, 3H, J = 7.2 Hz); FT-IR (ATR): ν = 2984, 2976, 2949, 2931, 2919, 2854, 1611, 1577, 1522, 1504, 1466, 1418, 1374, 1296, 1268, 1243, 1182, 1124, 1066, 995, 966, 940, 861, 806, 790, 786, 727, 668, 646, 622, 475, 445 cm^{-1} ; elemental analysis calcd (%) for $\text{C}_{22}\text{H}_{24}\text{BrFOS}_2$: C 56.53, H 5.17, Br 17.09, F 4.06, O 3.42, S 13.72; found: C 56.7, H 5.2; exact mass: 466.04; molecular weight: 467.46; m/z : 465.85, 466.81, 467.82, 468.82, 469.82.

10-Bromo-1-decene

To stirred DMF (600 mL) was slowly added dropwise PBr_3 (18.5 mL, 195 mmol) at 0 °C over 20 min and gradually warmed to room temperature. The mixture was stirred over 1 h. Then, 9-decen-1-ol (50.1 g, 321 mmol) with dry diethylether (50 mL) was slowly added to the cream-colored suspension over 20 min. After the addition of 9-decen-1-ol, the mixture was stirred for 24 h. The reaction mixture was quenched by H_2O (200 mL) cooling with ice bath. The product was extracted with *n*-hexane (200 mL \times 1, 100 mL \times 2, 75 mL \times 1). All collected organic fractions were combined and dried over Na_2SO_4 . After filtration and evaporation, the crude product was passed the silica gel column (eluent: *n*-hexane) and dried *in vacuo* to give 10-bromo-1-decene as a colorless clear liquid (57.7 g, 82 % yield).

$^1\text{H-NMR}$ (400 MHz, CDCl_3): δ = 5.81 (ddt, 1H, J = 17.0, 10.2, 6.8 Hz), 4.99 (ddd, 1H, J = 17.2, 3.6, 1.6 Hz), 4.93 (ddt, 1H, J = 10.2, 2.2, 1.2 Hz), 3.41 (t, 2H, J = 7.0 Hz), 2.04 (quartet, 2H, J = 7.2 Hz), 1.85 (quintet, 2H, J = 7.2 Hz), 1.46-1.27 (m, 10H).

2-(9-Decenyl)thiophene

To a solution of thiophene (15.0 g, 178 mmol) in dry THF (250 mL) was slowly added *n*-BuLi (1.6 M in *n*-hexane soln., 103 mL, 166 mmol) at -78 °C. After the addition of *n*-BuLi, the mixture was

allowed to warm to 0 °C and stirred for 1 h. Then, 9-bromo-1-decene (30.0 g, 137 mmol) with dry THF (50 mL) was slowly added to reactant mixture at 0 °C. The obtained pale-yellow suspension was gradually warmed to room temperature and stirred for overnight at room temperature. The mixture was quenched by H₂O (150 mL) cooling with ice-bath. The product was extracted with *n*-hexane (100 mL ×3, 50 mL ×1). The organic layer was washed with brine (150 mL) and water (100 mL) in this order. The collected organic fractions were combined and dried over Na₂SO₄. After filtration and evaporation, the crude solution was passed the silica gel column (eluent: *n*-hexane) and distilled *in vacuo* to give 2-(9-decenyl)thiophene as a pale-yellow clear liquid (21.2 g, 69 % yield).

¹H-NMR (400 MHz, CDCl₃): δ = 7.10 (dd, 1H, *J* = 5.2, 1.2 Hz), 6.91 (dd, 1H, *J* = 5.0, 3.4 Hz), 6.77 (dd, 1H, *J* = 3.4, 1.0 Hz), 5.81 (ddt, 1H, *J* = 17.0, 10.2, 6.8 Hz), 4.99 (ddd, 1H, *J* = 17.2, 3.6, 1.6 Hz), 4.93 (ddt, 1H, *J* = 10.2, 2.2, 1.2 Hz), 2.81 (t, 2H, *J* = 7.6 Hz), 2.04 (quartet, 2H, *J* = 6.8 Hz), 1.67 (quintet, 2H, *J* = 7.4 Hz), 1.41-1.28 (m, 10H).

2-(9-decenyl)thienylboric acid 2,2-dimethyl-1,3-propanediyl ester (4)

To a solution of 2-(9-decenyl)thiophene (13.5 g, 60.9 mmol) in dry THF (200 mL) was slowly added *n*-BuLi (1.6 M in *n*-hexane soln., 46.0 mL, 74.1 mmol) with dry THF (10 mL) at -78 °C. After the addition of *n*-BuLi, the mixture was stirred for 1 h at -78 °C. Then, the mixture was allowed to warm to 0 °C for 20 min and cooled down to -78 °C again. Trimethyl borate (9.60 mL, 85.9 mmol) was slowly dropwised over 5 min to reactant mixture at -78 °C. The obtained pale-yellow suspension was gradually warmed to room temperature and stirred for 20 h. Then, 2, 2-dimethylpropanediol (9.53 g, 91.5 mmol) with dry THF (40 mL) was added to the orange reactant mixture at 0 °C. The mixture was warmed to room temperature and stirred for 9 h. After the addition of H₂O (30 mL), the product was separated and washed with sat. NH₄Cl aq. (100 mL), brine (100 mL) and H₂O (100 mL) in this order. The aqueous layer was extracted with CHCl₃ (100 mL ×1, 50 mL ×3). All collected organic fractions were combined and dried over Na₂SO₄. After filtration and evaporation, the crude product was purified by the silica gel column chromatography (eluent: *n*-hexane → *n*-hexane/ethyl acetate = 10/1; v/v, gradient) and dried *in vacuo* to give 2-(9-decenyl)thienylboric acid 2,2-dimethyl-1,3-propanediyl ester as a pale yellow waxy crystal (10.6 g, 52 % yield).

¹H-NMR (400 MHz, CDCl₃): δ = 7.39 (d, 1H, *J* = 3.4 Hz), 6.83 (d, 1H, *J* = 3.4 Hz), 5.81 (ddt, 1H, *J* = 17.0, 10.2, 6.8 Hz), 4.99 (ddd, 1H, 17.0, 3.6, 1.6 Hz), 4.93 (ddt, 1H, *J* = 10.2, 2.2, 1.2 Hz), 3.74 (s, 4H), 2.83 (t, 2H, *J* = 7.6 Hz), 2.03 (quartet, 2H, *J* = 7.2 Hz), 1.67 (quintet, 2H, *J* = 7.4 Hz), 1.39-1.26 (m, 10H), 1.02 (s, 6H).

5-(9-Decenyl)-5''-[4-{{(S)-2-octyloxy}-3-fluorophenyl]-2,2':5',2''-terthiophene ((S)-1)

To a stirred solution of 5-Bromo-5'-[4-{{(S)-2-octyloxy}-3-fluorophenyl]-2,2'-bithiophene ((S)-3) (1.11 g, 2.37 mmol), 2-(9-decenyl)thienylboric acid 2,2-dimethyl-1,3-propanediyl ester (4) (0.87 g, 2.60 mmol) and Pd(PPh₃)₄ (91.3 mg, 0.079 mmol) in 1,2-dimethoxyethane (60 mL) was added 2 mol/L Na₂CO₃ aqueous solution (35 mL). After the reaction mixture was refluxed 6 h, 1,2-dimethoxyethane

was removed from the reaction mixture under the reduced pressure. The produced precipitates were collected by filtration. The filtrate was extracted with THF (100 mL ×1) and THF/ *n*-hexane (100 mL/50 mL ×1). The extract was dried over anhydrous MgSO₄. After filtration and evaporation, obtained solid was combined with former precipitate. The crude product was purified by silica gel column chromatography (eluent: *n*-hexane/toluene = 5/1; v/v). The product was recrystallized from *n*-hexane and dried in vacuo to afford 5-(9-decenyl)-5''-[4-{{(S)-2-octyloxy}-3-fluorophenyl}]-2,2':5',2''-terthiophene as a pale yellow crystal (1.16 g, 81 % yield).

¹H-NMR (400 MHz, CDCl₃): δ = 7.31 (dd, 1H, *J* = 12.2, 2.2 Hz), 7.26 (ddd, 1H, *J* = 8.4, 2.2, 1.2 Hz), 7.10 (d, 1H, *J* = 3.6 Hz), 7.09 (d, 1H, *J* = 3.6 Hz), 7.06 (d, 1H, *J* = 3.6 Hz), 7.00 (d, 1H, *J* = 3.6 Hz), 6.98 (d, 1H, *J* = 3.6 Hz), 6.96 (t, 1H, *J* = 8.8 Hz), 6.68 (d, 1H, *J* = 3.6 Hz), 5.81 (ddt, 1H, *J* = 17.2, 10.4, 6.8 Hz), 5.00 (m, 1H), 4.93 (ddt, 1H, *J* = 10.4, 2.4, 1.2 Hz), 4.37 (sextet, 1H, *J* = 6.0 Hz), 2.79 (t, 2H, *J* = 7.6 Hz), 2.04 (quartet, 2H, *J* = 7.2 Hz), 1.84-1.74 (m, 1H), 1.71 (quintet, 2H, *J* = 7.6 Hz), 1.65-1.55 (m, 1H), 1.51-1.25 (m, 18H), 1.33 (d, 3H, *J* = 6.0 Hz), 0.89 (t, 3H, *J* = 6.8 Hz); ¹³C-NMR (100 MHz, CDCl₃): δ = 145.8, 141.9, 139.4, 137.0, 136.4, 135.5, 134.6, 127.8, 125.0, 124.5, 124.3, 123.7, 123.5, 121.6, 121.5, 117.8, 114.3, 113.9, 113.7, 76.7, 36.6, 33.9, 31.9, 31.7, 30.3, 29.5, 29.4, 29.4, 29.2, 29.2, 29.1, 25.6, 22.8, 20.0, 14.2; FT-IR (ATR): ν = 3073, 2918, 2849, 1641, 1616, 1576, 1546, 1525, 1505, 1464, 1447, 1427, 1380, 1304, 1267, 1235, 1210, 1124, 1059, 996, 942, 912, 894, 856, 810, 799, 790, 726, 662, 631, 600, 550, 473, 447 cm⁻¹; elemental analysis calcd (%) for C₃₆H₄₅FOS₃: C 71.01, H 7.45, F 3.12, O 2.63, S 15.80; found: C 70.9, H 7.5; exact mass: 608.26; molecular weight: 608.94; *m/z*: 608.27, 609.27, 610.30, 611.30, 612.31, 613.31.

5-(9-Decenyl)-5''-[4-{{(R)-2-octyloxy}-3-fluorophenyl}]-2,2':5',2''-terthiophene ((R)-1)

The synthetic procedure is described in ref. 12.

¹H-NMR (400 MHz, CDCl₃): δ = 7.29 (dd, 1H, *J* = 12.0, 2.4 Hz), 7.25 (ddd, 1H, *J* = 8.4, 2.0, 1.2 Hz), 7.09 (d, 1H, *J* = 3.6 Hz), 7.07 (d, 1H, *J* = 3.6 Hz), 7.04 (d, 1H, *J* = 4.0 Hz), 6.98 (d, 1H, *J* = 3.6 Hz), 6.97 (d, 1H, *J* = 3.6 Hz), 6.94 (t, 1H, *J* = 6.3 Hz), 6.67 (d, 1H, *J* = 3.6 Hz), 5.80 (ddt, 1H, *J* = 16.8, 10.4, 6.8 Hz), 5.00 (ddd, 1H, *J* = 16.8, 3.6, 1.2 Hz), 4.92 (ddt, 1H, *J* = 10.4, 3.6, 1.2 Hz), 4.36 (sextet, 1H, *J* = 6.0 Hz), 2.78 (2H, t, *J* = 7.6 Hz), 2.03 (quartet, 2H, *J* = 6.8 Hz), 1.82-1.73 (m, 1H), 1.67 (quintet, 2H, *J* = 7.2 Hz), 1.64-1.56 (m, 1H), 1.40-1.25 (m, 18H), 1.31 (d, 3H, *J* = 6.4 Hz), 0.87 (t, 3H, *J* = 6.4 Hz); ¹³C-NMR (100 MHz, CDCl₃): δ = 145.9, 139.4, 137.0, 136.4, 135.6, 134.6, 125.0, 124.5, 124.3, 123.7, 123.6, 121.6, 121.5, 118.0, 114.3, 114.0, 113.8, 113.5, 76.8, 36.7, 34.0, 32.0, 31.8, 30.4, 29.6, 29.5, 29.4, 29.3, 29.2, 29.1, 25.6, 22.8, 20.0, 14.3, 14.2; FT-IR (ATR): ν = 3072, 2919, 2848, 1640, 1616, 1576, 1546, 1524, 1506, 1464, 1427, 1379, 1303, 1268, 1234, 1209, 1123, 1069, 996, 942, 911, 894, 857, 810, 799, 790, 726, 661, 630, 594, 549, 474, 447 cm⁻¹; elemental analysis calcd (%) for C₃₆H₄₅FOS₃: C 71.01, H 7.45, F 3.12, O 2.63, S 15.80; found: C 71.4, H 7.6; exact mass: 608.26; molecular weight: 608.94, *m/z*: 608.26, 609.27.¹²

3.2.2. Preparation of enantiomer mixtures of (S)-1 and (R)-1

Appropriate quantities of both enantiomers were weighed and dissolved in toluene. The solution was mixed and the solvent was evaporated by heating. Finally, the obtained solid was dried in vacuo to afford the enantiomeric mixture.

3.2.3. Characterization of mesomorphic properties

The mesomorphic properties of the phenylterthiophene derivatives were evaluated using polarizing optical microscopy (POM), differential scanning calorimetry (DSC), and X-ray diffraction (XRD). A polarizing optical microscope (Olympus DP70) equipped with a handmade hot stage was used for visual observation of optical textures. DSC measurements were conducted with a NETZSCH DSC 204 Phoenix system. XRD patterns were acquired with a Rigaku Rapid II diffractometer equipped with a handmade hot stage using Ni-filtered Cu K α radiation.

3.2.4. Evaluation of carrier transport properties

Hole mobilities were measured by a TOF method. Liquid crystal cells with a 25 μm gap were fabricated by combining two ITO-glass plates. The empty cells were put on a hot stage and heated above the clearing temperature of the LC compounds. The LC sample was melted and capillary-filled into the cells. After the required sample temperature was reached on the hot stage, a DC voltage was applied using an electrometer (ADC R8252), and a pulse laser was used to illuminate to the LC cell. The excitation source was the third harmonic of a Nd:YAG laser (Continuum MiniLite II, wavelength = 356 nm, pulse duration = 2 ns) and the photoinduced displacement currents were recorded using a digital oscilloscope (Tektronix TDS 3044B) through a serial resistor.

The photogenerated charge carriers obtained by pulse laser illumination drift across the sample under application of a DC electric field, inducing a transient photocurrent as a voltage drop across the serial resistor connected to the digital oscilloscope. When the photogenerated charge carriers arrive at the counter electrode, the transient photocurrent drops to zero. The transit time of the photogenerated charge carriers can be determined from the kink point in the transient photocurrent curve.

3.2.5. Evaluation of spontaneous polarization

Spontaneous polarization was evaluated by a Sawyer–Tower method using a triangular-wave bias ($\pm 25 \text{ kV cm}^{-1}$, 50–1000 Hz). The triangular-wave bias generated by a function generator (NF WF1973) was applied to the LC sample cells. The induced currents were recorded with a digital oscilloscope (Tektronics TDS 3044B) through a serial resistor. In this measurement, sample cells with a 2 μm gap were used. The sample cells were prepared in the same way as those for the TOF method.

3.2.6. Evaluation of the APV effect in SmC*/SmC phases

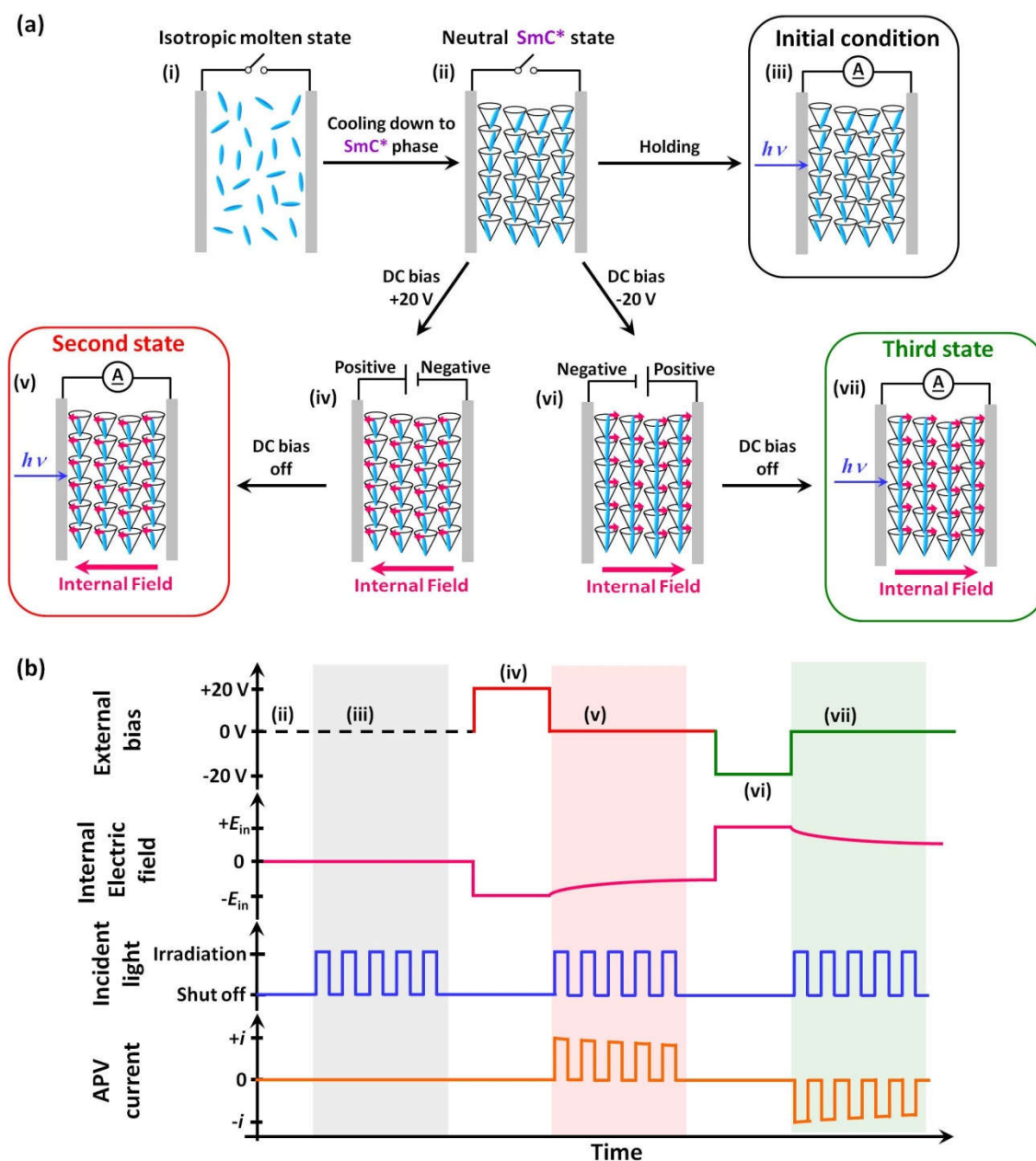


Figure 3-3. Schematic illustrations of measurement condition for the steady state photocurrent response under zero bias in SmC/SmC* phases.

Figure 3-3a depicts the formation of polarized states in the SmC* phase schematically. Randomly oriented LC molecules in the isotropic phase (state (i)) form a layer structure in the SmC* phase (state (ii)). In the SmC* phase, the direction of the LC molecules changes periodically along the layer normal to cancel the strong dipole moments, resulting in the formation of a helical structure owing to molecular chirality. This state is retained under short-circuit conditions (state (iii)). When a DC bias is applied to the sample, the helical structure is unwound to produce a polarized state in which the LC

molecules orient in one direction, tilted toward the layer normal (states (iv) and (vi)). Molecular dipoles align along the external electric field to produce polarization. When the external voltage is removed, the unidirectional molecular orientation is retained to produce an internal electric field (states (v) and (vii)).

The APV effect was confirmed by measuring the steady-state photocurrent response under zero bias (Figure 3-3b). In state (iii), no internal field is formed. When the front electrode is biased positively in the ferroelectric phase, spontaneous polarization is generated in the reverse direction in state (iv). After removing the DC external bias, the backward internal field remained (state (v)). UV illumination on the front electrode should produce a photocurrent with the opposite polarity to that of the DC field applied prior to illumination. In contrast, a forward internal field should be induced in the SmC* phase when the front electrode is biased negatively prior to UV illumination (state (vi)). After removal of the external DC bias, the polarized state with a forward internal field was retained (state (vii)). In this series of experiments, light irradiation was started just after removal of the DC voltage. Repeated illumination for 4 s was achieved using a mechanical shutter.

In the presence of an internal field, excitons generated by UV excitation separate to produce charge carriers. The photocarriers are transported to the electrodes, producing photocurrent without an external electric field.

3.3. Results and Discussion

3.3.1. Mesomorphic Properties of chiral phenylterthiophene derivatives

Table 3-1. Phase-transition behaviors of chiral compounds (*S*)-**1** and (*R*)-**1**.

| Compounds | Phase-transition temperature / °C |
|------------------------|------------------------------------|
| | (Enthalpy / kJ mol ⁻¹) |
| (<i>R</i>)- 1 | SmG* 124 (10) SmC* 140 (9) Iso |
| (<i>S</i>)- 1 | SmG* 125 (10) SmC* 140 (9) Iso |

The abbreviations SmG*, SmC*, and Iso denote chiral smectic G, chiral smectic C, and isotropic phases, respectively.

The mesomorphic properties of chiral fluorophenyl-terthiophene derivatives (*S*)-**1** and (*R*)-**1** are summarized in Table 1. The LC properties of (*R*)-**1** have been already discussed in the previous study.¹²

The mesomorphic properties of chiral fluorophenylterthiophene derivatives (*S*)-**1** and (*R*)-**1** are summarized in Table 1. The LC properties of (*R*)-**1** have been discussed in the previous study.¹² In POM, typical broken fan-like textures with disclination lines were observed on cooling from the isotropic molten state for compound (*S*)-**1** (Figure 3-4a). The appearance of characteristic broken fan-like domains suggests the formation of a SmC* structure, with the disclination lines derived from the helical structure of the SmC* phase (Figure 3-4a, inset). Upon further cooling from the SmC*

phase, the polarized optical textures were changed with the domain shapes maintained. It is noted that the LC molecules prefer a homeotropic alignment between the two glass substrates and the some fan-shaped domains appear. In this cooling process, tile-like domains drastically appeared in the homeotropic domains of the SmC* phases, which suggests the formation of an ordered smectic phase (Figure 3-4b).

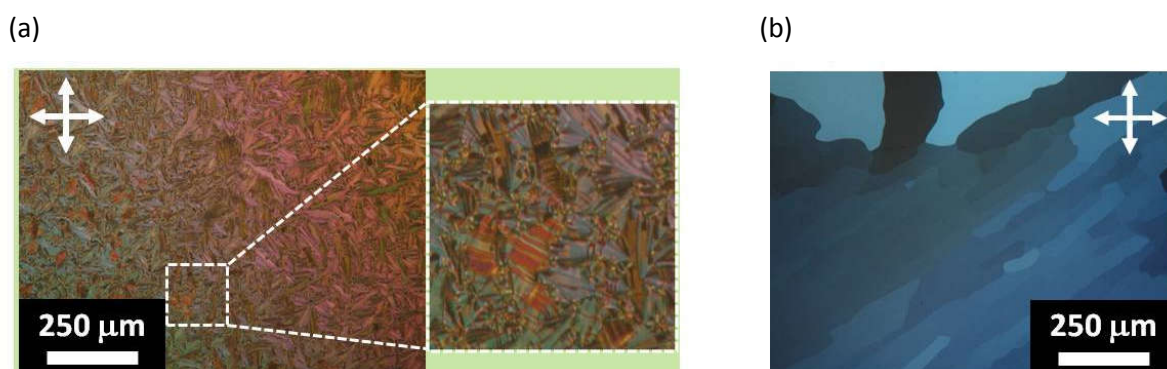


Figure 3-4. POM images of (a) the SmC* phase (125 °C) and (b) the SmG* phase (50 °C) of (S)-1 on cooling between two glass substrates. The inset is a magnified image of the SmC* phase at 125 °C.

The molecular reorientation behaviors induced by the external electric field were confirmed by the POM study under DC bias. For a 2 μm-thick cell of compound (S)-1, broken fan-like SmC* domains with periodic lines were obtained after cooling from the isotropic liquid phase (Figure 3-5a). The stripe patterns of the line defects implied the formation of SmC* helical structures. In the domains with stripe patterns, polarization should be cancelled. It should be noted that the formation of stripe patterns was random and was not observed in the whole area. That is, the polarization state should coexist microscopically, even in the electrically neutral state. When a DC bias was applied to the cell, the stripe patterns in the SmC* domains disappeared and clear broken fan-like textures, which are usually observed in achiral SmC phase, were observed in the POM images. This texture change suggested the reorientation of the LC molecules to form the polarized state. With the opposite external electric field, the POM texture change had a different color tone (Figure 3-5b and 3-5c). On removing the external bias, the original POM textures in the electrically neutral state were recovered. The stripes originating from the disclinations were only partially reproduced, owing to retention of the polarized state. After the discharge treatment, many disclination lines were formed in the broken fan-like domains (Figure 3-5d).

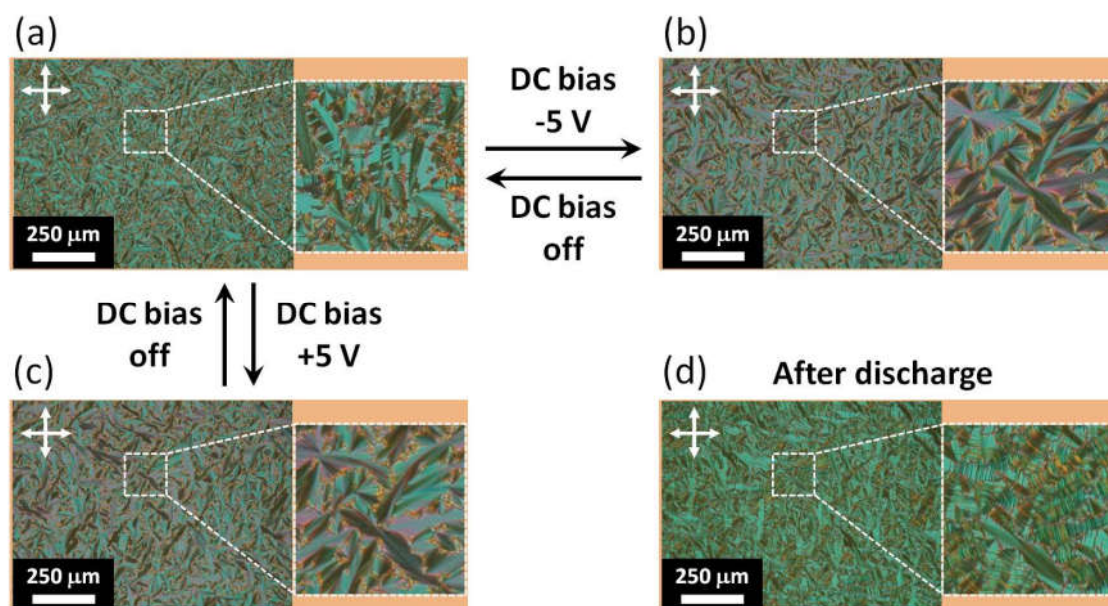


Figure 3-5. POM images of the SmC* phase (127 °C) in a 2 μm gap cell filled with (S)-1: (a) after cooling from the Iso phase without DC bias, (b) under application of a negative DC bias (-5 V), (c) under application of a positive DC bias (+5 V), and (d) after discharge. The insets are magnified images of the SmC* phase at 127 °C.

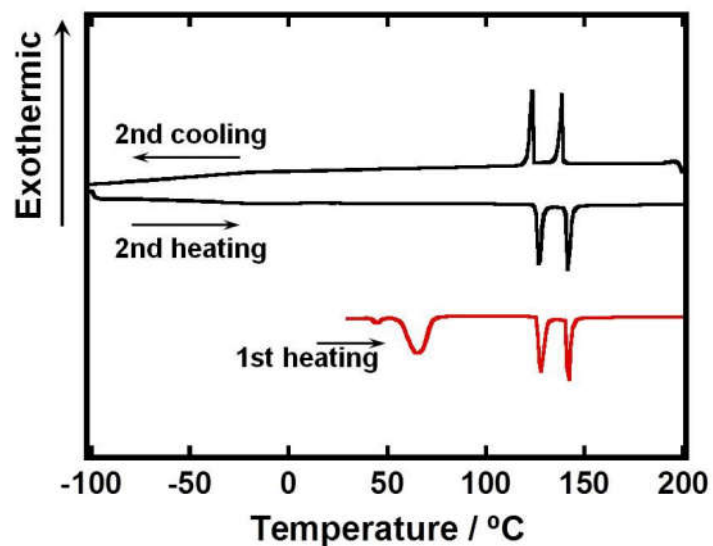


Figure 3-6. DSC thermograms of (S)-1 (The scanning rate was 10 K min⁻¹).

In the DSC thermogram of (S)-1 (Figure 3-6), clear two peaks are observed during the 2nd heating and cooling processes. These two peaks indicated transitions between ordered smectic and SmC* phases and between SmC* and isotropic phases. It is noted that a crystalline–LC phase transition

peak was observed around 50 °C only during the 1st heating process. The initial crystalline precipitates that were used for the DSC measurements were obtained by recrystallization from *n*-hexane solution. Once the precipitates melted to the isotropic phase, they did not crystallize during the cooling process. The DSC thermograms of (*S*)-**1** are identical to those of (*R*)-**1**, which were previously reported.¹²

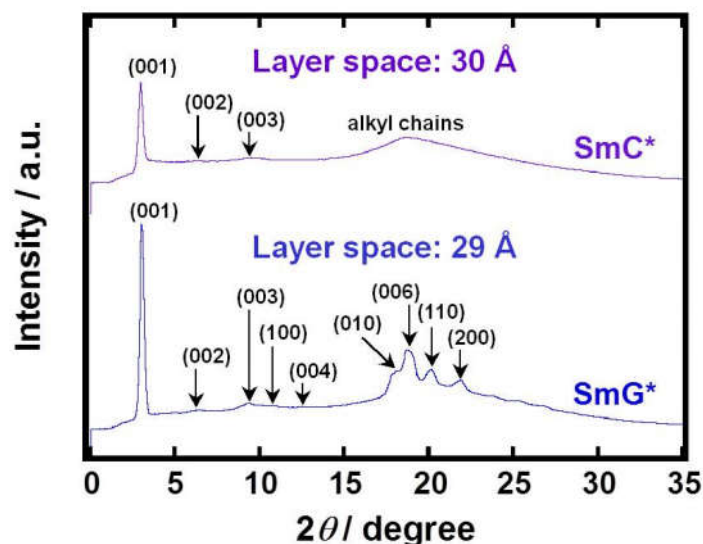


Figure 3-7. XRD patterns of (*S*)-**1** (upper: SmC* phase at 132 °C, bottom: SmG* phase at 100 °C).

The XRD pattern of the SmC* phase of (*S*)-**1** (Figure 3-7, upper) shows a strong small-angle diffraction and weak high-order peaks, which correspond to the (001), (002), and (003) diffraction planes. The ratio of the *d*-spacings for these diffraction planes is 3:2:1, supporting the smectic layer structure. The layer spacing is shorter than the extended molecular length of (*S*)-**1** estimated by MM2 calculation, indicating that the molecules are tilted to the layer normal. Therefore, the high-temperature LC phase was confirmed to be a SmC* phase. The low-temperature LC phase of (*S*)-**1** was identified as a chiral smectic G (SmG*) phase, as the wide-angle diffraction peaks observed in the XRD pattern of (*S*)-**1** (Figure 3-7, lower) suggest a rectangular order for the positions of LC molecules within the smectic layers. These diffraction patterns of (*S*)-**1** are identical with those of (*R*)-**1**.

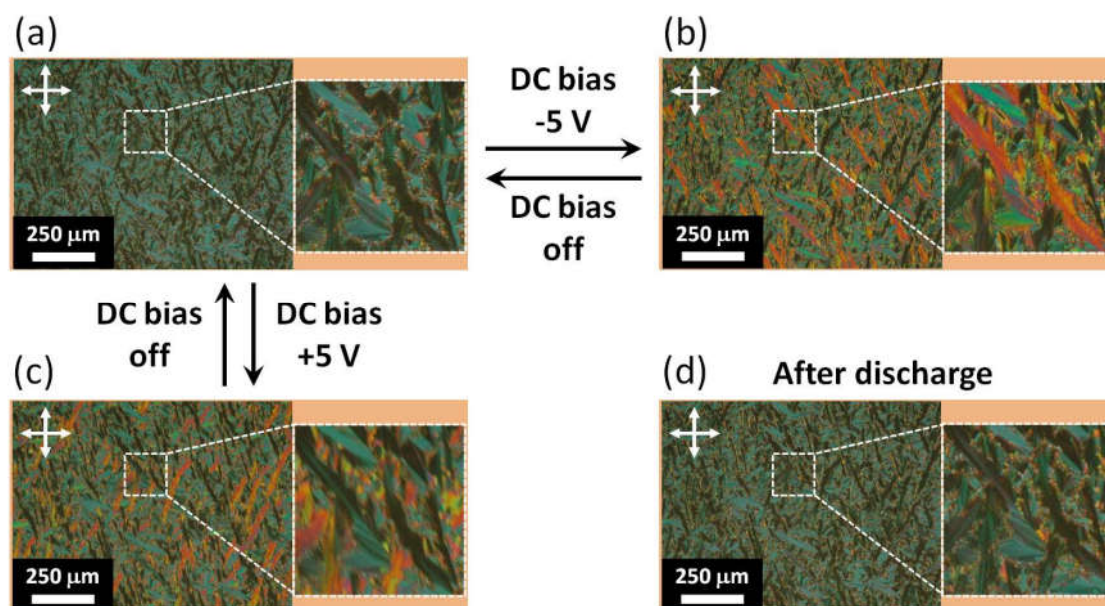


Figure 3-8. POM images of the SmC phase (127 °C) in a 2 μm gap cell filled with (*rac*)-1: (a) after cooling from the Iso phase without DC bias, (b) under application of a negative DC bias (-5 V), (c) under application of a positive DC bias (+5 V), and (d) after discharge. The insets are magnified images of the SmC phase at 127 °C.

The mesomorphic properties of LC enantiomeric mixtures composed of (*S*)-1 and (*R*)-1 were also evaluated in the same way. For the racemic mixture (*rac*)-1, broken fan-shaped domains without disclination lines were formed after cooling from the Iso phase in a 2- μm thick LC cell (Figure 3-8a). As an external bias was applied to the racemic SmC cell, the domain shapes and defect lines did not change, but the color tone changed slightly, regardless of the bias direction (Figure 3-8b and 3-8c). This color change should be attributed not to ferroelectric switching but to the electro-optic effect, which is observed in achiral SmC phases. Recovery of the original textures in the electrically neutral state was observed after removing the DC bias. It is noteworthy that no disclination lines were generated in the SmC phase of (*rac*)-1, even after discharge (Figure 3-8d). These results clearly indicated that achiral LC phases, not chiral LC phases, were formed in the racemic mixture system. Thus, the high-temperature and low-temperature LC phases of (*rac*)-1 were identified as smectic C (SmC) and smectic G (SmG) phases, respectively. (For details of the DSC thermograms and XRD profiles of (*rac*)-1, see the Figure 3-9 and 3-10, respectively.)

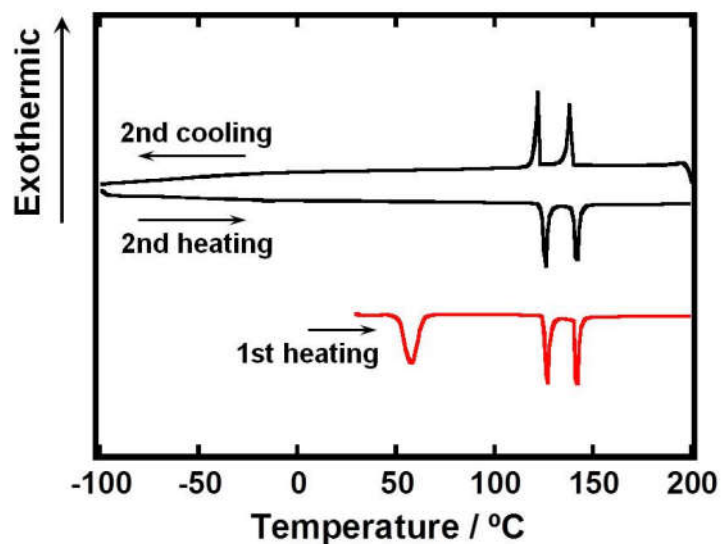


Figure 3-9. DSC thermograms of (*rac*)-1 (The scanning rate was 10 K min⁻¹).

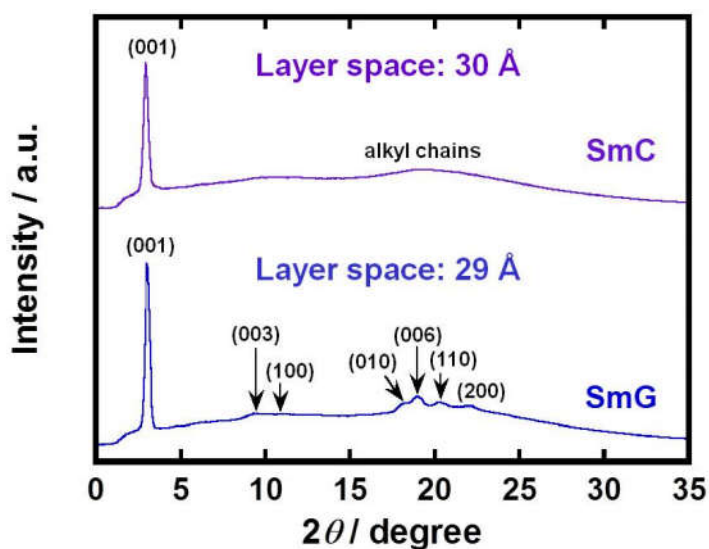


Figure 3-10. XRD patterns in the LC phases of (*rac*)-1 on cooling process (Upper: at 126 °C in the SmC phase, bottom: at 100 °C in the SmG phase).

Figure 3-11 shows the phase diagram for the LC mixtures of (*R*)- and (*S*)-1. With the exception of (*rac*)-1, all the samples exhibited SmC* and SmG* phases. The racemic mixture, (*rac*)-1, displays an achiral SmC phase. The phase transition temperatures and enthalpies were almost independent of the enantiomeric purity.

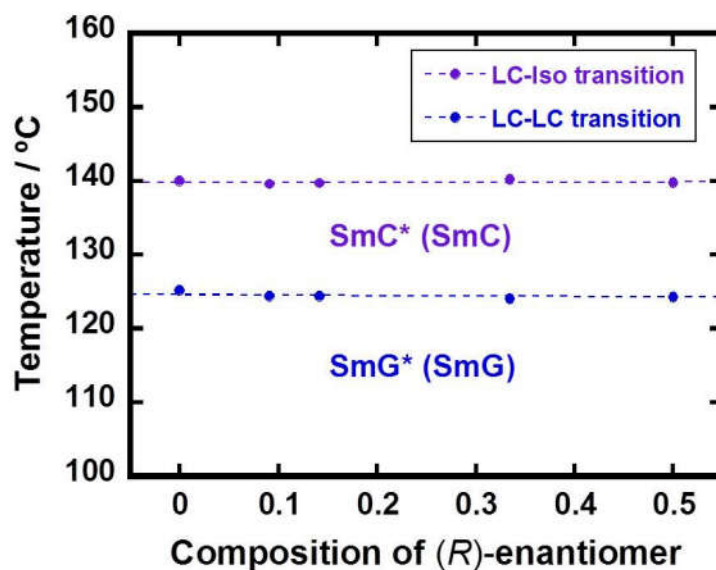


Figure 3-11. A phase diagram of the enantiomer mixtures of (S)-1 and (R)-1.

3.3.2. Carrier transport properties in SmC*/SmC phases

The carrier mobilities in the SmC* phase of (S)-1 were determined by the TOF technique using 25 μm gap cells. Figure 10a shows typical transient photocurrent curves for holes in the SmC* phase of (S)-1.

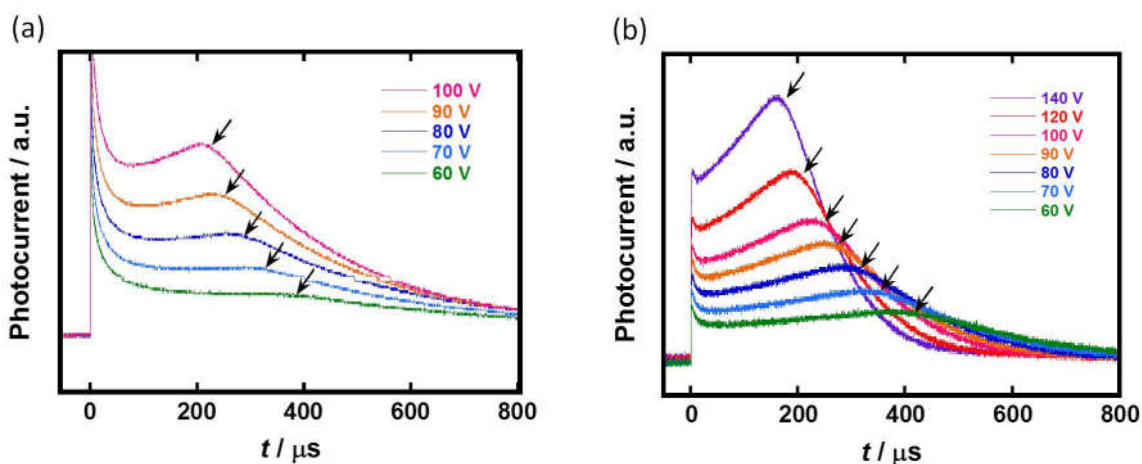


Figure 3-12. Transient photocurrent curves for positive charge (a) in the SmC* phase (130 °C) of (S)-1, and (b) in the SmC phase (130 °C) of (rac)-1. The measurements were performed using ITO/ITO sandwich cells (gap: 25 μm). The arrows indicate kink points corresponding to the transit times.

Nondispersive transient photocurrent curves were observed for the holes in the SmC* phase of (S)-**1** (Figure 3-12a). The kink points on the linear plots of the curves provided the transit times. In contrast, dispersive and weak transient photocurrent curves were observed for negative charge carriers, and the mobilities of the negative carriers could not be estimated.

In the SmC* phase of (S)-**1** at 130 °C, the hole mobility was determined to be $2.7 \times 10^{-4} \text{ cm}^2 \text{ V}^{-1} \text{ s}^{-1}$ from the transit times. This value is one or two orders of magnitude larger than ionic carrier mobilities in nematic phases.¹⁹ The hole mobility in the SmC* phase was independent of the temperature and the electric field (Figure 3-13a, 3-14a). The determined hole mobility is on the same order as those in the SmC* and SmC phases of other LC semiconductors.^{20, 21} Field- and temperature-independent charge carrier mobilities have also been observed in SmC* and SmC phases of oligothiophene and phenylanthracene derivatives.²²

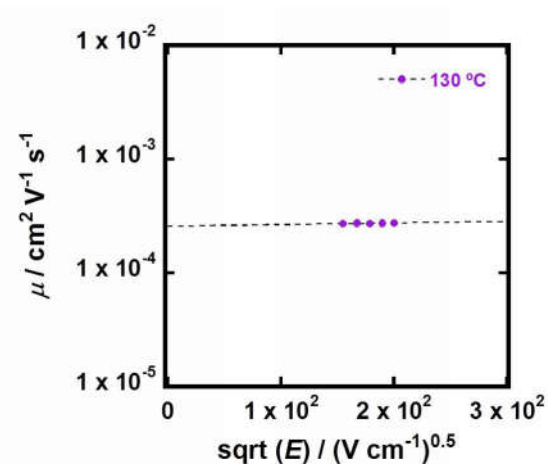
The hole-transport properties in the SmC phase of the racemic mixture, (*rac*)-**1**, were studied under similar conditions. Nondispersive transient photocurrent curves were observed for the holes in the SmC phase (Figure 3-12b). The hole mobility of (*rac*)-**1** was $2.5 \times 10^{-4} \text{ cm}^2 \text{ V}^{-1} \text{ s}^{-1}$ at 130 °C, which is comparable to that of (S)-**1**. In addition, the hole mobility in the SmC phase of the racemic sample was also independent of the temperature and electric field (Figure 3-13b, 3-14b). Thus, the hole-transport characteristics in the SmC* (or SmC) phase were not affected by the enantiomeric purity of the sample. Under the conditions used for TOF measurements, the helical structure of the SmC* phase was unwound and the molecular aggregation states are the same in the LC phases of the enantiomeric mixtures and the racemic sample. In the presence of an external voltage, the external voltage determines the electric field interacting with the photogenerated charge carriers, as observed in conventional dielectrics, including ferroelectrics.

In amorphous organic semiconductors,^{23a} temperature- and field-dependence of carrier mobilities is mainly attributed to distribution of energy levels of hopping sites. This is caused by the fluctuation of local electric fields produced by randomly oriented molecular dipole moments. Assuming the hopping transport,^{23b,c} hole transport characteristics in the SmC and SmC* phases should be different.

In columnar and smectic phases in high temperature region, thermal activation process of charge carrier hopping between the disordered energy levels competes with dynamic fluctuation of the LC structures.^{10c,10i,23b,23c} The SmC and SmC* phases have a dynamic nature. Because of thermal motion of the LC molecules, thermal fluctuation of the layer structures should cancel the thermal activation effect in the charge carrier hopping process which is influenced by the local electric field generated by molecular dipole moments. This thermal fluctuation of the LC supramolecular aggregation structures should make the difference of the characteristics between the two phases inconspicuous.

For electrons, only weak featureless current decays were observed in the SmC* and SmC phases of these samples. This result indicated that the generation efficiency of electrons was lower than that of holes.

(a) (S)-1



(b) (rac)-1

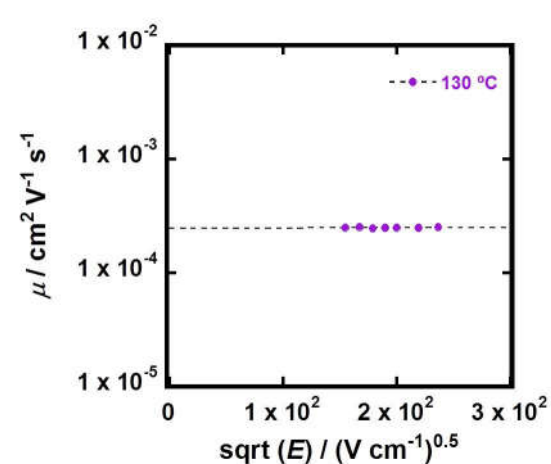
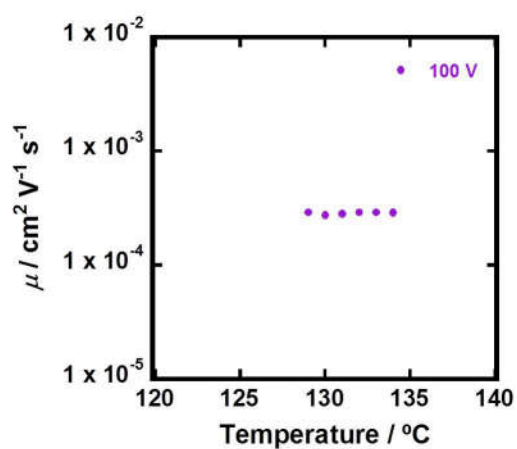


Figure 3-13. Hole mobilities as a function of the square root of electric field in (a) the SmC* phase of (S)-1 and (b) the SmC phase of (rac)-1.

(a) (S)-1



(b) (rac)-1

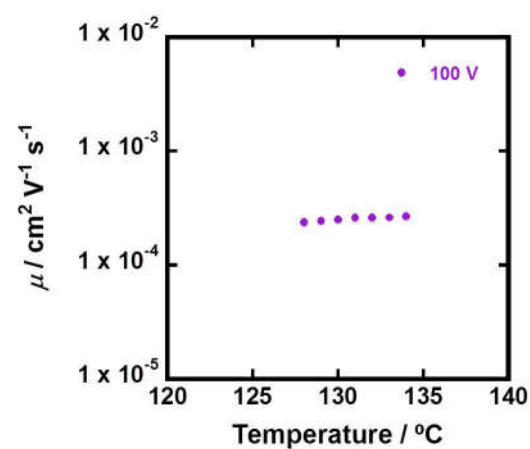


Figure 3-14. Hole mobilities as a function of temperature in (a) the SmC* phase of (S)-1 and (b) the SmC phase of (rac)-1.

3.3.3. Spontaneous polarizations

Spontaneous polarization in SmC* (SmC) phases of chiral (*S*)-**1** and the enantiomeric mixtures of (*S*)-**1** and (*R*)-**1** was evaluated by the Sawyer–Tower method using 2 μm gap LC cells ($\pm 25 \text{ kV cm}^{-1}$, 100 Hz). The value of the spontaneous polarization was determined by extrapolating the saturation region of the loop to the applied voltage of 0 V. The spontaneous polarization in the SmC* phase was almost constant up to the frequency of 1 kHz (Figure 3-15). As shown in Figure 3-16, hysteresis loops were observed for the dielectric properties in the SmC* phases, indicating ferroelectricity. In contrast, the racemic mixture did not exhibit ferroelectricity. The spontaneous polarization values were estimated by extrapolation of these polarization curves to zero bias. The estimated values are summarized in Table 3-2.

Table 3-2. Spontaneous polarization of the enantiomer mixtures for (*R*)-**1**/*(S)*-**1**.

| Sample | (<i>R</i>)-enantiomer composition | $P / \text{nC cm}^{-2}$ |
|-----------------------------------|-------------------------------------|-------------------------|
| (<i>S</i>)- 1 | 0.00 | 68 |
| 1 <i>R</i> 10 <i>S</i> - 1 | 0.09 | 55 |
| 1 <i>R</i> 6 <i>S</i> - 1 | 0.14 | 48 |
| 1 <i>R</i> 2 <i>S</i> - 1 | 0.33 | 23 |
| (<i>rac</i>)- 1 | 0.50 | 0 |

P denotes the value of spontaneous polarization. The notation of the sample is as follows. 1*R*10*S*-**1**: (*R*)-**1**/*(S)*-**1** = 1/10; w/w mixture, 1*R*6*S*-**1**: (*R*)-**1**/*(S)*-**1** = 1/6; w/w mixture, 1*R*2*S*-**1**: (*R*)-**1**/*(S)*-**1** = 1/10; w/w mixture, (*rac*)-**1**: (*R*)-**1**/*(S)*-**1** = 1/1; w/w mixture.

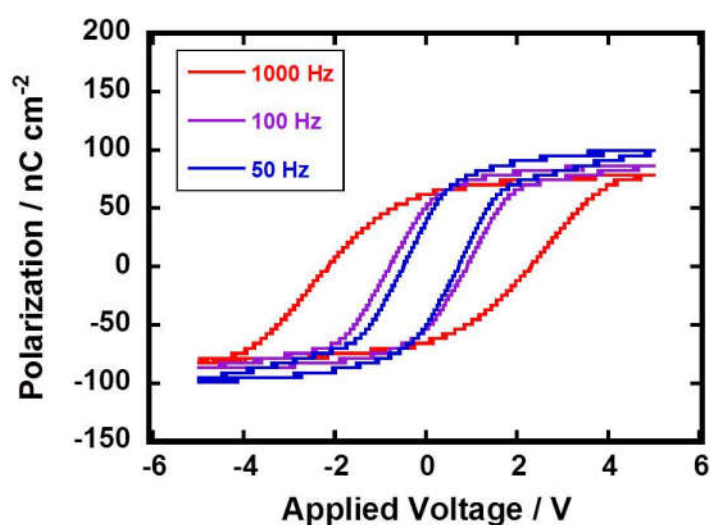


Figure 3-15. Dielectric hysteresis loops in the SmC* phase (130 °C) of (*S*)-**1**.

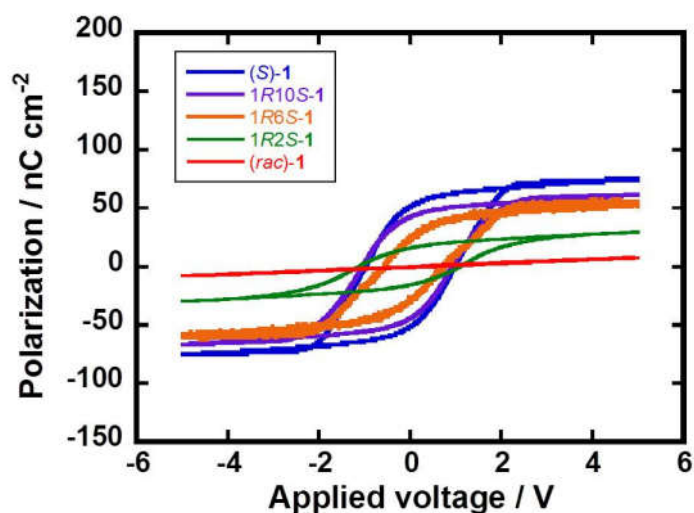


Figure 3-16. Dielectric hysteresis loops in SmC* (SmC) phases of the enantiomer mixtures for (S)-1/(R)-1.

Spontaneous polarization decreased as the enantiomeric purity was reduced. This result indicated that ferroelectricity in the SmC* phase is based on molecular chirality, as observed in conventional FLCs. Therefore, spontaneous polarization was generated by the directional orientation of the polar unit resulting from the symmetry break. Polarization inversion is determined by the precession dynamics of the chiral molecules.

3.3.4. APV response in SmC*/SmC phases

The APV response was evaluated in the SmC* (or SmC) phase using 2 μm gap ITO/ITO sandwich cells. Figure 3-17 shows the steady-state photocurrent response curves under zero bias in the SmC* phase of compound (S)-1.

In the initial state, a weak photocurrent response (ca. $0.12 \mu\text{A cm}^{-2}$) was observed (Figure 3-17, black line). The microscopic polarized domains might generate a weak internal electric field at the interface between the LC material and the ITO electrode.

In the second state, the polarity of the photocurrent response was reversed owing to the generated backward internal field (Figure 3-17, red line). In the third state, a strong photocurrent response ($>0.6 \mu\text{A cm}^{-2}$) was observed under the forward internal field (Figure 3-17, green line). It should be noted that the polarity of the photocurrent was opposite to that of the DC bias prior to UV illumination and that the polarity of the photocurrent response could be reversed by changing the polarity of the DC bias prior to UV illumination.

The photocurrent response at zero external bias in the third state was larger than that in the second state. As mentioned in previous papers,¹² the penetration depth of the UV excitation light is

less than 100 nm owing to the strong absorption coefficient of phenylterthiophene (*S*)-1 in the near-UV region. In this π -conjugated FLC system, the generation and the transport of holes are superior to those of electrons. Because the forward internal field in the third state enhanced hole conduction, a strong response was observed in the third state.

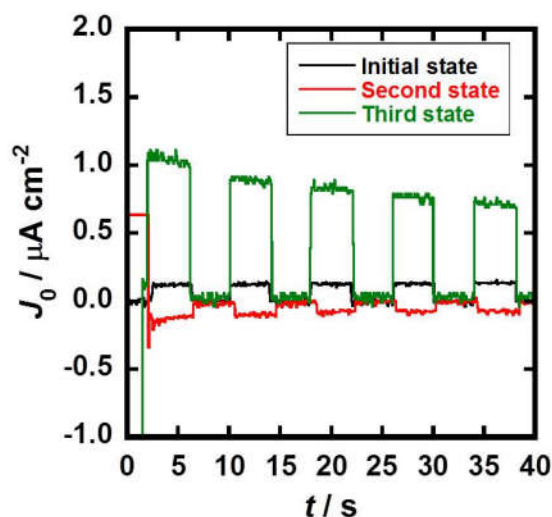


Figure 3-17. Steady state photocurrent response profiles in SmC* phases of (*S*)-1 (127 °C). The measurements were performed using ITO/ ITO sandwich cells whose gap was 2 μm . The APV current density (J_0) is determined as APV photocurrent density at zero external bias.

To confirm the origin of the spontaneous polarization for the APV effect, the APV responses of enantiomeric mixtures of (*S*)-1 and (*R*)-1 were evaluated under similar conditions using 2 μm gap LC cells. For the racemic mixture, (*rac*)-1, the APV response was suppressed, even in the third state. The APV photocurrent and spontaneous polarization are plotted as a function of the enantiomeric ratio in Figure 3-18. Both values are strongly correlated with the enantiomer composition, decreasing linearly as the enantiomeric purity decreases. In contrast, the carrier mobility is independent of the enantiomeric purity. Therefore, the origin of the APV effect in the SmC* phase of enantiomeric compound (*S*)-1 or (*R*)-1 was confirmed to be the spontaneous polarization based on ferroelectricity derived from the molecular chirality.

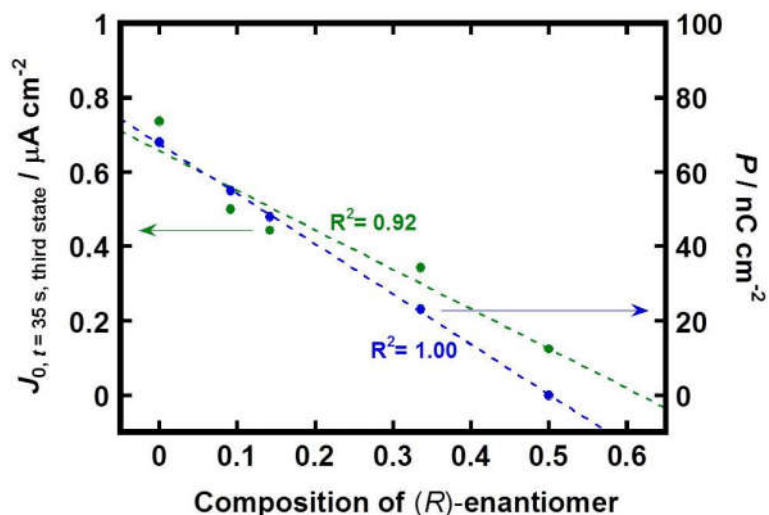


Figure 3-18. The plot of APV photocurrent of the mixtures for (S)-1/(R)-1 and the spontaneous polarization as a function of the enantiomer ratio (P : spontaneous polarization; $J_0, t=35 \text{ s, third state}$: APV photocurrent density at 35 s on the third state).

In all SmC* samples, the APV response was observed to decay (Figure 3-19). This response decay might originate from the dielectric relaxation behavior in the SmC* phases. When the LC sample thickness is larger than the SmC* helical pitch, the helical structure, which suppresses spontaneous polarization, is the most thermodynamically stable state. Thus, thermal relaxation of the polarized state to the nonpolarized helical structure should lead to a decay of the APV response. Because of this polarization relaxation, the open circuit voltage was about 0.4 V which was comparable to those of conventional organic photovoltaic cells based on p-n junction.

This APV effect in the SmC* phase of compound (S)-1 or (R)-1 originates from order-disorder-type ferroelectricity based on molecular chirality and is completely different from APV effects in ferroelectric ceramics^{14, 15} and antiferroelectric perovskites.²⁴ A few groups have recently reported photorefractive devices and polarity-switchable diodes based on electroactive FLC materials, but they did not mention the APV effect.²⁵

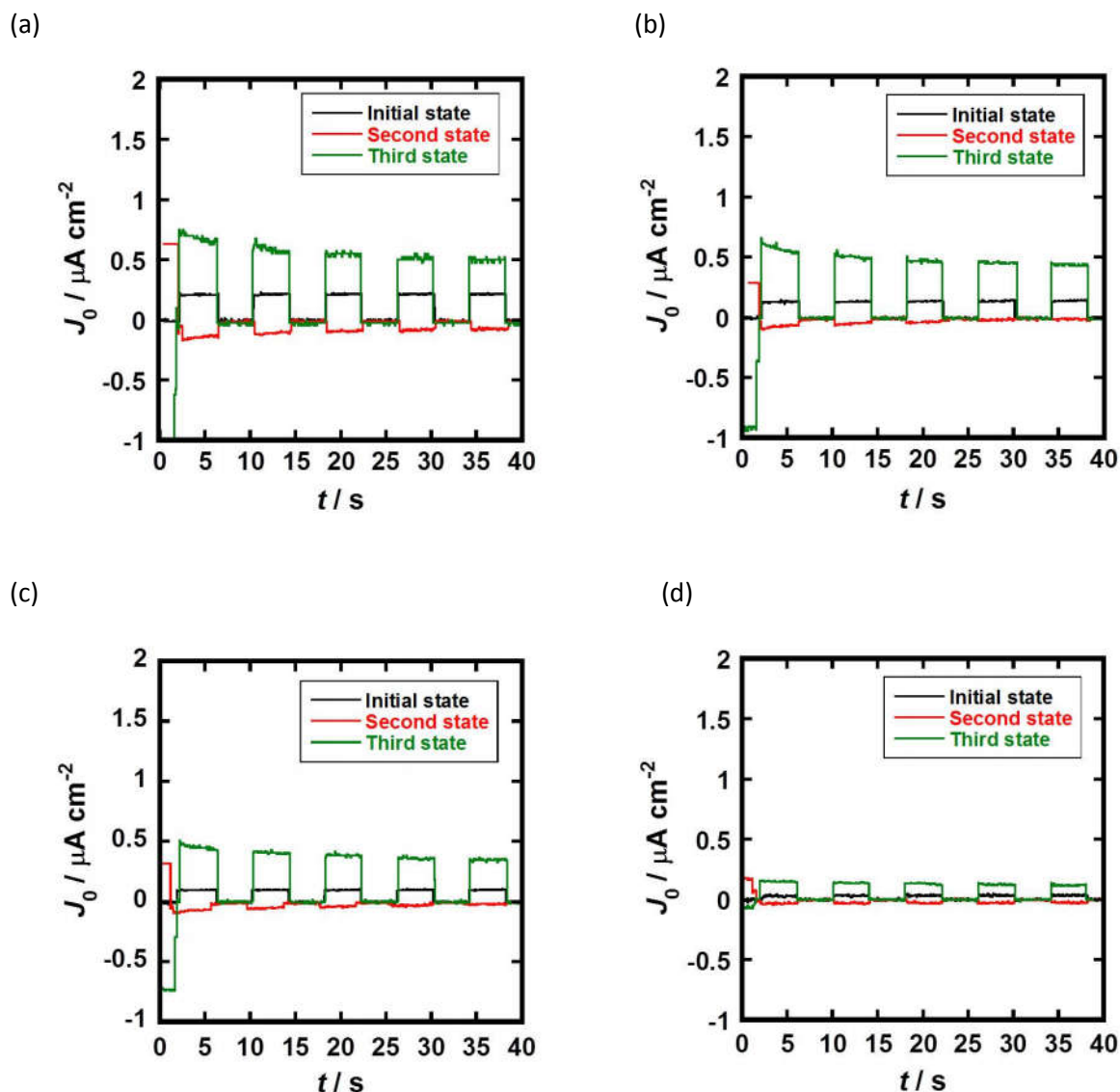


Figure 3-19. Steady state photocurrent response profiles at 127 °C for (a) 1R10S-1, (b) 1R6S-1, (c) 1R2S-1, and (d) (*rac*)-1, (b) The measurements were performed using ITO/ ITO sandwich cells whose gap was 2 μm . The APV current density (J_0) is determined as APV photocurrent density at zero external bias.

3.4. Conclusion

In conclusion, chiral π -conjugated compounds (*S*)-1 and (*R*)-1 were synthesized. Each enantiomer exhibited ferroelectric SmC* and ordered smectic phases. The ferroelectric properties in the SmC* phase were evaluated by the Sawyer–Tower method. The spontaneous polarization value reached 68 nC cm⁻² at 127 °C for (*S*)-1. Hole mobilities in the SmC* phase estimated by the TOF method were on the order of 10⁻⁴ cm² V⁻¹ s⁻¹. Each chiral enantiomer, (*S*)-1 and (*R*)-1, exhibited an APV response in the SmC* phase.

Further, enantiomeric mixtures of (*S*)-**1** and (*R*)-**1** were prepared. The APV effect was suppressed in the racemic mixture, (*rac*)-**1**. However, the APV photocurrent response increased with an increase in the enantiomeric purity. Thus, the origin of the APV response in this FLC system was not ionic impurities but instead the bulk internal field produced by spontaneous polarization based on molecular chirality.

3.5. References

1. (a) K. Hanabusa and M. Suzuki, *Bull. Chem. Soc. Jpn.*, 2016, **89**, 174. (b) S. Malik, S. Kawano, N. Fujita and S. Shinkai, *Tetrahedron*, 2007, **63**, 7326. (c) K. Yabuuchi, Y. Tochigi, N. Mizoshita, K. Hanabusa and T. Kato, *Tetrahedron*, 2007, **63**, 7358. (d) C. Bao, M. Jin, R. Lu, Z. Song, X. Yang, D. Song, T. Xu, G. Liu and Y. Zhao, *Tetrahedron*, 2007, **63**, 7443. (e) M. Takafuji, Y. Kira, H. Tsuji, S. Sawada, H. Hachisako and H. Ihara, *Tetrahedron*, 2007, **63**, 7489.
2. (a) N. Ousaka, F. Mamiya, Y. Iwata, K. Nishimura and E. Yashima, *Angew. Chem., Int. Ed.*, 2017, **56**, 791. (b) E. Yashima, N. Ousaka, D. Taura, K. Shimomura, T. Ikai and K. Maeda, *Chem. Rev.*, 2016, **116**, 13752.
3. (a) M. Oda, H.-G. Nothofer, G. Lieser, U. Scherf, S. C. J. Meskers and D. Neher, *Adv. Mater.* 2000, **12**, 362. (b) M. Nakamura, J. Suzuki, F. Ota, T. Takada, K. Akagi and K. Yamana, *Chem. Eur. J.*, 2016, **22**, 9121. (c) Y. Morisaki, R. Sawada, M. Gon and Y. Chujo, *Chem. Asian J.*, 2016, **11**, 2524. (d) K. Watanabe, Z. Sun and K. Akagi, *Chem. Mater.*, 2015, **27**, 2895. (e) K. Watanabe and K. Akagi, *Sci. Technol. Adv. Mater.*, 2014, **15**, 44203.
4. (a) D. Zhao, H. He, X. Gu, L. Guo, K. S. Wong, J. W. Y. Lam and B. Z. Tang, *Adv. Opt. Mater.*, 2016, **4**, 534. (b) T. Hamamoto and M. Funahashi, *J. Mater. Chem. C*, 2015, **3**, 6891. (c) K. L. Woon, M. O'Neill, G. J. Richards, M. P. Aldred, S. M. Kelly and A. M. Fox, *Adv. Mater.*, 2003, **15**, 1555. (d) S. H. Chen, D. Katsis, A. W. Schmid, J. C. Mastrangelo, T. Tsutsui and T. N. Blanton, *Nature*, 1999, **397**, 506.
5. (a) B. L. Feringa, *Science*, 2001, **292**, 2021. (b) N. Koumura, E. M. Geertsema, A. Meetsma and B. L. Feringa, *J. Am. Chem. Soc.*, 2000, **122**, 12005. (c) N. Koumura, R. W. J. Zijlstra, R. A. van Delden, N. Harada and B. L. Feringa, *Nature*, 1999, **401**, 152.
6. S. Wada, Y. Kitagawa, T. Nakanishi, K. Fushimi, Y. Morisaki, K. Fujita, K. Konishi, K. Tanaka, Y. Chujo and Y. Hasegawa, *NPG Asia Mater.*, 2016, **8**, e251.
7. (a) R. B. Meyer, L. Libert, L. Strzelecki and P. Keller, *J. Phys.*, 1975, **36**, L69; (b) C. Y. Young, R. Pindak, N. A. Clark and R. B. Meyer, *Phys. Rev. Lett.*, 1978, **40**, 773; (c) N. A. Clark and S. T. Lagerwall, *Appl. Phys. Lett.*, 1980, **36**, 899; (d) S. T. Lagerwall and I. Dahl, *Mol. Cryst. Liq. Cryst.*, 1984, **114**, 151; (e) Y. Takanishi, H. Takezoe, Y. Suzuki, I. Kobayashi, T. Yajima, M. Terada and K. Mikami, *Angew. Chem., Int. Ed.*, 1999, **38**, 2353.
8. W. J. A. M. Hartmann, *Ferroelectrics*, 1991, **122**, 1.
9. (a) T. Kato, M. Yoshio, T. Ichikawa, B. Soberats, H. Ohno and M. Funahashi, *Nat. Rev. Mater.*, 2017, **2**, 17001. (b) W. Pisula, M. Zorn, J. Y. Chang, K. Müllen and R. Zentel, *Macromol. Rapid Commun.*, 2009, **30**, 1179. (c) M. Funahashi, *Polym. J.*, 2009, **41**, 459. (d) M. Funahashi and T. Kato, *Liq. Cryst.*, 2015, **42**, 909. (e) A. Seki and M. Funahashi, *Heterocycles*, 2016, **92**, 3. (f) M. Funahashi, *J. Mater. Chem. C*, 2014, **2**, 7451. (g) M. O'Neill and S. M. Kelly, *Adv. Mater.*, 2011, **23**, 566.
10. (a) D. Adam, F. Closs, T. Frey, D. Funhoff, D. Haarer, H. Ringsdorf, P. Schuhmacher and K. Siemensmeyer, *Phys. Rev. Lett.*,

- 1993, **70**, 457. (b) N. Boden, R. J. Bushby, J. Clements, B. Movaghar, K. J. Donovan and T. Kreouzis, *Phys. Rev. B.*, 1995, **52**, 13274. (c) I. Bleyl, C. Erdelen, H.-W. Schmidt and D. Haarer, *Philos. Mag. B*, 1999, **79**, 463. (d) J. Simmerer, B. Glösen, W. Paulus, A. Kettner, P. Schuhmacher, D. Adam, K.-H. Etzbach, K. Siemensmeyer, J. H. Wendorf, H. Ringsdorf and D. Haarer, *Adv. Mater.*, 1996, **8**, 815. (e) D. Adam, P. Schumacher, J. Simmerer, L. Haussling, K. Siemensmeyer, K. H. Etzbach, H. Ringsdorf and D. Haarer, *Nature*, 1994, **371**, 141. (f) M. Funahashi and J. Hanna, *Jpn. J. Appl. Phys.*, 1996, **35**, L703. (g) M. Funahashi and J. Hanna, *Adv. Mater.*, 2005, **17**, 594. (h) M. Funahashi and A. Sonoda, *J. Mater. Chem.*, 2012, **22**, 25190. (i) M. Funahashi and A. Sonoda, *Phys. Chem. Chem. Phys.*, 2014, **16**, 7754. (j) A. M. van de Craats, J. M. Warman, A. Fechtenkötter, J. B. Brand, M. A. Harbison and K. Müllen, *Adv. Mater.*, 1999, **11**, 1469. (k) K. Ban, K. Nishikawa, K. Ohta, A. M. van de Craats, J. M. Warman, I. Yamamoto and H. Shirai, *J. Mater. Chem.*, 2001, **11**, 321. (l) A. Demenev, S. H. Eichhorn, T. Taerum, D. Perepichka, S. Patwardhan, F. C. Grozema, L. D. A. Siebbeles and R. Klenkler, *Chem. Mater.*, 2010, **22**, 1420. (m) C. Deibel, D. Janssen, P. Heremans, V. De Cupere, Y. Geerts, M. L. Benkhedir and G. J. Adriaenssens, *Org. Electron.*, 2006, **7**, 495. (n) Z. An, J. Yu, B. Domercq, S. C. Jones, S. Barlow, B. Kippelen and S. R. Marder, *J. Mater. Chem.*, 2009, **19**, 6688.
11. (a) T. Hassheider, S. A. Benning, H.-S. Kitzerow, M.-F. Achard and H. Bock, *Angew. Chem., Int. Ed.*, 2001, **40**, 2060. (b) M. P. Aldred, A. E. A. Contoret, S. R. Farrar, S. M. Kelly, D. Mathieson, M. O'Neill, W. C. Tsoi and P. Vlachos, *Adv. Mater.*, 2005, **17**, 1368. (c) S. A. Benning, R. Oesterhaus and H.-S. Kitzerow, *Liq. Cryst.*, 2004, **31**, 201. (d) A. J. J. M. van Breemen, P. T. Herwig, C. H. T. Chlon, J. Sweelssen, H. F. M. Schoo, S. Setayesh, W. M. Hardeman, C. A. Martin, D. M. de Leeuw, J. J. P. Valetton, C. W. M. Bastiaansen, D. J. Broer, A. R. Popa-Merticaru and S. C. J. Meskers, *J. Am. Chem. Soc.*, 2006, **128**, 2336. (e) M. Funahashi, F. Zhang and N. Tamaoki, *Adv. Mater.*, 2007, **19**, 353. (f) W. Pisula, A. Menon, M. Stepputat, I. Lieberwirth, U. Kolb, A. Tracz, H. Siringhaus, T. Pakula and K. Müllen, *Adv. Mater.*, 2005, **17**, 684. (g) T. Hori, Y. Miyake, N. Yamasaki, H. Yoshida, A. Fujii, Y. Shimizu and M. Ozaki, *Appl. Phys. Express*, 2010, **3**, 101602. (h) W. Shin, T. Yasuda, G. Watanabe, Y. S. Yang and C. Adachi, *Chem. Mater.*, 2013, **25**, 2549.
12. Y. Funatsu, A. Sonoda and M. Funahashi, *J. Mater. Chem. C*, 2015, **3**, 1982.
13. (a) Y. Zhang, X. Guo, B. Guo, W. Su, M. Zhang and Y. Li, *Adv. Funct. Mater.*, 2017, **27**, 1603892. (b) J. Zhang, B. Zhao, Y. Mi, H. Liu, Z. Guo, G. Bie, W. Wei, C. Gao and Z. An, *Dyes Pigm.*, 2017, **140**, 261.
14. (a) V. M. Fridkin and B. N. Popov, *Phys. Status Solidi A*, 1978, **46**, 729. (b) A. M. Glass, D. von der Linde and T. J. Negran, *Appl. Phys. Lett.*, 1974, **25**, 233. (c) T. Choi, S. Lee, Y. J. Choi, V. Kiryukhin and S.-W. Cheong, *Science*, 2009, **324**, 63. (d) A. Bhatnagar, A. R. Chaudhuri, Y. H. Kim, D. Hesse and M. Alexe, *Nat. Commun.*, 2013, **4**, 2835.
15. Y. Yuan, Z. Xiao, B. Yang and J. Huang, *J. Mater. Chem. A.*, 2014, **2**, 6027.
16. (a) T. Furukawa, M. Date, E. Fukada, Y. Tajitsu and A. Chiba, *Jpn. J. Appl. Phys.*, 1980, **19**, L109; (b) T. Furukawa, *Phase Transitions*, 1989, **18**, 143.
17. (a) A. Sugita, K. Suzuki and S. Tasaka, *Phys. Rev. B*, 2004, **69**, 212201; (b) H. Sasabe, T. Nakayama, K. Kumazawa, S. Miyata and E. Fukuda, *Polym. J.*, 1981, **13**, 967.
18. A. Kanazawa, T. Ikeda and J. Abe, *Angew. Chem., Int. Ed.*, 2000, **39**, 612.
19. (a) S. Murakami, H. Naito, M. Okuda and A. Sugimura, *J. Appl. Phys.*, 1995, **78**, 4533. (b) A. Sawada and S. Naemura, *Jpn. J. Appl. Phys.*, 2002, **41**, L195.
20. (a) M. Era, X. Zhang, T. Ishi-i, T. Thiemann, K. Kubo, A. Mori and S. Manaka, *Jpn. J. Appl. Phys.*, 2016, **55**, 03DE02. (b) K. Tokunaga, H. Iino and J. Hanna, *Mol. Cryst. Liq. Cryst.*, 2009, **510**, 241.

21. K. Kogo, H. Maeda, H. Kato, M. Funahashi and J. Hanna, *Appl. Phys. Lett.*, 1999, **75**, 3348.
22. (a) M. Funahashi and J. Hanna, *Appl. Phys. Lett.*, 2000, **76**, 2574. (b) M. Funahashi and N. Tamaoki, *Chem. Mater.*, 2007, **19**, 608.
23. (a) H. Bäessler, *Phys. Stat. Solidi*, 1993, **b 175**, 15. (b) M. Funahashi, T. Ishii and A. Sonoda, *ChemPhysChem*, 2013, **14**, 2750. (c) M. Funahashi, F. Zhang, N. Tamaoki and J. Hanna, *ChemPhysChem*, 2008, **9**, 1465.
24. (a) G. A. Sewvandi, D. Hu, C. Chen, H. Ma, T. Kusunose, Y. Tanaka, S. Nakanishi and Q. Feng, *Phys. Rev. Appl.*, 2016, **6**, 024007. (b) G. A. Sewvandi, K. Kodaera, H. Ma, S. Nakanishi and Q. Feng, *Sci. Rep.*, 2016, **6**, 30680.
25. (a) T. Sasaki, *Chem. Rec.*, 2006, **6**, 43. (b) H. Anetai, Y. Wada, T. Takeda, N. Hoshino, S. Yamamoto, M. Mitsuishi, T. Takenobu and T. Akutagawa, *J. Phys. Chem. Lett.*, 2015, **6**, 1813.

Chapter 4.

Anomalous Photovoltaic Effect in Chiral Ordered Smectic Phases of Phenylterthiophene Derivatives without Junctions: Immobilization of the Polarized Structure by Surface Stabilization

Abstract: The programmed liquid-crystalline (LC) system provides the realization strategy for multi-functional soft materials. Our interest is a development of the design strategy for LC semiconductors with some *exotic* functions. Recently, we have developed a π -conjugated ferroelectric liquid-crystalline (FLC) system exhibiting an anomalous photovoltaic (APV) effect. The mechanism of the APV phenomenon in FLC phases was clarified in the previous study. However, the APV efficiency was low because of the polarization behaviors and low carrier mobilities in FLC phases. To improve the APV performance, the stabilization of the polarized state based on the surface-stabilized FLC (SSFLC) system and the formation of the polarized ordered smectic structures were investigated.

The wide-gap and narrow-gap LC cells filled with chiral π -conjugated FLC compound (*S*)-1 were prepared. The SmC*-SmG* phase transition under the external bias promoted to the formation of polarized SmG* states. The APV response was observed in the SmG* phase as well as the SmC* phase. The response polarity was opposite to the poling external bias. After the formation of each SmG* state, the APV response was retained even under the reversed bias. However, the polarization relaxation behaviors made the APV response decayed in the wide-gap cell, because the polarized state was not thermodynamically stable state after removing the external bias. On the other hands, bistable polarized SmC* state was obtained in the narrow-gap LC cell. The polarized optical textures of the narrow-gap cell in the SmC* phase without external bias displayed different textures from those of the wide-gap cell. The polarization suppression behaviors in the narrow-gap cell seemed to be occurred by the different mechanism from the wide-gap one. The APV photocurrent in “the third state” could be enhanced in the initial stage. The APV responses in the SmG* phase showed the influence of the surface-stabilization effect clearly. The enhancement of the APV photocurrent was observed in the suitable configuration. This study will provide the improve strategy of the APV effect in π -conjugated FLC system.

4.1. Introduction

As described in chapters 2 and 3, π -conjugated FLC materials coupling with ferroelectric nature and electronic charge carrier transport properties have been developed.¹ Furthermore,

unconventional bulk photovoltaic effect originated from molecular chirality have been found in the π -conjugated FLC materials for the first time.^{1c} This photovoltaic effect is attributed to the photo-carrier generation and transport by the internal electric field produced by spontaneous polarization but not by p-n junction. However, the efficiency of the photovoltaic effect remains very low owing to the low carrier mobilities and polarization relaxation behaviors in the FLC phase.¹

In a polar environment with deviation of the electron density, internal electric field is generated and produces potential gradient. The potential gradient is essential to the charge separation. In conventional photovoltaic devices, built-in potential is produced by p-n junction near the interface. When uniaxial polarization is formed through long distance, the large internal field is generated in the bulk. Ferroelectric polarization can produce the large internal electric field in the bulk. The polarization behaviours depend on the stability of polar structure resulting from symmetry breaking. In the SmC*-based FLC system, the polarization state can be stabilized by surface-stabilization effect.² The surface-stabilized ferroelectric liquid crystal (SSFLC) geometry is obtained when the film thickness is smaller than the SmC* helical pitch. In the SSFLC system, the gain of the elastic free energy derived from the formation of the helical structure is impaired. As the helical structure becomes unstable, two polarization states in which the directions are opposite to each other are relatively stabilized (Figure 4-1).³

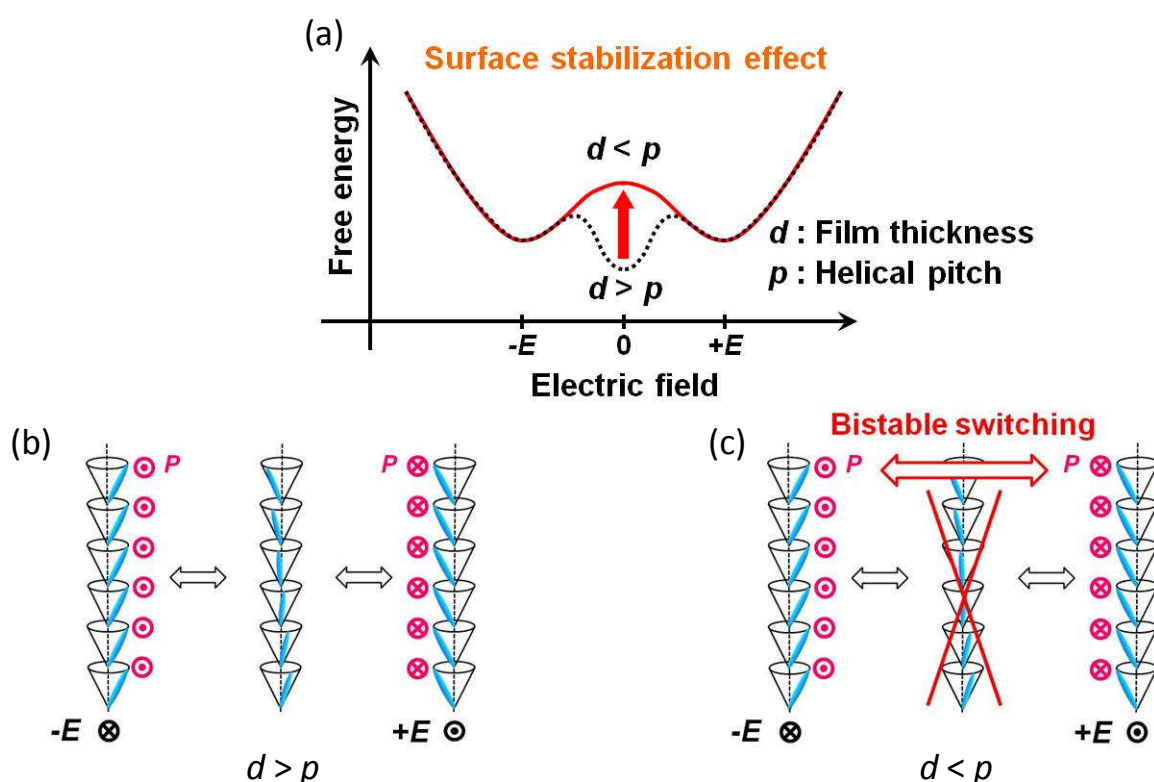


Figure 4-1. (a) Energy diagram of the FLC phase in the wide-gap and narrow-gap cells. Schematic illustrations of SmC* structures under the application of electric field in (b) wide-gap and (c) narrow-gap cells.

From the viewpoint of carrier transport property, defect-free dense packing structure is favourable. In fact, carrier mobilities in highly ordered smectic phase are one or two orders of magnitude larger than those in smectic C phase.⁴ If the polarization state can be fixed through the smectic-smectic phase transition, the balance between charge generation by the internal electric field and charge transport can be struck. The well-defined self-assembled structures assisted with external electric field can be formed in the electric-field-responsive molecular system. The control of molecular orientation by the electric field is realized in LC and the physical gel systems.⁵ The structural fixation through the FLC-ordered LC phase transition under the application of DC external bias provides one approach for obtaining the highly ordered LC structures with large internal field.

In this study, we investigated to improve the performance of bulk photovoltaic effect in the π -conjugated FLC material by combining high carrier mobilities and large polarization. As a realization strategy, we consider that surface-stabilization of the FLC system and the fixation of the polarized structure through the FLC—chiral ordered smectic phase transition under the application of electric field. Here, we will compare and discuss the bulk photovoltaic response of a chiral phenylterthiophene derivative (*S*)-**1** (Figure 4-2) for conventional cell and surface-stabilized cell in the FLC phase as well as ordered smectic phase.

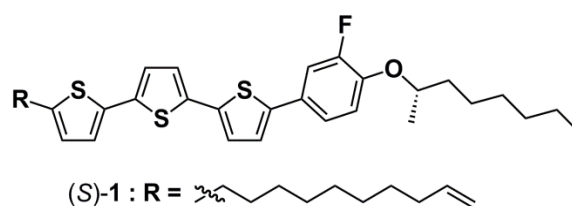


Figure 4-2. Chemical structure of the chiral fluorophenyl terthiophene derivative (*S*)-**1**.

4.2. Experimental Section

4.2.1. General Methods

All ¹H- and ¹³C-NMR spectra were performed in CDCl₃ solution on a Varian UNITY INOVA400NB spectrometer. Matrix-assisted laser desorption ionization time-of-flight (MALDI-TOF) mass spectra were performed using a Bruker Daltonics ultrafleXtreme™. FT-IR measurements were carried out on a JASCO FT/IR-660 Plus spectrometer. For electrical measurements, LC cells consisting of two ITO-coated glass plates were used. Narrow-gap cells (thickness < 1 μm) were purchased from EHC company.

4.2.2. Materials

Used compound (*S*)-**1** was synthesized as described in chapter 3.

5-(9-Decenyl)-5''-[4-*S*]-2-octyloxy-3-fluorophenyl]-2,2':5',2''-terthiophene (*S*-1)

¹H-NMR (400 MHz, CDCl₃): δ = 7.31 (dd, 1H, *J* = 12.2, 2.2 Hz), 7.26 (ddd, 1H, *J* = 8.4, 2.2, 1.2 Hz), 7.10 (d, 1H, *J* = 3.6 Hz), 7.09 (d, 1H, *J* = 3.6 Hz), 7.06 (d, 1H, *J* = 3.6 Hz), 7.00 (d, 1H, *J* = 3.6 Hz), 6.98 (d, 1H, *J* = 3.6 Hz), 6.96 (t, 1H, *J* = 8.8 Hz), 6.68 (d, 1H, *J* = 3.6 Hz), 5.81 (ddt, 1H, *J* = 17.2, 10.4, 6.8 Hz), 5.00 (m, 1H), 4.93 (ddt, 1H, *J* = 10.4, 2.4, 1.2 Hz), 4.37 (sextet, 1H, *J* = 6.0 Hz), 2.79 (t, 2H, *J* = 7.6 Hz), 2.04 (quartet, 2H, *J* = 7.2 Hz), 1.84-1.74 (m, 1H), 1.71 (quintet, 2H, *J* = 7.6 Hz), 1.65-1.55 (m, 1H), 1.51-1.25 (m, 18H), 1.33 (d, 3H, *J* = 6.0 Hz), 0.89 (t, 3H, *J* = 6.8 Hz); ¹³C-NMR (100 MHz, CDCl₃): δ = 145.8, 141.9, 139.4, 137.0, 136.4, 135.5, 134.6, 127.8, 125.0, 124.5, 124.3, 123.7, 123.5, 121.6, 121.5, 117.8, 114.3, 113.9, 113.7, 76.7, 36.6, 33.9, 31.9, 31.7, 30.3, 29.5, 29.4, 29.4, 29.2, 29.2, 29.1, 25.6, 22.8, 20.0, 14.2; FT-IR (ATR): ν = 3073, 2918, 2849, 1641, 1616, 1576, 1546, 1525, 1505, 1464, 1447, 1427, 1380, 1304, 1267, 1235, 1210, 1124, 1059, 996, 942, 912, 894, 856, 810, 799, 790, 726, 662, 631, 600, 550, 473, 447 cm⁻¹; elemental analysis calcd (%) for C₃₆H₄₅FOS₃: C 71.01, H 7.45, F 3.12, O 2.63, S 15.80; found: C 70.9, H 7.5; exact mass: 608.26; molecular weight: 608.94; *m/z*: 608.27, 609.27, 610.30, 611.30, 612.31, 613.31.

4.2.3. Evaluation of carrier transport properties

Hole mobilities were measured by the time-of-flight (TOF) method. A liquid crystal cell with 25-μm gap was fabricated by combining two ITO-glass plates. An empty cell was placed on a hot stage and heated above the clearing temperature of the LC compound. The LC sample was melted and capillary-filled into the cell. After the sample temperature was controlled on a hot stage, DC voltage was applied using an electrometer (ADC R8252). A laser pulse was then applied to the LC cell. The excitation source was the third harmonic generation of a Nd:YAG laser (Continuum MiniLite II, wavelength = 356 nm, pulse duration = 2 ns) and the photo-induced displacement currents were recorded using a digital oscilloscope (Tektronix TDS 3044B) through a serial resistor.

The charge carriers photogenerated by pulse laser illumination drifted across the sample under the application of the DC electric field, inducing a transient photocurrent as voltage drop across the serial resistor connected to the digital oscilloscope. When the photogenerated charge carriers arrived at the counter electrode, the transient photocurrent dropped to zero. The transit time of the photogenerated charge carriers could be determined from the kink point in the transient photocurrent curve.

4.2.4. Evaluation of spontaneous polarization

Dielectric properties were evaluated by the Sawyer-Tower method using triangular-wave bias (± 25 kV cm⁻¹, 100 Hz). Triangular-wave bias generated by a function generator (NF WF1973) was applied to the LC sample cells. The induced currents were recorded with a digital oscilloscope (Tektronics TDS 3044B) through a serial resistor. In this series of measurements, wide-gap (2 μm gap)

and narrow-gap (0.61 μm gap) sample cells supplied by EHC Co. were used. The sample cells were prepared similar to those for the TOF method.

4.2.5. Evaluation of the APV effect in the SmC* phase

The APV effect was confirmed by measurement of the steady-state photocurrent response under zero bias. The measurement conditions and sequence are schematically described in Chapter 3 (Figure 3-3). The SmC* state—after cooling from its isotropic liquid phase without DC bias—is defined as the “initial state” (Figure 3-3a, state (iii)). In this state, no internal field was formed. When the front electrode was biased positively in the SmC* phase, spontaneous polarization was generated in the reverse direction relative to the external DC bias (Figure 3-3a, state (iv)). Backward internal field remained after removal of the DC external bias, and maintained the polarized state as the “second state” (Figure 3-3a, state (v)). UV illumination on the front electrode could produce photocurrent with polarity opposite to that of the DC bias applied prior to illumination. An opposite internal field, in contrast, could be induced in the SmC* phase when the front electrode was biased negatively prior to UV illumination (Figure 3-3a, state (vi)). After removing the external DC bias, the forward internal field remained in the generated polarized state as the “third state” (Figure 3-3a, state (vii)). In the third state, photoexcitation could produce a photocurrent with polarity opposite to that in the “second state”. In this series of experiments, irradiation was started just after removal of DC voltage (Figure 3-3b). The light was illuminated for 4 seconds in each excitation, using a shutter. The light intensity at the LC sample cell position was about 6 mW cm^{-2} (290–390 nm light) as measured with a CUSTOM UV light meter UV-340C.

4.2.6. Evaluation of the APV effect in the SmG* phase

APV response in the SmG* phase was confirmed by the measurement of steady state photocurrent response under zero bias (Figure 4-3). The generated state—after cooling down from the SmC* to the SmG* phase, without the external bias—is defined as the standard SmG* (std-SmG*) state with no internal field (Figure 4-3, state (viii)). Polarized SmG* states were formed after cooling from the SmC* phase in the presence of external bias. The negatively polarized SmG* (np-SmG*) state was obtained when cooled from the SmC* phase with the front electrode biased positively (Figure 4-3, state (ix)). The positively polarized SmG* (pp-SmG*) state was formed when cooled from the SmC* phase under a reversed external field (Figure 4-3, state (x)). The measurement sequence followed to previous SmC* experimental system. The “initial state” in each SmG* state refers to the condition where no external field was applied. The “second state” in each SmG* state was obtained after removing the forward external bias (the front electrode was biased negatively for several minutes). The “third state” in each SmG* state corresponds to the condition after removing the backward external bias (the front electrode was biased positively for several minutes). In this

series of experiments, irradiation was started just after setting the conditions. The light was pulse illuminated for 4 s using a shutter.

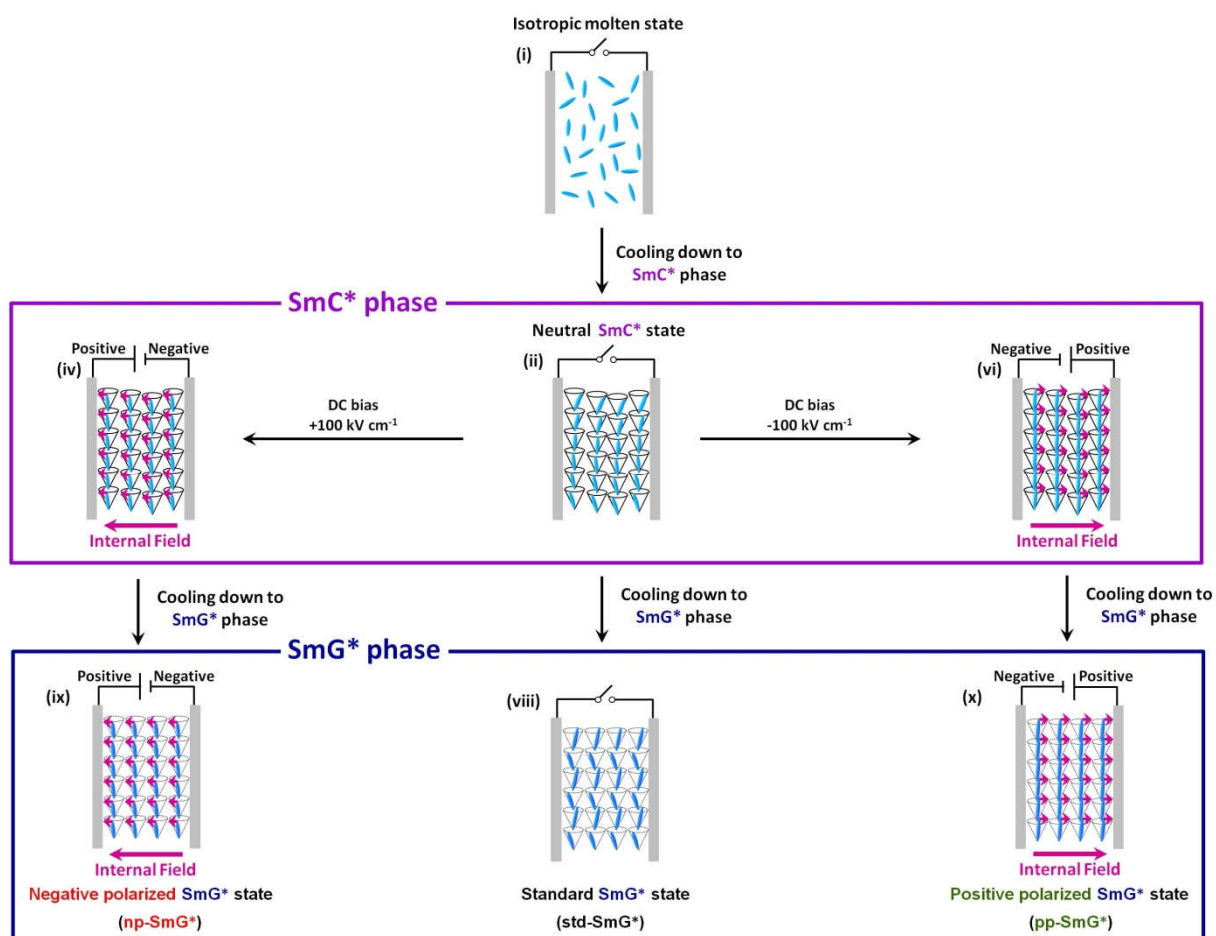


Figure 4-3. Schematics of molecular orientations and polarization states for steady-state photocurrent measurements under zero bias in each SmG* state.

4.3. Results and discussion

4.3.1. Mesomorphic properties and structures

The thermotropic mesomorphic property of chiral fluorophenylterthiophene derivative (*S*)-**1** is summarized in Table 4-1. The details of the mesomorphic properties of (*S*)-**1** have been discussed in the previous section (Chapter 3.3.1.).

Table 4-1. Phase transition behaviors of a chiral compound (*S*)-**1**.

| Compound | Phase-transition temperature / °C (Enthalpy / kJ mol ⁻¹) | | | | |
|----------|---|------|-----------|------|-----------|
| | (<i>S</i>)- 1 | SmG* | 125 (9.7) | SmC* | 140 (9.1) |

4.3.2. Carrier transport properties

4.3.2.1. In the SmC* phase

The carrier mobilities in the SmC* phase of (S)-1 were determined by TOF technique using 25- μm -gap cells. In the SmC* phase of (S)-1 at 130 °C, the hole mobility was determined to be $2.7 \times 10^{-4} \text{ cm}^2 \text{ V}^{-1} \text{ s}^{-1}$. The temperature- and field-independent hole mobility was observed in the SmC* phase. The details of carrier transport properties in the SmC* phase of (S)-1 have been discussed in the previous section (Chapter 3.3.2.).

4.3.2.2. In the SmG* phase

The carrier mobilities in the SmG* phase of (S)-1 were determined by a TOF technique using the same LC cells. Figure 4-4 shows typical transient photocurrent curves for holes in the ordered smectic phase.

In the SmG* phase of (S)-1 at 100 °C, the hole mobility estimated from the transit time was $2.3 \times 10^{-3} \text{ cm}^2 \text{ V}^{-1} \text{ s}^{-1}$. This value was one order of magnitude larger than that in the SmC* phase. In the SmG* phase, temperature- and field-dependent mobilities were observed. Thermal activation process was the predominant factor in hole hopping in the SmG* phase. On cooling, the close molecular packing in the SmG* structure enhanced charge carrier transport around the SmC*-SmG* phase transition temperature. When the temperature decreased to room temperature, lattice contraction of SmG* structures caused the formation of structural defects. The increase in defect density inhibited efficient carrier transport and resulted in positive temperature- and field-dependences of mobility.

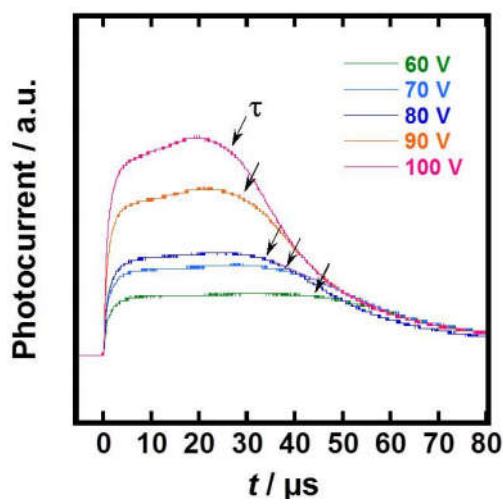


Figure 4-4. Transient photocurrent curves for positive charges in the SmG* phase of (S)-1 at 100 °C. The measurements were performed using ITO/ ITO sandwich cells (gap: 25 μm). The arrows indicate kink points corresponding to the transit times.

4.3.3. Ferroelectric properties

Spontaneous polarizations in the SmC* phase of chiral compound (S)-1 were evaluated using wide-gap (gap: 2.0 μm) and narrow-gap (gap: 0.61 μm) LC cells. The dielectric properties in the SmC* phase displayed ferroelectric hysteresis behaviors in both cells (Figure 4-5). Extrapolation of these hysteresis loops gave the values of spontaneous polarization (P). The estimated values are summarized in Table 4-2. The spontaneous polarization values were almost identical in these two cells with different gaps, indicating that the interaction on the electrode surface did not inhibit polarization inversion. No hysteresis behaviors were observed in the SmG* phase, as shown in Figure S-2. Molecular dipoles were immobilized because of the high viscosity of the SmG* phase, resulting in their dielectric behavior in the SmG* phase in the frequency range.

Table 4-2. The value of the spontaneous polarization in the SmC* phase of (S)-1 at 127 °C.

| Sample | Cell gap / μm | P / nC cm^{-2} |
|--------|--------------------------|---------------------------|
| (S)-1 | 0.61 | 68 |
| (S)-1 | 2.0 | 61 |

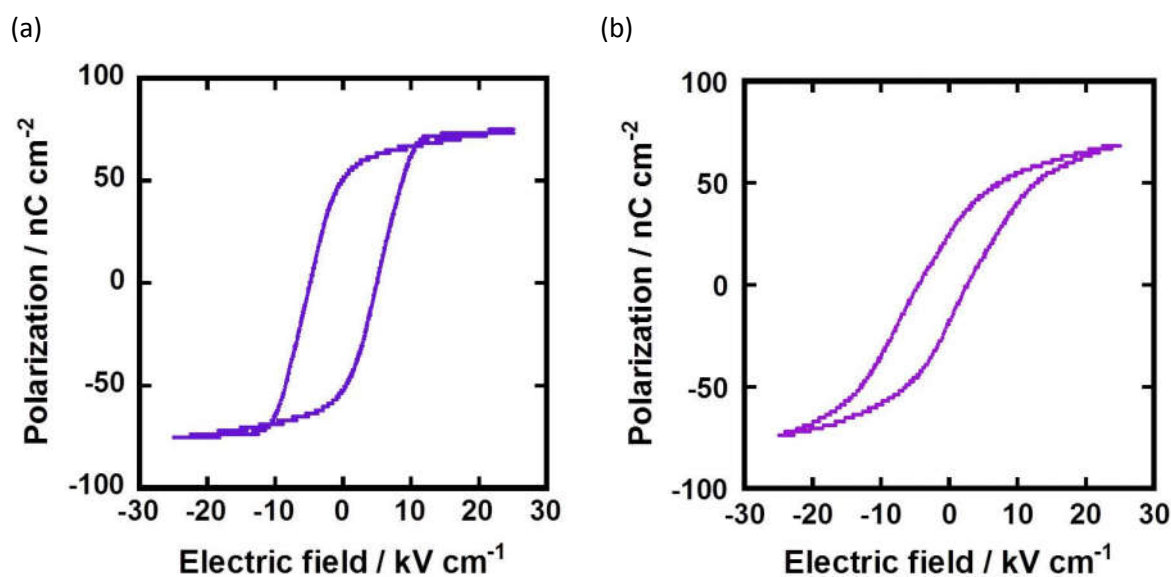


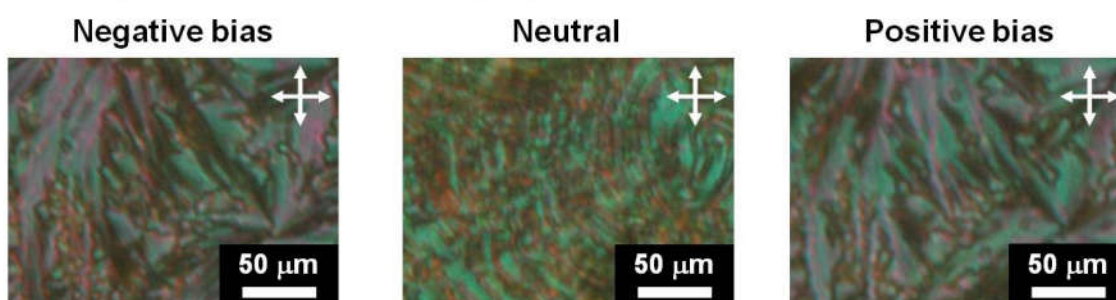
Figure 4-5. Dielectric hysteresis loops in the SmC* phase of (S)-1 for (a) the wide-gap LC cell (gap: 2.0 μm) and (b) the narrow-gap LC cell (gap: 0.61 μm).

4.3.4. POM study under bias

To obtain surface-stabilized π -conjugated ferroelectric LC cells, an empty narrow-gap ($< 1 \mu\text{m}$) cell was prepared. In LC cells with 2.0- μm gaps, a color tone change—equally-spaced by disclination lines—was observed and wedge-shaped defect lines did not appear in the fan-shaped domains

(Figure 4-6, upper, neutral). This indicated that the helical structure was formed without macroscopic polarization. For the capillary-filled narrow-gap cell of (S)-1, typical broken-fan like optical textures were observed in the POM when the narrow-gap sample cell was cooled from the isotropic temperature to the SmC* temperature without external bias (Figure 4-6, bottom, neutral). Wedge-shaped defect lines were found in some of the broken-fan like domains (area surrounded by dotted lines in Figure 4-6, bottom neutral). In the neutral state, negatively and positively polarized domains could coexist. The wedge-shaped defect lines (Figure 4-6, bottom, neutral) could display the boundaries of the two oppositely polarized domains. It was considered that the SmC* helical structures were destabilized in the neutral state of the narrow-gap cell. Clear broken-fan like domains were observed in the polarized states under the application of a DC electric field (Figure 4-6, upper and bottom, negative/positive bias) in both wide-gap and narrow-gap cells. After removing the external bias, disclination lines were regenerated in the SmC* phase of the 2.0 μm gap cell. The wedge-shaped defect lines reorganized to fan-shaped domains in the narrow-gap cell. Bistable switching in the narrow-gap cell was confirmed by the change of polarity in DC bias; the bright and dark domains were inverted, as shown in the dotted areas in Figure 4-6 (bottom right and left).

Wide-gap cell (reference, gap : 2 μm)



Narrow-gap cell (gap : 0.61 μm)

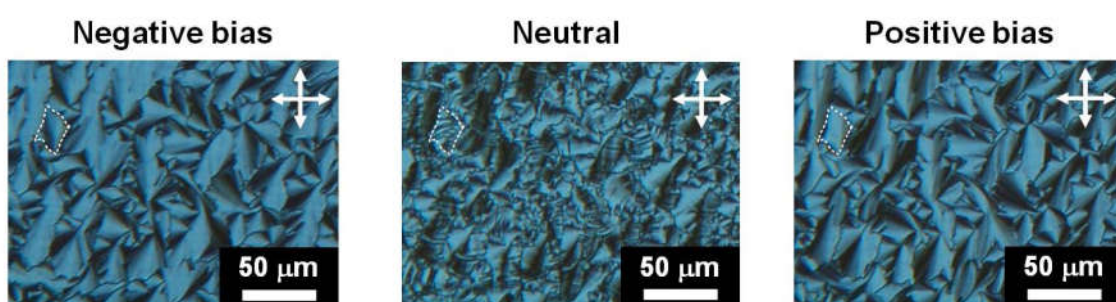


Figure 4-6. POM images of SmC* phases in (a) 2 μm -gap cell and (b) narrow-gap cell. The area surrounded by the white dotted line indicates a domain in which wedge-shaped defect lines were formed.

4.3.5. APV response of the wide-gap (gap: 2.0 μm) cell

4.3.5.1. In the SmC* phase

The initial evaluation of APV response was carried out in the SmC* phase using 2.0- μm gap ITO/ITO sandwich LC cells. Figure 4-7 shows the steady state photocurrent response curves under zero bias in the SmC* phase of compound (S)-1. In the “initial state”, a weak photocurrent response ($\sim 0.12 \mu\text{A cm}^{-2}$) was observed (Figure 4-7, black line). In the “second state”, the polarity of the photocurrent response was reversed due to the internal field (Figure 4-7, red line) generated. In the “third state”, a strong photocurrent response ($> 0.6 \mu\text{A cm}^{-2}$) was observed under an opposite internal field (Figure 4-7, green line). The polarity of the photocurrent was opposite to the polarity of the DC bias prior to UV light illumination. Compound (S)-1, thus exhibited the APV effect in the ferroelectric SmC* phase. Photocurrent response at zero external bias in the third state was larger than that in the second state. As mentioned in the previous reports,^{1a} the penetration depth of the excitation UV light was less than 100 nm due to strong absorption of phenylterthiophene (S)-1 in the near UV area. In this π -conjugated FLC system, the generation and transport efficiencies of holes were superior to those of electrons. Strong response based on hole transport was observed in the third state since the illuminated (front) electrode was positively charged.

In the SmC* phase of the wide-gap cell, decay of the APV response was observed. This response decay originated from dielectric relaxation behavior in the SmC* phase. When the LC sample thickness was larger than the SmC* helical pitch, the helical structure without macroscopic polarization was the most thermodynamically stable. Thermal relaxation behavior to form the helical structure, thus, led to decay of the APV response.

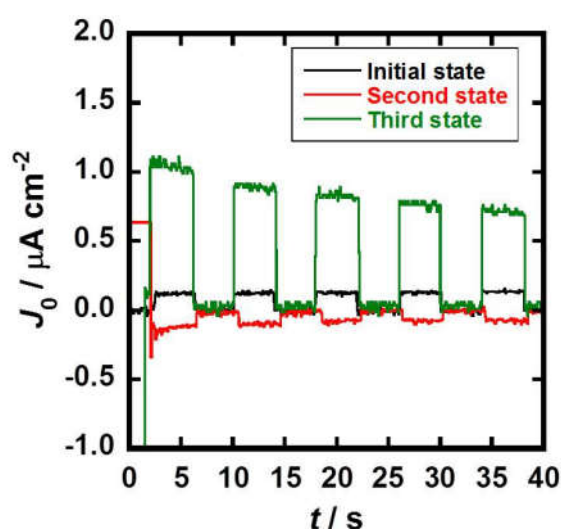


Figure 4-7. Steady-state photocurrent response profiles of the SmC* phases of (S)-1 at 127 °C in the wide-gap LC cell (gap: 2.0 μm). The measurements were performed using ITO/ ITO sandwich cells.

The J_0 is determined as APV photocurrent density at zero external bias. The decay of APV photocurrent for the “third state” in the SmC* phase of the wide-gap (gap: 2.0 μm) cell was approximated to curves shown in Equation 4-1.

$$|J_0(t)| = |J_0'| + k \cdot \exp(-t/\tau) \quad [\text{Equation 4-1}]$$

The fitting curve for the decay in the “third state” can be described as following equation.

$$|J_0(t)_{\text{third state, 2 } \mu\text{m}}| = 0.65 + 0.43 \cdot \exp(-0.052 \cdot t) \quad [\text{Equation 4-2}]$$

The inverse of decay time constant was obtained as $\tau^{-1} = 0.052 \text{ s}^{-1}$ from this fitting curve. The decay constant of the photocurrent (τ) was 19 s, assuming exponential decay of the photocurrent.

4.3.5.2. In the SmG* phase

The measurement of steady state photocurrent response was carried out for the same LC cells (2.0- μm gap) in the SmG* phase. The SmG* phase being more ordered and dense than a SmC* phase, carrier mobilities in the former were larger than those in the latter. As the photocurrent is proportional to the carrier mobility, the formation of polarized ordered smectic phase enhanced the APV response. The SmG* phase was very viscous and the orientation of molecular dipoles could be immobilized in the SmG* phase.

In the std-SmG* state of (S)-1 at the “initial condition”, photocurrent response was slightly enhanced relative to that in the SmC* phase at the “initial state” (Figure 4-8a, black line). The increase in carrier mobilities in the SmG* phase contributed to enhancing the APV response. In the std-SmG* state at the “second condition”, the polarization of the response was not reversed (Figure 4-8a, red line). In the std-SmG* state at the “third condition”, APV response did not change drastically (Figure 4-8a, green line). The densely packed structure of the SmG* phase inhibited polarity inversion and immobilized the molecular arrangement. In contrast to the result in the SmC* phase, APV response remained constant over the measurement time scale.

In the np-SmG* state, a weak polarity-reversed response was observed (Figure 4-8b). The response was comparable under every condition. This result indicated that the polarization was fixed against the external field in the SmG* phase and remained even under reversed bias. Inefficient generation and transport of electrons produced a small photocurrent response.

In the pp-SmG* state, enhancement of APV photocurrent was confirmed relative to the response in the std-SmG* phase (Figure 4-8c). The immobilized polarization state in the SmG* phase retained APV response due to efficient charge carrier generation and transport. The APV photocurrent was smaller than that in the initial stage of the third state in the SmC* phase, as shown in Figure 4-7. During the SmC*-SmG* phase transition, partial relaxation of polarity occurred due to molecular rearrangement. APV response, thus, could be maximized in the SmG* phase if the polarization in the SmC* phase was completely retained.

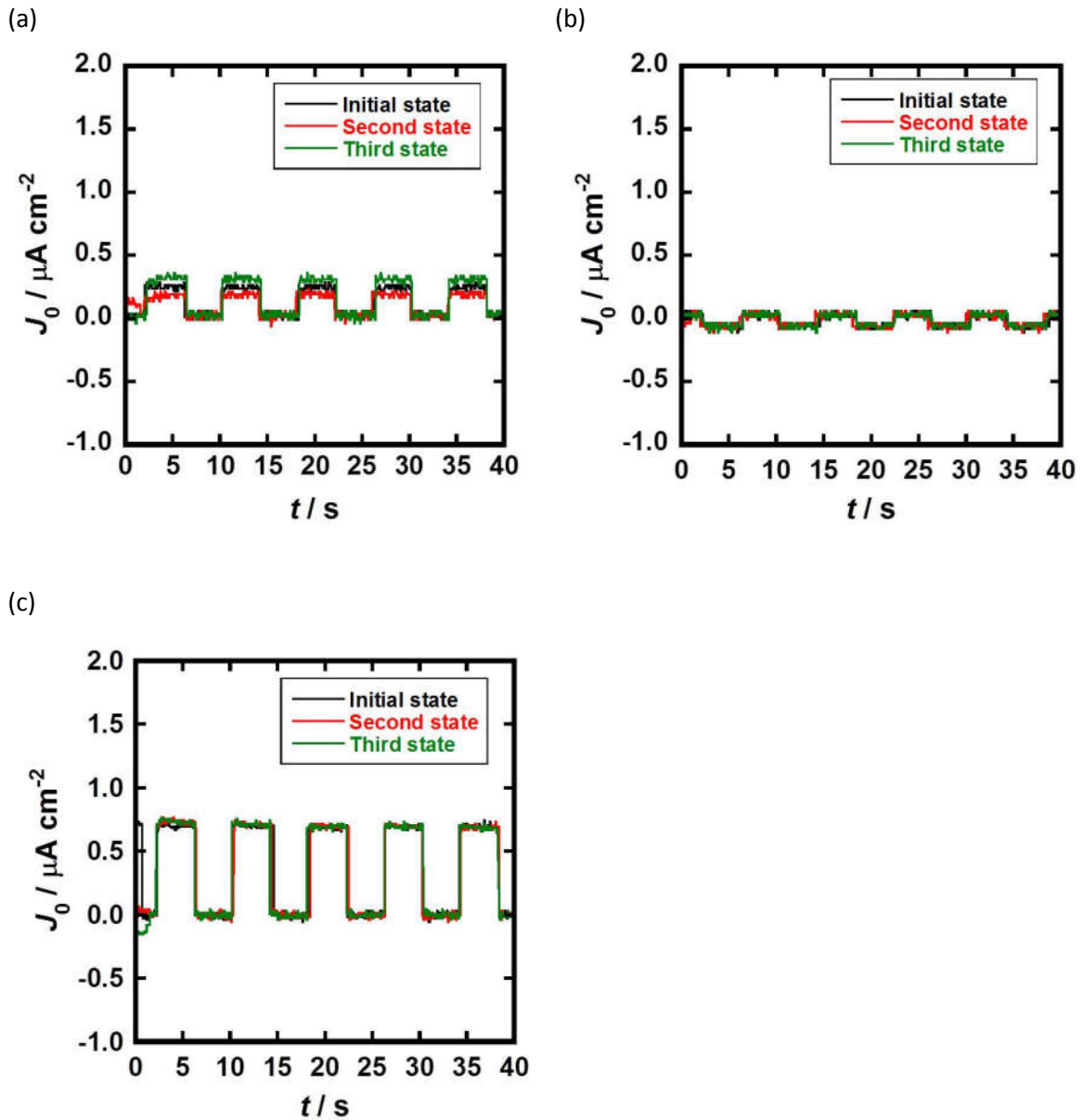


Figure 4-8. Steady-state photocurrent response profiles for the SmG* phase at 100 °C cooling from the SmC* phase in the wide-gap LC cell (gap: 2.0 μm). Prior to UV illumination, (a) no external electric field, (b) backward external field, and (c) forward external field were applied to the sample. The measurements were performed using ITO/ITO sandwich cells.

4.3.6. APV response of the narrow-gap (gap: 0.61 μm) cell: surface stabilization effect

4.3.6.1. In the SmC* phase

In the 2.0 μm gap LC cells, the polarization relaxed gradually. Relaxation behavior lowered the APV efficiency and deteriorated the long-term APV response. In the conventional FLC system, polarization state can be stabilized in an LC thin film state whose thickness is thinner than the helical pitch, called the “surface stabilization effect”. To inhibit the relaxation behavior, we considered the

application of the surface stabilization effect.

The APV response of the narrow-gap cell was evaluated by the measurement of steady state photocurrent response under zero bias. Weak photocurrent response ($\sim 0.2 \mu\text{A cm}^{-2}$) was observed in “the initial state” of the SmC* phase (Figure 4-9, black line) at 127 °C. In the second state, polarity of the photocurrent response was reversed due to the generation of a negatively polarized state (Figure 4-9, red line). In the initial stage of the measurement, APV photocurrent in “the second state” of the narrow-gap cell was enhanced to around 3 times than that in the 2.0 μm gap cell. This enhancement originated from effective charge generation and electron transport. In “the third state”, clear photocurrent response ($> 0.6 \mu\text{A cm}^{-2}$) was observed under an opposite internal field (Figure 4-9, green line). The APV photocurrent in “the third state” increased in the initial stage. The APV responses in the second and the third states were reduced. In the POM study, regeneration of wedge-shaped defect lines in the fan-shaped domains was observed just after removal of the external bias. Defect regeneration indicated that the polarization of domains was partially inverted to decrease the internal electric field. In spite of the narrow gap of the sample, the surface-stabilization effect was insufficient to immobilize macroscopic polarization because the gap of the sample was comparable to the helical pitch.

For the narrow-gap cell, the decay behaviors in the “second” and “third states” were also approximated to curves shown in former Equation 4-1. The fitting curve for the decays in the “second” and “third states” can be described as following equations.

$$|J_0(t)_{\text{second state, } 0.61 \mu\text{m}}| = 0.11 + 0.55 \cdot \exp(-0.10 \cdot t) \quad [\text{Equation 4-3}]$$

$$|J_0(t)_{\text{third state, } 0.61 \mu\text{m}}| = 0.70 + 0.57 \cdot \exp(-0.11 \cdot t) \quad [\text{Equation 4-4}]$$

The inverse of decay time constants for “second” and “third states” were obtained as $\tau^{-1} = 0.10$ and 0.11 s^{-1} , respectively. The decay constants of the photocurrents of the “second” and “third states” were 10 s and 9 s, respectively, assuming single exponential decay.

This indicated that APV photocurrent decay was caused by the same mechanism in all polarized state of the narrow-gap cell. Time constants for the narrow-gap cell were clearly different from those for the wide-gap (2.0 μm gap) cell. It was confirmed by the POM study of each LC cell that each APV response relaxation behavior resulted from a different mechanism. The different origins of the polarization relaxation behaviors were reflected in the different time constants. The small activation energy of the polarization relaxation behavior led to short decay time constant in the narrow-gap cell.

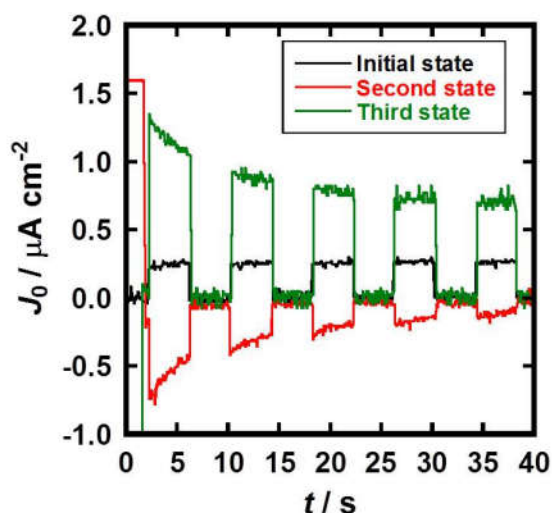


Figure 4-9. Steady-state photocurrent response profiles for the SmC* phase at 127 °C in the narrow-gap LC cell. The measurements were performed using ITO/ITO sandwich cells.

4.3.6.2. In the SmG* phase

The influence of surface stabilization effect in the narrow-gap cell was confirmed by measurement at 100 °C (SmG* phase of (S)-1). In the std-SmG* state of the sample cell at “initial state”, a comparable APV photocurrent response was observed (Figure 4-10, black line). The strongest APV photocurrent response ($>1.5 \mu\text{A cm}^{-2}$), however, was confirmed in the pp-SmG* state of the narrow-gap cell (Figure 4-10, green line). The APV photocurrent in the pp-SmG* state of the 0.61- μm -gap cell was twice that in the pp-SmG* state of the 2.0- μm -gap cell (Figure 4-8). This was larger than the maximum APV photocurrent in the third state of the 2.0- μm -gap SmC* sample, as shown in Figure 4-7. The APV current was constant. This enhancement resulted from surface stabilization, higher carrier mobility in the SmG* phase than that in the SmC* phase, and immobilization of macroscopic polarization in the viscous ordered smectic phase.

No enhancement of APV response was observed for the np-SmG* state in the narrow-gap cell. Majority carriers of the APV effect in the np-SmG* state were electrons, although the phenylterthiophene system was more suitable for hole transport than electron transport due to the existence of traps formed at domain boundaries and dissolved oxygen.

To confirm the formation of the polarized SmG* state, POM observation was conducted in each state. The polarized-SmG* state gave different optical textures in the crossed Nicole state than the std-SmG* state (Figure 4-11). The interval of disclination lines was not evenly spaced in the polarized-SmG* state and the patterns were not identical when compared to those in the std-SmG* state (Figure 4-11b, c). The disclination lines were derived from the lattice reduction of LC structures through the SmC*-SmG* phase transition. In the std-SmG* phase, two polarized SmG* states with opposite polarization directions were formed in the phase-transition process. In the polarized SmG* phases, domains polarized in one direction were predominant over the domains polarized in the

other direction and the residual polarization contributed to the generation of an internal electric field, which was essential to the APV phenomenon.

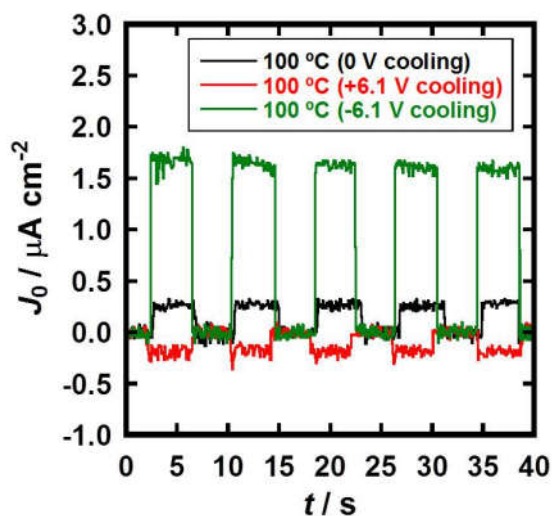


Figure 4-10. Steady-state photocurrent response profiles for the SmG* phase of (S)-1 at 100 °C in the narrow-gap LC cell. The measurements were performed using ITO/ ITO sandwich cells.

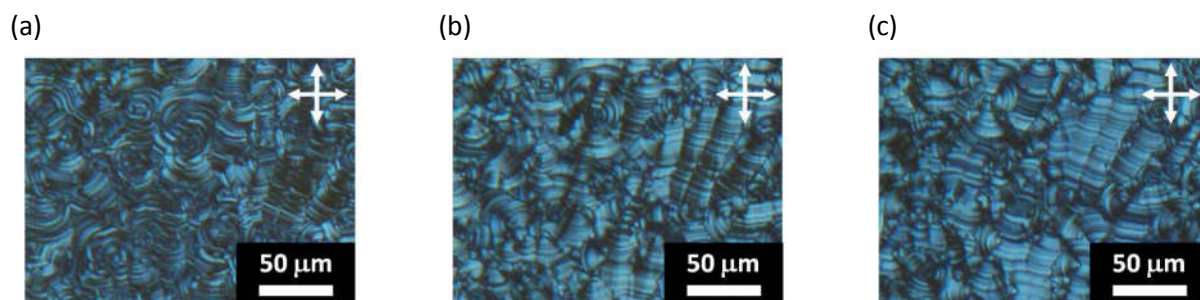


Figure 4-11. POM images of (S)-1 at 100 °C in narrow-gap LC cell: (a) std-SmG*, (b) np-SmG*, and (c) pp-SmG* states.

4.3.7. Current-voltage characteristics of the narrow-gap LC cell

Current-voltage characteristics under the dark and illuminated conditions exhibited different behaviors in each SmG* state (Figure 4-12). Current density-electric field (J - E) plots shifted in response to the polarization direction. The maximum open circuit voltage (electric field) and short circuit current under 6 mW cm^{-2} UV illumination condition reached -0.24 V (-3.9 kV cm^{-1}) and 2.25 μA cm^{-2} in the pp-SmG* state, respectively.

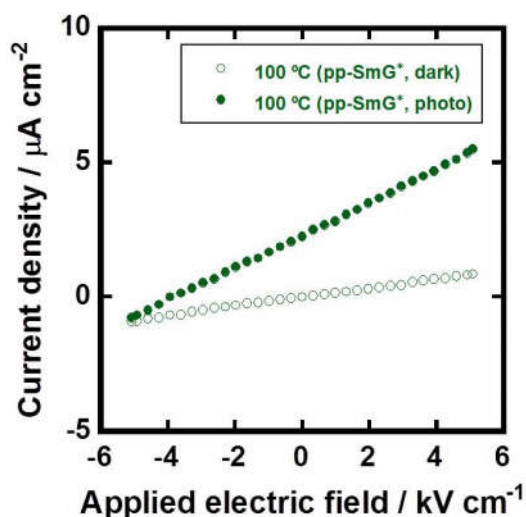


Figure 4-12. J - E curves of the narrow-gap LC cell in the mesophases of (S)-1 under the dark and illuminated conditions. UV intensity was 6 mW cm^{-2} .

4.4. Conclusion

Wide-gap and narrow-gap LC cells filled with chiral π -conjugated FLC compound (S)-1 were prepared. Through the SmC^* - SmG^* phase transition under external bias, the formation of polarized SmG^* states was achieved. APV response was observed in the SmG^* phase and the SmC^* phase. The polarity of the photocurrent response was opposite to that of the poling external bias. In the polarized SmG^* states, APV response remained even under reversed bias. Polarization relaxation behaviors made the APV response decay in the wide-gap cell. This was because the polarized state was not thermodynamically stable after removal of the external bias. Bistable polarized SmC^* state was obtained in the narrow-gap LC cell. Polarized optical textures of the narrow-gap cell in the SmC^* phase without external bias displayed different textures from those of the wide-gap cell. Polarization suppression behaviors in the narrow-gap cell seemed to be caused by a different mechanism than the wide-gap one. The APV photocurrent in “the third state” was enhanced in the initial stage. The APV responses in the SmG^* phase showed the influence of surface-stabilization effect clearly. Enhancement of the APV photocurrent was observed in the suitable configuration. This study will provide a strategy for improving the APV effect in π -conjugated FLC systems.

In the $2 \mu\text{m}$ -gap LC cells, the polarization relaxation should be gradually occurred. The relaxation behaviors lower the APV efficiency and impair the longer-term APV response. In the conventional FLC system, the polarization state can be stabilized in a LC thin film state whose thickness is thinner than the helical pitch, which is called “surface stabilization effect” (Figure 4-1). To inhibit the relaxation behaviours, we consider the application of this stabilization effect.

The APV response of the narrow-gap cell was also evaluated by the measurement of steady state photocurrent response under zero bias. On the measurement at $127 \text{ }^\circ\text{C}$ (SmC^* phase), the weak photocurrent response ($\sim 0.2 \mu\text{A cm}^{-2}$) was observed in “the initial state” (Figure 4-9, black line). In

the second state, the polarity of the photocurrent response was reversed due to the generation of the negatively polarized state (Figure 4-9, red line). In the initial stage of the measurement, the APV photocurrent in “the second state” of the narrow-gap cell was enhanced around 3 times larger than that of the 2 μm gap cell. This enhancement should be originated from the effective charge generation and electron transport. In “the third states”, the clear photocurrent response ($> 0.6 \mu\text{A cm}^{-2}$) was observed under the opposite internal field (Figure 4-9, green line). The APV photocurrent in “the third state” seemed to be also enhanced in the initial stage. However, the APV responses in the second and third states were decayed. In the POM study, the regeneration of the wedge-shaped defect lines in the fan-shaped domains was observed just after removing the external bias. The defect regeneration should show the reorganization of the reversed polarized domains and relax the electric polarization. Thus, the APV photocurrent was decayed in the “second” and “third” states. However, it could not be strongly assertive that the enhancement of the APV effect by the surface-stabilization effect.

4.5. Reference

1. (a) Y. Funatsu, A. Sonoda and M. Funahashi, *J. Mater. Chem. C*, 2015, **3**, 1982. (b) A. Seki and M. Funahashi, *Chem. Lett.*, 2016, **45**, 616. (c) A. Seki and M. Funahashi, *Phys. Chem. Chem. Phys.*, 2017, **19**, accepted.
2. N. A. Clark and S. T. Lagerwall, *Appl. Phys. Lett.*, 1980, **36**, 899.
3. J. P. F. Lagerwall and F. Giesselmann, *ChemPhysChem*, 2006, **7**, 20.
4. (a) M. Funahashi, *EKISHO*, 2006, **10**, 359. (b) M. Funahashi and J. Hanna, *Adv. Mater.*, 2005, **17**, 594. (c) M. Funahashi, T. Ishii and A. Sonoda, *ChemPhysChem*, 2013, **14**, 2750.
5. (a) Y. Shoji, M. Yoshio, T. Yasuda, M. Funahashi and T. Kato, *J. Mater. Chem.*, 2010, **20**, 173. (b) M. Yoshio, Y. Shoji, Y. Tochigi, Y. Nishikawa and T. Kato, *J. Am. Chem. Soc.*, 2009, **131**, 6763. (c) H. Shimura, M. Yoshio, A. Hamasaki, T. Mukai, H. Ohno and T. Kato, *Adv. Mater.*, 2009, **21**, 1591.

Chapter 5.

Conclusion of this thesis

5.1. Overall conclusion

In this doctoral study, the potential of π -conjugated FLC systems was investigated. The LC self-assembled material coupled with ferroelectrics and semiconductors exhibits *exotic* and attractive functions such as bulk photovoltaic effect. Through the study, it was found that bulk photovoltaic effect in π -conjugated FLC system is novel phenomenon based on the molecular chirality. The molecular chirality broken the structural symmetry and generated the polar environment. Although the ferroelectric polymer and their ferroelectric liquid crystal are common in that polarization are caused by uniaxial alignment of polar groups, molecular chirality is essential in the SmC*-based FLC system for inducing the gradient in the mean residence time of suitable positions. The polar environment produced by ferroelectric material induces the potential drops and internal electric field in the bulk. In the π -conjugated FLC system, the generated internal field promotes charge separation from excitons. The generation of excitons should be caused near the interface between front electrode and LC layer because the penetration depth of the excitation light is less than 100 nm due to strong absorption of phenylterthiophenes in the near UV area. The generated charge carriers can transport to electrodes by hopping between π -conjugated units. Thus, bulk photovoltaic effect is generated in the π -conjugated FLC materials. Although FLC phenylterthiophenes exhibit ambipolar carrier transport properties, hole transport is preferred over electron transport. Therefore, the characteristics of bulk photovoltaic effect depend on the polarity.

The internal electric field derived from spontaneous polarization is effective to charge separation as well as generation of some optical phenomena such as nonlinear optical phenomena. Moreover, the enhancement and amplification of some opto-physical processes can be expected by stabilization of polar nanostructures comprised of multifunctional self-assemblies. The investigated approaches in this study would provide several characters for each molecule in the hierarchical self-assembled structures. This material design concept would lead to construction of highly organized advanced functional materials which could not be achieved by conventional techniques. In addition, the material design philosophy will contribute to effective utilization of finite elements.

5.2. Perspective

Through the doctoral study, the mechanism of photovoltaic effect in the π -conjugated FLC systems was clarified. However, the characteristics of the photovoltaic effect remain low level. At the end of this doctoral thesis, the author points out some present drawbacks as follows.

(1) Low absorption efficiency of solar spectrum over wide wavelength range

The visible and near infrared light did not contribute to the bulk photovoltaic effect, because the main absorption band of FLC phenylterthiophenes lies in the near UV area. Therefore, total incident photon-to-current conversion efficiency was very low. For improving the efficiency, the development of π -conjugated ferroelectric liquid crystal systems with strong absorption band in the visible light region will be desired. The extension of π -conjugated unit provides one approach. The other strategy is π -conjugated FLC compound-dye composite system for utilizing a spectral sensitization.

(2) Imperfect surface stabilization and immobilization of polarized state

The suppression of polarization relaxation behavior is important to retain the characteristics of bulk photovoltaic effect for long term. Although the improvement of the APV characteristics was found as described in Chapter 4, the polarized state was only partially retained. The control of helical pitch and tuning of phase transition temperature should be required. To overcome this drawback, the molecular design must be optimized. In addition, the introduction of network structures into the FLC structures provides a structural immobilization method.

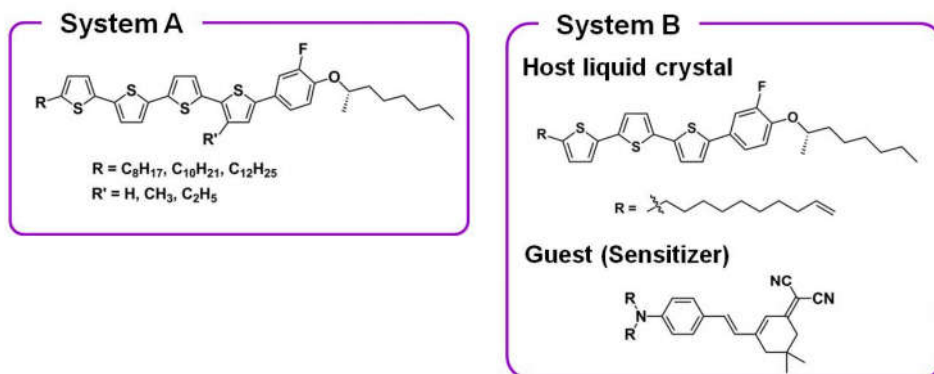
(3) Imperfect control of molecular orientation

The ferroelectricity is affected by the molecular orientation and uniaxial planer arrangement is the most suitable orientation. In this study, the molecular orientation in LC cells was random planer arrangement. In order to obtain a large-area monodomain structures with uniaxial planer alignment, LC materials exhibiting Iso-N*-SmA*-SmC* phase transition behaviors on cooling process is required.

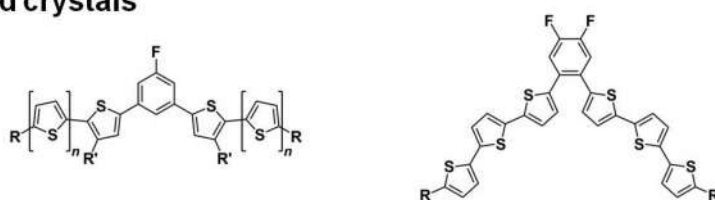
As demonstrated in this study, spontaneous polarization and carrier mobility of π -conjugated FLC system are key factors which affect the APV characteristics. Therefore, the optimization of molecular structures is also important for improving both properties and for realizing the large open-circuit voltage exceeding the band-gap. In order to realize high carrier mobility, the utilization of high ordered LC phases and the control of structural defects are key strategies. To obtain a large spontaneous polarization, the increase of polar groups and the introduction of polar unit on a chiral carbon can offer effective strategies. In addition, bent-shaped π -conjugated FLC materials have the potential of providing another type material system exhibiting the APV effect.

Some examples of material design strategies for overcome these drawbacks are as shown in Figure 5-1.

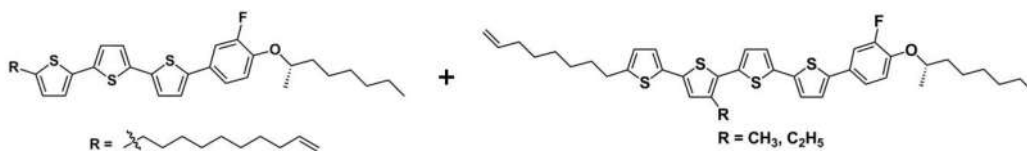
◆ The development of π -conjugated ferroelectric liquid crystal systems with strong absorption band in the visible light region



◆ The development of bent-shaped π -conjugated ferroelectric liquid crystals



◆ Control of the molecular orientation by using conventional techniques (Iso \rightarrow N* \rightarrow SmA* \rightarrow SmC* \rightarrow SmG*)



◆ *In situ* polymerization of surface-stabilized π -conjugated ferroelectric liquid crystal films by using photoacid generators

◆ π -conjugated ferroelectric liquid crystal with network molecules (LC physical gel, Polymer dispersed liquid crystals)

Figure 5-1. Some examples of material design strategies for future work.

Accomplishments

Publications

Original papers

1. "Photovoltaic effects in ferroelectric liquid crystals based on phenylterthiophene derivatives" (in Chapter 2)
Atsushi Seki and Masahiro Funahashi, *Chem. Lett.*, 2016, **45**, 616-618.
2. "Anomalous photovoltaic effect based on molecular chirality: Influence of enantiomeric purity on the photocurrent response in π -conjugated ferroelectric liquid crystals" (in Chapter 3)
Atsushi Seki, Yusuke Funatsu and Masahiro Funahashi, *Phys. Chem. Chem. Phys.*, 2017, **19**, accepted.
3. "Anomalous photovoltaic effect in chiral ordered smectic phases of phenylterthiophene derivatives without Junctions: Immobilization of the polarized structure by surface stabilization" (in Chapter 4)
Atsushi Seki and Masahiro Funahashi, To be submitted.

Reference

1. "Dipole-driven self-organization of liquid-crystalline *N*-heteroacene derivatives showing redox-properties"
Kyosuke Isoda, Ippei Kawamoto, Atsushi Seki, Masafumi Funahashi and Makoto Tadokoro, *ChemistrySelect*, 2017, **2**, 300-303.

Proceeding

1. "Oligothiophene-based chiral LC semiconductors: Circularly polarized light emission and anomalous photovoltaic effect"
Masahiro Funahashi, Taichi Hamamoto, Yusuke Funatsu and Atsushi Seki, *Proceedings of IDW 15'*, 2015, 23-26.

Review

1. "Nanostructure formation based on the functionalized side chains in liquid-crystalline heteroaromatic compounds"
Atsushi Seki and Masahiro Funahashi, *Heterocycles*, 2016, **92**, 3-30.

Symposium

International symposium (Oral)

1. "Bulk photovoltaic effect in π -conjugated ferroelectric liquid crystals"
Atsushi Seki, Jumpei Nakagawa, Yusuke Funatsu and Masahiro Funahashi, third Asian Conference on Liquid Crystals (ACLIC 2017), LCC-013, Feb., 2017, Tainan, Taiwan.
2. "Mesomorphic properties of phenylquaterthiophene derivatives comprised of an extended π -conjugated unit"

Atsushi Seki and Masahiro Funahashi, IUMRS-ICAM 2017 (The 15th International Conference on Advanced Materials), C3-O30-011, Kyoto (Japan), August, 2017.

International symposium (Poster)

1. “Mechanistic study on anomalous photovoltaic effect in the ferroelectric liquid-crystalline phase of phenylterthiophene derivatives”
Atsushi Seki and Masahiro Funahashi, The 2015 International Chemical Congress of Pacific Basin Societies (Pacifichem 2015), MACR1237, Dec., 2015, Honolulu, Hawaii, USA.
2. “Anomalous photovoltaic effect in ferroelectric liquid crystals based on phenylterthiophene unit”
Atsushi Seki, Jumpei Nakagawa and Masahiro Funahashi, the 26th International Liquid Crystal Conference (ILCC 2016), ILCC2016-211, Aug., 2016, Kent, Ohio, USA.
3. “Stabilization of spontaneous polarization by polymerization in thin films based on ferroelectric liquid-crystalline phenylterthiophene derivatives”
Jumpei Nakagawa, Atsushi Seki and Masahiro Funahashi, Korea-Japan Joint Forum International Conference on Organic Materials for Electronics and Photonics 2016 (KJF-ICOMEF 2016), PS-164, Sept. 2016, Fukuoka, Fukuoka, Japan.

Domestic symposium (Oral, in English session)

1. “Influence of the enantiomer ratio upon bulk photovoltaic effect of ferroelectric phenylterthiophene-based liquid crystals”
Atsushi Seki and Masahiro Funahashi, The 96th CSJ Annual Meeting (2016), 2B8-47*, Mar., 2016, Kyo-Tanabe, Kyoto.
2. “Mesomorphic and ferroelectric properties of phenylterthiophene derivatives bearing a polymerizable cyclotetrasiloxane moiety at the terminal of side chain”
Atsushi Seki, Jumpei Nakagawa and Masahiro Funahashi, 65th SPSJ Annual Meeting (2016), 1L-15, May, 2016, Kobe, Hyogo.
3. “An anomalous photovoltaic effect in a surface-stabilized π -conjugated ferroelectric liquid crystal”
Atsushi Seki and Masahiro Funahashi, The 97th CSJ Annual Meeting (2017), 3E1-03*, Mar., 2017, Yokohama, Kanagawa.

Domestic symposium (Oral, in Japanese session)

1. 「フェニルターチオフェン骨格を有する液晶性半導体の薄膜状態での強誘電性評価」
関 淳志, 舟橋 正浩, 2015 年日本液晶学会討論会, 3B05, 2015 年 9 月, 横浜, 神奈川.
2. 「側鎖に重合性シクロテトラシロキサン環を有するフェニルターチオフェンの液晶性と強誘電性」
関 淳志, 舟橋 正浩, 第 64 回高分子討論会, 1K18, 2015 年 9 月, 仙台, 宮城.
3. 「表面安定化を利用した π 共役系強誘電性液晶の異常光起電力効果の特性改善」
関 淳志, 舟橋 正浩, 2016 年日本液晶学会討論会, 3B-09, 2016 年 9 月, 大阪, 大阪.

4. 「*In situ* 重合を利用した π 共役系強誘電性液晶の高分子薄膜の作製」
関 淳志, 舟橋 正浩, 第 65 回高分子討論会, 3E09, 2016 年 9 月, 横浜, 神奈川.
5. 「 π 共役系強誘電性液晶における異常光起電力効果」
関 淳志, 船津 佑介, 中川 順平, 舟橋 正浩, 第 2 回液晶若手勉強会, 2016 年 9 月, 加賀, 石川.
6. 「 π 共役系強誘電性液晶における異常光起電力効果」
関 淳志, 舟橋 正浩, 第 26 回日本 MRS 年次大会, C2-O19-008, 2016 年 12 月, 横浜, 神奈川.
7. 「キラルな側鎖を有するフェニルクォーターチオフェン誘導体の液晶性評価」
関 淳志, 舟橋 正浩, 2017 年日本液晶学会討論会, 1B01, 2017 年 9 月, 弘前, 青森.
8. 「機能集積型液晶性半導体の開発: π 共役強誘電性液晶の分子不斉に由来したバルク光起電力効果」
関 淳志, 舟橋 正浩, 第 66 回高分子討論会, 3T07, 2017 年 9 月, 松山, 愛媛.

Domestic symposium (Poster)

1. 「フェニルターチオフェンをコアとして有する強誘電性液晶のスメクチック相での電荷輸送特性」
関 淳志, 舟橋 正浩, 第 19 回液晶化学研究会シンポジウム, P-11, 2015 年 5 月, 名古屋, 愛知.
2. 「側鎖末端に環状シロキサン部位を有する液晶性フェニルターチオフェン類縁体の強誘電性評価」
関 淳志, 舟橋 正浩, 第 5 回 CSJ 化学フェスタ 2015, P2-116, 2015 年 10 月, 江戸川, 東京.
3. 「強誘電性液晶での異常光起電力効果」
関 淳志, 舟橋 正浩, 日本化学会新領域研究グループ「エキゾチック自己組織化材料」全体講演会, P-5, 2015 年 11 月, つくば, 茨城.
4. 「自発分極を有するスメクチック液晶における異常光起電力効果」
関 淳志, 舟橋 正浩, 第 25 回日本 MRS 年次大会, C2-P8-005, 2015 年 12 月, 横浜, 神奈川.
5. “The production of polymerized thin films based on ferroelectric liquid-crystalline phenylterthiophene bearing a cyclotetrasiloxane ring”
中川 順平, 関 淳志, 舟橋 正浩, 第 96 回日本化学会春季年会 (2016), 3PC-209, 2016 年 3 月, 京田辺, 京都.
6. 「強誘電性液晶における異常光起電力効果に対する自発分極の影響」
関 淳志, 舟橋 正浩, 新学術研究領域「元素ブロック高分子材料の創出」第 3 回若手シンポジウム, 2016 年 3 月, 淡路, 兵庫.
7. 「重合性環状シロキサン部位を有する強誘電性液晶の液晶性と電荷輸送特性」
中川 順平, 関 淳志, 舟橋 正浩, 第 20 回液晶化学研究会シンポジウム, P02, 2016 年 7 月, 文京, 東京.
8. 「屈曲型 1,3-Bis(2,2'-bithienyl)-5-fluorobenzene 誘導体の相転移挙動」
関 淳志, 舟橋 正浩, 第 20 回液晶化学研究会シンポジウム, P37, 2016 年 7 月, 文京, 東京.

9. 「側鎖末端に重合性の環状シロキサンを有する π 共役系強誘電性液晶の異常光起電力効果」
中川 順平, 関 淳志, 舟橋 正浩, 2016 年日本液晶学会討論会, PB-64, 2016 年 9 月, 大阪, 大阪.
10. 「側鎖末端に環状シロキサンを有する π 共役系強誘電性液晶の重合薄膜の作製」
中川 順平, 関 淳志, 舟橋 正浩, 第 6 回 CSJ 化学フェスタ 2016, P5-138, 2016 年 11 月, 江戸川, 東京.
11. 「機能性シロキサンポリマーを指向した π 共役系強誘電性液晶」
関 淳志, 中川 順平, 舟橋 正浩, 新学術研究領域「元素ブロック高分子材料の創出」 第 4 回若手シンポジウム, 2016 年 12 月, 大津, 滋賀.
12. 「 π 共役系強誘電性液晶の構造固定化とその効果」
関 淳志, 舟橋 正浩, ExOM&CMS 合同シンポジウム, P6, 2017 年 1 月, 福岡, 福岡.
13. “Electronic property of thin films of π -conjugated ferroelectric liquid crystal exhibiting anomalous photovoltaic effect”
中川 順平, 関 淳志, 舟橋 正浩, 第 97 回日本化学会春季年会 (2017), 1PB-171, 2017 年 3 月, 横浜, 神奈川.
14. 「重合性環状シロキサン部位を導入した π 共役強誘電性液晶のスピンコート薄膜特性」 中川 順平, 関 淳志, 舟橋 正浩, 第 21 回液晶化学研究会シンポジウム, P6, 2017 年 7 月, 大分, 大分.
15. 「高次のスメクチック相における表面安定化を利用したバルク光起電力効果の特性改善」 関 淳志, 舟橋 正浩, 第 21 回液晶化学研究会シンポジウム, P29, 第 21 回液晶化学研究会シンポジウム, P6, 2017 年 7 月, 大分, 大分.
16. 「重合性環状シロキサン部位を導入した π 共役強誘電性液晶のスピンコート薄膜特性」 中川 順平, 関 淳志, 舟橋 正浩, 2017 年日本液晶学会討論会, PA57, 2017 年 9 月, 弘前, 青森.

Award

1. 第 25 回日本 MRS 年次大会, 横浜, 2015 年 12 月, 奨励賞.
「自発分極を有するスメクチック液晶における異常光起電力効果」
関 淳志, 舟橋 正浩.
2. 第 21 回液晶化学研究会シンポジウム, 大分, 2017 年 7 月, 優秀ポスター発表賞.
「高次のスメクチック相における表面安定化を利用したバルク光起電力効果の特性改善」
関 淳志, 舟橋 正浩.

Acknowledgements

The author expresses his deepest appreciation to Professor Masahiro Funahashi at Kagawa University for kind guidance and encouragement throughout the present study. His supervision led the author to fascinating field of liquid-crystal science, softmatter electronics and fusion material science. Professor Funahashi has taught to the author the wide knowledge about solid state physics as well as liquid crystal science. Furthermore, he provided a lot of opportunity to present our study in many of symposiums and to be acquaintance with many scientists of various research fields.

The author also would like to dedicate his gratitude to Professor Tomohiko Ishii and Professor Noriaki Tsurumachi who advise him to improve and summarize this Ph.D. study.

The author greatly appreciates Professor Shinobu Uemura and Professor Kyosuke Isoda at Kagawa University for many experimental supports.

The author would like to thank Dr. Mizuho Kondo in University of Hyogo for molecular calculation.

The author expresses his gratitude to Professor Takashi Kato in the University of Tokyo, who is a supervisor of master degree and cared about him.

The author thanks all his colleagues in Funahashi laboratory.

This study was financially supported by a Grant-in-Aid for Scientific Research on Innovative Areas (Element-Block Polymers, no. 15H00753) from the Ministry of Education, Culture, Sports, Science and Technology (MEXT), a Grant-in-Aid for Scientific Research (B) (no. 15H03797) from the Japan Society for the Promotion of Science (JSPS), the TEPCO memorial foundation, the Ogasawara Foundation for Promotion of Science and Engineering, the Kato Foundation for Promotion of Science, the Iketani Science and Technology Foundation, the Murata Science Foundation, the Iwatani Naoji Foundation, and the Asahi Glass Foundation.

Finally, the author sincerely acknowledges his family, Hideyuki Seki, Tomie Seki and Kokoro Seki and devotes to his grandmother, Isami Seki.